EXPLORING METAMATERIALS FOR THE CONTROL OF MASS DIFFUSION

A Dissertation
Presented to
The Academic Faculty

by

Juan Manuel Restrepo Flórez

In Partial Fulfillment
Of the Requirements for the Degree
Doctor of Philosophy in the
School of Chemical and Biomolecular Engineering

Georgia Institute of Technology

May, 2019

EXPLORING METAMATERIALS FOR THE CONTROL OF MASS DIFFUSION

Approved by:

Dr. Martin Maldovan, Advisor.
School of Chemical and
Biomolecular Engineering
Georgia Institute of Technology

Dr. David Sholl
School of Chemical and
Biomolecular Engineering
Georgia Institute of Technology

Dr. Christopher W. Jones
School of Chemical and
Biomolecular Engineering
Georgia Institute of Technology

Dr. Ryan P. Lively
School of Chemical and
Biomolecular Engineering
Georgia Institute of Technology

Dr. Massimo Ruzzene
School of Aerospace Engineering
Georgia Institute of Technology

Date approved: May 8th 2019

34. Busca por el agrado de buscar, no por el de encontrar…

Jorge Luis Borges, El Elogio de la Sombra

DEDICATION

To my parents Oscar and Gloria, and to my wife Any Carolina

ACKNOWLEDGMENTS

I must start by saying that I have enjoyed the journey. I have enjoyed being here, learning a lot, and at times failing a lot. I want to thank God for my joy and also the many people that made it possible.

First to my advisor, Dr. Martin Maldovan, his patience, support, rigorous sense of science, and attention to detail shaped my character as a scientist. I have always appreciated the possibility of asking questions openly. I am really grateful for being part of a group where discussion and learning are encouraged and pursued.

To my committee members: Dr. David Sholl, Dr. Christopher W. Jones, Dr. Ryan P. Lively, and Dr. Massimo Ruzzene, for their valuable comments and suggestions. I want to thank specially to Dr. Ryan P. Lively for opening the doors of his lab allowing me to learn the challenges of experimental research.

I also want to thank my group mates Kartik and Abhinav, they have listened countless times with attention to my presentations. Furthermore, they have answered patiently to my numerous "outsider" questions on phononics. It has been a pleasure to learn from them.

I also want to thank my friends at the CEED, Dr. Felicia Benton-Johnson, Jacky Cox, Cedric Trice, and Valentina de la Fe. They gave me the opportunity of making an impact on the community and gave me a sense of belonging.

To my mom Gloria Flórez, for being a model of honesty and hard work, for her love and unconditional support. To my dad Oscar Restrepo, for craving the wood with patience showing me that perfect things are the result of dedication and time. To my

grandpa Pastor Restrepo, who does not believe in anything and has shown me how to doubt of established truths. To my grandma Ester Perez, for being generous with her love. To my aunts, Nena Flórez, Monica Restrepo, and Catalina Restrepo, for helping me all my life walking by my side. To my brother, Isidro Restrepo, and my sister Isidra Restrepo, it's been an enormous amount of fun to grow (and get older) with them.

Finally, I want to thank my wife, Any Carolina Cuervo, for her unconditional love, for her adventurous character, for her company, for reading instruction manuals, for her help with drawings, and for giving meaning to everything I do.

TABLE OF CONTENTS

ACKNOWLEDGMENTS v

LIST OF TABLES x

LIST OF FIGUES xi

LIST OF SYMBOLS xviii

SUMMARY xxiii

CHAPTER 1: INTRODUCTION 1
1.1 Flux control in mass diffusion processes 1
1.2 Tailoring diffusion in membrane based gas separations: Current status and opportunities 3
1.3 Dissertation outline 5
1.4 References 6

CHAPTER 2: THEORY AND BACKGROUND 9
2.1 Metamaterials 9
2.1.1 Coordinate transformations 11
2.1.1.1 Metamaterial Functionalities 15
2.1.2 Topology optimization 19
2.1.3 Heuristic design 20
2.2 Membrane based gas separations 21
2.3 Numerical solution of the diffusion equation 26
2.4 References 27

CHAPTER 3: RATIONAL DESIGN OF MASS DIFFUSION CONCENTRATORS USING COORDINATE TRANSFORMATIONS 34
3.1 Introduction 34
3.2 Theoretical approach 35
3.3 Results and discussion 40
3.4 Conclusions 52
3.5 References 53

CHAPTER 4: A COMPLETE FRAMEWORK FOR THE REALIZATION OF MASS DIFFUSION METAMATERIALS 55
4.1 Introduction 55
4.2 Theoretical approach 56
4.3 Results and discussion 58
4.4 Conclusions 65
4.4 References 66

CHAPTER 5: TAILORING DIFFUSION OF A BINARY MIXTURE IN A CYLINDRICAL SYSTEM: A FIRST STEP TOWARD THE DESIGN OF METAMATERIALS FOR MASS SEPARATIONS **68**
5.1 Introduction **68**
5.2 Theoretical approach **69**
5.3 Results and discussion **70**
5.4 Conclusions **76**
5.5 References **77**

CHAPTER 6: DESIGN OF A PLANAR METAMATERIAL TO SORT CHEMICAL SPECIES **78**
6.1 Introduction **78**
6.2 Theoretical approach **78**
6.3 Results and Discussion **81**
6.4 Conclusions **84**
6.5 References **84**

CHAPTER 7: DESING OF CYLINDRICAL ANISOTROPIC MEMBRANES WITH APPLICATIONS TO O_2/N_2 SEPARATIONS **86**
7.1 Introduction **86**
7.2 Theoretical approach **89**
7.3 Results and discussion **92**
7.4 Conclusions **99**
7.5 References **99**

CHAPTER 8: GENERAL CONSIDERATIONS FOR THE DESIGN OF ANISOTROPIC MEMBRANES FOR GAS SEPARATIONS **102**
8.1 Introduction **102**
8.2 Theoretical analysis **103**
8.3 Results and Discussion **110**
8.4 Conclusions **118**
8.5 References **118**

CHPATER 9: ANALYSIS AND CHARACTERIZATION OF ANISOTROPIC HOLLOW FIBERS FOR GAS SEPARATIONS **120**
9.1 Introduction **120**
9.2 Theoretical analysis **120**
9.3 Results and Discussion **125**
9.4 Conclusions **132**
9.5 References **132**

CHPATER 10: PERMEABILITIES AND SELECTIVITIES IN ANISOTROPIC PLANAR MEMBRANES FOR GAS SEPARATIONS **134**
10.1 Introduction **134**
10.2 Results and Discussion **136**
10.2.1 Rerouting one species (Ideal case) 136

10.2.2 Rerouting one species (Real case) 141
10.2.3 Rerouting two species (Ideal case) 144
10.2.4 Rerouting two species (Real case) 146
10.4 Conclusions 149
10.5 References 150

CHPATER 11: CONCLUSIONS AND FUTURE DIRECTIONS 152
11.1 Conclusions 152
11.2 Future work 155
11.3 References 157

LIST OF TABLES

Table 7.1. Solubilities and diffusivities for polydimethylsiloxane (PDMS), polysulfone (PSF) (Refs. [40,41]) and for an anisotropic shell made of layered PDMS (M_1) and PSF (M_2) with f_{PDMS}=0.5...……97

Table 8.1. Diffusion properties of the shell materials in Figure 8.7. The effective properties for the shells are calculated using effective medium theory...……117

Table 10.1. Material properties for separation of species A and B (left), and O_2 and N_2 (right). For O_2/N_2 separation M_1 is PDMS and M_2 is PSF. Units [D]=m^2/s, [S]=mol/m^3Pa …….....139

Table 10.2. Material properties for separation of species A and B (left), and H_2 and CH_4 (right), which are designed to independently control the diffusion trajectory of the two species. For H_2/CH_4 separation M_1 is PTMSP, M_2 PDMS, M_3 PIM-7, and M_4 PMDA-BATPHF. Units [D]=m^2/s, [S]=mol/m^3Pa……...145

LIST OF FIGURES

Figure 2.1. Schematic representation of the transformation process. Red lines represent flux trajectories while black lines represent isoconcentrations……..……13

Figure 2.2. Schematic representation of the four possible transformations: rotation, translation, compression and expansion. In the figure we have presented two regions, a core (small square) surrounded by a larger square delimiting the portion of the space in which the transformation is performed. As an example we have applied the transformation to the core region. In general the metamaterial is the space where the transformation is applied, i.e. the region between the small and big squares……14

Figure 2.3. Transformation process for different *2D* metamaterials with simple geometries. The first column contains a representation of the original space, with broken lines indicating the position of the metamaterial; the second column illustrates the metamaterial structure (light blue) as well as the effect of the device presence on the isothermal(isoconcentration) (black) and flux lines (red); the third column presents the homogenization strategy that can be used in the cases where it is necessary while the forth column shows the effective medium arrangement of isotropic materials that can be used to reproduce the required anisotropicity; finally, in the fifth column an example of the temperature(concentration) profile observed in the presence of the metamaterial is presented. (a) Cloak, (b) concentrator, (c) beam shifter. In figures (a) and (b) the following boundary conditions were used for the simulations: left/right boundary at high/low temperature(concentration) and upper and lower boundaries insulated. In figure (c) same left and right boundaries were used but periodic conditions were implemented in the upper and lower boundaries. ……...15

Figure 2.4. Schematic of the operation of a typical isotropic membrane for the separation of a binary mixture. Ideally one of the species will permeate the membrane (Species B) while the other one will be rejected (Species A). ……22

Figure 2.5. Robeson representation of selectivity vs permeability for a hypothetical separation. The red line is known as the upper bound (an experimentally observed trade-off limit between selectivity and permeability for polymeric materials). The figure also illustrates how and ideal material would have high selectivity and permeability, breaking the upper-bound limit. ……...24

Figure 2.6. Comsol multhyphysics enviroment for the solution of mass diffusion problems…….27

Figure 3.1. Coordinate transformation scheme for mass diffusion concentrators. The figure shows the three major design steps. (a)(b) A coordinate transformation is applied and a homogenization process (c)(e) is used to simplify the initial device. (d)(f) A

segmentation step is employed where isotropic homogeneous materials reproduce the prescribed anisotropy. (a) Initial isotropic region. (b) Ideal anisotropic, non homogeneous metamaterial. (c) Homogeneous, anisotropic metamaterial (with *m* rings) after homogenization of (b) based on mean value theorem. (d) Multilayer mass concentrator where the anisotropy of each *m* ring is reproduced by two isotropic materials. (e) Homogeneous, anisotropic metamaterial (with one ring) after homogenization of (b) using Eq. (3.3). (f) Multilayer lamellar structure, anisotropy is reproduced by two isotropic materials A and B. The average concentration gradient is measured between P1 and P2 (f), the standard deviation of the concentration along the lines at x=±3.05cm….36

Figure 3.2. Performance of ideal mass concentrator devices as a function of metamaterial shell geometry. (a) Functional relation among $\langle D_{r(i)}/D_{(i)} \rangle$, R_1/R_3 and R_2/R_3 (b) Concentration gradient normalized with respect to the external gradient. (c) Incoming mass flow rate towards the core normalized against the mass flow rate entering the system at the boundary……..……43

Figure 3.3. Covariance as a function of R_1/R_3 and R_2/R_3…….……44

Figure 3.4. Mass diffusivity contrast T of the isotropic homogeneous constituent materials. (a) T as a function of the geometrical parameters of the system, where the gray area shows the more accessible region in terms of finding required constituent materials. (b) T as a function of the relative radial diffusivity and the volume fraction of the highly diffusive material…….……..46

Figure 3.5. Effect of the volume fraction of highly diffusive material f_A on the performance of the metamaterial shell. (a) Concentration gradient normalized with respect to the external gradient. (b) Mass flow rate towards the core normalized against the incoming flow rate. (c) Standard deviation of the concentration on a vertical line outside the device (x=±3.05cm). No significant differences were found between the standard deviations measured at both sides of the device ((i.e. at x=-3.05cm (left side), and x=3.05cm (right side))…….49

Figure 3.6. Performance of the device as a function of the number of bilayers N. (a) Normalized gradient in the interior of the device. (b) Normalized total mass flow rate towards the core. (c) Standard deviation of the concentration at a vertical position outside the device. ……...…..51

Figure 3.7. Color maps for the mass concentration profiles for different number of bilayers N. A mass concentrator metamaterial shell (white lines) made of N=18 provides a similar mass spatial distribution as N=∞…….51

Figure 4.1. Schematic representation for mass diffusion metamaterial devices. Ideal (i.e. homogeneous and isotropic) cloaking (a) and concentrator (b) shells with internal radius R_1 and external radius R_3. (c) and (d) Multilayer metamaterial shells that reproduce the anisotropic properties of the corresponding ideal metamaterials……..57

Figure 4.2. Color maps of the concentration profiles for homogeneous and isotropic mass diffusion metamaterials ($D_{r(cl)(i)}/D_{(i)}$=1/10, $D_{r(cn)(i)}/D_{(i)}$=10, ($D_{r(i)}/D_{(i)}$)($D_{\theta(i)}/D_{(i)}$)=1) for different external partition coefficient $k_{ex(i)}$=1/10, 1/2, 1, 2, 10. (a)-(e) Cloaks. (f)-(j) Concentrators. Standard deviation for cloak (k) and concentrator (l) and relative concentration gradient for cloak (m) and concentrator (n) as a function of the external partition coefficient $k_{ex(i)}$. Insets show concentration profiles along a vertical line outside the metamaterial device $x=-1.05R_3$, $-L/2<y<L/2$ (k),(l) and relative concentration gradient along the horizontal line $y=0$, $-L/2<x<L/2$ (m), (n). ……61

Figure 4.3. (a), (g) Color maps for the predicted concentration of layered mass diffusion metamaterial shells under the assumption $k_{in(i)}=k_{ex(i)}=1$ (EMA-∇C approach) for cloak and concentrator, respectively ($D_{r(cl)(i)}/D_{(i)}$=1/10, $D_{r(cn)(i)}/D_{(i)}$=10, ($D_{r(i)}/D_{(i)}$)($D_{\theta(i)}/D_{(i)}$)=1). (b)-(f) and (h)-(l) Actual concentration profiles when the constituent materials calculated using the EMA-∇C approach possess solubilities $k_{in(i)}$ =1/10, 1/2, 1, 2, and 10. (m)-(p) Standard deviation and relative concentration gradient calculated using the EMA-∇C approach (designed EMA-∇C), the actual values when discontinuities at interfaces are present (actual EMA-∇C), and the values obtained when using EMA-$\nabla\mu$. (m),(o) Cloak. (n),(p) Concentrator. ……64

Figure 4.4. Concentration profiles in layered metamaterials designed using the EMA-$\nabla\mu$ for different internal partition coefficients $k_{in(i)}$. (a)-(e) Cloaks. (f)-(j) Concentrators…..65

Figure. 5.1. (a) Cloaking: A point is transformed into a circle of radius R_1 while the adjacent region is being compressed. Experimental realization of such transformation is obtained by a multilayer structure made of concentric rings (b) Concentrator: Compression of a circular region $0<r<R_2$ into $0<r<R_1$ followed by expansion of the adjacent annulus from R_2 to R_1. The experimental realization is obtained by a lamellar structure (c) Bi-functional multilayer device: the design requires four different materials depicted by dark blue, grey, light blue, and light green colors, respectively. ……...…69

Figure 5.2. Concentration profiles for *cloaked* compound A at different times and steady-state. (a-e), background media without metamaterial. (f-j) Anisotropic homogeneous cloak. (k-o) Multilayer cloaking device. ……...……71

Figure 5.3. Concentration profiles for *concentrated* compound B at different times and steady-state. Insets (a-e), background media without metamaterial. (f-j) Anisotropic homogeneous concentrator. (k-o) Multilayer concentrator device……71

Figure 5.4. (a) (b) Concentration values at two different locations inside the mass-separator device (locations are highlighted in Figure 1(c) with numbers 1 and 2) as a function of time for cloaked and concentrated species, respectively. (c) (d) Concentration gradients inside the bi-functional device for cloaked and concentrated species……...75

Figure 6.1. (a) Schematic of a metamaterial membrane. Due to their anisotropic properties, unit cell Type I simultaneously redirects compound *A* to the right and compound *B* to the left, while in unit cell Type II the effect is inverted. As a result, *A* and

B are separated by guiding them to different spatial areas. (b) Design of a metamaterial membrane to achieve compound separations using four homogeneous isotropic materials. Rhomboidal elements with same color have the same diffusivity for compound *B*, while elements with same geometric pattern have the same diffusivity for compound *A*. P_1 and P_2 are representative points to study the transient behavior of the system. …….……79

Figure 6.2. Color maps describing the transient and steady-state concentrations for compounds *A* and *B* in the case of an ideal (left) and a multilayer (right) metamaterial membrane. Diffusion of compound *A* in ideal (a-d) and multilayer (e-h) metamaterial. Diffusion of compound *B* in ideal (i-l) and multilayer (m-p) metamaterial. After crossing the metamaterial membrane from top to bottom, compounds *A* and *B* are guided to different spatial locations, as it can be seen by analyzing the location of maximal concentration (red area) at the bottom of the metamaterial membrane for the upper panels (Compound *A*) and the lower panels (Compound *B*). Note that the metamaterial membrane (indicated by horizontal black lines) is embedded in a homogeneous background medium..…….83

Figure 6.3. Transient and steady-state profiles for compound *A* (a),(b) and compound *B* (c),(d) along the horizontal direction *y* at the bottom surface of the metamaterial membrane for ideal (a), (c) and multilayer (b), (d) devices……..…….84

Figure 7.1. (a) Isotropic hollow fiber working for separation in countercurrent flow. The cylindrical membrane is highly selective for compound A (spheres) thus creating a permeate enriched in A. Inset shows the radial flux lines due to the cylindrical symmetry. (b) Proposed anisotropic membrane separation device consisting of an isotropic cylindrical core of radius R_1 covered by an anisotropic cylindrical shell with internal radius R_1 and external radius R_2. In this case, the two molecules (spheres and cubes) permeate in the membrane. The schematics show the ideal case where one compound (cubes) is directed around the core and the other compound (spheres) is focused towards the core. We are interested in collecting molecules A (spheres) at the core region ($-R_1<x<R_1$, $y=0$). Inset shows the flux lines for the two compounds, which are bent as a consequence of the anisotropicity of the shell. Simultaneous control of the flux trajectory for the two compounds is the basic principle of operation of the anisotropic membrane. (c) The anisotropic shell can be constructed using multilayer structures made of two isotropic materials M_1 and M_2 with mass resistances adding in series in the radial direction and in parallel in the azimuthal direction……...88

Figure 7.2. (a) Selectivity and (b) permeance for our anisotropic membrane device as a function of R_2/R_1 in the case of separation of a binary mixture of oxygen and nitrogen. The cylindrical core is made of PDMS. Red, blue, and green lines correspond to anisotropic, PSF, and PDMS shells respectively. The anisotropic shell is made of layered PSF and PDMS materials. For the permeance, two R_1 values are considered 1μm and 10μm……..94

Figure 7.3. Robeson plot for selectivity vs. permeance for anisotropic (red), PSF (blue), and PDMS (green) shells respectively where R_1=1μm. Black solid line shows selectivity

vs. permeance upper bounds for a planar isotropic membrane of thickness 1μm. We note that if R_1 is increased (reduced) the plot will shift to the left (right)…….94

Figure 7.4. Selectivity vs. permeance for a membrane separation device with R_1=1μm and R_2/R_1=2 for different volume fractions of PDMS in the shell…….97

Figure 7.5. Insets: Selectivity (left) and permeability (right) of our membrane design for separation of a binary mixture of oxygen (50%) and nitrogen (50%) as a function of the number *N* of bilayers. The layered anisotropic shell is made of isotropic PDMS and PSF materials. R_1=1μm (top line), R_1=10μm (bottom line) and R_2/R_1=2. Main panel: Robeson plot of selectivity vs. permeance for a layered anisotropic shell with R_1=1μm and R_2/R_1=2 and increasing number of layers (orange line). For large numbers of bilayers (~20), the performance corresponds to the continuous case (red dot). For reference, PSF and PDMS shells are also shown in the figure…….98

Figure 8.1. Schematic of the proposed anisotropic membranes. The core region is isotropic while the surrounding shell is anisotropic. The role of the shell is to reroute compounds *A* and *B* through the membrane. The driving force is the chemical potential difference at the top and bottom of the membrane. Separation of *A* from *B* is obtained for permeate 1 leaving the core. A schematic of a module design is shown on the right where two permeate streams are generated requiring two independent collection channels (Permeate 1 and Permeate 2). ……..105
.
Figure 8.2. Schematic for the effect of the anisotropic shell on the trajectory of compounds *A* and *B* (a) $l_{(A)}$<1, $l_{(B)}$>1 (b) $l_{(A)}$>1, $l_{(B)}$>1 (c) $l_{(A)}$<1, $l_{(B)}$<1 (d) $l_{(A)}$>1, $l_{(B)}$<1. The shell structures made of isotropic materials that can create such mass diffusion trajectories are shown on the right……...…107

Figure 8.3. Normalized selectivity as a function of the non-dimensional variables $l_{(i)}$ and $\delta_{(i)}$ for a shell/core ratio R_2/R_1=2. (a) l_A=0.1, (b) l_A=10. ……112

Figure 8.4. Normalized permeance as a function of $l_{(i)}$ and $\delta_{(i)}$ for a ratio R_2/R_1=2….112

Figure 8.5. Selectivity vs. permeance for different values of the non-dimensional variables $\delta_{(A)}$, $\delta_{(B)}$, $l_{(A)}$ and $l_{(B)}$. ……....114

Figure 8.6. Color maps for concentration distribution of compounds *A* (left) and *B* (right) inside the anisotropic membranes. We show both homogeneous anisotropic shells (top) and the corresponding multilayer shells (bottom) obtained by effective medium theory (a) $l_{(A)}$<1, $l_{(B)}$>1 (b) $l_{(A)}$>1, $l_{(B)}$>1 (c) $l_{(A)}$<1, $l_{(B)}$<1 (d) $l_{(A)}$>1, $l_{(B)}$<1. For simplicity, the materials are assumed to have similar solubilities. ……..…115

Figure 8.7. Selectivity vs. permeance for different anisotropic membranes for separation of H_2/CH_4 with different number of azimuthal *N* and radial *m* layers (blue circles) (a) CH_4 shielded from the core and H_2 focused towards the core (b) Both CH_4 and H_2 are shielded from the core. (c) Both CH_4 and H_2 are focused towards the core (d) CH_4 is focused

towards the core and H_2 is shielded from the core. The black stars correspond to homogeneous anisotropic shells. Results are presented for R_1=1μm. ……117

Figure 9.1. (a) Anisotropic membrane slab (light green) and operating conditions. The slab can be transformed into a cylindrical shell via bending/rotation. (b) A schematic of the anisotropic membrane slab with different preferred directions of transport for *A* and *B* as a function of $l_{(A)}$ and $l_{(B)}$ (left). Effective medium architectures for the required anisotropicity (center. A resistors network analogy representing the resistance to diffusion in different effective media (right). The resistor network analogy is used to calculate the effective properties of the composites……122

Figure 9.2. (a) Normalized permeability $P'_{(i)}/P^{*\prime}_{(i)}$ as a function of $l_{(i)}$ for different aspect ratios H/L. Dashed line represents the permeability for an isotropic material with $l_{(i)} = 1$. (b) Local permeability $P'_{(i)}(x)$ of the system at the bottom of the membrane as a function of the *x*-coordinate for representative values of $l_{(i)}$ and $H/L = 2$. (c) Color maps of the concentration profiles for representative values of $l_{(i)}$ and H/L. Isoconcentration lines are presented in black, and flux lines are displayed in white……..128

Figure 9.3. Selectivity as a function of $l_{(A)}$ and $l_{(B)}$ for three representative aspect ratios $H/L = 1/5$, $H/L = 1/2$, $H/L = 1$**.** The dashed red line represents the set of materials for which $l_{(A)} = l_{(B)}$ and $\alpha_{A/B(i)}/\alpha^*_{A/B(i)} = 1$……...131

Figure 9.4. Modified Robeson representation of relative selectivity $\alpha_{A/B}/\alpha^*_{A/B}$ vs. relative permeability $P'_{(i)}/P^{*\prime}_{(i)}$ for representative membranes. The upper panel present membranes with $l_{(A)} > l_{(B)} = 0.1$. Different lines correspond to different values of $l_{(A)}$ increasing from bottom to top from $l_{(A)} = 0.12$ to $l_{(A)} = 10$. The lower panel presents membranes with $l_{(A)} = 0.1 < l_{(B)}$. Different lines correspond to different $l_{(B)}$ increasing increases from top to bottom from $l_{(B)} = 0.12$ to $l_{(B)} = 10$……...132

Figure 10.1. Schematic representation of a planar membrane of thickness *H* and length *L* (a) Isotropic membrane: Difference in flux magnitude creates a permeate enriched in one of the species diffusing through the membrane (species *A* in this case). (b) Anisotropic membrane: flux directional control of species *B*, creates a permeate depleted on this species at the left side, thus if the collection area is located at the left the side the permeate will be enriched in species *A* (c) Anisotropic membrane: flux directional control of both species *A* and *B* creates a permeate in which the flux of these species is a function of the position on the permeate side. If the collection area is located on the left, the permeate is enriched in species *A*, whereas if the collection area is located on the right the permeate is enriched in species *B*. ……..135

Figure 10.2. Separation of a binary mixture of species *A* and *B* using an anisotropic planar membrane that reroutes species *B* toward the right side while not affecting the diffusion of *A*. The figure also presents the performance of related isotropic systems and

their series and parallel arrangements (a)-(b) Permeability of species *B* as a function of the position *x* on the permeate side for $D_{\parallel(B)}/D_{\perp(B)}$ = 100 and $D_{\parallel(B)}/D_{\perp(B)}$ = 4, with $D_{\parallel(A)}/D_{\perp(A)}$ =1. (c)-(d) Corresponding selectivities $\alpha_{A/B}$ as a function of the length *s* of a collection area placed at the left side of the membrane. Color maps show the concentration profiles for *A* and *B*……...…138

Figure 10.3. Effect of the rotation angle of the multilayer material on the local permeability for systems L=5μm..……...141

Figure 10.4. Separation of a binary mixture of O_2 and N_2 using an anisotropic planar membrane that preferentially reroutes N_2 to the right. O_2 is also rerouted to the right but to a lesser extent (a)-(b) Permeabilities of N_2 and O_2 as a function of the position *x* on the permeate side. (c) Selectivity α_{O_2/N_2} as a function of the length *s* of a collection area placed at the left side of the membrane. Inset shows collected permeate proportion (CPP). ……..143

Figure 10.5. Modified Robeson plot for the separation of O_2 and N_2 using an anisotropic planar membrane. The plot shows the relation between the selectivity, permeability, and CPP. For comparison we show the results for the isotropic constituent materials PDMS and PSF, and their series and parallel arrangements. The blue plane is the upper bound……....144

Figure 10.6. Separation of a binary mixture of species *A* and *B* using an anisotropic membrane that reroutes species *B* to the right side and species *A* toward the left side. (a)-(c) Permeabilities of species *A* and *B* as a function of the position on the permeate side. (b)-(d) Selectivities ($\alpha_{A/B}$) as a function of the length *s* of a collection area placed at the left side (b) and right side (d) of the membrane. Inset: CPP of species *A* as a function of the length *s* of a collection area placed at the left side of the membrane....……146

Figure 10.7. Separation of H_2 and CH_4 in a planar membrane that reroutes CH_4 to the right side and H_2 to the left side. (Note: The effect on H_2 is very small). (a)-(c) Permeability of CH_4 and H_2 as a function of the position *x* on the permeate side. (b)-(d) Ideal selectivity α_{H_2/CH_4} as a function of the length *s* of a collection area placed at the left (b) and right (d) side of the membrane. Inset: CPP of H_2 as a function of the length *s* of a collection area placed at the left side of the membrane……...148

Figure 10.8. Modified Robeson plot for the separation of N_2 and CH_4 using an anisotropic planar membrane. The plot shows the relation between the selectivity, permeability, and CPP. For comparison we also show the selectivity and permeability for the isotropic constituent materials PTMSP, PDMS, PIM-7, and PMDA-BATPHF), as well as their series and parallel arrangements. The blue plane represents the upper bound for this separation……149

LIST OF SYMBOLS

b	Transformation constant	[-]
$b_{l(i)}$	Langmuir affinity constant for species *i*	[1/Pa]
$C_{(i)}$	Concentration of species *i*	[mol/m^3]
$C_{bg(i)}$	Concentration of species *i* in a background material	[mol/m^3]
$C_{c(i)}$	Concentration of species *i* in the core	[mol/m^3]
$C_{sh(i)}$	Concentration of species *i* in the shell	[mol/m^3]
$C_{mm(i)}$	Concentration of species *i* in a metamaterial	[mol/m^3]
$C'_{H(i)}$	Langmuir capacity constant for species *i*	[mol/m^3]
$C_{D(i)}$	Concentration of the fast moving fraction of species *i* in the partial immobilization model	[mol/m^3]
$C_{H(i)}$	Concentration of the slow moving fraction of species *i* in the partial immobilization model	[mol/m^3]
C_{pbg}	Heat capacity of a background material	[J/kg-K]
C'_p	Transformed heat capacity	[J/kg-K]
CPP	Collected permeate proportion	[%]
$D_{(i)}$	Isotropic diffusivity of species *i*	[m^2/s]
$D_{bg(i)}$	Isotropic diffusivity of species *i* in a background material	[m^2/s]
$D_{c(i)}$	Diffusivity of species *i* in a cylindrical core	
$D_{D(i)}$	Diffusivity of the fast moving fraction of species *i* in the partial immobilization model	[m^2/s]

$D_{H(i)}$	Diffusivity of the slow moving fraction of species *i* in the partial immobilization model	[m^2/s]
$D_{j(i)}$	Isotropic diffusivity of species *i* in material *j*	[m^2/s]
$D_{P(i)}$	Effective diffusion coefficient of materials connected in parallel in a planar membrane	[m^2/s]
$D_{r(i)}$	Radial anisotropic diffusivity of species *i*	[m^2/s]
$D_{r(cl)(i)}$	Radial anisotropic diffusivity of a cloaked species *i*	[m^2/s]
$D_{r(cn)(i)}$	Radial anisotropic diffusivity of a concentrated species *i*	[m^2/s]
$D_{r(sh)(i)}$	Radial anisotropic diffusivity of species *i* in the shell	[m^2/s]
$D_{sh(i)}^{Parallel}$	Effective diffusivity of species *i* in shell for materials connected in parallel	[m^2/s]
$D_{sh(i)}^{Series}$	Effective diffusivity of species *i* in shell for materials connected in series	[m^2/s]
$D_{S(i)}$	Effective diffusion coefficient of materials connected in series in a planar membrane	[m^2/s]
$D_{x(i)}$	Anisotropic diffusivity of species *i* in the *x*-direction	[m^2/s]
$D_{xx(i)}$	Anisotropic diffusivity tensorial component of species *i*	[m^2/s]
$D_{xy(i)}$	Anisotropic diffusivity tensorial component of species *i*	[m^2/s]
$D_{yx(i)}$	Anisotropic diffusivity tensorial component of species *i*	[m^2/s]
$D_{yy(i)}$	Anisotropic diffusivity tensorial component of species *i*	[m^2/s]
$D_{y(i)}$	Anisotropic diffusivity of species *i* in the *y*-direction	[m^2/s]
$D_{\theta(i)}$	Azimuthal anisotropic diffusivity of species *i*	[m^2/s]

$D_{\theta(cl)(i)}$	Azimuthal anisotropic diffusivity of a cloaked species *i*	[m^2/s]
$D_{\theta(cn)(i)}$	Azimuthal anisotropic diffusivity of a concentrated species *i*	[m^2/s]
$D_{\theta(sh)(i)}$	Azimuthal anisotropic diffusivity of species *i* in the shell	[m^2/s]
$D_{\parallel(i)}$	Effective diffusion coefficient in one of the main components of the diffusivity tensor	[m^2/s]
$D_{\perp(i)}$	Effective diffusion coefficient in one of the main components of the diffusivity tensor	[m^2/s]
$\bar{\bar{D}}_{(i)}$	Anisotropic tensorial diffusivity	[m^2/s]
d	Thickness of a planar metamaterial membrane	[m]
EMA	Effective Medium Approximation	
f_j	Volume fraction of material *j*	-
$\mathcal{H}_{(i)}$	Henrry's constant (solubility) of species *i*	[mol/m^3-Pa]
H	Membrane thickness	[m]
$J_{(i)}$	Molar flux of species *i*	[mol/m^2-s]
$\bar{\bar{J}}$	Jacobian of a transformation	[-]
κ_{bg}	Isotropic thermal conductivity of a background medium	[W/m-K]
$\bar{\bar{\kappa}}$	Tensorial anisotropic thermal conductivity	[W/m-K]
$\bar{\bar{\kappa}}'$	Transformed tensorial anisotropic thermal conductivity	[W/m-K]
$K_{(i)}$	Partition coefficient between the core and the shell for species *i* in an anisotropic membrane	[-]
k_i^*	Partition coefficient for species *i* between two constituent	[-]

	shell materials in an effective anisotropic membrane	
$k_{ex(i)}$	Partition coefficient between a metamaterial and the background material	[-]
$k_{in(i)}$	Partition coefficient between two materials in an effective anisotropic metamaterial	[-]
$k_{jk(i)}$	Partition coefficient for species *i* between materials *j* and *k*	[-]
$l_{(i)}^2$	Ratio of components along the main axis of the anisotropic diffusion coefficient for species *i*	[-]
L	Membrane length	[m]
m	Number of bilayers arranged in the radial direction in the shell	[-]
m'	Geometric parameter in the design of beam shifter metamaterial membranes	[m]
N	Number of bilayers arranged in the azimuthal direction in the shell	[-]
$P'_{(i)}$	Permeability of species *i*	[Barrer] [mol-m/ m2-s-Pa]
$P_{(i)}$	Permeance of species *i*	[GPU]
$P^*_{(i)}$	Permeance of species *i* in an isotropic material	[GPU]
$P^{*\prime}_{(i)}$	Permeability of species *i* in an isotropic material	[GPU]
$p_{(i)}$	Partial pressure	[Pa]
R	Radius	[m]

$S_{(i)}$	Solubility	[mol/m^3]
$S_{bg(i)}$	Solubility of species *i* in a background material	[mol/m^3]
$S_{c(i)}$	Solubility of species *i* in the core	[mol/m^3]
$S_{mm(i)}$	Solubility of species "*i*" in a metamaterial	[mol/m^3]
$S_{sh(i)}$	Solubility of species *i* in the shell	[mol/m^3]
$S_{j(i)}$	Solubility of species *i* in material *j*	[mol/m^3]
T_c	Diffusivity contrast	[-]
T	Temperature	[K]
$\alpha_{A/B}$	Selectivity	[-]
$\alpha^*_{A/B}$	Selectivity of the core material	[-]
$\delta_{(i)}$	Core/shell material permeability ratio	
$\theta_{(i)}$	Rotation angle in a multilayer composite	[rad]
ρ_{bg}	Density of the background medium	[kg/m^3]
ϕ	Bending angle of a flux line	[rad]
ρ'	Transformed density	[kg/m^3]
μ	Chemical potential	[J/mol]

SUMMARY

Understanding and controlling mass diffusion processes is a fundamental scientific challenge with impact in many technological applications. Toward this end different efforts in materials science and engineering have been developed in recent years with the aim of providing new materials with improved mass diffusion properties. Most of these efforts have centered on the design of isotropic materials that control the mass flux magnitude. The use of isotropic materials, however, does not provide opportunities to exploit the vectorial nature of the flux and the possibility of controlling the flux direction. The design of mass diffusion systems that can simultaneously control flux direction and magnitude requires the development of engineered materials in which anisotropy is being tailored locally. One avenue for the development of these materials with tailored anisotropic properties is metamaterials theory. Metamaterials are structured composites whose effective properties are radically different from those of the constituent materials and depend strongly on the architecture of the composite structure. The most common approach for the design of metamaterials is coordinate transformations, a mathematical technique that correlates a desired spatial trajectory for a mass flux line with a set of required spatially-dependent material properties to realize such trajectory. Importantly coordinate transformations have been extensively employed to manipulate heat conduction but they have been barely explored for the design of materials and devices to control mass diffusion.

From a technological perspective the development and use of materials that can control the trajectory of mass flux can have a significant impact in the design of

membrane separation processes. Membranes are particularly attractive in the current search for energy-saving industrial processes since their energy demand can be one order of magnitude lower than dominant separation technologies such as distillation. Membranes are typically designed with the goal of controlling the flux magnitude of the species in a chemical blend as the species cross the membrane. To date, the basic goal in membrane-based separations has been the design of membrane materials for which the flux of one of the species is very high while for the others is very low as the species cross the membrane under a driving force. Importantly, the development and use of membrane materials that can also control the direction of flux in order to perform separations has never been attempted before and the requirements and benefits of such novel approach are unknown.

In this thesis we have explored the use of metamaterials theory for the design of new materials and devices that provide unprecedented control of mass diffusion and proposed new mechanisms to perform separations. First, we focus on the design of metamaterials to control the diffusion trajectory of a chemical species (Chapters 3-4) as it crosses the metamaterial structure. In this part, we present the use of coordinate transformation techniques to obtain benchmark mass diffusion metamaterials such as cloaks and concentrators. We explore the design space for these metamaterial devices and establish a proper effective medium framework allowing the realization of mass diffusion metamaterials. In the second part of this thesis, we extend our findings to the design of metamaterial devices that can simultaneously control the flux trajectory of two arbitrary chemical species (Chapters 5-6). We show that these novel metamaterial devices can sort chemical species by directing molecules toward different spatial places. Finally, in the

third part of this thesis, we study the use of tailored anisotropic materials (metamaterials) in the context of membrane-based gas separations (Chapters 7-10). We show how anisotropic metamaterial membranes operate differently from typical isotropic membranes. Specifically, our anisotropic metamaterial membranes generally create two permeate fractions. We also show how the use of anisotropic materials can significantly increase the selectivity in membrane separation processes. Such increase in selectivity however occurs at the expense of reducing the collection area on the permeate site. The design, use, and characterization of anisotropic metamaterial membranes in the context of membrane separations is a new research area that provides novel opportunities to devise alternative separation processes and to reconceive well-established classical processes.

CHAPTER 1: INTRODUCTION

1.1 Flux control in mass diffusion processes

Understanding and controlling mass transfer in engineered materials and devices is crucial for improved efficiencies in numerous modern technologies, and specifically in the field of chemical engineering. Mass diffusion is a determinant factor in catalytic reactions[1], chemical separations[2], drug delivery[3] and environmental pollution[4]. The large number of different research areas involving mass transfer illustrates how gaining a deeper understanding of the physical principles behind diffusive transport can have an impact in the development of a broad range of technologies. The ultimate goal from an engineering perspective is to be able to design materials and devices where the transport coefficients are arbitrarily manipulated to enable specific functionalities for mass transfer. Over the last decades, a significant amount of work has focused on manipulating mass transfer resulting in the advent of novel materials with extreme and diverse transport properties. An example of these efforts is the vast amount of work devoted to chemically tune the mass diffusion coefficients of various molecules (e.g. O_2, N_2, CO_2, H_2 and CH_4) in polymeric materials and molecular sieves[5–8].

To date, most strategies employed in the design of mass diffusion materials have been based on controlling the magnitude of mass fluxes. In other words, most proposed approaches make use of isotropic materials in which the mass diffusivity $D_{(i)}$ is a scalar quantity. The use of isotropic materials has been extremely successful in controlling mass transfer rates but these materials are limited in the sense that mass diffusivities are in general tensors (not scalars) and resultant fluxes are not necessarily parallel to the driving

force. Mathematically, the relation between the resulting flux and a concentration driving force can be described in many situations by the tensorial Fick's law equation (Eq. (1.1))[9,10]

$$J_{(i)} = -\overline{\overline{D}}_{(i)} \nabla C_{(i)} \tag{1.1}$$

where $J_{(i)}$ is the molar flux, $\overline{\overline{D}}_{(i)}$ the mass diffusivity tensor, and $C_{(i)}$ the concentration of the species *i*. Note that by considering anisotropic materials, in which mass diffusivities are tensors, it is possible to tune not only the magnitude, but also the direction of the fluxes. Anisotropic materials can thus have as strong impact in the development of materials and devices that can "guide" mass transfer to specific locations. Achieving a directional control over mass transfer requires the development of new approaches to design anisotropic materials where the transport coefficient $\overline{\overline{D}}_{(i)}$ can be manipulated such that specific trajectories for the flux can be established. In addition, the relationship between desired trajectories for mass flux and the anisotropic material properties that would create such trajectories needs to be established. Since the resultant anisotropic materials may have spatially dependent transport coefficients, there is also a need for experimental methods to fabricate these engineered materials for mass diffusion. Toward this end, theoretical approaches based on coordinate transformations and metamaterial theory have recently been introduced to provide strategies to find the anisotropic material properties required to generate specific flux trajectories[11–13]. The field of heat and mass diffusion metamaterials has been mainly focused on heat transport and it has recently provided novel devices with various functionalities such as heat shielding, focusing, and flux rotation[14–17]. Significantly, the design of metamaterials for controlling mass diffusion has been scarcely attempted[16,18–20].

1.2 Tailoring diffusion in membrane based gas separations: current status and opportunities[1]

One particular area in which material science innovations in the field of mass diffusion may have a significant impact is in the design of separation processes. Specifically, in the design of novel materials for membrane separations. Separations in the chemical industry are responsible for 10-15% of the total world energy consumption and the emission of more than 100 million tons of CO_2 per year in the U.S.[21,22]. This high energy demand is due to the predominance of energy-intensive separation processes such as distillation and drying which require a phase change. A more efficient alternative for separations is the use of membranes where the energy demand can be an order of magnitude lower than distillation[21,22]. A sub-set of particularly challenging membrane processes is gas separations. In many cases, the sizes of gas molecules are very similar and materials that separate gas molecules should be able to sort chemical species despite their size similarity[6,7,23]. Gas separations are relevant in a number of industries, and applications range from specialized uses of inert gases in the microelectronic industry to natural gas sweeting in fuel and gas industries[23,24]. From an energetic perspective the use of membranes in gas separations would represent an enormous advance in terms of energy sustainability, provided that the most common technology used in this kind of separations is cryogenic distillation[7,8,23].

The ability of membranes to selectively permeate gases has been studied for more than a century. However, the use of membranes in commercial applications has started nearly forty years ago[8,25,26]. The gradual advancement from scientific discovery to fully

[1] Portions of this chapter have been published in: "Restrepo-Flórez, J.M.; Maldovan, M.; Anisotropic membranes for gas separations. *AIChE journal.* ***2019***"

developed technologies can be partially explained by the lack of materials and fabrication processes that can produce membranes with large efficiencies[8,26]. Despite the success of membranes in the separation of gas mixtures such as N_2/O_2, CO_2/CH_4, H_2/CO, and N_2/Ar, widespread use of membranes is still far from reaching several important systems such as CO_2/N_2, CO_2/H_2, and Olefin/paraffin[8,24,25]. Challenges hindering the use of membranes in new separation processes include efficiency, stability, and processability[5,7,8,25,27,28]. In particular, being able to improve membrane efficiency is one of the challenges that has received significant attention in recent years, with several works aimed at designing membrane materials that simultaneously maximize selectivity and permeability[6,7,27–29].

From a material science perspective significant attempts have been made in order to design new materials for gas separations with improved capabilities. New materials such as advanced polymers (Thermally rearranged polymers and Polymers of Intrinsic Microporosity), and metal organic frameworks are good examples of recent efforts to achieve better control of the diffusion process of gases in membranes[6,30]. Additionally, it must also be highlighted the steady increase of techniques for the fabrication of composite materials such as Mixed Matrix Membranes[6,31]. From a physical perspective all these research efforts rely on a fundamental concept about the separation process: membrane separations can be improved by controlling the magnitude of the flux of the molecules diffusing through the system. That is, membrane materials are commonly designed by considering isotropic media for the transport of gases. Separation is thus the result of differences in the flux magnitude of the species of interests. However, as previously stated, mass flux is a vector and it is thus possible to design materials that can control its direction. It is interesting to note that, to date, there is no research work

exploring the possibility of controlling mass flux direction within the membrane as an alternative to enhance the performance of membrane separations. In this context, rationally designed anisotropic metamaterials appear as an ideal platform to explore the possibilities offered by mass flux directional control in membrane-based separations.

1.3 Dissertation outline

The overarching goal in this thesis is to explore the possibilities offered by metamaterials theory to engineer mass diffusion processes, with a special emphasis on mass transport applied to gas separations. Around this central theme, the work contained in this dissertation can be divided into four main sections:

- First, in Chapter 2 we present the theoretical foundations behind metamaterials theory for mass diffusion. We also discuss some fundamental concepts related with membrane based gas separations and briefly explain the numerical approach used to solve the problems arising through this dissertation.
- Second, in Chapters 3 and 4 we study coordinate transformation techniques in the field of mass diffusion and establish an adequate effective medium approach for the design of benchmark mass diffusion metamaterials (cloaks and concentrators). The work in these chapters focuses on controlling the diffusion trajectory of a chemical species *i*. We developed a complete framework allowing to find the metamaterial properties required to achieve a specific and desired mass flux trajectory.
- Third, in Chapters 5 and 6, we study the design of metamaterials that simultaneously control the diffusion of two arbitrary chemical species *A* and *B*. These metamaterials have been tailored such that each diffusing species is directed toward a different place

thus paving the way for the design of systems that can achieve separations based on flux directional control.

- Finally, in Chapters 7-10 we apply the metamaterial concepts developed in previous chapters for the design of anisotropic membrane materials for gas separations. In these novel materials separation occurs due to control of both flux direction and flux magnitude. Importantly, we establish the relations between different structural variables and the performance of the system, and we also present practical examples associated with relevant gas separations.

1.4 References

(1) Davis, E. M.; Davis, R. J. *Fundamentals of Chemical Reaction Engineering*, 1st Ed.; McGraw-Hill: New York, 2003.

(2) Seader, J. D.; Henley, E. J.; Roper, D. K. *Separation Process Principles-Chemical and Biochemical Operations*, 3rd Ed.; John Wiley & Sons, Inc.: United States of America, 2011.

(3) Saltzman, W. M. *Drug Delivery: Engineering Principles for Drug Therapy*, 1st Ed.; Oxford University Press: New York, 2001.

(4) Brun, A.; Engesgaard, P. Modelling of Transport and Biogeochemical Processes in Pollution Plumes: Literature Review and Model Development. *J. Hydrol.* **2002**, *256* (3–4), 211–227.

(5) Koros, W. J.; Coleman, M. R.; Walker, D. R. B. Controlled Permeability Polymer Membranes. *Annu. Rev. Mater. Sci.* **1992**, *22*, 47–89.

(6) Koros, W. J.; Zhang, C. Materials for Next-Generation Molecularly Selective Synthetic Membranes. *Nat. Mater.* **2017**, *16* (3), 289–297.

(7) Jue, M. L.; Lively, R. P. Targeted Gas Separations through Polymer Membrane Functionalization. *React. Funct. Polym.* **2015**, *86*, 40–43.

(8) Baker, R. W.; Low, B. T. Gas Separation Membrane Materials: A Perspective. *Macromolecules* **2014**, *47* (20), 6999–7013.

(9) Fourier, J. *The Analytical Theory of Heat*; Cambridge University Press: London, Cambridge, Leipzig, 1878.

(10) Fick, A. On Liquid Diffusion. *J. Memb. Sci.* **1995**, *100*, 33–38.

(11) Restrepo-Flórez, J. M.; Maldovan, M. Mass Separation by Metamaterials. *Sci. Rep.* **2016**, *6* (2), 21971.

(12) Guenneau, S.; Amra, C.; Veynante, D. Transformation Thermodynamics: Cloaking and Concentrating Heat Flux. *Opt. Express* **2012**, *20* (7), 8207–8218.

(13) Narayana, S.; Sato, Y. Heat Flux Manipulation with Engineered Thermal Materials. *Phys. Rev. Lett.* **2012**, *108* (21), 214303.

(14) Kadic, M.; Bückmann, T.; Schittny, R.; Wegener, M. Metamaterials beyond Electromagnetism. *Reports Prog. Phys.* **2013**, *76* (12), 126501.

(15) Kadic, M.; Bückmann, T.; Schittny, R.; Wegener, M. Experiments on Cloaking in Optics, Thermodynamics and Mechanics. *Philos. Trans. R. Soc. A Math. Phys. Eng. Sci.* **2015**, *373* (2049), 20140357.

(16) Guenneau, S.; Petiteau, D.; Zerrad, M.; Amra, C.; Puvirajesinghe, T. Transformed Fourier and Fick Equations for the Control of Heat and Mass Diffusion. *AIP Adv.* **2015**, *5* (5), 053404.

(17) Bandaru, P. R.; Vemuri, K. P.; Canbazoglu, F. M.; Kapadia, R. S. Layered Thermal Metamaterials for the Directing and Harvesting of Conductive Heat. *AIP Adv.* **2015**, *5* (5), 053403.

(18) Guenneau, S.; Puvirajesinghe, T. M. Fick's Second Law Transformed: One Path to Cloaking in Mass Diffusion. *J. R. Soc. Interface* **2013**, *10* (83), 20130106.

(19) Zeng, L.; Song, R. Controlling Chloride Ions Diffusion in Concrete. *Sci. Rep.* **2013**, *3*, 3359.

(20) Li, Y.; Liu, C.; Bai, Y.; Qiao, L.; Zhou, J. Ultrathin Hydrogen Diffusion Cloak. *Adv. Theory Simulations* **2017**, *1* (1), 1700004.

(21) Sholl, D. S.; Lively, R. P. Seven Chemical Separations to Change the World. *Nature* **2016**, *532* (4), 435–437.

(22) Oak Ridge National Laboratory. *Materials for Separation Technologies: Energy and Emission Reduction Opportunities*; Oak Ridge, 2005.

(23) Baker, R. W. *Membrane Technology and Applications*, 3rd Ed.; John Wiley & Sons, Inc., 2012.

(24) Bernardo, P.; Drioli, E.; Golemme, G. Membrane Gas Separation: A Review/State of the Art. *Ind. Eng. Chem. Res.* **2009**, *48* (10), 4638–4663.

(25) Sanders, D. F.; Smith, Z. P.; Guo, R.; Robeson, L. M.; McGrath, J. E.; Paul, D. R.;

Freeman, B. D. Energy-Efficient Polymeric Gas Separation Membranes for a Sustainable Future: A Review. *Polymer.* **2013**, *54* (18), 4729–4761.

(26) Baker, R. W. Future Directions of Membrane Gas Separation Technology. *Ind. Eng. Chem. Res.* **2002**, *41* (6), 1393–1411.

(27) Robeson, L. M. The Upper Bound Revisited. *J. Memb. Sci.* **2008**, *320* (1–2), 390–400.

(28) Koros, W. J.; Fleming, G. K. Membrane-Based Gas Separation. *J. Memb. Sci.* **1993**, *83*, 1–80.

(29) Robeson, L. M. Correlation of Separation Factor versus Permeability for Polymeric Membranes. *J. Memb. Sci.* **1991**, *62* (2), 165–185.

(30) Bezzu, C. G.; Carta, M.; Tonkins, A.; Jansen, J. C.; Bernardo, P.; Bazzarelli, F.; Mckeown, N. B. A Spirobifluorene-Based Polymer of Intrinsic Microporosity with Improved Performance for Gas Separation. *Adv. Mater.* **2012**, *24* (44), 5930–5933.

(31) Zimmerman, C. M.; Singh, A.; Koros, W. J. Tailoring Mixed Matrix Composite Membranes for Gas Separations. *J. Memb. Sci.* **1997**, *137* (1–2), 145–154.

CHAPTER 2: THEORY AND BACKGROUND

This chapter has been written with the goal of presenting fundamental concepts associated with this dissertation. Structurally it is divided into three main sections: in the first section (section 2.1) metamaterials theory for mass diffusion is summarized; in the second section (section 2.2) the theoretical background associated with membrane based gas separations is presented; and in the third section (section 2.3) the numerical methods used throughout this dissertation are briefly discussed.

2.1 Metamaterials

A metamaterial is an artificially structured composite that has been engineered to obtain extreme properties (e.g. strong anisotropy) typically not found in nature[1]. Metamaterials properties arise from the arrangement of building blocks in a particular spatial configuration within the composite, meaning that the observed properties of the structure are not directly the result of the chemistry of the system but rather of its particular architecture. Importantly the building blocks are made of common materials thus explaining the prefix *meta* which is used to indicate that the resulting composite has properties beyond those of its constituents. Most commonly, metamaterials have been used in the field of electromagnetism where metamaterial theory has gained prominence since 2006[2]. In this year John Pendry working at the Imperial College in London proved that unprecedented functionalities such as electromagnetic invisibility were theoretically achievable by using metamaterials[2,3]. Motivated by this initial success, scientists from other disciplines interested in controlling the propagation of different physical fields, such as acoustic[4], thermal[5,6], and mass diffusion[7], have extended metamaterials theory to

these non-conventional areas with significant success and a growing body of literature[8–12]. In the field of heat transport, the first attempts to design metamaterials to control the diffusion of heat were performed at Fudan University by the group of Jiping Huang[13]. After this initial proof-of-concept, the interest in thermal metamaterials increased significantly after 2012, when the group of Sebastién Guenneau at Aix Marseille University presented a detailed theoretical analysis of heat transport in metamaterials discussing the design of thermal cloaks and concentrators[5]. This theoretical work subsequently motivated experimental studies by the groups of Yuki Sato at Harvard University[6] and Martin Wegener at KIT[14]. In the case of mass diffusion metamaterials, a seminal contribution was introduced by Guenneau's group in 2013 where a detailed analysis of Fick's law was presented in the context of mass diffusion metamaterials theory[7]. Theoretical approaches describing anisotropic diffusion have been known for a long time both in the case of heat[15] and mass transport[16,17]. What is new in metamaterial design is the possibility of tailoring the structure anisotropy to achieve precise control of the mass flux trajectory; in other words, in metamaterials theory anisotropy becomes a degree of freedom that can be engineered to guide flux.

From a general perspective, the metamaterial design process requires first the calculation of the structure properties that will create a particular functionality. This functionality is determined by the specific trajectory that the flux lines will follow. To obtain such structure properties, there exist three different approaches: coordinate transformations[5,11], topology optimization[18] or heuristic design[19], being coordinate transformations the dominant approach in the literature. For transport processes such as heat and mass diffusion, it is often found that these structure properties are non-

homogeneous, anisotropic, and in some cases singular (i.e. they become infinity at specific locations inside the domain of interest). Therefore, the prescribed properties are difficult to be satisfied by naturally occurring materials. For this reason, the design process in metamaterials requires a second stage in which effective medium theory is used to obtain a structured composite made of homogeneous isotropic materials whose effective structural properties resemble those calculated in the first stage, thus allowing the experimental realization of the metamaterial and the desired functionality.

2.1.1 Coordinate transformations

Coordinate transformation is a mathematical technique that allows designing metamaterial devices with specific functions[2]. This technique has been widely used in the design of optical devices such as invisibility cloaks[2], superlenses [20], and field rotators[1,21]. In order to exploit its advantages, the equations governing the physical phenomena of interest must be invariant under coordinate transformations[2]. For example, in the case of heat conduction, if the Fourier equation is transformed under an arbitrary coordinate transformation $\mathbf{x}=(x,y,z) \rightarrow \mathbf{x'}=(x',y',z')$

$$\rho_{bg} C_{pbg} \frac{\partial T}{\partial t} = -\nabla \cdot \kappa_{bg} \nabla T \quad \xrightarrow{Transformation} \quad \rho' C_p' \frac{\partial T}{\partial t} = -\nabla' \cdot \bar{\bar{\kappa}}' \nabla' T \tag{2.1}$$

the equation remains invariant after the transformation is applied (Eq. (2.1), right) provided that the density ρ_{bg}, heat capacity C_{pbg}, and thermal conductivity κ_{bg} of the background medium where the transformation is applied are transformed as

$$\rho' C_p' = \frac{\rho_{bg} C_{pbg}}{det(\bar{\bar{J}})}; \quad \bar{\bar{\kappa}}' = \frac{\bar{\bar{J}} \kappa_{bg} \bar{\bar{J}}^T}{det(\bar{\bar{J}})} \tag{2.2}$$

where $\bar{\bar{J}}$ is the Jacobian matrix of the transformation[5].

Analogously, in the case of mass diffusion, if the Fick's equation is transformed under an arbitrary coordinate transformation $\mathbf{x}=(x,y,z) \rightarrow \mathbf{x'}=(x',y',z')$

$$\frac{\partial C_{(i)}}{\partial t} = -\nabla \cdot D_{bg(i)} \nabla C_{(i)} \quad \xrightarrow{Transformation} \quad \frac{1}{\det(\bar{\bar{J}})} \frac{\partial C_{(i)}}{\partial t} = -\nabla' \cdot \bar{\bar{D}}'_{(i)} \nabla' C_{(i)} \qquad (2.3)$$

the equation remains invariant at steady state provided that $D_{bg(i)}$ is transformed as

$$\bar{\bar{D}}'_{(i)} = \frac{\bar{\bar{J}} D_{bg(i)} \bar{\bar{J}}^T}{det\,(\bar{\bar{J}})} \qquad (2.4)$$

or in transient if the determinant of $\bar{\bar{J}}$ is equal to one [7,22].

To understand how these mathematical concepts can be applied to engineer devices with specific functions, we introduce a graphical description of the transformation process (Figure 2.1). We characterize the spatial geometry of the medium where the transformation is applied by plotting the isoconcentration or isothermal lines as well as the flux lines (Figure 2.1(a)). We consider that the original space is filled with an isotropic material where the flux lines follow a linear trajectory in the direction of the gradient (*x*-direction). In this representation, if the lines are considered as being "elastic", applying a transformation is equivalent to stretching these lines to accommodate a desired flux trajectory (Figure 2.1(b)). Note that by applying a transformation, the original space is transformed into a curved space in which the flux lines follow a different trajectory. Importantly, the original (Figure 2.1(a)) and transformed (Figure 2.1(b)) spaces are connected in such a way that the transformed (curved) space can be reproduced in the original (real) space by an anisotropic material whose properties are given by $\bar{\bar{\kappa}}'$ and $\bar{\bar{D}}'_{(i)}$ (Eqs (2.2) and (2.4))[8]. In other words, the trajectory of a flux line in the curved space can be achieved in real space by using a tailored anisotropic material. If a certain

functionality requires a flux trajectory that can be described by a transformation $f \rightarrow f'$, a metamaterial whose properties are given by Eqs (2.2) and (2.4) would yield that functionality.

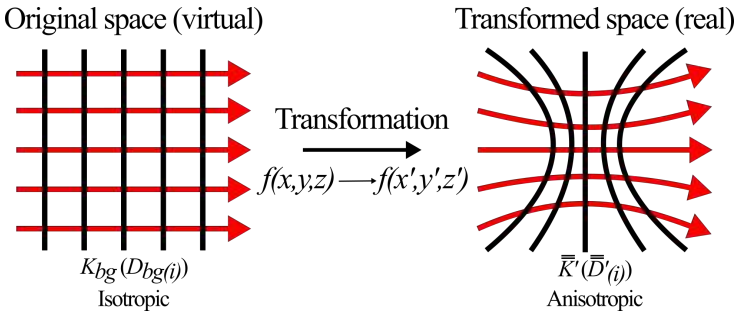

Figure 2.1. Schematic representation of the coordinate transformation process. Red lines represent flux trajectories while black lines represent isotherms (or isoconcentrations).

Among the infinite number of coordinate transformations that will create curved spaces, there are four basic transformations commonly used to tune the trajectory of a flux line. These are rotation, translation, compression and expansion, and the corresponding transformed curved spaces are shown in Figure 2.2[23]. Note that these transformations can be applied individually or simultaneously to attain a particular functionality. In many cases, the transformations can be represented analytically allowing a direct calculation of the transformed property tensors $\bar{\bar{\kappa}}'$ and $\bar{\bar{D}}'_{(i)}$ [5,11,24–26]. If the required flux path is more complex or if the geometry of the region in which flux control is to be attained is irregular, an analytical representation is difficult and numerical approaches based on a grid generation equation or domain discretization can be used to calculate the required anisotropic properties[27–31]. For simplicity sake, most transformation functions are linear with respect to the spatial coordinates and can be written as $x'_j = \sum_{j=1}^{3} a_j x_j$,

where a_j are constants coefficients, x_j' are the coordinates in the transformed space, and x_j are the coordinates in the original space. We note that although linear transformations are commonly used, non-linear dependences have also been considered[32–34]. Non-linear transformations allow for broader changes in the spatial dependence of the transformed space[33,34]. In addition, the transformation functions can be considered to be dependent on temperature T (heat transport) or concentration $C_{(i)}$ (mass diffusion)[35–39] allowing for the design of "adaptive devices" that respond differently to changes in the environment[40]. A general expression for the metamaterial thermal conductivity $\bar{\bar{\kappa}}'$ and mass diffusivity $\bar{\bar{D}}'_{(i)}$ tensors resulting from coordinate transformations that depend on spatial non-linearities, temperature T or concentration $C_{(i)}$, and time t can be written as

$$\bar{\bar{\kappa}}' = \frac{\bar{\bar{J}}[f(\bar{x}(T,t))]\kappa_{bg}\,\bar{\bar{J}}[f(\bar{x}(T,t))]^T}{det\left(\bar{\bar{J}}[f(\bar{x}(T,t))]\right)}\ \bar{\bar{D}}'_{(i)} = \frac{\bar{\bar{J}}\left(f(\bar{x}(C_i,t))\right) D_{bg(i)}\,\bar{\bar{J}}\left(f\left((\bar{x}(C_i,t))\right)\right)^T}{det\left(\bar{\bar{J}}\left(f(\bar{x}(C_i,t))\right)\right)} \tag{2.5}$$

these generalized equations constitute the basis to perform non-linear, temperature or concentration, and time-dependent coordinate transformations.

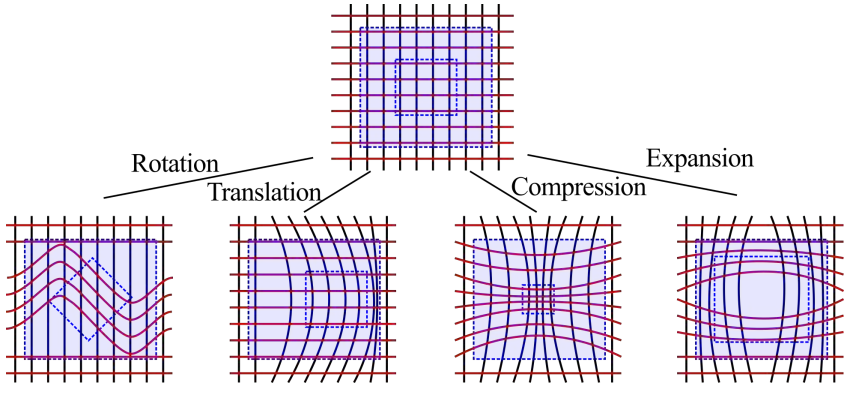

Figure 2.2. Schematic representation of four possible coordinate transformations: rotation, translation, compression and expansion.

2.1.1.1 Metamaterial Functionalities

The number of possible trajectories for heat or mass diffusion is infinite and only constrained by the second law of thermodynamics. This means that the number of conceivable metamaterial devices is also infinite. There are however some benchmark devices with specific capabilities which are of particular interest. In this section, we briefly introduce three of these benchmark devices which are of significant relevance for this thesis (Figure 2.3): cloaks (Chapters 4,5,7 and 8), concentrators (Chapters 3,4,5,7 and 8) and beam shifters (Chapters 6 and 10).

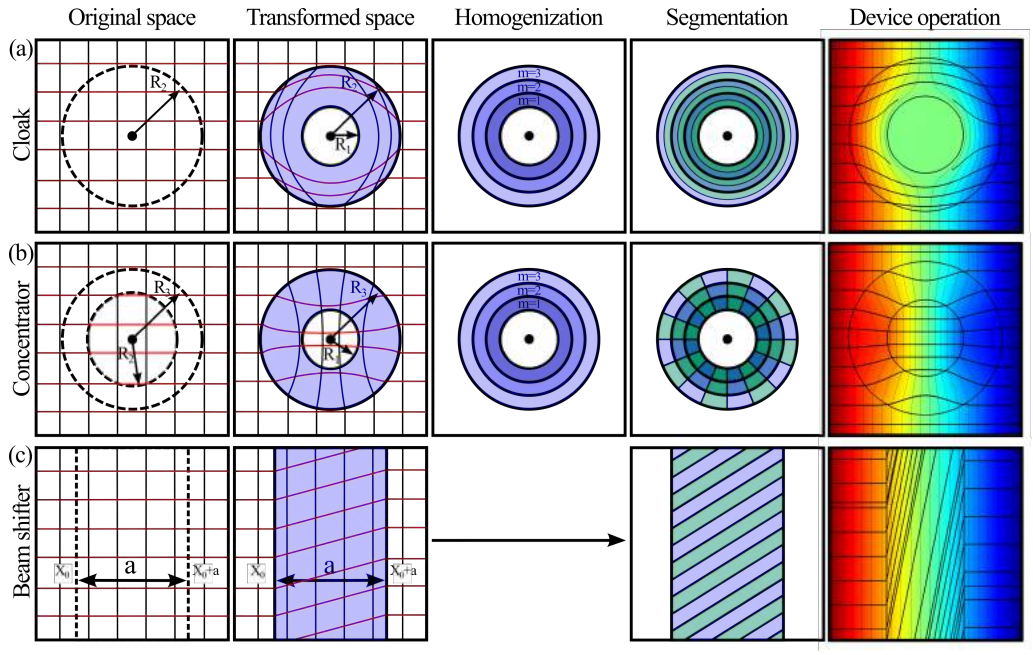

Figure 2.3. Coordinate transformation process for several different metamaterials with geometries in two-dimensions. First column: Original space with dashed lines indicating the space to be transformed. Second column: Metamaterial structure (light blue) as well as the effect of the coordinate transformation on the isoconcentration (isothermal) lines (black) and flux lines (red). Third column: Homogenization strategy to obtain the anisotropic metamaterial structure. Forth column: Effective medium arrangement of isotropic materials that reproduce the required anisotropicity. Fifth column: Concentration (temperature) profiles. (a) Cloak, (b) concentrator, (c) beam shifter. Left boundaries are at high concentration and right boundaries at low concentration. In figure (c) periodic conditions are considered at the upper and lower boundaries.

Cloaks: In metamaterial's literature, cloaks are the devices to which more attention has been devoted. This is in part due to the fact that in electromagnetism, cloaking devices provide the possibility of rendering objects invisible, and as a consequence cloaks have received especial attention both from scientists and the general public[2]. In the context of heat and mass diffusion, a cloak can be described as a metamaterial that prevents the penetration of mass (or heat) into a core area due to the rerouting of the flux lines around it[5,7,11]. In other words, a cloak acts as a shield, creating a core region of nearly constant temperature or concentration[5,41–43] (Figure 2.3(a)). In addition, when the cloak is embedded in a background medium, it does not disturb the external field. This means that, the isoconcentration or isothermal lines in the background medium in which the cloak is embedded are unaltered as if the metamaterial device was not present.

The most common approach to design cloaks is to consider a coordinate transformation that maps a point in the original space into an annulus in the transformed space (Figure 2.3(a)). One can consider that the original space is compressed within the annular region and a hole thus appears at the center. Note that the transformation maintains unaltered the region outside the original circular area. If we associate the geometry of the transformed space with the isothermal and flux lines distribution in the real space, this transformation results in the exclusion of the flux lines from the core region (i.e. the hole)[8] thus creating a mass or heat shielding device. Mathematically the coordinate transformation that creates a 2D cylindrical cloak is given by Eq. (2.6). Note that in this equation, the center point in the original space (i.e. $r = 0$) is transformed into a circular boundary in the transformed space (i.e. $r'(0) = R_1$)

$$r' = \frac{(R_2 - R_1)}{R_2} r + R_1; \quad \theta' = \theta \tag{2.6}$$

Using the transformation given by Eq. 2.6 and the metamaterial properties $\bar{\bar{\kappa}}'$and $\bar{\bar{D}}'_{(i)}$ (Eqs (2.2) and (2.4)) it is possible to determine the properties of the metamaterial structure that would yield a mass diffusion or thermal cloak

$$\frac{\bar{\bar{D}}'_{(i)}}{D_{bg(i)}} = \begin{bmatrix} \frac{D_{r(i)}}{D_{bg(i)}} & 0 \\ 0 & \frac{D_{\theta(i)}}{D_{bg(i)}} \end{bmatrix} = \frac{\bar{\bar{k}}'}{\kappa_{bg}} = \begin{bmatrix} \frac{k_r}{\kappa_{bg}} & 0 \\ 0 & \frac{k_\theta}{\kappa_{bg}} \end{bmatrix} = A; \quad A = \begin{bmatrix} \frac{r'-R_1}{r'} & 0 \\ 0 & \frac{r'}{r'-R_1} \end{bmatrix} \tag{2.7}$$

The ability of the cloak to detour mass or heat flux around the core is explained by noting that in Eqs (2.7) the radial diffusivity $D_{r(i)}$ (or conductivity κ_r) is always smaller than the azimuthal component, ensuring a preferential transport along the azimuthal direction and not towards the core[41,42]. The experimental realization of metamaterial cloaks can be achieved by using effective medium theory (for a detailed treatment see chapter 4). It can be shown that a multilayer composite consisting of a set of concentric rings made of different and alternating materials *A* and *B* behaves anisotropically with azimuthal preferential transport (Figure 2.3(a)) and thus provides a material platform for achieving mass diffusion cloaks. The anisotropy of the composite is explained by realizing that in the radial direction the resistances for diffusion are arranged in series, while in the azimuthal direction they are arranged in parallel.

Concentrators*:* A concentrator is a metamaterial whose main functionality consists in focusing flux lines toward a region in space (the core)[5,6]. When the device is designed using transformation techniques it has the additional property of been mass-diffusion/thermally "invisible" as well[5,44]. The redirecting of the flux lines towards the core region can be observed as a displacement of the isothermal/ isoconcentration lines in

the direction of the core and an increase in their density, thus causing an increment in the concentration (thermal) gradient in the core region in comparison with the external gradient (this is the reason for these devices to be called concentrators)[44,45] (Figure 2.3(b)).

Mathematically, we consider a mass diffusion concentrator in a circular geometry in two-dimensions. The coordinate transformation in this case ($r \to r'$) can be represented as a process in which the annular region $R_2 \le r \le R_3$ is stretched to a final state in which $R_1 \le r' \le R_3$ with $R_1 < R_2$ (Figure 2.3(b)). The coordinate transformation process can be represented as two simultaneous operations (Eq. (2.8)): the compression of the central region ($r \le R_2$) and the expansion of the adjacent area ($R_2 \le r \le R_3$) such that no empty space is left within the structure[5,41,44,45]. The required metamaterial properties are given by Eqs (2.9).

$$r' = \frac{R_1}{R_2} r \ (r \le R_1), \qquad r' = \left(\frac{R_3 - R_1}{R_3 - R_2}\right) r + R_3 \left(\frac{R_1 - R_2}{R_3 - R_2}\right) \ (R_1 \le r \le R_2) \tag{2.8}$$

$$\frac{\bar{\bar{D}}'_{(i)}}{D_{bg(i)}}\left(\frac{\bar{\bar{k}}'}{k_{bg}}\right) = \begin{bmatrix} \dfrac{r' - R_3\left(\frac{R_1 - R_2}{R_3 - R_2}\right)}{r'} & 0 \\ 0 & \dfrac{r'}{r' - R_3\left(\frac{R_1 - R_2}{R_3 - R_2}\right)} \end{bmatrix} (R_1 \le r \le R_2); \frac{\bar{\bar{D}}'_{(i)}}{D_{bg(i)}}\left(\frac{\bar{\bar{k}}'}{k_{bg}}\right) = 1 \ (r \le R_1) \tag{2.9}$$

In terms of experimental realization, two important characteristics of these equations must be highlighted: first, opposite to cloaks, the radial diffusivity (conductivity) is larger than the azimuthal diffusivity, therefore the radial direction is the preferred direction for diffusion[5]. Second, unlike cloaks, the properties of the material at the core are relevant to the metamaterial structural properties[6]. Note that if a material with different properties from those prescribed by Eq. (2.9) is placed at $r \le R_1$ then the "invisibility" functionality will be lost but the structure will still detour mass flux toward

the core. In general, a two-dimensional cylindrical concentrator can be realized experimentally by using a lamellar arrangement of isotropic materials *A* and *B* (Figure 2.3(b)). This layered geometry ensures a parallel connection between materials in the radial direction, while a series connection in the azimuthal direction; thus assuring that the radial direction is the preferred direction for diffusion[6,46–49].

Beam shifters: A beam shifter is a transformation-based metamaterial in which a flux line, that otherwise would diffuse in a straight path in an isotropic material, changes its trajectory by an angle ϕ[25]. The beam-shifter coordinate transformation is represented by Eq. (2.10) (Figure 2.3(d)), where b is the slope of the detoured flux line and x_0 the x-coordinate denoting the position at which the metamaterial is placed[25,50]. The anisotropic properties of the metamaterial structure associated with this transformation are presented in Eq. (2.11). It is interesting to note that, in this transformation, the components of the diffusivity (conductivity) tensor are constants. It has been proved that the anisotropic characteristics required to obtain beam shifters (Eq. (2.11)) can be provided by rotated multilayer composites (Figure 2.3(d)). Layered materials thus constitute a material platform for the experimental realization of mass diffusion beam-shifters[25,51–53].

$$y' = y + b(x - x_0) \tag{2.10}$$

$$\frac{\bar{\bar{D}}'_{(i)}}{D_{bg(i)}}\left(\frac{\bar{\bar{k}}'}{k_{bg}}\right) = \begin{bmatrix} 1 & b \\ b & b^2 + 1 \end{bmatrix} \tag{2.11}$$

2.1.2 Topology optimization

Topology optimization is a technique that has its origins in structural engineering where it was developed for the design of elements such as bridges and cantilevers[54–56]. The scientific/engineering problem the technique addresses can be formulated as follows:

if two materials (e.g. air and concrete) are to be used to manufacture a structure, which spatial distribution of air and concrete minimizes the amount of concrete used while simultaneously satisfying a required set of constraints imposed by loadings applied to the system[56]. In addition to structure mechanics, topology optimization can also be used for the design of anisotropic composites (metamaterials) that control diffusion processes[18,57–66]. In the case of mass diffusion, the problem can be stated as follows: if a metamaterial structure with a desired functionality is to be made by using a set of isotropic materials, what is the local arrangement of these materials (orientation and composition) yielding an effective non-homogeneous anisotropic conductivity or diffusivity that optimizes the performance in terms of the desired functionality. Mathematically, topology optimization is based on the simultaneous use of optimization techniques and the finite element method to solve the mass diffusion problem and find the required material arrangement and composition[60]. The metamaterial domain is divided into an arbitrary number of cells J using a typical finite element discretization process and the selected optimization algorithm finds the composition in terms of material selection in each of these J cells such that an objective function is maximized or minimized.

2.1.3 Heuristic design

The development of coordinate transformations and topology optimization techniques has enabled the design of several unprecedented metamaterial devices as it has been presented in the previous sections. However, one may still ask whether is possible to design metamaterial structures using only physical intuition about mass diffusion processes and thus avoiding complex mathematical formalisms or numerical complications. The answer to this question is positive, in fact, one can certainly use as a

general design rule that the preferred direction for mass (heat) diffusion is along the path with higher diffusivity (conductivity), that is minimum resistance. However, despite the simplicity of this rule, there are two underlying assumptions constraining its applicability: first, heuristic design can be essentially implemented when a single functionality is required (*e.g.* mass shielding, mass concentration) making it difficult to apply to complex multicomponent mass diffusion functionalities. Second, although heuristic design can be used in functionalities clearly determined by the direction of mass flux, it will also be difficult to apply this method to complex functionalities such as "invisibility".

2.2 Membrane based gas separations[1]

In the context of chemical separations, a membrane is a device that allows the selective permeation of chemical species (Figure 2.4). Depending on the type of material, different mechanisms can be associated with the transport of molecules across the membrane and with the separation process itself[67]. More specifically, membrane materials can be generally divided in two main groups: porous and dense. In porous membranes (microfiltration and ultrafiltration membranes are good examples) transport can be described using a pore-flow model and separation occurs due to size exclusion, i.e. some molecules will be unable to cross the pore[67,68]. On the other hand, in dense membranes, mass transport is described in terms of a solution diffusion process, in which molecules in the phase outside the membrane first dissolve in the membrane and then diffuse across the membrane material in the direction of a chemical potential gradient[67,68]. Separation in these membranes is achieved due to a difference in the permeation rate for

[1] Portions of this section have been published in: "Restrepo-Flórez, J.M.; Maldovan, M.; Anisotropic membranes for gas separations. *AIChE journal.* ***2019***"

different species. In particular, membrane based gas separations are generally performed by using dense membranes.

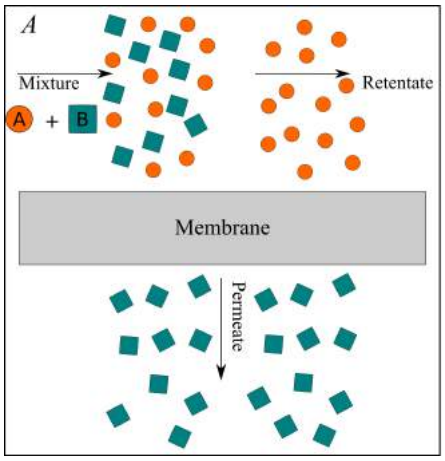

Figure 2.4. Schematic of a typical isotropic membrane for separation of a binary mixture. Ideally, one of the species (Species B) permeates the membrane while the other species (Species A) is rejected.

Mathematically, the modeling of solution-diffusion processes requires the use of theoretical approaches for the two physical processes involved: solution and diffusion[68–70]. In the simplest case scenario, the solution process is modeled using Henry's law (Eq. (2.12)) where $C_{(i)}$ is the concentration of species i in the polymer phase which is in equilibrium with a gas phase with partial pressure $p_{(i)}$. In Eq. 2.12, $\mathcal{H}_{(i)}$ is the Henry's constant, which can be interpreted as the solubility of species i into the polymer[69,70]. On the other hand, mass diffusion processes can be modeled by using Fick's law (Eq. (1.1))[69,70].

$$C_{(i)} = \mathcal{H}_{(i)} p_{(i)} \tag{2.12}$$

$$J_{(i)} = D_{(i)} \nabla C_{(i)} \tag{1.1}$$

Although Henry's and Fick's law offer significant advantages in terms of mathematical treatment of mass diffusion processes, and they are used throughout this dissertation, it is worth mentioning, for completeness, that deviations from this behavior can be observed in real materials. An important example is the case of glassy polymers, which are known for exhibiting dual sorption (Eq. 2.13) and partial immobilization (Eq. (2.14)) [70–72]. Another source of deviation from ideality is multicomponent effects, which are better described by extending Fick's law formulation to [73,74]

$$C_{(i)} = \mathcal{H}_{(i)} p_{(i)} + \frac{C'_{H(i)} b_{l(i)} p_{(i)}}{1 + b_{l(i)} p_{(i)}} \tag{2.13}$$

$$J_{(i)} = -\left(D_{H(i)} \frac{\partial C_{H(i)}}{\partial x} + D_{D(i)} \frac{\partial C_{D(i)}}{\partial x} \right) \tag{2.14}$$

The performance of a membrane material for gas separation is usually characterized in terms of permeability and selectivity[69,75]. Permeability is defined as a normalized flux with respect to the driving force multiplied by the membrane thickness (Eq. (2.15)), while selectivity is defined as the ratio of the permeabilities of two species diffusing throughout the membrane (Eq. (2.16))[76]. In general, the permeability provides a measurement of the ability of a membrane to allow the passage of a given species, and the selectivity characterizes the ability of the membrane to perform a separation. Therefore membrane materials with high permeability and selectivity for the species of interest are desired[75,77]. A useful representation that allows measuring the ability of a membrane material to perform separation is a plot of selectivity vs. permeability of the fast diffusing species (Figure 2.5). This representation is known as a Robeson plot[78,79].

$$P'_{(i)} = \frac{J_{(i)} H}{\Delta p_{(i)}} \tag{2.15}$$

$$\alpha_{A/B} = \frac{P'_{(A)}}{P'_{(B)}} = \frac{J_{(A)}/\Delta P_{(A)}}{J_{(B)}/\Delta P_{(B)}} \tag{2.16}$$

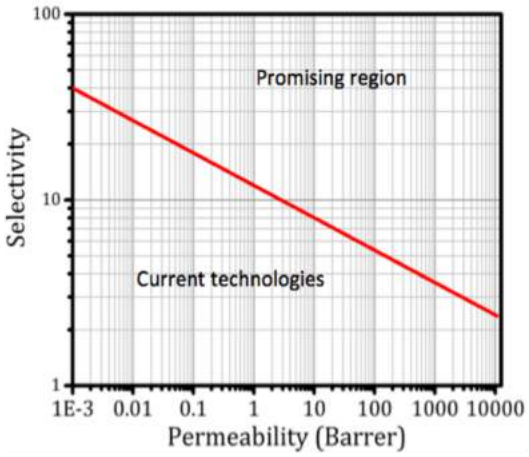

Figure 2.5. Robeson plot of selectivity vs. permeability for separation of an arbitrary mix. The red line represents the upper bound (an experimentally observed limit between selectivity and permeability for polymeric materials).

Theoretical and experimental approaches to design membrane materials for gas separations can be classified into two different "generations". The first generation can be characterized by the use of homogeneous isotropic materials[69,80]. Materials in this group, mainly polymers, have been widely used in gas separation processes due to their ease of fabrication and material availability. Membranes made of homogeneous isotropic materials have spatially-independent scalar diffusion coefficients[68,77]. Depending on their structural properties, homogeneous isotropic membranes for gas separations can be further divided into dense membranes and molecular sieves. Dense membranes are comprised of flexible polymers (rubbery and glassy) or semi-rigid polymers (polymers of intrinsic micro porosity PIM and thermally rearranged polymers)[77]. In polymeric membranes, chemical modifications to the material can result in changes in polymer

backbone mobility, chemical affinity for the different gases, and/or packing efficiency. All these physical properties provide an avenue to manipulate the solubility and diffusivity of the gas species in the polymer. The ultimate goal is to establish the relation between chemical functionalization and the resultant transport properties such that permeabilities can be chemically tuned[69,80]. On the other hand, in molecular sieves such as Zeolites, Metal Organic Frameworks (MOFs) and Carbon Molecular Sieves (CMS), the transport of gases is governed by the size of the nanopores in the sieve. In these nanoporous membranes, chemical functionalization is used to control the nanopore dimensions with the aim of tuning the membrane permeability[77,81–83]. Despite of the wide use of homogeneous isotropic membranes for gas separations, flexible and semi-rigid polymers present limitations in terms of trade-off relations between selectivity and permeability (Figure 2.5), while molecular sieves often require difficult manufacturing processes[75].

The second generation of membranes can be characterized by the use of non-homogeneous materials. These membranes have recently been developed with the aim of partially overcoming the limitations of homogeneous materials[84–86]. In this case, two or more materials are combined to yield an effective isotropic composite with tailored transport properties and separation efficiencies. Ideally, the resultant composite material should have the advantages of its constituents and none of its limitations[75]. In non-homogeneous isotropic membranes, the diffusion coefficient is spatially dependent and effective medium approaches are generally used to predict the effective properties of the membrane[77,84]. One type of non-homogeneous membranes, known as mixed matrix membranes (MMM), consists of molecular sieves dispersed in a polymer matrix (either

flexible or semi-rigid)[77,84]. MMM are expected to have high selectivity and permeability as the molecular sieves can be easily processed as the polymer matrix. In practice however, challenging issues associated with polymer-sieve interactions often limit their performance[84,86,87]. The effective membrane permeability is typically calculated by using Maxwell's effective medium formulation[84].

2.3 Numerical solution of the diffusion equation

In this thesis, in order to characterize the mass diffusion properties of metamaterial structures, we solve the two-dimensional mass diffusion differential equation (or second's Ficks law). We note that in a few cases, analytical solutions using Fourier series expansions can be found (See chapters 7-9); however, in many cases such analytical solutions can not be found and numerical solutions are thus obtained. In this thesis, we have used the finite element software COMSOL Multiphysics® to find solutions to the mass diffusion differential equation both for isotropic and anisotropic systems. In Figure 2.6 we show a sample of the comsol enviroment for a representative metamaterial problem.

The Finite element method rely on the discretization of the original continuous space in a finite number of subdomains. The coarsness of this discretization depends on the selection of a discretization mesh such that a more accurate solutions is obtained as the discretization is refined. In each of these subdomains, an interpolation scheme for the variable of interest (e.g. species concentration) is established. The solution is obtained once the interpolations in all of the subdomains are assembled as a system of algebraic equations. The linearity of the system of equations depends on the interpolation scheme.

Corresponding boundary conditions are implemented during the numerical process allowing to find a solution to mass diffusion in anisotropic metamaterial structures.

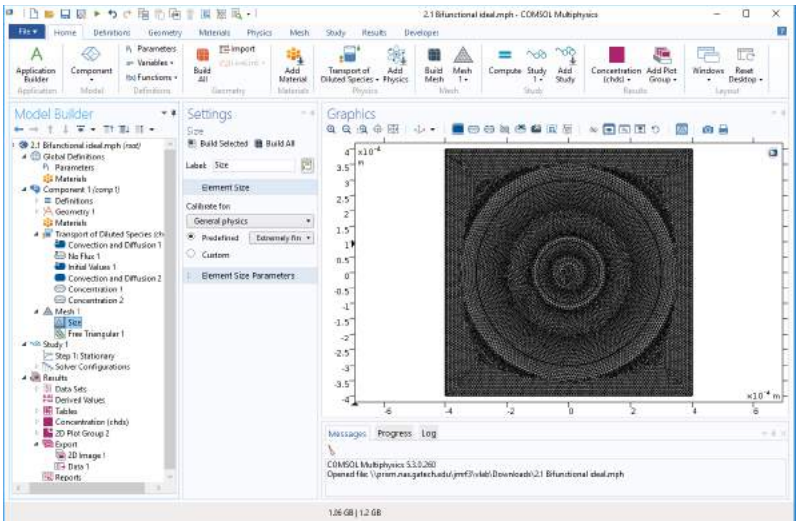

Figure 2.6. Comsol multiphysics® environment for the solution of mass diffusion problems

2.4 References

(1) Chen, H.; Chan, C. T.; Sheng, P. Transformation Optics and Metamaterials. *Nat. Mater.* **2010**, *9* (5), 387–396.

(2) Pendry, J. B.; Schurig, D.; Smith, D. R. Controlling Electromagnetic Fields. *Science.* **2006**, *312* (5781), 1780–1782.

(3) Schurig, D.; Mock, J. J.; Justice, B. J.; Cummer, S. a; Pendry, J. B.; Starr, a F.; Smith, D. R. Metamaterial Electromagnetic Cloak at Microwave Frequencies. *Science.* **2006**, *314* (5801), 977–980.

(4) Cummer, S. A.; Schurig, D. One Path to Acoustic Cloaking. *New J. Phys.* **2007**, *9*, 45.

(5) Guenneau, S.; Amra, C.; Veynante, D. Transformation Thermodynamics: Cloaking and Concentrating Heat Flux. *Opt. Express* **2012**, *20* (7), 8207–8218.

(6) Narayana, S.; Sato, Y. Heat Flux Manipulation with Engineered Thermal Materials. *Phys. Rev. Lett.* **2012**, *108* (21), 214303.

(7) Guenneau, S.; Puvirajesinghe, T. M. Fick's Second Law Transformed: One Path to

Cloaking in Mass Diffusion. *J. R. Soc. Interface* **2013**, *10* (83), 20130106.

(8) Kadic, M.; Bückmann, T.; Schittny, R.; Wegener, M. Metamaterials beyond Electromagnetism. *Reports Prog. Phys.* **2013**, *76* (12), 126501.

(9) Raza, M.; Liu, Y.; Lee, E. H.; Ma, Y. Transformation Thermodynamics and Heat Cloaking: A Review. *J. Opt.* **2016**, *18* (4), 044002.

(10) Han, T.; Qiu, C.-W. Transformation Laplacian Metamaterials: Recent Advances in Manipulating Thermal and Dc Fields. *J. Opt.* **2016**, *18* (4), 044003.

(11) Guenneau, S.; Petiteau, D.; Zerrad, M.; Amra, C.; Puvirajesinghe, T. Transformed Fourier and Fick Equations for the Control of Heat and Mass Diffusion. *AIP Adv.* **2015**, *5* (5), 053404.

(12) Bandaru, P. R.; Vemuri, K. P.; Canbazoglu, F. M.; Kapadia, R. S. Layered Thermal Metamaterials for the Directing and Harvesting of Conductive Heat. *AIP Adv.* **2015**, *5* (5), 053403.

(13) Fan, C. Z.; Gao, Y.; Huang, J. Shaped Graded Materials with an Apparent Negative Thermal Conductivity. *Appl. Phys. Lett.* **2008**, *92* (25), 251907.

(14) Schittny, R.; Kadic, M.; Guenneau, S.; Wegener, M. Experiments on Transformation Thermodynamics: Molding the Flow of Heat. *Phys. Rev. Lett.* **2013**, *110* (19), 195901.

(15) Domenicali, C. A. Irreversible Thermodynamics of Thermoelectric Effects in Inhomogeneous, Anisotropic Media. *Phys. Rev.* **1953**, *92* (4), 877–881.

(16) Sax, J.; Ottino, J. M. Modeling of Transport of Small Molecules in Polymer Blends: Application of Effective Medium Theory. *Polym. Eng. Sci.* **1983**, *23* (1 l), 165–176.

(17) Shah, N.; Sax, J. E.; Ottino, J. M. Influence of Morphology on the Transport Properties of Polystyrene/Polybutadiene Blends: 2. Modelling Results. *Polymer.* **1985**, *26* (8), 1239–1246.

(18) Dede, E. M.; Nomura, T.; Lee, J. Thermal-Composite Design Optimization for Heat Flux Shielding, Focusing, and Reversal. *Struct. Multidiscip. Optim.* **2014**, *49* (1), 59–68.

(19) Narayana, S.; Savo, S.; Sato, Y. Transient Heat Flux Shielding Using Thermal Metamaterials. *Appl. Phys. Lett.* **2013**, *102* (20), 201904.

(20) Pendry, J. B. Negative Refraction Makes a Perfect Lens. *Phys. Rev. Lett.* **2000**, *85* (18), 3996–3969.

(21) Chen, H.; Chan, C. T. Transformation Media That Rotate Electromagnetic Fields.

Appl. Phys. Lett. **2007**, *90* (24), 241105.

(22) Schittny, R.; Niemeyer, A.; Kadic, M.; Bückmann, T.; Naber, A.; Wegener, M. Transient Behavior of Invisibility Cloaks for Diffusive Light Propagation: Supplementary Material. *Optica* **2015**, *2* (2), 84–87.

(23) Shen, X.; Jiang, C.; Li, Y.; Huang, J. Thermal Metamaterial for Convergent Transfer of Conductive Heat with High Efficiency. *Appl. Phys. Lett.* **2016**, *109*, 201906.

(24) Guenneau, S.; Amra, C. Anisotropic Conductivity Rotates Heat Fluxes in Transient Regimes. *Opt. Express* **2013**, *21* (5), 6587.

(25) Restrepo-Flórez, J.-M.; Maldovan, M. Metamaterial Membranes. *J. Phys. D. Appl. Phys.* **2017**, *50*, 25104.

(26) Hou, Q.; Zhao, X.; Meng, T.; Liu, C. Illusion Thermal Device Based on Material with Constant Anisotropic Thermal Conductivity for Location Camouflage. *Appl. Phys. Lett.* **2016**, *109* (10).

(27) Chang, Z.; Liu, X.; Hu, G. Heat Flow Control by Transformation Method with Grid Generation Method. *Acta Mech. Solida Sin.* **2014**, *27* (5), 454–460.

(28) Park, G.; Kang, S.; Lee, H.; Choi, W. Tunable Multifunctional Thermal Metamaterials: Manipulation of Local Heat Flux via Assembly of Unit-Cell Thermal Shifters. *Sci. Rep.* **2017**, *7* (January), 41000.

(29) Athanasopoulos, N.; Siakavellas, N. J. Heat Flux Manipulation Using Highly Anisotropic Pitch-Based Carbon Fiber Composites. *Adv. Eng. Mater.* **2015**, *17* (10), 1494–1503.

(30) Vemuri, K. P.; Canbazoglu, F. M.; Diego, S.; Jolla, L. Guiding Conductive Heat Flux through Thermal Metamaterials-Supplementary Information. *Appl. Phys. Lett.* **2014**, *115* (19), 193904.

(31) Liu, D.-P.; Chen, P.-J.; Huang, H.-H. Realization of a Thermal Cloak–Concentrator Using a Metamaterial Transformer. *Sci. Rep.* **2018**, *8* (1), 2493.

(32) Petiteau, D.; Guenneau, S.; Bellieud, M.; Zerrad, M.; Amra, C. Spectral Effectiveness of Engineered Thermal Cloaks in the Frequency Regime. *Sci. Rep.* **2014**, *4* (December), 7386.

(33) Ooi, E. H.; Popov, V. Transformation Thermodynamics for Heat Flux Management Based on Segmented Thermal Cloaks. *Eur. Phys. J. Appl. Phys.* **2013**, *63* (1), 10903.

(34) Yuan, X. B.; Lin, G. C.; Wang, Y. S. Influence of Nonlinear Coordinate Transformation on Thermal Cloaking Performances of Multilayered Cylindrical

Thermal Cloaks. *AIP Adv.* **2016**, *6* (4), 045013.

(35) Li, Y.; Shen, X.; Wu, Z.; Huang, J.; Chen, Y.; Ni, Y.; Huang, J. Temperature-Dependent Transformation Thermotics: From Switchable Thermal Cloaks to Macroscopic Thermal Diodes. *Phys. Rev. Lett.* **2015**, *115* (19), 195503.

(36) Li, Y.; Shen, X.; Huang, J.; Ni, Y. Temperature-Dependent Transformation Thermotics for Unsteady States: Switchable Concentrator for Transient Heat Flow. *Phys. Lett. Sect. A Gen. At. Solid State Phys.* **2016**, *380* (18–19), 1641–1647.

(37) Shen, X.; Li, Y.; Jiang, C.; Huang, J. Temperature Trapping: Energy-Free Maintenance of Constant Temperatures as Ambient Temperature Gradients Change. *Phys. Rev. Lett.* **2016**, *117* (5), 055501.

(38) Shen, X.; Li, Y.; Jiang, C.; Ni, Y.; Huang, J. Thermal Cloak-Concentrator. *Appl. Phys. Lett.* **2016**, *109* (3), 031907.

(39) Sklan, S. R.; Li, B. A Unified Approach to Nonlinear Transformation Materials. *Sci. Rep.* **2018**, *8*, 4436.

(40) Garcia-Meca, C.; Barceló, C. Dynamically Tunable Transformation Thermodynamics. *J. Opt.* **2016**, *18* (4), 44026.

(41) Restrepo-Flórez, J. M.; Maldovan, M. Mass Separation by Metamaterials. *Sci. Rep.* **2016**, *6* (2), 21971.

(42) Restrepo-Flórez, J. M.; Maldovan, M. Mass Diffusion Cloaking and Focusing with Metamaterials. *Appl. Phys. Lett.* **2017**, *111* (7), 071903.

(43) Li, Y.; Liu, C.; Bai, Y.; Qiao, L.; Zhou, J. Ultrathin Hydrogen Diffusion Cloak. *Adv. Theory Simulations* **2017**, *1* (1), 1700004.

(44) Restrepo-Flórez, J. M.; Maldovan, M. Rational Design of Mass Diffusion Metamaterial Concentrators Based on Coordinate Transformations. *J. Appl. Phys.* **2016**, *120* (8), 084902.

(45) Petiteau, D.; Guenneau, S.; Bellieud, M.; Zerrad, M.; Amra, C. *Thermal Concentrator Homogenized with Solar-Shaped Mantle*; 2015.

(46) Dede, E. M.; Nomura, T.; Schmalenberg, P.; Seung Lee, J. Heat Flux Cloaking, Focusing, and Reversal in Ultra-Thin Composites Considering Conduction-Convection Effects. *Appl. Phys. Lett.* **2013**, *103* (6), 063501.

(47) Hu, R.; Wei, X.; Hu, J.; Luo, X. Local Heating Realization by Reverse Thermal Cloak. *Sci. Rep.* **2014**, *4* (January), 3600.

(48) Chen, F.; Yuan Lei, D. Experimental Realization of Extreme Heat Flux Concentration with Easy-to-Make Thermal Metamaterials. *Sci. Rep.* **2015**, *5*

(May), 11552.

(49) Han, T.; Bai, X.; Liu, D.; Gao, D.; Li, B.; Thong, J. T. L. Manipulating Steady Heat Conduction by Sensu-Shaped Thermal Metamaterials. *Sci. Rep.* **2015**, *5* (May), 10242.

(50) Rahm, M.; Cummer, S. A.; Schurig, D.; Pendry, J. B.; Smith, D. R. Optical Design of Reflectionless Complex Media by Finite Embedded Coordinate Transformations. *Phys. Rev. Lett.* **2008**, *100* (6), 063903.

(51) Chen, H.; Chan, C. T. Electromagnetic Wave Manipulation by Layered Systems Using the Transformation Media Concept. *Phys. Rev. B* **2008**, *78* (5), 054204.

(52) Vemuri, K. P.; Bandaru, P. R. Geometrical Considerations in the Control and Manipulation of Conductive Heat Flux in Multilayered Thermal Metamaterials. *Appl. Phys. Lett.* **2013**, *103* (13), 133111.

(53) Vemuri, K. P.; Canbazoglu, F. M.; Bandaru, P. R. Guiding Conductive Heat Flux through Thermal Metamaterials. *Appl. Phys. Lett.* **2014**, *105* (19), 193904.

(54) Svanberg, K. The Method of Moving Asymptotes—a New Method for Structural Optimization. *International Journal for Numerical Methods in Engineering*. 1987, pp 359–373.

(55) Harzheim, L.; Graf, G. A Review of Optimization of Cast Parts Using Topology Optimization : III-Topology Optimization with Manufacturing Constraints. *Struct. Multidiscip. Optim.* **2006**, *31* (5), 388–399.

(56) Bendsøe, M. P.; Sigmund, O. *Topology Optimization: Theory, Methods, and Applications*, 2nd Ed.; Springer: Berlin, Heidelberg, New York, 2003.

(57) Dede, E. M.; Zhou, F.; Schmalenberg, P.; Nomura, T. Thermal Metamaterials for Heat Control in Electronics. In *Proceedings of the ASME 2017 International Technical Conference and Exhibit on PAcking and Integration of Electronic and Photonic Microsystems*; 2017.

(58) Fujii, G.; Akimoto, Y.; Takahashi, M. Exploring Optimal Topology of Thermal Cloaks by CMA-ES. *Appl. Phys. Lett.* **2018**, *112* (6).

(59) Dede, E. M. Simulation and Optimization of Heat Flow via Anisotropic Material Thermal Conductivity. *Comput. Mater. Sci.* **2010**, *50* (2), 510–515.

(60) Dede, E. M. Multiphysics Topology Optimization of Heat Transfer and Fluid Flow Systems. In *Proceedings of the COMSOL Users Conference*; 2009.

(61) Dede, E. M.; Schmalenberg, P.; Wang, C. M.; Zhou, F.; Nomura, T. Collection of Low-Grade Waste Heat for Enhanced Energy Harvesting. *AIP Adv.* **2016**, *6* (5), 055113.

(62) Peralta, I.; Fachinotti, V. D. Optimization-Based Design of a Heat Flux Manipulation Devices with Emphasis on Fabricability. *Sci. Rep.* **2017**, *7*, 40591.

(63) Fachinotti, D.; Peralta, I.; Huespe, A. E.; Ciarbonetti, A. Control of Heat Flux Using Computationally Designed Metamaterials. In *5th International Conference on Engineering Optimization*; 2016; pp 19–23.

(64) Peralta, I.; Fachinotti, V. D.; Ciarbonetti, Á. A. Optimization-Based Design of a Heat Flux Concentrator. *Sci. Rep.* **2017**, *7*, 40591.

(65) Neofytou, A. Topology Optimization for Heat Flow Manipulation, Delft University of Technology, 2016.

(66) Fachinotti, V. D.; Ciarbonetti, Á. A.; Peralta, I.; Rintoul, I. Optimization-Based Design of Easy-to-Make Devices for Heat Flux Manipulation. *Int. J. Therm. Sci.* **2018**, *128* (April 2017), 38–48.

(67) Baker, R. W. *Membrane Technology and Applications*, 3rd Ed.; John Wiley & Sons, Inc., 2012.

(68) Wijmans, J. G.; Baker, R. W. The Solution-Diffusion Model: A Review. *J. Memb. Sci.* **1995**, *107* (1–2), 1–21.

(69) Jue, M. L.; Lively, R. P. Targeted Gas Separations through Polymer Membrane Functionalization. *React. Funct. Polym.* **2015**, *86*, 40–43.

(70) Klopffer, M. H.; Flaconneche, B. Transport Properties of Gases in Polymers: Bibliographic Review. *Oil Gas Sci. Technol.* **2001**, *56* (3), 223–244.

(71) Wang, L.; Corriou, J. P.; Castel, C.; Favre, E. Transport of Gases in Glassy Polymers under Transient Conditions: Limit-Behavior Investigations of Dual-Mode Sorption Theory. *Ind. Eng. Chem. Res.* **2013**, *52* (3), 1089–1101.

(72) Paul, D. R.; Koros, W. J. Effect of Partially Immobilizing Sorption on Permeability and the Diffusion Time Lag. *J. Polym. Sci. Polym. Phys. Ed.* **1976**, *14* (4), 675–685.

(73) Taylor, R.; Krishna, R. *Multicomponent Mass Transfer*, 1st Ed.; John Wiley & Sons, Inc: New York, 1995.

(74) Krishna, R.; Wesselingh, J. A. The Maxwell-Stefan Approach to Mass Transfer. *Chem. Eng. Sci.* **1997**, *52* (6), 861–911.

(75) Park, H. B.; Kamcev, J.; Robeson, L. M.; Elimelech, M.; Freeman, B. D. Maximizing the Right Stuff: The Trade-off between Membrane Permeability and Selectivity. *Science (80-.).* **2017**, *356*, eab0530.

(76) Koros, W. J.; Fleming, G. K. Membrane-Based Gas Separation. *J. Memb. Sci.*

1993, *83*, 1–80.

(77) Koros, W. J.; Zhang, C. Materials for Next-Generation Molecularly Selective Synthetic Membranes. *Nat. Mater.* **2017**, *16* (3), 289–297.

(78) Robeson, L. M. The Upper Bound Revisited. *J. Memb. Sci.* **2008**, *320* (1–2), 390–400.

(79) Robeson, L. M. Correlation of Separation Factor versus Permeability for Polymeric Membranes. *J. Memb. Sci.* **1991**, *62* (2), 165–185.

(80) Koros, W. J.; Coleman, M. R.; Walker, D. R. B. Controlled Permeability Polymer Membranes. *Annu. Rev. Mater. Sci.* **1992**, *22*, 47–89.

(81) Kim, W. gwi; Nair, S. Membranes from Nanoporous 1D and 2D Materials: A Review of Opportunities, Developments, and Challenges. *Chem. Eng. Sci.* **2013**, *104*, 908–924.

(82) Shah, M.; McCarthy, M. C.; Sachdeva, S.; Lee, A. K.; Jeong, H. K. Current Status of Metal-Organic Framework Membranes for Gas Separations: Promises and Challenges. *Ind. Eng. Chem. Res.* **2012**, *51* (5), 2179–2199.

(83) Singh, A.; Koros, W. J. Significance of Entropic Selectivity for Advanced Gas Separation Membranes. *Ind. Eng. Chem. Res.* **1996**, *35* (4), 1231–1234.

(84) Zimmerman, C. M.; Singh, A.; Koros, W. J. Tailoring Mixed Matrix Composite Membranes for Gas Separations. *J. Memb. Sci.* **1997**, *137* (1–2), 145–154.

(85) Robeson, L. M. Polymer Blends in Membrane Transport Processes. *Ind. Eng. Chem. Res.* **2010**, *49* (23), 11859–11865.

(86) Vu, D. Q.; Koros, W. J.; Miller, S. J. Mixed Matrix Membranes Using Carbon Molecular Sieves I. Preparation and Experimental Results. *J. Memb. Sci.* **2003**, *211* (2), 311–334.

(87) Chung, T. S.; Jiang, L. Y.; Li, Y.; Kulprathipanja, S. Mixed Matrix Membranes (MMMs) Comprising Organic Polymers with Dispersed Inorganic Fillers for Gas Separation. *Prog. Polym. Sci.* **2007**, *32* (4), 483–507.

CHAPTER 3: RATIONAL DESIGN OF MASS DIFFUSION CONCENTRATORS USING COORDINATE TRANSFORMATIONS[1]

3.1 Introduction

In this chapter, our goal is to use coordinate transformations [1–4] in order to design mass diffusion concentrators (see chapter 2.1.1.1)[3,4]. We systematically study the physical behavior of mass diffusion concentrators under different design conditions. First, we analyze the efficiency of the concentrators as a function of the different variables associated with the coordinate transformation process, and subsequently discuss the different homogenization strategies that can be employed to obtain devices that can be fabricated. In addition, we investigate the use of effective medium approach and the influence of using composite materials to obtain functional devices. We evaluate the performance in terms of the gradient developed in the interior of the device, the total mass flow rate of the compound towards the core, the disturbance of the external field, and the material requirements to fabricate the device. Ideally we seek devices that can maximize the concentration gradient and the mass flow rate at the core. For fabrication purposes, however, we look for simple metamaterial designs that require the smallest number of material layers and consist of homogeneous materials. We note that in catalytic or separation applications, the concentration gradient and the mass flow rate towards the core of the concentrator are more relevant functional properties than the disturbance of the external field. Our results help to understand the control of mass

[1] Portions of this chapter have been published in: "Restrepo-Flórez, J.M.; Maldovan, M.; Rational design of mass diffusion metamaterial concentrators based on coordinate transformations. *J. App Phys.* ***2016,*** 120 (8), 084902"

diffusion in metamaterial systems and clarify the role of the different design variables in the performance of metamaterial concentrators. This initial work on the use of coordinate transformation techniques to control mass diffusion pave the way toward using these novel devices to rationally design the flux trajectory of molecular compounds in chemical and biomolecular systems.

3.2 Theoretical approach

Mass flux manipulation via coordinate transformation techniques and metamaterials requires a series of steps for rational design[5,6] (Figure 3.1). First, it is necessary to select a spatial coordinate transformation that provides the desired functionality and obtain the material requirements in terms of the spatial distribution of the diffusivity. These requirements generally translate into the need of an anisotropic and inhomogeneous constituent material. A second step is the application of a *homogenization* strategy that simplifies the spatial dependence of the anisotropic diffusivity. After such homogenization, a *segmentation* method is required where the anisotropic features of the metamaterial shell are reproduced by using appropriate combinations of *isotropic and homogeneous* materials (Figure 3.1).

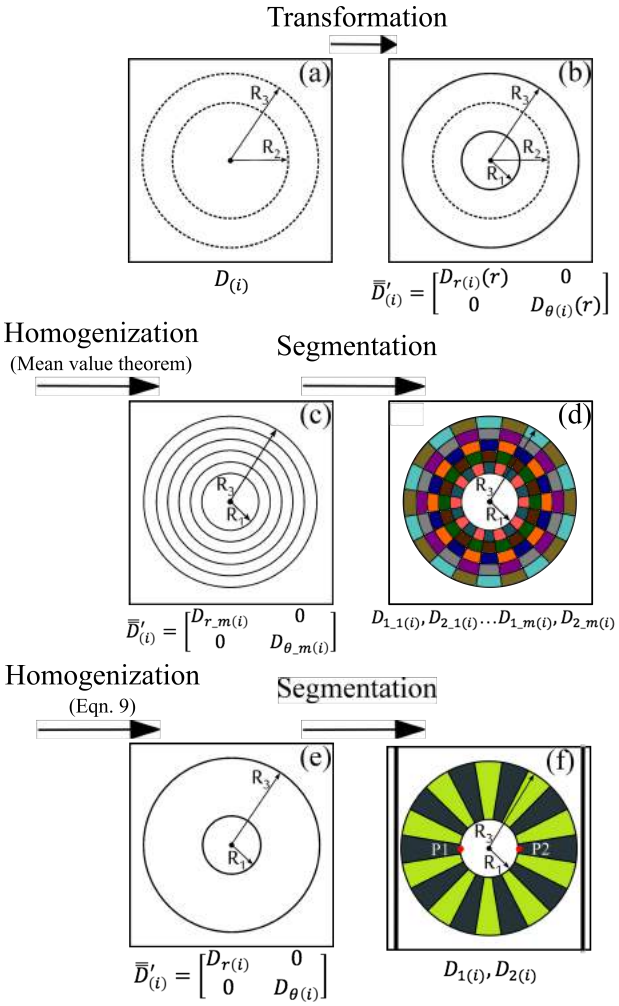

Figure 3.1. Coordinate transformation scheme for mass diffusion concentrators. The figure shows the three major design steps. (a)(b) A coordinate transformation is applied and a homogenization process (c)(e) is used to simplify the initial device. (d)(f) A segmentation step is employed where isotropic homogeneous materials reproduce the prescribed anisotropy. (a) Initial isotropic region. (b) Ideal anisotropic, non homogeneous metamaterial. (c) Homogeneous, anisotropic metamaterial (with *m* rings) after homogenization of (b) based on mean value theorem. (d) Multilayer mass concentrator where the anisotropy of each *m* ring is reproduced by two isotropic materials. (e) Homogeneous, anisotropic metamaterial (with one ring) after homogenization of (b) using Eq. (3.3). (f) Multilayer lamellar structure, anisotropy is reproduced by two isotropic materials *1* and *2*. The average concentration gradient is measured between P1 and P2 (f), the standard deviation of the concentration along the lines at x=±3.05cm.

In this chapter, we follow the above procedure and use linear transformations to design two-dimensional metamaterial mass diffusion concentrators as described in

chapter 2.1.1.1. The coordinate transformation process allows to calculate the required radial $D_{r(i)}$ and azimuthal $D_{\theta(i)}$ diffusivities that yield a mass concentrator[3] device for species *i*

$$\frac{\bar{\bar{D}}'_{(i)}}{D_{bg(i)}} = \begin{bmatrix} \frac{r' - R_3\left(\frac{R_1 - R_2}{R_3 - R_2}\right)}{r'} & 0 \\ 0 & \frac{r'}{r' - R_3\left(\frac{R_1 - R_2}{R_3 - R_2}\right)} \end{bmatrix} (R_1 \leq r \leq R_2); \frac{\bar{\bar{D}}'_{(i)}}{D_{bg(i)}} = 1 \ (r \leq R_1) \qquad (2.9)$$

Eq. (2.9) shows that the metamaterial structure is both non-homogeneous and anisotropic. It is important to note that satisfying such complex requirements using naturally occurring materials is difficult and strategies that allow for the design of metamaterials using homogeneous and isotropic materials are critically required.

We first investigate and compare the two more common homogenization strategies to simplify the material requirements[3,7,8]. The first approach consists of dividing the metamaterial shell in an arbitrary number *m* of concentric rings. In each *j* ring, the average radial and azimuthal diffusivities are calculated using the mean value theorem[3,9], i.e. $\langle {D_{r(i)}}/{D_{bg(i)}} \rangle = \frac{2\pi}{A_j} \int_{r=R'_j}^{r=R'_{j+1}} D_{r(i)}(r) r dr$ and $\langle {D_{\theta(i)}}/{D_{bg(i)}} \rangle = \frac{2\pi}{A_j} \int_{r=R'_j}^{r=R'_{j+1}} D_{\theta(i)}(r)\, r dr$ respectively; where *j* runs from 1 to *m*, A_j is the area and R'_j and R'_{j+1} are the radius of the *j* ring. The higher the number of rings, the more difficult the fabrication of the structure. The second strategy analyzed considers the fact that the product of the radial and azimuthal diffusivities is equal to one (Eq. (3.1))[7,8]. Note that taking the average value of Eq. (3.1) throughout the spatial domain, results in Eq. (3.2). In practice, the covariance is neglected, and the metamaterial diffusivities for the concentrator are obtained by calculating the average relative radial diffusivity and using Eq. (3.3) to approximate the average relative azimuthal diffusivity[4,8,10]. This assumption however should be examined

carefully as shown later in this thesis. For this second approach, it has been indicated that the value of the relative radial diffusivity can be selected arbitrarily[7,8,11], however, it is important to keep in mind that selecting the value of the relative radial diffusivity requires a specific combination for the radii R_1, R_2 and R_3 as shown below.

$$\left(\frac{D_{r(i)}}{D_{bg(i)}}\right)\left(\frac{D_{\theta(i)}}{D_{bg(i)}}\right) = 1 \tag{3.1}$$

$$\left\langle\left(\frac{D_{r(i)}}{D_{bg(i)}}\right)\left(\frac{D_{\theta(i)}}{D_{bg(i)}}\right)\right\rangle = \left\langle\frac{D_{r(i)}}{D_{bg(i)}}\right\rangle\left\langle\frac{D_{\theta(i)}}{D_{bg(i)}}\right\rangle + Cov\left[\left(\frac{D_{r(i)}}{D_{bg(i)}}\right)\left(\frac{D_{\theta(i)}}{D_{bg(i)}}\right)\right] = 1 \tag{3.2}$$

$$\left\langle\frac{D_{r(i)}}{D_{bg(i)}}\right\rangle\left\langle\frac{D_{\theta(i)}}{D_{bg(i)}}\right\rangle \cong 1 \tag{3.3}$$

Once the transformation function and the homogenization approach are applied, the expected values for the relative radial and azimuthal diffusivities are function exclusively of the geometry of the system (i.e. R_1, R_2, R_3). Independently of the homogenization strategy employed, the anisotropy requirements in each of the *m* rings are fulfilled by considering *N* bilayers made of homogeneous isotropic materials. Specifically, in the case of a concentrator, a large radial diffusivity and a small azimuthal diffusivity are required simultaneously. As it has been explained, this can be achieved by assembling a lamellar structure with resistances in parallel in the radial direction and in series in the azimuthal direction. The effective diffusivities $\langle D_{r(i)}/D_{bg(i)}\rangle_m$ and $\langle D_{\theta(i)}/D_{bg(i)}\rangle_m$ for each bilayer *N* made of two homogeneous and isotropic materials *1* and *2* are calculated using Eq. (3.4), where f_1 and f_2 are the corresponding volume fractions[8]; note that these equations rely on the assumption of constant solubility[2,12].

$$\left\langle\frac{D_{r(i)}}{D_{bg(i)}}\right\rangle_m = f_1\frac{D_{1(i)}}{D_{bg(i)}} + f_2\frac{D_{2(i)}}{D_{bg(i)}}\ ; \quad \frac{1}{\left\langle\frac{D_{\theta(i)}}{D_{bg(i)}}\right\rangle_m} = \frac{f_1}{\frac{D_{1(i)}}{D_{bg(i)}}} + \frac{f_2}{\frac{D_{2(i)}}{D_{bg(i)}}} \tag{3.4}$$

Although the number of bilayers N is not an explicit variable, N needs to be large enough such that the metamaterial behaves as composed of a single anisotropic material. However, there is an upper bound for N imposed by the continuum medium theory, since the size of a material layer should be larger than the mean free path of the compound in that layer. In general, one constituent isotropic material (*1)* shows a higher diffusion coefficient than the background medium, while the other material (*2)* has a lower diffusion coefficient. The above analysis shows that the design of mass diffusion concentrators involves eleven material/structural variables ($D_{r(i)}$,$D_{\theta(i)}$,$D_{1(i)}$, $D_{2(i)}$, f_1, f_2, N, m R_1, R_2 and R_3) and there are five equations establishing relations among them. For homogenization strategy 1, these equations are Eqs (2.9), Eqs (3.4), and f_1+f_2=1, while for homogenization strategy 2 we have Eq. (2.9) (left), Eq. (3.3), Eqs (3.4), and f_1+f_2=1. Therefore there are six degrees of freedom, whose values can be arbitrarily selected during the design process. We would like to highlight that in the design of metamaterials we deal with two simultaneous requirements that need a practical solution: (1) the device is anisotropic, i.e. the diffusivity $\overline{\overline{D}}'_{(i)}$ is a tensor, and (2) the device is inhomogeneous, i.e. $\overline{\overline{D}}'_{(i)}$ is a function of position. To solve the anisotropic requirement, we consider effective medium theory and use an arrangement of bilayers, where the total number of bilayers is N. When N is large the metamaterial reproduces the original anisotropicity. On the other hand, to solve for the inhomogeneity, we divide the system in rings "m" and for each of these rings, we calculate the spatial average of the radial and azimuthal conductivities. When m is large the metamaterial reproduces the original inhomogeneity.

3.3 Results and discussion

Without losing generality, we consider that the external metamaterial radius is R_3=3cm and the spatial domain where the concentrator is placed consists of a square of side L=8cm. The structure radius R_1 and the transformation radius R_2 are thus physical variables that can be exploited to achieve desired mass concentration effects. We note that diffusion problems at steady-state are scale independent, meaning that the performance can be calculated by knowing the solution at one scale and using a scaling factor[9]. Since the metamaterials are two-dimensional, the z direction is considered to be infinite. Initially we will analyze ideal devices (i.e. anisotropic and homogeneous) obtained by linear coordinate transformation functions. Figure 3.2(a) shows the relationship between the average relative radial diffusivity $\langle D_{r(i)}/D_{bg(i)} \rangle$ and the metamaterial structural design variables R_1/R_3 and R_2/R_3. The functional dependence is obtained by averaging Eq. (2.9) within the metamaterial shell ($R_1<r<R_3$ and $0<\theta<2\pi$) and it is given by $\langle D_{r(i)}/D_{bg(i)} \rangle = 1-[2b/(R_3+R_1)]$, where $b=R_3(R_1-R_2)/(R_3-R_2)$. Note that, for fixed R_3, when R_1 is constant one can increase the anisotropy (i.e. the value of $\langle D_{r(i)}/D_{bg(i)} \rangle$) by increasing R_2, and also for constant R_2 the anisotropy increases for small R_1. This is due to the fact that the degree of anisotropy depends on the amount of space that is compressed, which is determined by $r' = (R_2/R_1)\, r$ (Eq. (2.8)). The ratio R_2/R_1 thus establishes the amount of space compressed (e.g. for R_2/R_1=1 no transformation is performed) and the trends observed in Figure 3.2(a). Note that the geometry of the system critically influences the performance of a concentrator by establishing not only the surface area of the core and the thickness of the shell, but also, importantly, the values of the relative radial and azimuthal diffusivities of the constituent metamaterial.

Understanding this functionality is important because it helps to clarify the role of geometry in metamaterial design.

The performance of metamaterial concentrators can be measured in terms of three important physical properties (quantities of interest): the average gradient in the interior of the device ($\langle \nabla C_{(i)} \rangle = \frac{1}{2R_1} \int_{x=-R_1}^{x=R_1} \nabla C_{(i)} dx$, measured along the line y=0); the average magnitude of the mass flow rate towards the core ($\langle \dot{m} \rangle = \int_{y=-R_1}^{y=R_1} D_{bg(i)} \nabla C_{(i)} dy$, measured along the line x=0); and the ability of the system to keep the external field undisturbed, measured as the standard deviation of the concentration along the lines located at x=±3.05cm (see Figure 3.1(f) for location of the lines). Note that for ideal metamaterials, any vertical line outside the device must be an iso-concentration line whose standard deviation is equal to zero[13]. We show in Figure 3.2(b-c) the numerical calculations for $\langle \nabla C_{(i)} \rangle$ and $\langle \dot{m} \rangle$ as a function of R_1/R_3 and $\langle D_{r(i)}/D_{bg(i)} \rangle$ relative to the external fields. In particular, the numerical predictions show how these physical properties can be increased by considering larger $\langle D_{r(i)}/D_{bg(i)} \rangle$ values. This behavior is consistent, since increasing the radial diffusivity not only favors transport in the radial direction but also, in this type of designs, generates a decrease in the azimuthal diffusivity as given by Eq. (3.3). In other words, by increasing $\langle D_{r(i)}/D_{bg(i)} \rangle$, mass transport along the radial/azimuthal direction is enhanced/reduced, focusing the flux lines towards the core. Therefore the net effect is an increase in the relative concentration gradient and relative mass flow rate, as observed in the figures. Another important aspect in Figure 3.2(b-c) is that when $\langle D_{r(i)}/D_{bg(i)} \rangle$ is kept constant, decreasing R_1 (i.e. thicker metamaterial shell) leads to higher concentration gradients but lower total mass flow rates. Note that increasing the gradient in the core is related to the amount of space

compressed during the transformation process, i.e. the more the compression, the higher the gradient. The same behavior is not observed when the mass flow rate is analyzed, note that this variable depends on the concentration gradient and the total area for transport, and in this case the increase in the concentration gradient does not compensate the decrease in the core area when R_1 decreases. There is therefore an opposite dependence for the concentration gradient and mass flow rate in the metamaterial device. The presence of the metamaterial can increase the concentration gradient in the core by a factor of 30× in comparison with the external gradient if an internal radius R_1=0.1cm is used (limit not shown) and by a 3× factor if an internal radius of R_1=1cm is used. The relative mass flow rate has also a strong dependence on both the internal radius and the radial mass diffusivity (Figure 3.2(c)). For a fixed R_1, the mass flow rate is enhanced with increasing $D_{r(i)}$ due to an improved performance of the metamaterial device. On the other hand, for a fixed $D_{r(i)}$, the mass flow rate is enhanced with R_1 due to a larger core area.

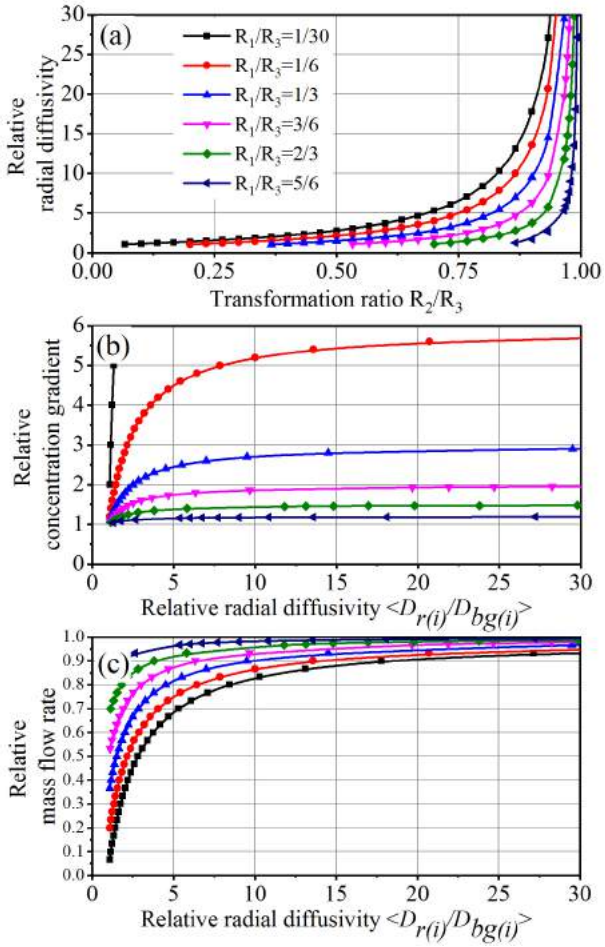

Figure 3.2. Performance of ideal mass concentrator devices as a function of metamaterial shell geometry. (a) Functional relation among $\langle D_{r(i)}/D_{bg(i)} \rangle$, R_1/R_3 and R_2/R_3 (b) Concentration gradient normalized with respect to the external gradient. (c) Mass flow rate towards the core normalized against the mass flow rate entering the system.

After selecting the geometrical parameters and applying the coordinate transformation, a critical objective is to practically achieve the complex metamaterial shell; the first step towards this goal is the selection of an appropriate *homogenization* strategy. As mentioned before, two procedures can be used: the metamaterial shell can be divided in *m* concentric rings and use the mean value theorem to calculate the radial and azimuthal diffusivities for each ring; or alternatively, the mean value theorem can be used to obtain the average radial diffusivity for the entire metamaterial shell and use equation

(3.3) to calculate the average azimuthal diffusivity. Note that even if in the first approach the number of rings is equal to one, the two approaches are not the same, yielding slightly different values in the estimation of the diffusivity tensor; however, we found that the differences in performance obtained by the two approaches are not significant in terms of the gradient and the mass flow rate toward the core. It is important to highlight that increasing the number of rings significantly increases the difficulties for manufacturing since the number of homogeneous and isotropic materials also increases. Since our numerical calculations show that increasing the number of rings from m=1 does not have a significant effect on the performance of the device (data not shown), from a practical standpoint, the use of one ring is a more convenient strategy. We therefore investigate the difficulties associated with finding the required constituent materials when m=1. Due to its simplicity, we will use Eq. (3.3) for the homogenization process. It is important to keep in mind that when considering Eq. (3.3), the covariance between the relative radial and azimuthal diffusivities is neglected. To establish the accuracy of this assumption, we plot in Figure 3.3 the covariance as a function of R_1/R_3 and R_2/R_3. Note that the larger the compression of space, the larger the covariance. The area in blue corresponds to a region where the covariance can be essentially neglected (<0.1) and Eq. (3.3) can be applied.

In general, it is desirable to find metamaterial designs in which the required constituent materials present low contrast for the diffusivities (Eq. (3.5)) since the range of mass diffusivity contrast that can be obtained by using naturally occurring materials is restricted[47]. Importantly, since the diffusivity of the *isotropic* materials required to fabricate the concentrator is a direct function of the anisotropic diffusivities $\langle D_{r(i)}/D_{bg(i)} \rangle$ and $\langle D_{\theta(i)}/D_{bg(i)} \rangle$ (Eqs (3.4)), the material requirements for fabrication are also function

of the metamaterial radius R_1/R_3 and R_2/R_3. We show in Figure 3.4(a) the dependence of the contrast between the diffusivity of the *isotropic* constituent materials on the choice of the design variables R_1/R_3 and R_2/R_3 of the metamaterial structure. In our calculations, the material contrast T is calculated as the logarithm of the ratio of the diffusivities of the two isotropic constituent materials, we thus have

$$T_c = \mathrm{Log}\left(\frac{D_{1(i)}}{D_{2(i)}}\right) = \mathrm{Log}\left[\left(\frac{1-f_1}{f_1}\right)\left(\frac{\left(\langle D_{r(i)}^2/D_{bg(i)}^2\rangle+2f_1-1\right)+\sqrt{\left(\langle D_{r(i)}^2/D_{bg(i)}^2\rangle+2f_1-1\right)^2-\left(2\langle D_{r(i)}/D_{bg(i)}\rangle f_1\right)^2}}{\left(\langle D_{r(i)}^2/D_{bg(i)}^2\rangle-2f_1+1\right)-\sqrt{\left(\langle D_{r(i)}^2/D_{bg(i)}^2\rangle+2f_1-1\right)^2-\left(2\langle D_{r(i)}/D_{bg(i)}\rangle f_1\right)^2}}\right)\right] \quad (3.5)$$

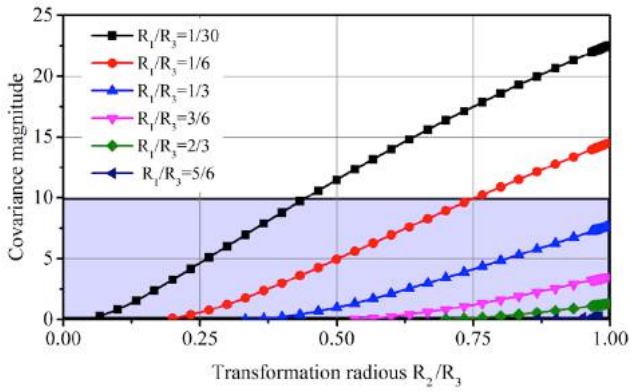

Figure 3.3. Covariance magnitude in a metamaterial concentrator as a function of R_1/R_3 and R_2/R_3.

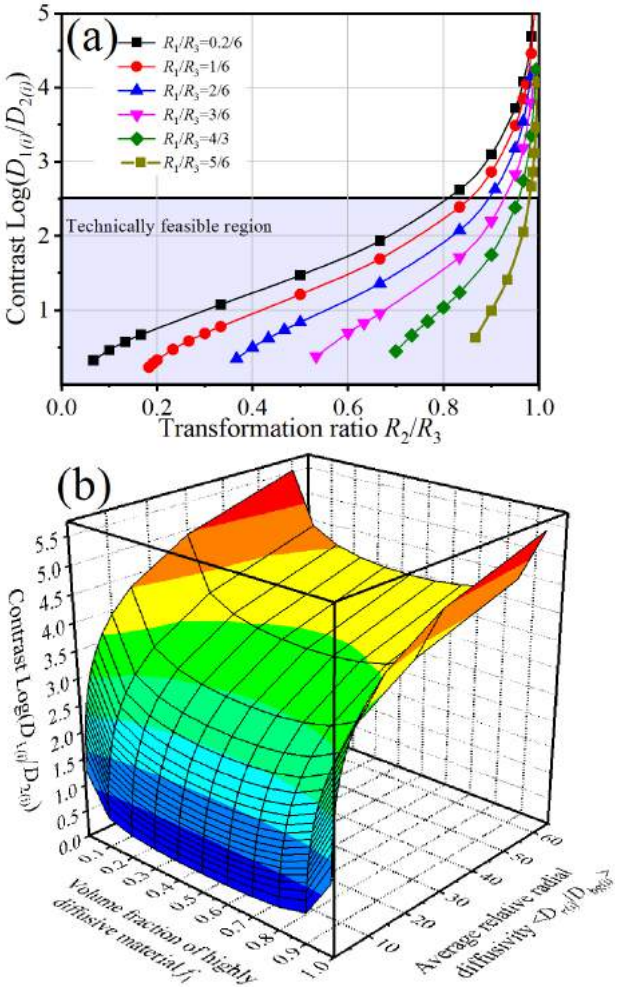

Figure 3.4. Mass diffusivity contrast (T_c) of the isotropic homogeneous constituent materials. (a) T_c as a function of the geometrical parameters of the system, where the gray area shows the more accessible region in terms of finding required constituent materials. (b) T_c as a function of the relative radial diffusivity and the volume fraction of the highly diffusive material.

Two conclusions can be extracted from the figure: first, for given R_2 and R_3, the thinner the concentrator's shell, the less the diffusivity contrast required to build the metamaterial; second, for given R_1 and R_3, the higher the value of R_2, the higher the value of the material diffusivity contrast. This is because the relative radial and azimuthal mass

diffusivities are both function of R_2 and $D_{r(i)}D_{\theta(i)} = D_{bg(i)}^2$, (Eqs (2.9) and (3.1)), such that increasing the value of R_2 increases the anisotropy (i.e. the ratio $D_{r(i)}/D_{\theta(i)}$) of the system, as determined by Eqs (2.9). Note that maximum anisotropy is obtained when R_2 tends to R_3. The direct relation between the diffusivity contrast of the materials, the metamaterial anisotropy, and the volume fraction of the high diffusivity material is shown in Figure 3.4(b). A continuous increase in the diffusivity contrast is observed when the average radial diffusivity increases (and therefore the anisotropicity), as established by Eqs (3.4). This is because materials with more contrasting diffusivities are required to create higher anisotropy (i.e. large $<D_{r(i)}/D_{bg(i)}>$). For constant $<D_{r(i)}/D_{bg(i)}>$, the diffusivity contrast presents a minimum when f_1=0.5 and increases when $f_1 \rightarrow 0$ or $f_1 \rightarrow 1$. The functional relation that explains this behavior is presented in Eq. (3.5). Importantly, considering that these novel systems have the potential to control mass diffusion in catalytic or separation systems – where flux and gradient are the most relevant variables – from the design point of view, the value of R_1/R_3 should be chosen based on applications and fabrication limitations by considering that a small internal radius yields higher gradients but lower mass flow rates. On the other hand, the value of R_2/R_3 should be increased up to the point where manufacturing difficulties arise in terms of the high diffusivity contrast required for the constituent materials (i.e. material availability). Figure 3.4(a) therefore provides guidelines for the selection of the geometry of the system based on material availability. For gases diffusing in polymers, it is convenient to select the geometrical parameters such that the diffusivity contrast between the required constituent polymers is less than 2.5 orders of magnitude, since within this region it is more likely to find two candidate polymers with the required characteristics

(i.e. with the same solubility such that Fick's law can be applied and with prescribed mass diffusivities)[14–16].

The final step in the design of a mass concentrator is the *segmentation* process. Based on the above discussion, to study the effects of segmentation on the performance of metamaterial concentrator devices, we consider an internal radius R_1 of 1cm and a transformation radius R_2 equal to 2.72cm (a value of R_2 selected such that the diffusivity contrast required between the materials is still within the feasible region defined in Figure 3.4(a)). Note that for R_1=1cm, R_2=2.72cm and R_3=3cm, the covariance ~0.06 can be neglected (Figure 3.3). At this stage the volume fraction of the highly diffusive material f_1 and the total number of bilayers N are still two degrees of freedom (f_2, $D_{1(i)}$, $D_{2(i)}$ are fixed and given by Eq. (3.4)). We should note especially that by selecting the volume fraction f_1 we are also implicitly determining the isotropic mass diffusivities of the materials in the shell. We studied the effect of varying the volume fraction of the highly diffusive material f_1 on the efficiency of the metamaterial device for three different values of bilayers ($N=20,40,80$) and the results are shown in Figure 3.5. We found that a maximum mass concentration gradient and mass flow rate are obtained when the volume fraction of the highly diffusive material f_1 is approximately 0.6; the minimum disturbance of the external field also occurs at f_1~0.6 but it is slightly displaced to the left due to the convergence of the multilayer approximation towards the ideal device when the number of bilayers increases. Besides performance, material availability is also important. Since it is observed that the diffusivity contrast between the isotropic homogeneous materials reaches a minimum when f_1 is ~0.5 (Figure 3.4(b)) a compromise between efficiency and material availability should be contemplated.

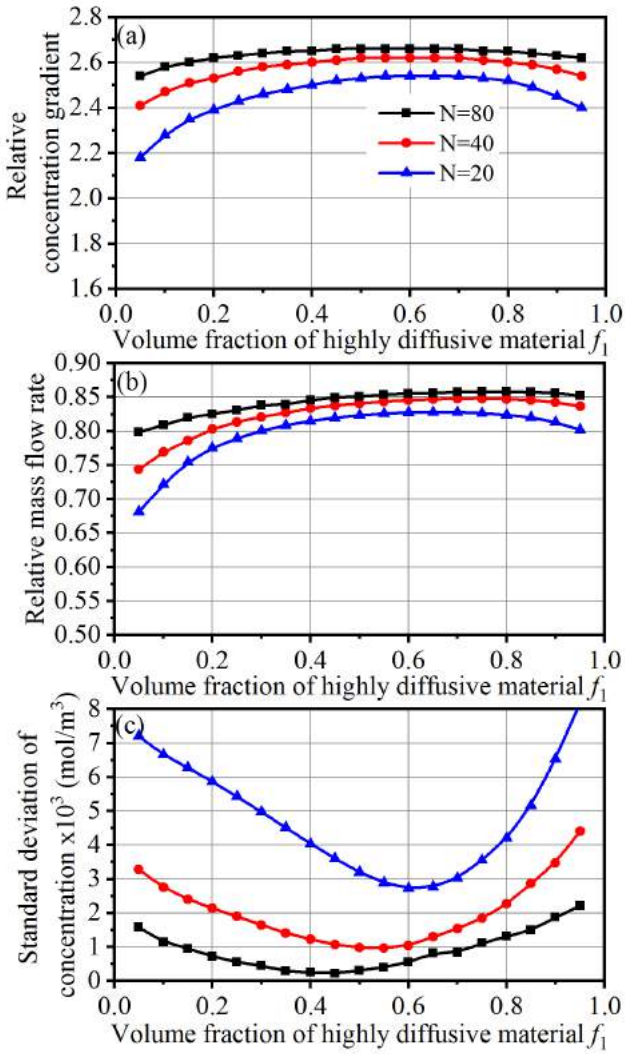

Figure 3.5. Effect of the volume fraction of highly diffusive material f_1 on the performance of the metamaterial shell. (a) Concentration gradient normalized with respect to the external gradient. (b) Mass flow rate towards the core normalized against the incoming flow rate. (c) Standard deviation of the concentration on a vertical line outside the device (x=±3.05cm). No significant differences were found between the standard deviations measured at both sides of the device ((i.e. at x=-3.05cm (left side), and x=3.05cm (right side)).

For a volume fraction of f_1=0.5, Figures 3.6(a-c) show how the total number of bilayers N modifies the mass concentration field, showing that the concentration gradient and mass flow rate toward the core increase while the standard deviation decreases when the number N of bilayers is increased. Note, however, that an oscillating behavior is

observed as a function of N in the discretized shell due to the broken symmetry of the system, since materials *1* and *2* organize differently with respect to the external gradient (i.e. high and low symmetry) when the number of bilayers is even or odd. Figure 3.6 shows that the performance of the segmented device is lower in comparison with the anisotropic homogeneous device, providing a quantitative measurement of the consequences of approximating the original non-homogeneous anisotropic system with isotropic materials. As N goes to infinity, the performance of the segmented device certainly approaches the ideal case. Importantly, despite the fact that the performance improves with increased number of bilayers, it is necessary to establish a reasonable number of bilayers for fabrication purposes. From the graphs, we found that N=18 generates a concentration gradient which is ~95% of the maximum gradient (which corresponds to the ideal device) and also ~95% of the maximum mass flow rate. A metamaterial shell made of 18 bilayers is therefore an excellent approximation (within 5%) of the ideal device. We note that reducing the number of bilayers is more practical in terms of fabrication but it will also reduce the efficiency of the device. In addition, we compare in Figure 3.7 the concentration profiles for the metamaterial shell with N=10, N=18, and the ideal shell, where it can be seen comparable concentration fields in the case of N=18 and the ideal case.

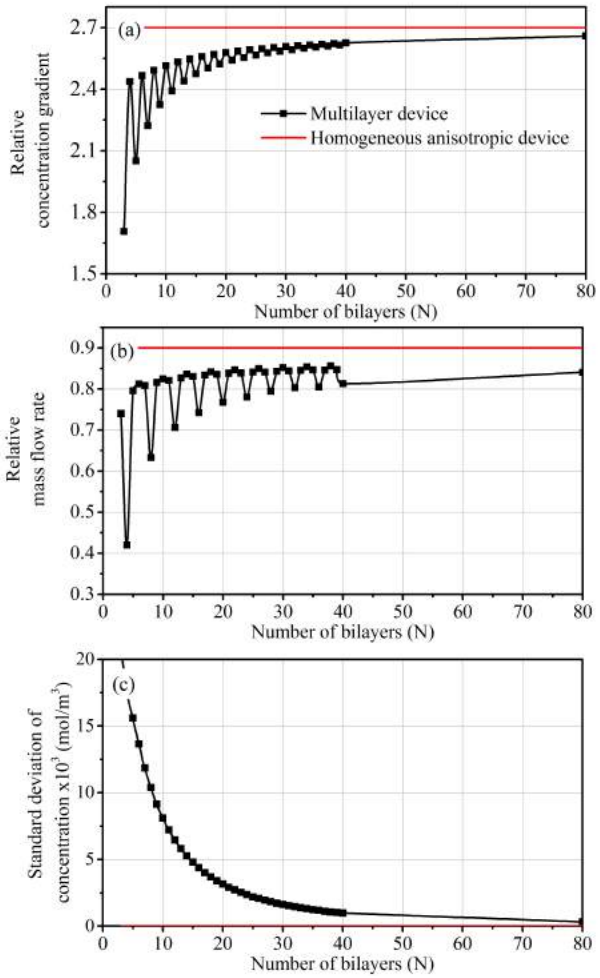

Figure 3.6. Performance of the device as a function of the number of bilayers *N*. (a) Normalized gradient in the interior of the device. (b) Normalized total mass flow rate towards the core. (c) Standard deviation of the concentration at a vertical position outside the device.

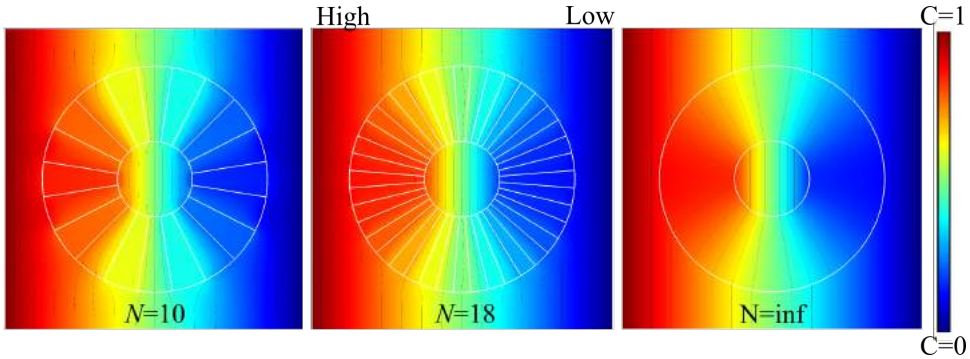

Figure 3.7. Color maps for the mass concentration profiles for different number of bilayers *N*. A mass concentrator metamaterial shell (white lines) made of *N*=18 provides a similar mass spatial distribution as *N*=∞.

We should notice that there are different variables associated with each of the steps in the design of a metamaterial concentrator. For example, during the transformation step, the geometric parameters R_1, R_2 and R_3 need to be chosen, which control the anisotropicity of the system (Eq. (2.9)) and have a strong influence on the performance of the concentrator in terms of gradient and mass flow rate (as well as on material requirements in terms of diffusivity contrast). Also, during the homogenization and segmentation processes, the number of rings m and the effective medium approach variables f_1 and N need to be selected, variables that primarily impact the disturbance of the external field but are not critical in terms of other performance criteria (e.g. gradient and mass flow rate). Note that none of these variables is associated with the anisotropy of the system (Eq. (2.9)), therefore their influence on the performance of the device in terms of gradient and mass flow rate, although relevant, is less critical than the geometric parameters.

3.4 Conclusions

Achieving precise manipulation of mass transfer provides vast opportunities for improving a broad band of chemical and biomolecular engineering processes where mass diffusion is critically important. A practical and novel way to achieve such a precise control of mass flow is through the use of mass-diffusion metamaterials. The objective of this chapter was to understand and design coordinate-transformation based metamaterial concentrators with the purpose of developing a new physical approach to control mass-diffusion. Despite the fact that metamaterial concentrators offer the potential of controlling mass diffusion in catalytic and separation systems, a systematic analysis of the physical properties provided by mass diffusion metamaterial concentrators has not

been reported in the literature. We presented a comprehensive study of the effects of structural and material properties on the efficiency of mass concentrator metamaterial shells. We systematically examined the concentration gradient at the core, the total mass flow rate towards the core, and the disturbance of the external concentration field, and provided fabrication guidelines to rationally design metamaterial concentrators. The results in this chapter help to understand, design, and control mass diffusion in metamaterials, which offer the possibility of initiating significant advances in chemical and biomolecular systems by introducing novel effects and devices such as mass diffusion rotators, concentrators, cloaking of arbitrary objects, and mass diffusion dividers.

3.5 References

(1) Pendry, J. B.; Schurig, D.; Smith, D. R. Controlling Electromagnetic Fields. *Science.* **2006**, *312* (5781), 1780–1782.

(2) Guenneau, S.; Petiteau, D.; Zerrad, M.; Amra, C.; Puvirajesinghe, T. Transformed Fourier and Fick Equations for the Control of Heat and Mass Diffusion. *AIP Adv.* **2015**, *5* (5), 053404.

(3) Guenneau, S.; Amra, C.; Veynante, D. Transformation Thermodynamics: Cloaking and Concentrating Heat Flux. *Opt. Express* **2012**, *20* (7), 8207–8218.

(4) Narayana, S.; Sato, Y. Heat Flux Manipulation with Engineered Thermal Materials. *Phys. Rev. Lett.* **2012**, *108* (21), 214303.

(5) Ooi, E. H.; Popov, V. Thermal Invisibility through Geometrical Transformation: A Segmented Cloaking Approach. *WIT Trans. Eng. Sci.* **2012**, *75*, 39–46.

(6) Ooi, E. H.; Popov, V. Transformation Thermodynamics for Heat Flux Management Based on Segmented Thermal Cloaks. *Eur. Phys. J. Appl. Phys.* **2013**, *63* (1), 10903.

(7) Han, T.; Yuan, T.; Li, B.; Qiu, C.-W. Homogeneous Thermal Cloak with Constant Conductivity and Tunable Heat Localization. *Sci. Rep.* **2013**, *3* (April), 1593.

(8) Hu, R.; Wei, X.; Hu, J.; Luo, X. Local Heating Realization by Reverse Thermal Cloak. *Sci. Rep.* **2014**, *4* (January), 3600.

(9) Schittny, R.; Kadic, M.; Guenneau, S.; Wegener, M. Experiments on Transformation Thermodynamics: Molding the Flow of Heat. *Phys. Rev. Lett.* **2013**, *110* (19), 195901.

(10) Chen, T.; Weng, C. N.; Tsai, Y. L. Materials with Constant Anisotropic Conductivity as a Thermal Cloak or Concentrator. *J. Appl. Phys.* **2015**, *117* (5), 054904.

(11) Chen, F.; Yuan Lei, D. Experimental Realization of Extreme Heat Flux Concentration with Easy-to-Make Thermal Metamaterials. *Sci. Rep.* **2015**, *5* (May), 11552.

(12) Guenneau, S.; Puvirajesinghe, T. M. Fick's Second Law Transformed: One Path to Cloaking in Mass Diffusion. *J. R. Soc. Interface* **2013**, *10* (83), 20130106.

(13) Petiteau, D.; Guenneau, S.; Bellieud, M.; Zerrad, M.; Amra, C. Spectral Effectiveness of Engineered Thermal Cloaks in the Frequency Regime. *Sci. Rep.* **2014**, *4* (December), 7386.

(14) Shelby, J. E. *Handbook of Gas Diffusion*, 1st Ed.; ASM International: United States of America, 1996.

(15) Koros, W. J.; Coleman, M. R.; Walker, D. R. B. Controlled Permeability. *Annu. Rev. Mater. Sci.* **1992**, *22*, 47–89.

(16) Jue, M. L.; Lively, R. P. Targeted Gas Separations through Polymer Membrane Functionalization. *React. Funct. Polym.* **2015**, *86*, 40–43.

CHAPTER 4: A COMPLETE THEORETICAL FRAMEWORK FOR THE REALIZATION OF MASS DIFFUSION METAMATERIALS[1]

4.1 Introduction

In mass diffusion metamaterials it has been commonly assumed that the concentration gradient is the driving force for the diffusion of atoms and molecules[1–4]. However, in general, the driving force is the gradient of the chemical potential[5–7]. In particular cases (such as homogeneous ideal dilute systems) concentration and chemical potential are equivalent, and they can be considered as the driving force for diffusion[5,8,9]. Since metamaterials are non-homogeneous systems, the driving force for mass transport is thus the chemical potential, and equilibrium is reached when the chemical potential (and not the concentration) is spatially constant throughout the system. The concentration, while being constant in each phase at equilibrium, can show discontinuities at the interfaces due to different solubilities in the different phases[5,6,10]. To date there is no theoretical framework to study mass diffusion in non-homogenous systems using coordinate transformations and metamaterial theory[2–4,11,12], this limitation has constrained the design and fabrication of metamaterial devices that would enable new tools to control mass diffusion in general and realistic systems[1–3,13]. It is thus important to develop a general approach to design mass diffusion metamaterials that adequately incorporates the correct driving forces behind molecular diffusion.

In this chapter we develop a general approach to manipulate mass diffusion using rationally designed metamaterial devices. Our method is based on an effective medium

[1] Portions of this chapter have been published in: "Restrepo-Flórez, .JM.; Maldovan, M.; Mass diffusion cloaking and focusing with metamaterials. *Appl Phys Lett.* ***2017***, 111 (7), 071903"

approximation which is derived by using chemical potential as the driving force for diffusion[14–16], and correctly accounts for discontinuities of mass concentration at the interfaces in the metamaterial systems. We study the role of concentration discontinuities on the performance of metamaterial devices for cloaking and concentration of atoms and molecules. Our results show that neglecting changes in solubility across interphases can lead to unrealistic predictions for the mass concentration profiles, gradients, and disturbance of the external field.

4.2 Theoretical approach

In this chapter we will use as benchmark metamaterial examples cloaks and concentrators designed using coordinate transformations as described in chapter 2. The radial $D_{r(i)}$ and azimuthal $D_{\theta(i)}$ components of the diffusivity tensor of the metamaterial shells, which are limited to the annular region $R_1<r<R_3$, are given by

$$\frac{D_{r(cl)(i)}}{D_{bg(i)}} = \frac{r'-R_1}{r'}; \quad \frac{D_{\theta(cl)(i)}}{D_{bg(i)}} = \frac{r'}{r'-R_1} \quad (cloak) \tag{2.7}$$

$$\frac{D_{r(cn)(i)}}{D_{bg(i)}} = \frac{r'-R_3\left(\frac{R_1-R_2}{R_3-R_2}\right)}{r'}; \quad \frac{D_{\theta(cn)(i)}}{D_{bg(i)}} = \frac{r'}{r'-R_3\left(\frac{R_1-R_2}{R_3-R_2}\right)} \quad (concentrator) \tag{2.9}$$

Since non-homogeneous anisotropic metamaterials are difficult to obtain in practice, approaches that simplify the diffusivity requirements are needed to achieve metamaterials that can be fabricated. To simplify the spatial dependence of the diffusivity tensor (non-homogeneity), it is important to note that for cloaks and concentrators $\left(D_{r(i)}/D_{bg(i)}\right)\left(D_{\theta(i)}/D_{bg(i)}\right) = 1$[17,18]. In the simplified version, the relative radial diffusivity is thus considered constant and the relative azimuthal diffusivity is calculated as its inverse[4]. Note that for cloaking, we need $D_{\theta(cl)(i)}>D_{r(cl)(i)}$ to prevent mass diffusion from moving inside the core, while for a concentrator, we need $D_{r(cn)(i)}>D_{\theta(cn)(i)}$ to focus mass

diffusion. To obtain the required anisotropy, we consider two homogeneous isotropic materials *1* and *2*. As it has been discussed for cloaking, we alternate materials *1* and *2* in concentric cylindrical rings such that mass diffusion resistances add in series (parallel) in the radial (azimuthal) direction, and thus $D_{\theta(cl)(i)}>D_{r(cl)(i)}$[19,20] (Figure 4.1(c)). For concentrators, we combine materials *1* and *2* in a radial lamellar structure where resistances add in parallel (series) in the radial (azimuthal) direction, thus satisfying $D_{r(cn)(i)}>D_{\theta(cn)(i)}$[20–22] (Figure 4.1(d)). Materials *1* and *2* need to be carefully selected such that based on effective medium theory, they reproduce the required values of the anisotropic mass diffusivities $D_{r(i)}$ and $D_{\theta(i)}$. We note that standard effective medium theories[1–3] do not consider concentration discontinuities at the interfaces since they are formulated considering the gradient of concentration as the driving force, restricting all studies to metamaterial devices made of materials with similar solubilities[11].

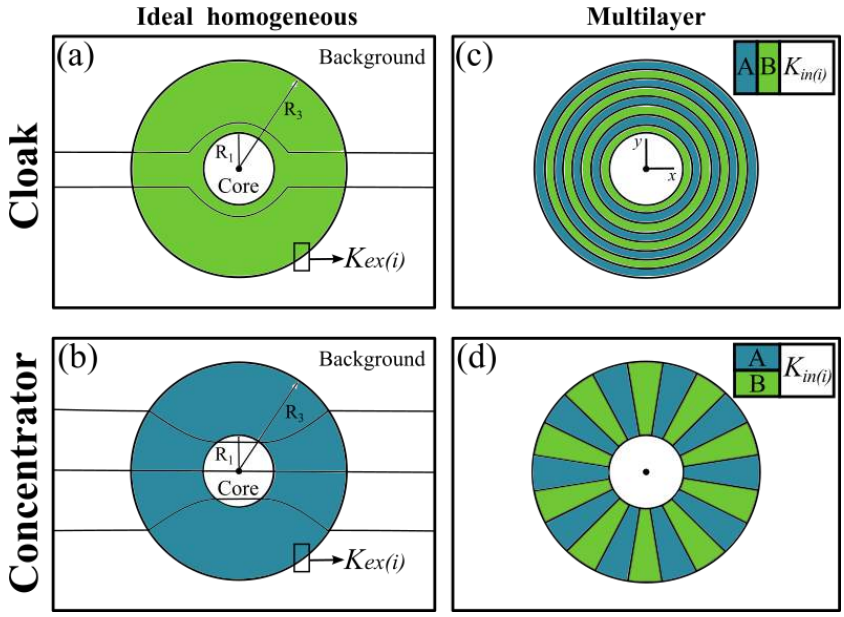

Figure 4.1. Schematic representation for mass diffusion metamaterial devices. Ideal (i.e. homogeneous and isotropic) cloaking (a) and concentrator (b) shells with internal radius R_1 and external radius R_3. (c) and (d) Multilayer metamaterial shells that reproduce the anisotropic properties of the corresponding ideal metamaterials.

In this chapter, we consider a general effective medium theory formulated based on the chemical potential as the driving force for diffusion[5,6,15,16,23–27] where the effects of both *diffusivity* and *concentration discontinuity* at interfaces are taken into account. The effective radial and azimuthal mass diffusivities are given by Eq. (4.1) and the effective solubility by Eq. (4.2)[6,15,25]

$$\left\langle \frac{D_{r(cn)(i)} | D_{\theta(cl)(i)}}{D_{bg(i)}} \right\rangle = \frac{1}{(f_1 + f_2 k_{in(i)})} \left(f_1 \frac{D_{1(i)}}{D_{bg(i)}} + f_2 k_{in(i)} \frac{D_{2(i)}}{D_{bg(i)}} \right); \quad \frac{1}{\left\langle \frac{D_{\theta(cn)(i)} | D_{r(cl)(i)}}{D_{bg(i)}} \right\rangle} = (f_1 + f_2 k_{in(i)}) \left(\frac{f_1}{\frac{D_{1(i)}}{D_{bg(i)}}} + \frac{f_2}{k_{i\_in} \frac{D_{2(i)}}{D_{bg(i)}}} \right) \quad (4.1)$$

$$S_{mm(i)} = f_1 S_{1(i)} + f_2 S_{2(i)} \quad (4.2)$$

In this formulation, concentration discontinuities at interfaces are described by the partition coefficient $k_{(i)}$, which is defined as the ratio of the concentrations $C_{(i)}$ (or solubilities $S_{(i)}$) of compound *i* in materials *1* and *2* at opposite sides of an interface[5,25,28]

$$k_{in(i)} = \frac{S_{2(i)}}{S_{1(i)}} = \frac{C_{2(i)}}{C_{1(i)}}; \quad k_{ex(i)} = \frac{S_{bg(i)}}{S_{mm(i)}} = \frac{C_{bg(i)}}{C_{mm(i)}} \quad (4.3)$$

where $k_{in(i)}$ corresponds to discontinuities in concentration at interfaces between materials *1* and *2* within the metamaterial shell, and $k_{ex(i)}$ corresponds to concentration discontinuities at the interface between the background material (*bg*) and the metamaterial shell (*mm*). Note that when $k_{in(i)}$=1, Eq. (4.1) reduces to a standard effective medium approach for conduction. Importantly, the role of concentration discontinuities on the performance of mass diffusion metamaterial devices has not been investigated.

4.3 Results and discussion

We study and design the diffusion of a compound *i* within metamaterial devices embedded in an isotropic and homogeneous background. Without losing generality we assume a background diffusivity $D_{bg(i)}$=1 cm^2/s. The system consists of a square

background material of side L=8 cm in which a metamaterial shell of internal radius R_1=1 cm and external radius R_3=3 cm is embedded (Figure 4.1). An external horizontal mass flux is established by imposing concentrations C_L=1 mol/m^3 and C_R=0 mol/m^3 on the left and right boundaries, respectively, and no flux across the top and bottom boundaries. We first study ideal (i.e. homogeneous and anisotropic) cloak and concentrator metamaterial devices for which the anisotropic mass diffusivity is $D_{r(cl)(i)}/D_{bg(i)}$=1/10, $D_{r(cn)(i)}/D_{bg(i)}$=10, and $(D_{\theta(i)}/D_{bg(i)}) = \left(D_{r(i)}/D_{bg(i)}\right)^{-1}$. In this ideal case, concentration discontinuities occur only at the interfaces between the metamaterial shell and the background material. We establish the role of such concentration discontinuity on the performance of mass diffusion metamaterials. Figures 4.2(a)-(j) shows the steady-state spatial distribution of compound concentration $C_{(i)}$ both for cloaking (upper panels) and concentrators (lower panels) metamaterials where $k_{ex(i)}$ ranges from 1/10 to 10. Note that for $k_{ex(i)}$>1, we have $S_{bg(i)} > S_{mm(i)}$, and the "affinity" of the compound for the metamaterial is low and only a small amount of compound i diffuses through the cloak or concentrator (blue/light-blue colors). Contrarily, when $k_{ex(i)}$<1, we have $S_{mm(i)} > S_{bg(i)}$ and high concentration levels develop within the shells (red/yellow colors). In the latter case, the concentration in the metamaterial shell can be higher than that at the left boundary, a phenomenon with no equivalence in heat transport clearly showing the fundamental differences between heat and mass diffusion. We study the disturbance of the external field and the concentration gradient at the core as a function of $k_{ex(i)}$ in Figure 4.2(k)-(n). We calculate the spatial standard deviation of the concentration along the vertical line x=–1.05R_3, $-L/2<y<L/2$ outside the metamaterial (Figure 4.2(k) and 4.2(l)), and the relative concentration gradient averaged along the central horizontal line within the core $-R_1<x<R_1$, y=0 and

normalized with respect to the external gradient (Figure 4.2(m) and 4.2(n)). Since cloaks divert the flux around the core, the concentration gradient within the core is nearly zero (Figure 4.2(m)). In contrast, concentrators focus the flux towards the core and the gradient in the core is increased with respect to the external gradient (Figure 4.2(n)). Note that the standard deviation and the concentration gradient at the core strongly depend on the concentration discontinuity at the metamaterial surface. Insets in Figure 4.2 show the effects of $k_{ex(i)}$ on the concentration profiles along a vertical (Figure 4.2(k) and 4.2(l)) and a horizontal (Figure 4.2(m) and 4.2(n)) line passing through the center of the core. For both cloaks and concentrators the standard deviation of the concentration reaches a minimum when $k_{ex(i)}=1$, i.e. $S_{bg(i)} = S_{mm(i)}$ (Figure 4.2(k) and 4.2(l)), which is in agreement with the insets where the concentration is essentially constant for $k_{ex(i)}=1$ (Note that for $k_{ex(i)}\neq1$, the concentration profile assumes a bell shape). This means that in order to minimally disrupt the external concentration field (i.e. minimize standard deviation of the concentration), it is required that $S_{bg(i)} = S_{mm(i)}$. However, the concentration gradient at the core is neither maximal nor minimal for $S_{bg(i)} = S_{mm(i)}$. For a cloak, lower concentration gradients are achieved for $k_{ex(i)}>>1$ or $k_{ex(i)}<<1$, while for a concentrator, a higher concentration gradient is obtained for $k_{ex(i)}<1$. Note that the minimal standard deviation for the external field and the optimal concentration gradient (minimal for cloaks, maximal for concentrators) do not occur at the same value of $k_{ex(i)}$. These results demonstrate that having different background and metamaterial solubilities (i.e. $k_{ex(i)}\neq1$) is an important physical factor that needs to be accurately incorporated when designing mass diffusion metamaterial devices.

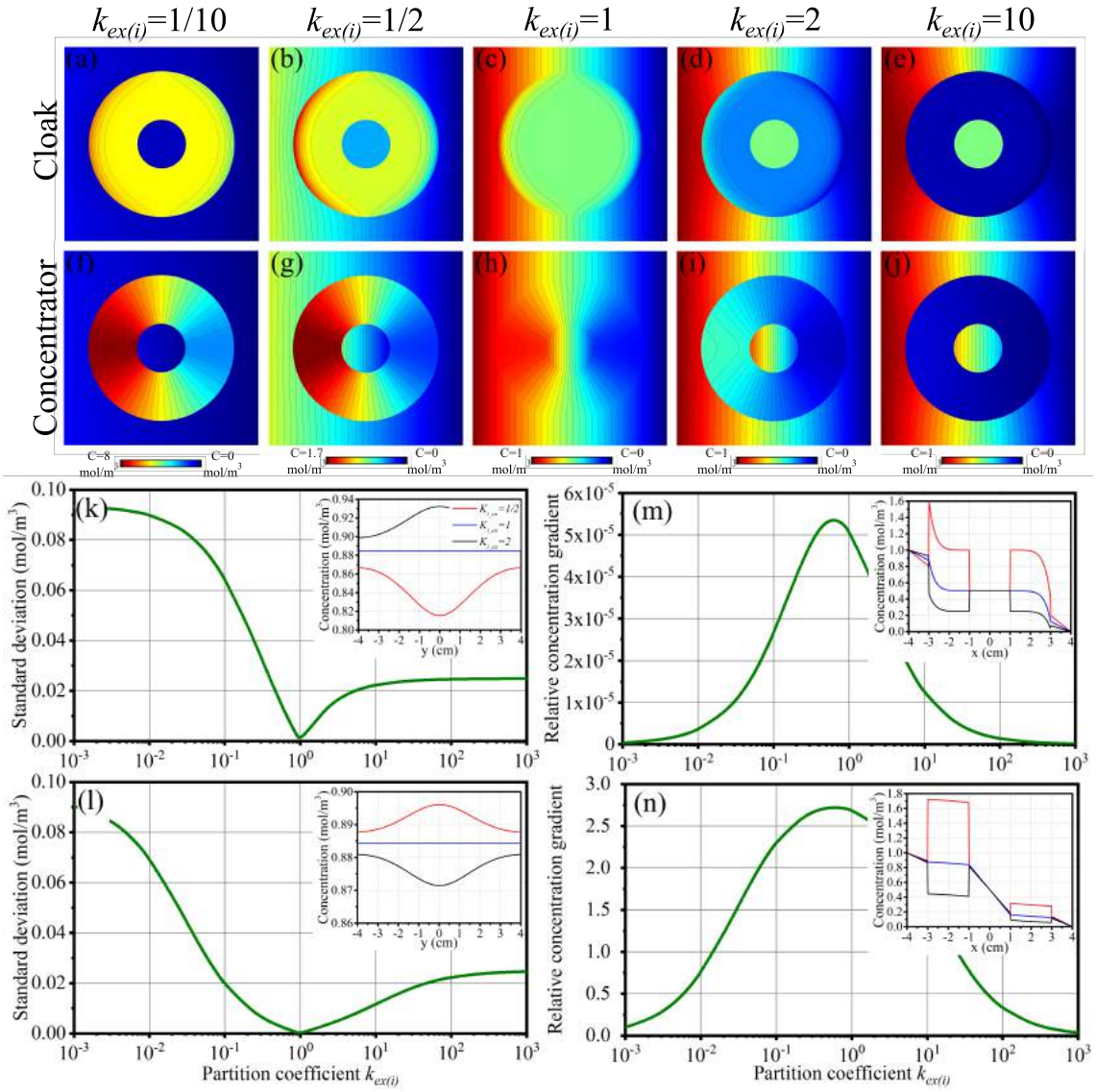

Figure 4.2. Color maps of the concentration profiles for homogeneous and isotropic mass diffusion metamaterials ($D_{r(cl)(i)}/D_{bg(i)}$=1/10, $D_{r(cn)(i)}/D_{bg(i)}$=10, ($D_{r(i)}/D_{bg(i)}$)($D_{\theta(i)}/D_{bg(i)}$)=1) for different external partition coefficient $k_{ex(i)}$=1/10, 1/2, 1, 2, 10. (a)-(e) Cloaks. (f)-(j) Concentrators. Standard deviation for cloak (k) and concentrator (l) and relative concentration gradient for cloak (m) and concentrator (n) as a function of the external partition coefficient $k_{ex(i)}$. Insets show concentration profiles along a vertical line outside the metamaterial device x=–1.05R_3, $-L/2<y<L/2$ (k),(l) and relative concentration gradient along the horizontal line y=0, $-L/2<x<L/2$ (m), (n).

Since homogeneous anisotropic metamaterials are difficult to obtain in practice, we next study cloaks and concentrators made of two homogeneous and isotropic layered materials *1* and *2* which reproduce the diffusivities of the homogeneous and anisotropic systems[17–20]. Since layered metamaterials can have different solubilities due to the different component materials, the role of concentration discontinuities at the interfaces between materials *1* and *2* needs to be investigated. For consistency, we maintain $D_{r(cl)(i)}/D_{bg(i)}$=1/10 and $D_{r(cn)(i)}/D_{bg(i)}$=10 for the layered metamaterials. For simplicity, we choose f_1=f_2=0.5 and the number of bilayers is N=36 to ensure effective medium response[4]. To separately analyze the effects of concentration discontinuities at internal surfaces, we consider $k_{ex(i)}$=1. We calculate the required material diffusivities $D_{1(i)}$ and $D_{2(i)}$ and solubilities $S_{1(i)}$ and $S_{2(i)}$ by following two different approaches. In the first approach, it is assumed that all solubilities are equal (i.e. $k_{in(i)}$=$k_{ex(i)}$=1) and Eqs (4.1) are used to find $D_{1(i)}$ and $D_{2(i)}$, this strategy has been commonly used in the literature to study and design mass diffusion metamaterials[2–4,11,12]. Assuming that the partition coefficients are equal to one means that the concentration gradient can be considered as the driving force[5], hence we will refer to this approach as effective medium approach based on concentration gradient (EMA-∇C). The second approach uses the general effective medium approach based on the chemical potential (EMA-$\nabla\mu$)[6,15,25], in this case Eqs (4.1)-(4.3) are solved simultaneously yielding both the required solubilities and diffusivities for the materials. We show in Figure 4.3 the color maps for the predicted concentration profiles under the assumption $k_{in(i)}$=$k_{ex(i)}$=1 (EMA-∇C approach) (Figure 4.3(a), cloak and 4.3(g), concentrator) and compare them against the observed concentration profiles

when the constituent materials calculated using the EMA-∇C approach possess different solubilities ($k_{in(i)} \neq 1$) (Figure 4.3(b)-4.3(f), cloak and 4.3(h)-(l), concentrator). We can see that neglecting differences in solubilities can lead to significant inaccuracies for the concentration profiles. Furthermore, the disturbance of the external concentration (Figure 4.3(m) and 4.3(n)) and relative concentration gradient (Figure 4.3(o) and 4.3(p)) designed by the EMA-∇C approach (red line) are significantly different to the observed values (orange line). In contrast, when the EMA-$\nabla \mu$ approach is used, the designed and obtained concentration profiles, gradients, and standard deviations are in agreement. In this approach, the discontinuities in mass concentrations at the interfaces are accurately incorporated in the formulation. The agreement can be seen in Figure 4.3(m)-(p) where the standard deviation and concentration gradients for the general EMA-$\nabla \mu$ approach (blue squares) agree with the designed values for all $k_{in(i)}$. The color maps for the realistic concentrations profiles using EMA-$\nabla \mu$ which include discontinuities at the interfaces and satisfy the conditions $D_{r(cl)(i)}/D_{bg(i)}=1/10$, $D_{r(cn)(i)}/D_{bg(i)}=10$ are shown in Figure 4.4. Our results demonstrate that a general effective medium approach formulated based on the chemical potential as the driving force is required in order to rationally design metamaterials for general and realistic cases where the chemical species solubility is not constant throughout the system.

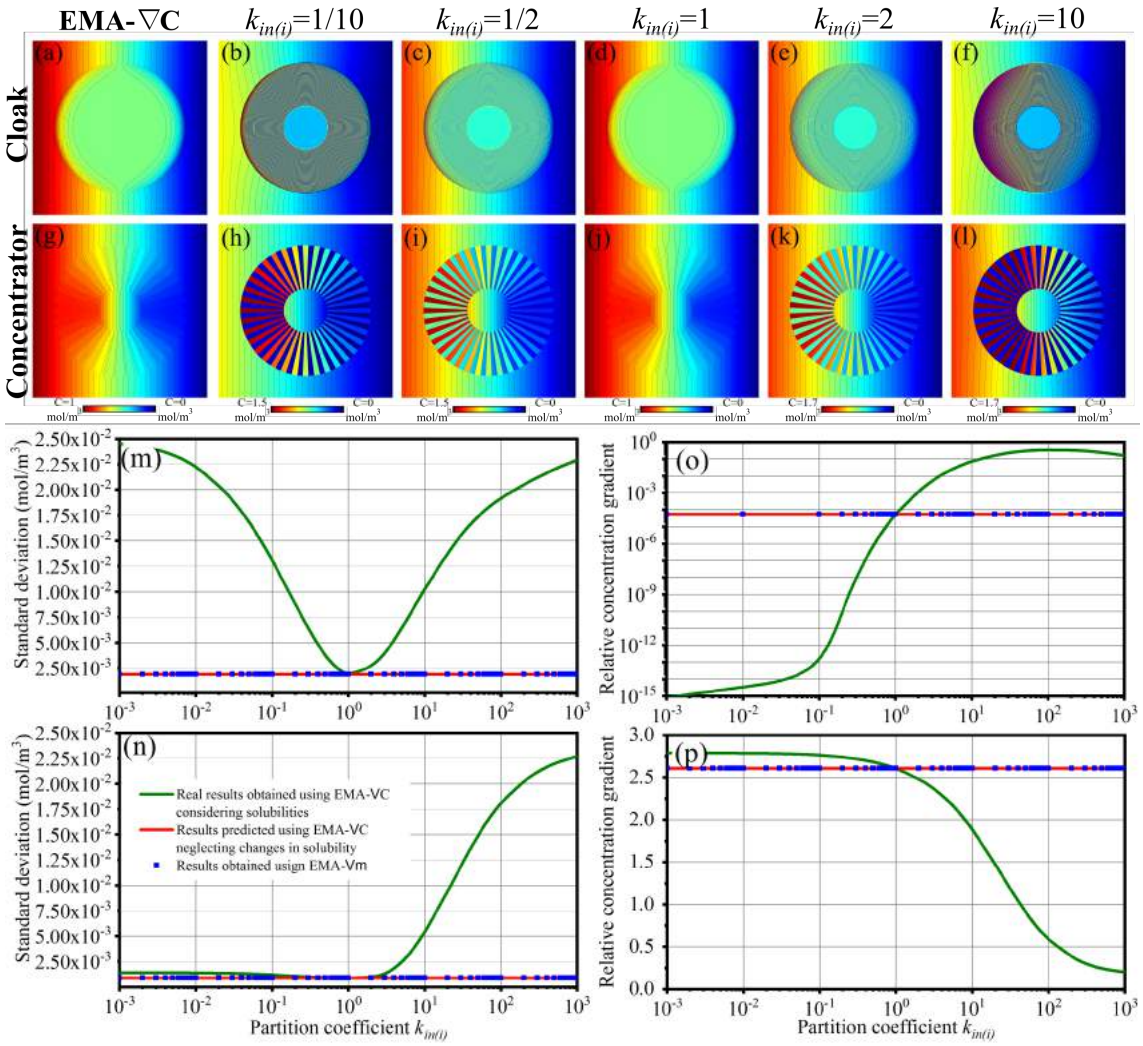

Figure 4.3. (a) and (g) Color maps for the predicted concentration of layered mass diffusion metamaterial shells under the assumption $k_{in(i)}=k_{ex(i)}=1$ (EMA-∇C approach) for a cloak and a concentrator, respectively ($D_{r(cl)(i)}/D_{bg(i)}$=1/10, $D_{r(cn)(i)}/D_{bg(i)}$=10, ($D_{r(i)}/D_{bg(i)}$)($D_{\theta(i)}/D_{bg(i)}$)=1). (b)-(f) and (h)-(l) Actual concentration profiles when the constituent materials calculated using the EMA-∇C approach possess solubilities $k_{in(i)}$ =1/10, 1/2, 1, 2, and 10. (m)-(p) Standard deviation and relative concentration gradient calculated using the EMA-∇C approach (designed EMA-∇C), the actual values when discontinuities at interfaces are present (actual EMA-∇C), and the values obtained when using EMA-$\nabla\mu$. (m),(o) Cloak. (n),(p) Concentrator.

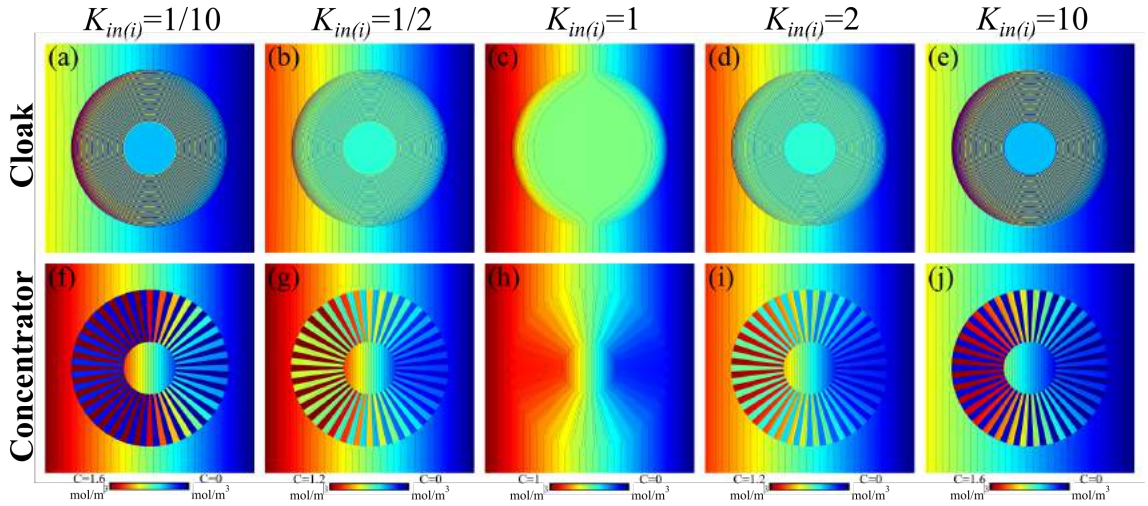

Figure 4.4. Concentration profiles in layered metamaterials designed using the EMA-$\nabla\mu$ for different internal partition coefficients $k_{in(i)}$. (a)-(e) Cloaks. (f)-(j) Concentrators.

4.4 Conclusions

In this chapter we introduced a general approach to study and design mass diffusion in coordinate-transformation metamaterial devices that incorporates the effects of concentration discontinuities at interfaces due to differences in material solubilities. Our approach takes into account the mass concentration discontinuities by means of partition coefficients and it is based on an effective medium theory derived using the chemical potential (rather than the concentration) as driving force for diffusion. We found that concentration discontinuities have a significant impact on the performance and design of metamaterial devices and must therefore be carefully considered when designing mass diffusion metamaterials in order to properly describe the transport process and select constituent materials. The results in this chapter contribute to fundamentally understand the physical principles behind mass diffusion in metamaterials and to improve and enable the design of metamaterials as components of functional devices.

4.4 References

(1) Guenneau, S.; Petiteau, D.; Zerrad, M.; Amra, C.; Puvirajesinghe, T. Transformed Fourier and Fick Equations for the Control of Heat and Mass Diffusion. *AIP Adv.* **2015**, *5* (5), 053404.

(2) Guenneau, S.; Puvirajesinghe, T. M. Fick's Second Law Transformed: One Path to Cloaking in Mass Diffusion. *J. R. Soc. Interface* **2013**, *10* (83), 20130106.

(3) Zeng, L.; Song, R. Controlling Chloride Ions Diffusion in Concrete. *Sci. Rep.* **2013**, *3*, 3359.

(4) Restrepo-Flórez, J. M.; Maldovan, M. Rational Design of Mass Diffusion Metamaterial Concentrators Based on Coordinate Transformations. *J. Appl. Phys.* **2016**, *120* (8), 084902.

(5) Davis, H. T. The Effective Medium Theory of Diffusion in Composite Media. *J. Am. Ceram. Soc.* **1977**, *60* (11–12), 499–501.

(6) Zhang, Y.; Liu, L. On Diffusion in Heterogeneous Media. *Am. J. Sci.* **2012**, *312* (9), 1028–1047.

(7) Seader, J. D.; Henley, E. J.; Roper, D. K. *Separation Process Principles-Chemical and Biochemical Operations*, 3rd Ed.; John Wiley & Sons, Inc.: United States of America, 2011.

(8) Seader, J. D.; Henley, E. J.; Roper, K. D. *Separation Process Principles*, 3rd Ed.; John Wiley & Sons:New York, Inc., 2011.

(9) Deen, W. M. *Analysis of Transport Phenomena*, Second.; Oxford University Press: New York, 2013.

(10) Singh, T.; Kang, D. Y.; Nair, S. Rigorous Calculations of Permeation in Mixed-Matrix Membranes: Evaluation of Interfacial Equilibrium Effects and Permeability-Based Models. *J. Memb. Sci.* **2013**, *448*, 160–169.

(11) Restrepo-Flórez, J. M.; Maldovan, M. Mass Separation by Metamaterials. *Sci. Rep.* **2016**, *6* (2), 21971.

(12) Restrepo-Flórez, J.-M.; Maldovan, M. Metamaterial Membranes. *J. Phys. D. Appl. Phys.* **2017**, *50*, 25104.

(13) Zeng, L.; Song, R.; Zhao, Y.; Zhao, Z. Experimental Measure Mass Diffusion Transparency. *Solid State Commun.* **2014**, *186*, 23–27.

(14) Davis, H. T.; Velencourt, I. R.; Johnson, C. E. Transport Processes in Composite Media. *J. Am. Cer. Soc.* **1975**, *58* (9), 446–452.

(15) Belova, I. V.; Murch, G. E. Diffusion in Nanocrystalline Materials. *J. Phys. Chem. Solids* **2003**, *64*, 873–878.

(16) Belova, I. V; Murch, G. E. Analysis of the Effective Diffusivity in Nanocrystalline Materials. *J. Metastable Nanocrystalline Mater.* **2004**, *19*, 25–34.

(17) Hu, R.; Wei, X.; Hu, J.; Luo, X. Local Heating Realization by Reverse Thermal Cloak. *Sci. Rep.* **2014**, *4* (January), 3600.

(18) Han, T.; Yuan, T.; Li, B.; Qiu, C.-W. Homogeneous Thermal Cloak with Constant Conductivity and Tunable Heat Localization. *Sci. Rep.* **2013**, *3* (April), 1593.

(19) Guenneau, S.; Amra, C.; Veynante, D. Transformation Thermodynamics: Cloaking and Concentrating Heat Flux. *Opt. Express* **2012**, *20* (7), 8207–8218.

(20) Narayana, S.; Sato, Y. Heat Flux Manipulation with Engineered Thermal Materials. *Phys. Rev. Lett.* **2012**, *108* (21), 214303.

(21) Han, T.; Bai, X.; Liu, D.; Gao, D.; Li, B.; Thong, J. T. L. Manipulating Steady Heat Conduction by Sensu-Shaped Thermal Metamaterials. *Sci. Rep.* **2015**, *5* (May), 10242.

(22) Han, T.; Zhao, J.; Yuan, T.; Lei, D. Y.; Li, B.; Qiu, C.-W. Theoretical Realization of an Ultra-Efficient Thermal-Energy Harvesting Cell Made of Natural Materials. *Energy Environ. Sci.* **2013**, *6* (12), 3537.

(23) Barrer, R. M.; Petropoulos, J. H. Diffusion in Heterogeneous Media: Lattices of Parallelepipeds in a Continuous Phase. *Br. J. Appl. Phys.* **1961**, *12* (12), 691–697.

(24) Ash, R.; Barrer, R. M.; Petropoulus, J. H. Diffusion in Heterogeneous Media - Properties of a Laminated Slab. *Br. J. Appl. Phys.* **1963**, *14* (12), 854–862.

(25) Sax, J.; Ottino, J. M. Modeling of Transport of Small Molecules in Polymer Blends: Application of Effective Medium Theory. *Polym. Eng. Sci.* **1983**, *23* (1 l), 165–176.

(26) Zimmerman, C. M.; Singh, A.; Koros, W. J. Tailoring Mixed Matrix Composite Membranes for Gas Separations. *J. Memb. Sci.* **1997**, *137* (1–2), 145–154.

(27) Van Siclen, C. D. Effective Diffusivity of Solute in Multiphase Materials with Segregation. *J. Phys. Chem. Solids* **2004**, *65* (6), 1199–1200.

(28) Wijmans, J. G.; Baker, R. W. The Solution-Diffusion Model: A Review. *J. Memb. Sci.* **1995**, *107* (1–2), 1–21.

CHAPTER 5: TAILORING THE DIFFUSION OF A BINARY MIXTURE: A FIRST STEP TOWARD DESIGNING METAMATERIALS FOR MASS SEPARATIONS[1]

5.1 Introduction

In this chapter, we introduce a novel physical principle for mass separation using transformation based[1] mass-diffusion metamaterials. The designed metamaterials are able to sort the chemical species in an arbitrary binary mixture by controlling their flux direction such that different species are induced to follow different trajectories. These metamaterials provide the basis for a new approach to manipulate mass diffusion and achieve separations in biomedical, biophysics, and chemical applications. We employ coordinate transformations to the Fick's law equation to simultaneously manipulate the diffusion paths of different species in both transient and steady state regimes[2–5]. The design of an ideal, non-homogeneous, anisotropic mass-separator metamaterial device is first introduced. We next present a design strategy that allows for the experimental realization of such metamaterial using homogeneous isotropic materials. The simultaneous metamaterial manipulation of two different chemical species has not been reported in the literature. This is the first attempt to achieve mass separations using metamaterials devices in chemical and biomolecular science and technology.

[1] Portions of this chapter have been published in: "Restrepo-Flórez, J.M.; Maldovan, M.; Mass separation by metamaterials. *Sci Rep.* ***2016,*** 6 (1), 21971"

5.2 Theoretical approach

Let us consider an arbitrary dilute binary mixture consisting of species *A* and *B* diffusing in a background medium with diffusion coefficient $D_{bg(i)}$. Since, in a dilute solution, diffusion of *A* is independent of diffusion of *B*, we propose a metamaterial structure that acts as a cloak for species *A* and simultaneously as a concentrator for species *B*. The key concept in the design of such metamaterial structure is that the cloaking effects on *A* will not have a significant impact on the diffusion of *B*, while the concentrating effects on *B* will not have a significant influence on *A*. We thus perform two different coordinate transformations in the same spatial domain (each related to one of the compounds of interest (Figure 5.1)) in order to direct *A* and *B* to different spatial locations

$$\frac{D_{r(cl)(i)}}{D_{bg(i)}} = \frac{r'-R_1}{r'}; \quad \frac{D_{\theta(cl)(i)}}{D_{bg(i)}} = \frac{r'}{r'-R_1} \ (\textit{cloak-species A}) \tag{2.7}$$

$$\frac{D_{r(cn)(i)}}{D_{bg(i)}} = \frac{r'-R_3\left(\frac{R_1-R_2}{R_3-R_2}\right)}{r'}; \quad \frac{D_{\theta(cn)(i)}}{D_{bg(i)}} = \frac{r'}{r'-R_3\left(\frac{R_1-R_2}{R_3-R_2}\right)} \ (\textit{concentrator-species B}) \tag{2.9}$$

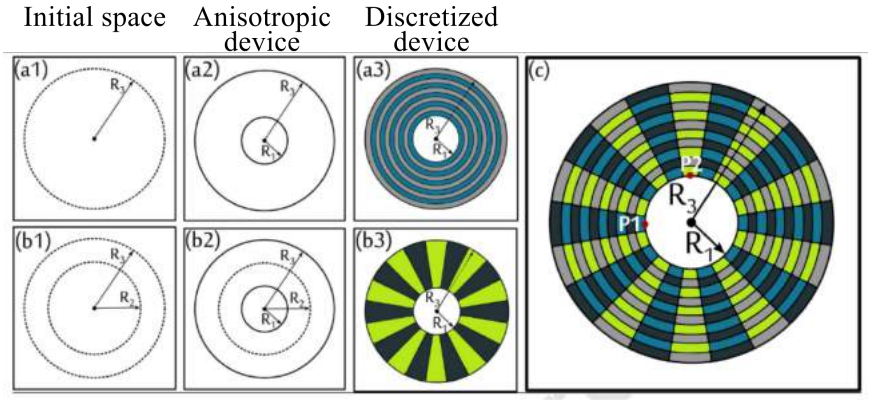

Figure 5.1. (a) Cloaking: A point is transformed into a circle of radius R_1 while the adjacent region is compressed. The experimental realization is obtained by a multilayer a structure made of concentric rings (b) Concentrator: Compression of a circular region $0<r<R_2$ into $0<r<R_1$ followed by expansion of the adjacent annulus from R_2 to R_1. The experimental realization is obtained by a lamellar structure (c) Bi-functional multilayer device: the design requires four materials: dark blue, grey, light blue, and light green.

5.3 Results and discussion

As an initial proof of concept we select the relative radial diffusivities (i.e. $D_{r(i)}/D_{bg(i)}$) to be 0.1 and 10 in the proposed metamaterial shell for the cloaked and concentrated species, respectively. The azimuthal diffusivities are calculated using Eq. (3.3)[6,7] such that $D_{\theta(i)}D_{r(i)} = D_{bg(i)}^2$. The spatial domain consists of a square of side 0.8 mm and the external and internal cloaking shell radius are R_3=0.3mm and R_1=0.1mm, respectively. We have assumed that the solubility of species *A* and *B* is constant thought the system. Results for the unperturbed concentration gradients without the metamaterial (Figures 5.2-5.3 (a-e)) and the concentration profiles of species *A* (cloaked) and species *B* (concentrated) are shown in Figures 5.2-5.3 (f-j), respectively. The metamaterial device controls the trajectory of species *A* and *B* both in transient and steady-state. A near zero concentration gradient for the cloaked species (*A*) is observed inside the device all along the process (Figure 5.4(c)). On the other hand, a larger concentration gradient is observed for the concentrated species (*B*) (Figure 5.4(d)). Comparison between concentration fields in the presence (Figures 5.2-5.3 (f-j)) and absence (Figures 5.2-5.3 (a-e)) of the metamaterial reveals that for both species the field outside the device remains largely undisturbed (Figures 5.2-5.3 (g-j)) except at early stages (Figures 5.2-5.3 (f)).

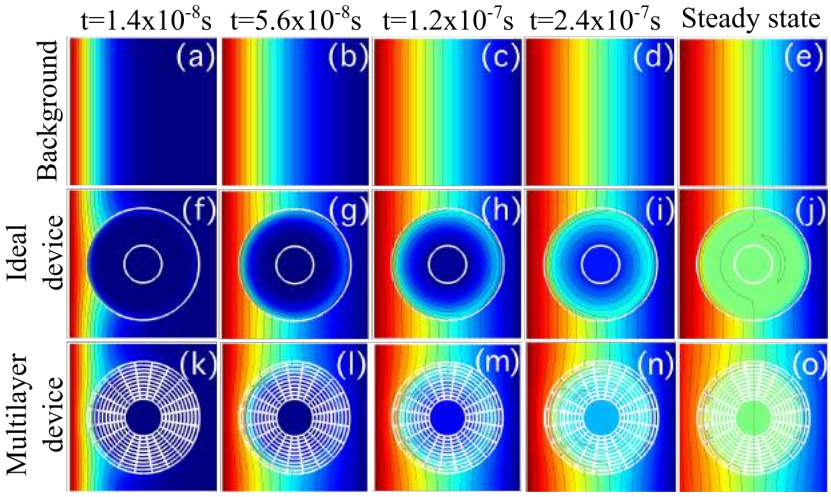

Figure 5.2. Concentration profiles for *cloaked* compound A at different times and steady-state. (a-e), background media without metamaterial. (f-j) Anisotropic homogeneous cloak. (k-o) Multilayer cloaking device.

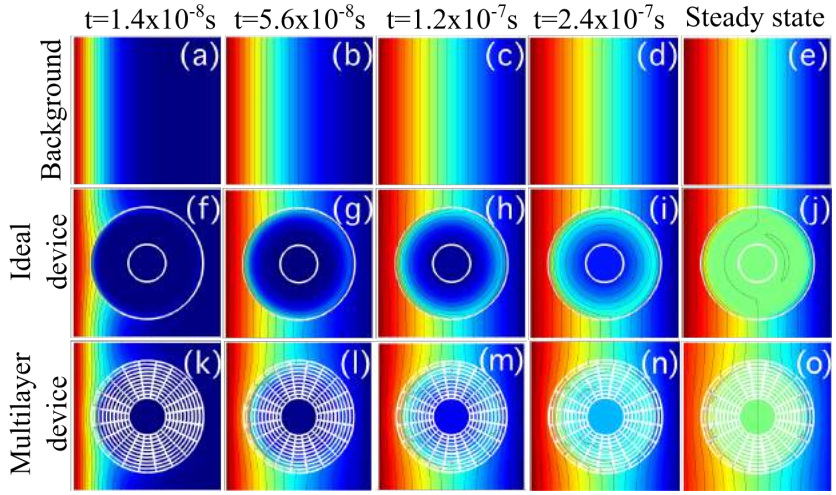

Figure 5.3. Concentration profiles for *concentrated* compound B at different times and steady-state. Insets (a-e), background media without metamaterial. (f-j) Anisotropic homogeneous concentrator. (k-o) Multilayer concentrator device.

Although these results provide the basis for mass separation by metamaterials, the requirements in terms of diffusion-coefficient anisotropy are difficult to fulfill experimentally. We thus propose a simple scheme that provides the prescribed anisotropy

for simultaneous mass cloaking of (A) and concentration of (B) by using four isotropic materials. It is important to note that the solubility of (A) and (B) within these four materials is considered to be constant. A stack of layered materials with different diffusivities creates a system of resistors in parallel (longitudinal direction) and in series (perpendicular direction) in which the spatial anisotropy can be controlled[8,9]. For a *cloak*, resistors are required in parallel along the azimuthal direction and in series along the radial direction. A structure made of concentric rings with alternating diffusivities, as shown in Figure 5.1(a), satisfies such requirement. Contrarily, for a *concentrator*, resistors are in parallel along the radial direction and in series along the azimuthal direction. A lamellar structure as shown in Figure 5.1(b) is thus required. Note the contrary requirements for a cloak or a concentrator in terms of the alignment of the layered materials. Effective medium approaches (assuming constant solubility) show that the radial and azimuthal diffusivities for bi-layered materials are given by $1/D_{\theta(i)} = f_1/D_{1(i)} + f_2/D_{2(i)}$, $D_{r(i)} = f_1 D_{1(i)} + f_2 D_{2(i)}$, where $D_{1(i)}$ and $D_{2(i)}$ are the diffusivities of the homogeneous isotropic materials and f_1 and f_2 are their volume fractions. Note that although the same equations apply, radial and azimuthal diffusivities must be flipped in a concentrator with respect to a cloak.

We apply the discretization procedure described above to the diffusivity tensors of species A and B. In doing so, one must consider four constrains imposed by the effective medium solutions for cloaked and concentrated species. Thus the minimum number of isotropic materials that will satisfy these constrains is four. One arrangement that yields the desired results is presented in Figure 5.1(c). Note that this metamaterial structure consists of simultaneous concentric rings and adjacent lamellae. The idea

behind the design of such metamaterial is that the diffusivity for the cloaked species is constant in the azimuthal direction, and for the concentrated species is constant in the radial direction. For simulations, 10 concentric layers were used in the radial direction and 20 layers in the azimuthal direction. The relative diffusivities of the homogeneous materials were calculated by the effective medium approach using radial and azimuthal diffusivities $D_{r(i)}$ and $D_{\theta(i)}$ determined in the previous section. Without losing generality, we consider volume fractions f_1=f_2=0.5. The material diffusivities are $D_{1(A)}$=$D_{2(A)}$ =19.95, $D_{3(A)}$=$D_{4(A)}$=0.05, $D_{1(B)}$=$D_{3(B)}$=19.95, $D_{2(B)}$=$D_{4(B)}$=0.05. The concentration profiles for species *A* and *B* are shown in Figures 5.2-5.3 (k-o). From the plots, it is clear that both cloaking and concentrating effects for *A* and *B* respectively are simultaneously achieved. Some small disturbances in the iso-concentration lines are observed as a consequence of the discretization procedure. However, the performance of the multilayer device can be improved by increasing the number of layers. Figures 5.2-5.3 show that it is thus possible to construct a bi-functional metamaterial device that simultaneously controls the diffusion paths of two different species, cloaking *A* while focusing *B*, using *homogeneous isotropic* materials.

Time-dependent concentration for species *A* and *B* at two different locations (points 1 and 2 in Figure 5.1) are shown in Figures 5.4(a) and 5.4(b) for both ideal and multilayer designs. Three conclusions can be stated: first, the performance of the ideal device is comparable to that of the multilayer device for both cloaked and concentrated species; however, when comparing ideal and multilayer devices there are slight differences in the concentrations at the beginning of the process and the multilayer cloak reaches the steady-state regime faster than the ideal device. Second, when comparing

concentrations at the two different locations, it is clear that for the cloaked species *A* the concentration is constant. On the other hand, for the concentrated species *B*, it is observed, at steady-state, a concentration difference of around 80% between the two points evaluated. Finally, the steady-state regime is reached faster in the case of the concentrated species than in the case of the cloaked species. Figures 5.4(c) and 5.4(d) show the time-dependence of the concentration gradient at the core of the metamaterial device for cloaked and concentrated species, from which the transient performance can be evaluated. For the cloaked species (Figure 5.4(c)), the internal concentration gradient – for ideal and multilayer cases – is approximately zero during the entire experiment. In addition, in the case of the concentrated species (Figure 5.4(d)), the concentration gradient in the device is always greater than that in the background media (without metamaterial). Importantly, the differences in concentration for species *A* and *B* can be employed for the design of metamaterial devices with applications in chemical and biophysical separations. The metamaterial design presented achieves separation of species *A* and *B*, provided that that the differences in concentration gradient for the species at the core is large, a physical effect that can be exploited to design separation processes.

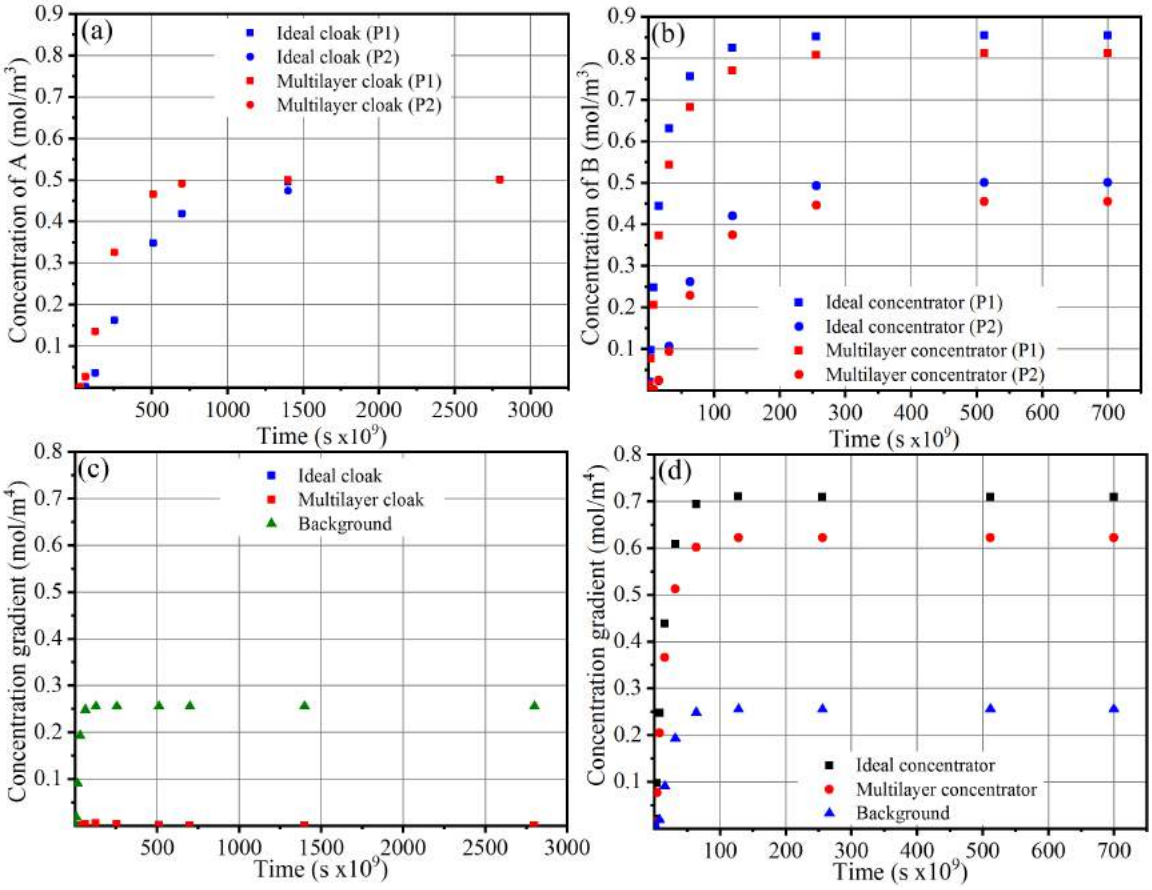

Figure 5.4. (a) (b) Concentration values at two different locations inside the mass-separator device (locations are highlighted in Figure 5.1(c) with numbers 1 and 2) as a function of time for cloaked and concentrated species, respectively. (c) (d) Concentration gradients inside the bi-functional device for cloaked and concentrated species.

We note that replacing the structure by a single isotropic material is less efficient for separation. Using a single material, the optimal field distribution to obtain separation in the core at steady-state will be having a zero gradient for *A*, and the external gradient for *B* (or vice versa). Even such a configuration is less efficient than our design. In our results, the concentration gradient for *B* in the core is larger than the external gradient due to concentration effects, providing larger separation efficiency. This difference in efficiency arises from the fact that a single isotropic material cannot shield *A* and concentrate *B* at the same time. In addition, if we consider the transient regime, a layered

structure can be better to protect a region from a diffusing compound than a single material[10]. Although heat and mass diffusion can be described by similar equations it should be noted that simultaneous manipulation of two or more species is only possible in mass diffusion, this kind of treatment is different from previous results reported in the case of heat transport[7,8,11–14] where cloaking or concentrating have been reported, note that these two effects cannot be achieved simultaneously in the case of heat.

5.4 Conclusions

In this chapter, we introduced a new physical approach to rationally design mass-separator metamaterial devices that can cloak one molecular species while concentrate another, enabling the development of the first metamaterial for sorting molecular compounds. Moreover we proved that there exists a feasible geometric metamaterial configuration to achieve such effects using isotropic homogeneous materials. It is important to note that the proposed approach considers similar material solubilities. More generally, mass concentration can be discontinuous at interfaces due to the different solubilities. A general solution requires the application of the concepts developed in Chapter 4. A complete treatment extending the above concepts for the manipulation of two chemical species in separations is presented in Chapters 7-10. The simultaneous control of the diffusion of chemical species is extremely relevant in biophysics, biomolecular, and chemical science and technology, both in separation and catalysis processes. The concept of mass separation by metamaterials introduced here thus provides an important tool to control the diffusion paths of chemical and biomolecular species, opening the opportunity for the simultaneous manipulation of different molecular species.

5.5 References

(1) Pendry, J. B.; Schurig, D.; Smith, D. R. Controlling Electromagnetic Fields. *Science.* **2006**, *312* (5781), 1780–1782.

(2) Guenneau, S.; Petiteau, D.; Zerrad, M.; Amra, C.; Puvirajesinghe, T. Transformed Fourier and Fick Equations for the Control of Heat and Mass Diffusion. *AIP Adv.* **2015**, *5* (5), 053404.

(3) Guenneau, S.; Amra, C.; Veynante, D. Transformation Thermodynamics: Cloaking and Concentrating Heat Flux. *Opt. Express* **2012**, *20* (7), 8207–8218.

(4) Guenneau, S.; Puvirajesinghe, T. M. Fick's Second Law Transformed: One Path to Cloaking in Mass Diffusion. *J. R. Soc. Interface* **2013**, *10* (83), 20130106.

(5) Zeng, L.; Song, R. Controlling Chloride Ions Diffusion in Concrete. *Sci. Rep.* **2013**, *3*, 3359.

(6) Restrepo-Flórez, J. M.; Maldovan, M. Rational Design of Mass Diffusion Metamaterial Concentrators Based on Coordinate Transformations. *J. Appl. Phys.* **2016**, *120* (8), 084902.

(7) Han, T.; Yuan, T.; Li, B.; Qiu, C.-W. Homogeneous Thermal Cloak with Constant Conductivity and Tunable Heat Localization. *Sci. Rep.* **2013**, *3* (April), 1593.

(8) Narayana, S.; Sato, Y. Heat Flux Manipulation with Engineered Thermal Materials. *Phys. Rev. Lett.* **2012**, *108* (21), 214303.

(9) Ooi, E. H.; Popov, V. Thermal Invisibility through Geometrical Transformation: A Segmented Cloaking Approach. *WIT Trans. Eng. Sci.* **2012**, *75*, 39–46.

(10) Narayana, S.; Savo, S.; Sato, Y. Transient Heat Flux Shielding Using Thermal Metamaterials. *Appl. Phys. Lett.* **2013**, *102* (20), 201904.

(11) Han, T.; Bai, X.; Gao, D.; Thong, J. T. L.; Li, B. Experimental Demonstration of Bilayer Thermal Cloak. *Phys. Rev. Lett.* **2014**, *112* (5), 054302.

(12) Schittny, R.; Kadic, M.; Guenneau, S.; Wegener, M. Experiments on Transformation Thermodynamics: Molding the Flow of Heat. *Phys. Rev. Lett.* **2013**, *110* (19), 195901.

(13) Farhat, M.; Chen, P.-Y.; Bagci, H.; Amra, C.; Guenneau, S.; Alù, A. Thermal Invisibility Based on Scattering Cancellation and Mantle Cloaking. *Sci. Rep.* **2015**, *5* (9876), 9876.

(14) Maldovan, M. Sound and Heat Revolutions in Phononics. *Nature* **2013**, *503* (7475), 209–217.

CHAPTER 6: DESIGN OF A PLANAR METAMATERIAL TO SORT CHEMICAL SPECIES[1]

6.1 Introduction

In this chapter, we elaborate on the ideas presented in Chapter 5[1], where we introduced a new class of metamaterial system that can sort chemical species by rationally designing their trajectory by means of coordinate transformations[2–4] and effective medium theory[1]. Here, we apply the metamaterial principles to a physical system consisting of a planar membrane. The basic idea is to guide the diffusion paths of two different species towards opposite spatial locations. We show that by carefully designing anisotropic mass diffusivities by means of a "beam shifter" transformation[5–7] it is possible to achieve the separation of compounds as they diffuse through a metamaterial planar membrane. Our results show that coordinate transformations and metamaterial principles can be incorporated into design strategies for membrane separations with diverse geometries, leading to new functionalities and modes of operation for separations.

6.2 Theoretical approach

We start by considering the diffusion of two dilute compounds *A* and *B* in a finite slab with a concentration gradient in the *x* direction (Figure 6.1). At steady-state, the diffusion of each compound can be described by Fick's law. We divide the slab into regions I, II, and III (Figure 6.1(a)) and apply a beam-shifter transformation function (Eq. (2.10))[8,9]:

$$x' = x; \qquad y' = y + b_{(i)}(x - x_0) \tag{2.10}$$

[1] Portions of this chapter have been published in: "Restrepo-Flórez, J.M.; Maldovan, M.; Metamaterial membranes. *J. Phys D: Appl Phys.* ***2016,*** 50 (2), 025104"

to region II such that a metamaterial is embedded between the two isotropic regions I and III. Conceptually, a beam shifter transformation allows us to bend the trajectory of a flux line by an angle Φ, which is controlled by b_i. In our mass diffusion metamaterial device, the net effect of such transformation is to redirect molecules along specific spatial directions. We consider two repeating *unit cells* (Type 1 and 2) in region II, having thickness d and length L, in each of which we apply two different beam-shifter transformations (one for each compound). Specifically, in the Type 1 unit cell, the transformations redirect the flux of compound A to the right and compound B to the left, while in the Type 2 the transformations are reversed (Figure 6.1(a)). Our objective is to combine the two unit cells to redirect compounds A and B to different spatial locations after they diffuse through the metamaterial. The maximum concentration for species A will be exactly at the point where species B has its minimum and vice versa.

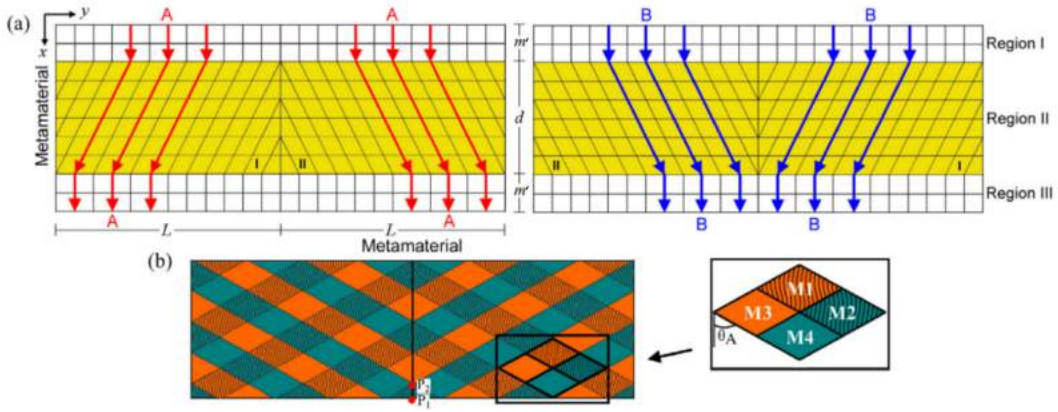

Figure 6.1. (a) Schematic of a metamaterial membrane. Due to their anisotropic properties, unit cell Type I simultaneously redirects compound A to the right and compound B to the left, while in unit cell Type II the effect is inverted. As a result, A and B are separated by guiding them to different spatial areas. (b) Design of a metamaterial membrane to achieve compound separations using four homogeneous isotropic materials. Rhomboidal elements with same color have the same diffusivity for compound B, while elements with same geometric pattern have the same diffusivity for compound A. P_1 and P_2 are representative points to study the transient behavior of the system.

The required diffusivity tensors $\overline{\overline{D}}'_{(i)}$ is given by Eq. (2.11). For each transformation, we have

$$\frac{\overline{\overline{D}}'_{(i)}}{D_{bg(i)}} = \begin{bmatrix} 1 & b_{(i)} \\ b_{(i)} & b_{(i)}^2 + 1 \end{bmatrix} \tag{2.11}$$

Note that the resultant diffusivity tensors $\overline{\overline{D}}'_{(i)}$ are homogeneous. In order to reproduce the spatial diffusivity $\overline{\overline{D}}'_{(i)}$ given by Eq. (2.11), we consider multilayer structures (made of two layered materials with different diffusivities) rotated by an angle $\theta_{(i)}$ with respect to the *x*-axis. The diffusivity tensor for such multilayer system is given by [10]

$$\begin{bmatrix} D_{\parallel(i)}\, cos^2\theta_{(i)} + D_{\perp(i)}\, sin^2\theta_{(i)} & \left(D_{\perp(i)} - D_{\parallel(i)}\right) sin\theta_{(i)}\, cos\theta_{(i)} \\ \left(D_{\perp(i)} - D_{\parallel(i)}\right) sin\theta_{(i)}\, cos\theta_{(i)} & D_{\perp(i)}\, cos^2\theta_{(i)} + D_{\parallel(i)}\, sin^2\theta_{(i)} \end{bmatrix} \tag{6.1}$$

where $D_{\parallel(i)}$and $D_{\perp(i)}$are the diffusivities of compound *i* along the principal components of the effective diffusivity tensor associated the multilayer structure, respectively. By comparing Eqs (2.11) and (6.1), the rotation angle and the diffusivities $D_{\parallel(i)}$and $D_{\perp(i)}$of the multilayer structure that reproduces the tensor in Eq. (2.11) can be calculated as

$$\theta_{(i)} = \frac{1}{2} tan^{-1}\left(\frac{2}{b_i}\right); \quad \frac{D_{\parallel(i)}}{D_{bg(i)}} = \frac{b_{(i)}^2}{2} - \frac{b_i}{\sin(2\theta_{(i)})} + 1; \quad \frac{D_{\perp(i)}}{D_{bg(i)}} = \frac{b_{(i)}^2}{2} + \frac{b_{(i)}}{\sin(2\theta_{(i)})} + 1 \tag{6.2}$$

Since the objective is to guide compounds *A* and *B* to different locations, the next step is to design a metamaterial structure that *simultaneously* fulfills the constraints imposed by Eq. (6.2) to the diffusivities of both compounds. Note that for each unit cell, we need to satisfy the requirements given by two beam-shifter transformations for which $b_{(A)} = -b_{(B)}$. To achieve this, we use effective medium theory, for which the effective normal and parallel multilayer diffusivities $D_{\perp(i)}$ and $D_{\parallel(i)}$ are given by

$$\frac{1}{D_{\perp(i)}} = \frac{f_{1(i)}}{D_{1(i)}} + \frac{f_{2(i)}}{D_{2(i)}}; \quad D_{\parallel} = f_{1(i)}D_{1(i)} + f_{2(i)}D_{2(i)} \tag{6.3}$$

where $D_{1(i)}$ and $D_{2(i)}$ are the diffusivities of compound *i* in the layered materials *1* and *2*, and $f_{(i)}$ are the corresponding volume fractions. For simplicity, we assume $f_{1(i)}$= $f_{2(i)}$=0.5 in our simulations. To obtain a unit cell that redirects compound *A* to the right and compound *B* to the left, we need a metamaterial in which, normally to the $\theta_{(A)}$ direction, compound *A* "sees" alternating layered materials with constant diffusivities $D_{1(A)}$ and $D_{2(A)}$, and at the same time, along the $\theta_{(A)}$ direction, compound *B* sees alternating layered materials with constant diffusivities $D_{1(B)}$ and $D_{2(B)}$. This mass diffusivity spatial distribution can be obtained by arranging four materials in a rhomboidal pattern as shown in Figure 6.1(b). The four constituent materials must be carefully selected such that the diffusivities are given by: Material 1 ($D_{(A)}$=$D_{1(A)}$, D_B=$D_{1(B)}$), Material 2 ($D_{(A)}$=$D_{1(A)}$, $D_{(B)}$=$D_{2(B)}$), Material 3 ($D_{(A)}$=$D_{2(A)}$, $D_{(B)}$=$D_{1(B)}$) and Material 4 ($D_{(A)}$=$D_{2(A)}$, $D_{(B)}$=$D_{2(B)}$). The values of $D_{1(A)}$ and $D_{2(A)}$ as well as those of $D_{1(B)}$ and $D_{2(B)}$ are obtained by simultaneously solving Eqs (6.2) and (6.3) for each compound *A* or *B*, using the selected parameters $b_{(i)}$, $f_{(i)}$. We note that the proposed independent manipulation of diffusion paths can be accomplished provided that the system is dilute. Also, note that we have assumed for simplicity that the solubilities are constant within the metamaterial.

6.3 Results and Discussion

We next study the diffusion of compounds *A* and *B* across the proposed membrane-based metamaterial separation device. We assume concentration values of 1 mol/m^3 and 0 mol/m^3 at the top and bottom boundaries to create a concentration-gradient driving force. Because of symmetry, there is no flux along the *y* direction at the right and left

boundaries. For the transformation functions (Eq. (2.10)), we consider beam-shifters with $b_{(i)}=\pm 5$. The background material has diffusivity $D_{bg(i)}=1\text{m}^2/\text{s}$ and the geometric parameters are $L=10$ cm, $m'=2$ cm and $d=1$ cm (Figure 6.1). Color maps and graphs in Figures 6.2 and 6.3 show the predicted results for the spatial distribution of the concentration for both compounds for an ideal metamaterial device made of a single homogeneous anisotropic material embedded in the background material. The results in Figures 6.2 and 6.3 show how, after crossing the metamaterial, the concentration of *A* is higher in those areas where the concentration of *B* is lower (and vice versa) (Figures 6.2(a)-(d), 6.2(i)-(l) and Figures 6.3(a) and 6.3(c)). Specifically, below the metamaterial membrane, the concentration of *A* reaches a maximum at the right side of unit cell I, while the concentration of *B* is maximal at the right side of unit cell II. Such rationally designed localization of *A* and *B* in different regions demonstrates the possibility of using planar metamaterial membranes for the separation of binary mixtures. We note, however, that an ideal metamaterial is difficult to obtain in practice. For this reason, we reproduce the ideal metamaterial by engineering a composite structure that, along different directions in space, acts as a multilayer system for the different compounds. The selected four isotropic materials have diffusivities: Material 1 ($D_{1(A)}=11.6$ m/s, $D_{1(B)}=0.06$ m/s), Material 2 ($D_{2(A)}=11.6$ m/s, $D_{2(B)}=11.6$ m/s), Material 3 ($D_{3(A)}=0.06$ m/s, $D_{3(B)}=0.06$ m/s) and Material 4 ($D_{4(A)}=0.06$ m/s, $D_{4(B)}=11.6$ m/s) and are assembled as shown in Figure 6.1(b). The concentration distribution for *A* and *B* in the case of the rationally structured metamaterial is shown in Figures 6.2(e)-(h), 6.2(m)-(p) and 6.3(b) and 6.3(d), respectively. Similarly to the ideal device, we obtain high concentration of *A* in areas where *B* has low concentration, both in transient and steady-state regimes. This shows

that it is possible to realize a membrane-based separation metamaterial device using homogeneous and isotropic materials. We note that the concentration profiles for the multilayer device (Figures 6.3(b) and 6.3(d)) show small spatial irregularities due to the piecewise isotropic materials of finite dimensions employed to reproduce the completely homogeneous anisotropic material of the ideal device.

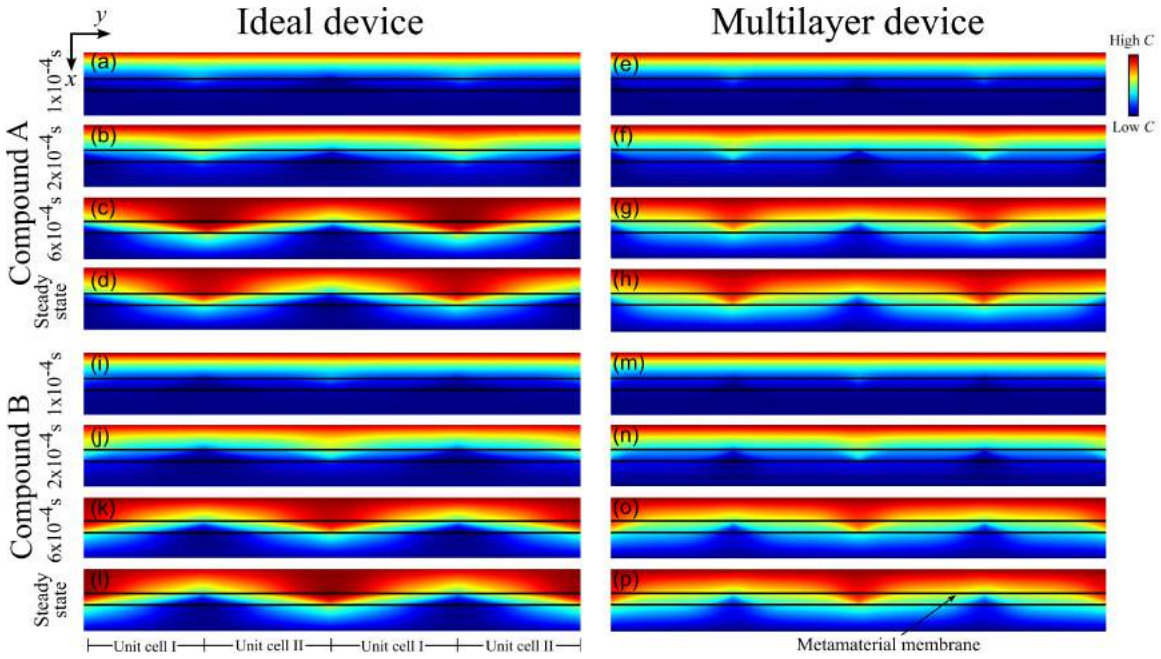

Figure 6.2. Color maps describing the transient and steady-state concentrations for compounds *A* and *B* in the case of an ideal (left) and a multilayer (right) metamaterial membrane. Diffusion of compound *A* in ideal (a-d) and multilayer (e-h) metamaterial. Diffusion of compound *B* in ideal (i-l) and multilayer (m-p) metamaterial. After crossing the metamaterial membrane from top to bottom, compounds *A* and *B* are guided to different spatial locations, as it can be seen by analyzing the location of maximal concentration (red area) at the bottom of the metamaterial membrane for the upper panels (Compound *A*) and the lower panels (Compound *B*). Note that the metamaterial membrane (indicated by horizontal black lines) is embedded in a homogeneous background medium.

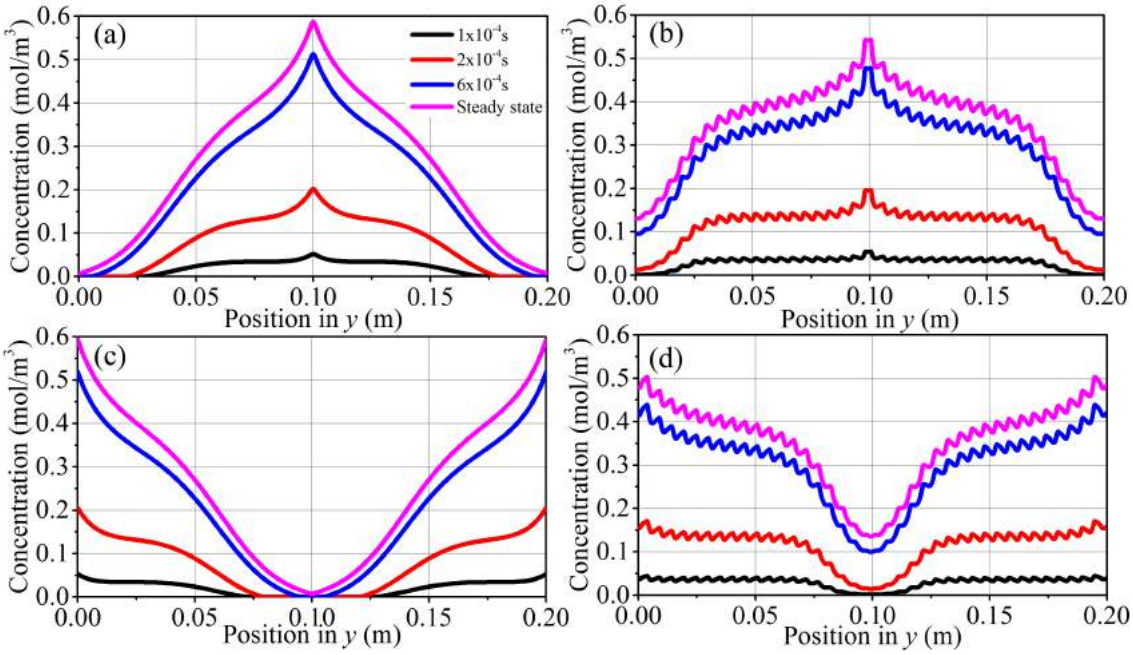

Figure 6.3. Transient and steady-state profiles for compound *A* (a),(b) and compound *B* (c),(d) along the horizontal direction *y* at the bottom surface of the metamaterial membrane for ideal (a), (c) and multilayer (b), (d) devices.

6.4 Conclusions

In conclusion, using a beam shifter coordinate transformation we have introduced a new class of engineered planar metamaterial membrane to control mass diffusion. We showed that this rationally designed metamaterials are able to guide the species in a binary mixture to opposite spatial locations in a planar membrane. Interestingly this behavior can be realized by using four isotropic materials with specific properties arranged in a particular architecture associated with this functionality. The ability of these metamaterial membranes guide the diffusion of two different species can be used to design new separation processes as it will be elaborated in detail in Chapter 10.

6.5 References

(1) Restrepo-Flórez, J. M.; Maldovan, M. Mass Separation by Metamaterials. *Sci. Rep.*

2016, *6* (2), 21971.

(2) Pendry, J. B.; Schurig, D.; Smith, D. R. Controlling Electromagnetic Fields. *Science.* **2006**, *312* (5781), 1780–1782.

(3) Guenneau, S.; Petiteau, D.; Zerrad, M.; Amra, C.; Puvirajesinghe, T. Transformed Fourier and Fick Equations for the Control of Heat and Mass Diffusion. *AIP Adv.* **2015**, *5* (5), 053404.

(4) Guenneau, S.; Amra, C.; Veynante, D. Transformation Thermodynamics: Cloaking and Concentrating Heat Flux. *Opt. Express* **2012**, *20* (7), 8207–8218.

(5) Wei, P.; Liu, F.; Liang, Z.; Xu, Y.; Chu, S. T.; Li, J. An Acoustic Beam Shifter with Enhanced Transmission Using Perforated Metamaterials. *Epl* **2015**, *14004*.

(6) Wang, M. Y.; Zhang, J. J.; Chen, H. S.; Luo, Y.; Xi, S.; Ran, L. X.; Kong, J. A. Design and Application of a Beam Shifter by by Transformation Media. *Prog. Electromagn. Res.* **2008**, *83*, 147–155.

(7) Rahm, M.; Roberts, D. a; Pendry, J. B.; Smith, D. R. Transformation-Optical Design of Adaptive Beam Bends and Beam Expanders. *Opt. Express* **2008**, *16* (15), 11555–11567.

(8) Rahm, M.; Cummer, S. A.; Schurig, D.; Pendry, J. B.; Smith, D. R. Optical Design of Reflectionless Complex Media by Finite Embedded Coordinate Transformations. *Phys. Rev. Lett.* **2008**, *100* (6), 063903.

(9) Huidobro, P. A.; Nesterov, M. L.; Martín-Moreno, L.; García-Vidal, F. J. Moulding the Flow of Surface Plasmons Using Conformal and Quasiconformal Mappings. *New J. Phys.* **2011**, *13*, 033011.

(10) Nye, J. F. *Physical Properties of Crystals*, 1st Ed.; Clarendon Press, 1957.

CHAPTER 7: DESING OF CYLINDRICAL ANISOTROPIC MEMBRANES WITH APPLICATIONS TO O_2/N_2 SEPARATIONS[1]

7.1 Introduction

In chapters 5 and 6 we have demonstrated that anisotropic materials designed using coordinate transformations can be use to tailor the diffusion trajectory of the species in a binary mixture. In this chapter we characterize the performance of anisotropic membranes for gas separations with emphasis on the separation of O_2/N_2. Importantly, the designs presented here are inspired by the results obtained in previous chapters. We note that established approaches for mass separation assume that the membrane material is isotropic (Figure 7.1(a)). This means that mass-flow cannot be "guided" in controlled ways to perform separations. In contrast, we propose rationally designed anisotropic membranes that purposely guide molecular diffusion (O_2 and N_2) to specific places and this translates into a completely new physical mechanism to improve current separation processes. In contrast to conventional isotropic membranes, the use of anisotropic membranes allows controlling both *direction* and *magnitude* of the mass flux. It is important to highlight that the flux directional control has already been proven both experimentally and theoretically for mass and heat diffusion but has not been used in the design of separation technologies[1–6]. Significantly, using our anisotropic design we found remarkable selectivities for O_2/N_2 separations. Clearly the proposed concept for separation can also be applied to other gas mixtures.

[1] Portions of this chapter have been published in: "Restrepo-Flórez, J.M.; Maldovan, M.; Breaking separation limits in membrane technology. *J. Memb Sci.* ***2018,*** 566, 301-306"

We show in Figure 7.1(b) how our separation device that controls the direction of mass flow using an anisotropic membrane operates significantly different from typical isotropic membranes such as planar, hollow fibers, or dual-layer hollow fiber membranes. In the isotropic case, membranes separate two compounds by selectively permeating one compound through the membrane while rejecting the other one (Figure 7.1(a)). As a result, two streams with different compositions develop – a permeate enriched with the permeated compound and a retentate enriched with the rejected compound[7,8]. In contrast the proposed separation device using an anisotropic membrane (Figure 7.1(b)) is selective for one of the compounds by simultaneously guiding the molecules that have permeated into the membrane toward different locations on the "permeate" side. Three streams develop: the retentate and two permeate fractions, with compositions that depend on the effectiveness of the anisotropic membrane to reroute the different species. Also note that our separation device does not possess a hollow core but rather a solid material core, in contrast to hollow fiber membranes. Furthermore, separation processes in hollow fiber membranes occur under a one-dimensional radial concentration gradient (Figure 7.1(a)), while our device requires a two-dimensional concentration gradient for operation (Figure 7.1(b)). A number of fundamental questions arise when considering anisotropic membranes for separation. What structural geometry would allow taking full control of the direction of mass flux and separation capabilities? How does an anisotropic membrane perform in comparison with a typical isotropic membrane? And how can we construct such anisotropic membrane considering that most currently available membrane materials are isotropic? In this chapter, we address these questions in the context of gas separations (e.g. O_2 and N_2) and prove that anisotropic layered structures made of

isotropic materials can be used to enhance the separation performance of typical isotropic membranes breaking the limits imposed by the conventional upper bound relation. Specifically, we discuss these findings in the case of O_2/N_2 separation where we propose a structure/material design consisting of rationally arranged isotropic polymeric materials.

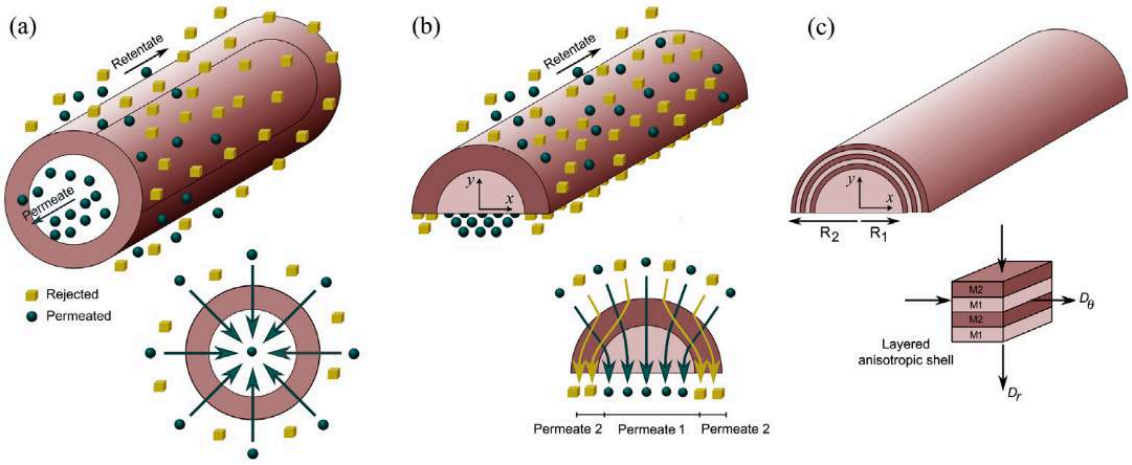

Figure 7.1. (a) Isotropic hollow fiber working for separation in countercurrent flow. The cylindrical membrane is highly selective for compound A (spheres) thus creating a permeate enriched in A. Inset shows the radial flux lines due to the cylindrical symmetry. (b) Proposed anisotropic membrane separation device consisting of an isotropic cylindrical core of radius R_1 covered by an anisotropic cylindrical shell with internal radius R_1 and external radius R_2. In this case, the two molecules (spheres and cubes) permeate in the membrane. The schematics show the ideal case where one compound (cubes) is directed around the core and the other compound (spheres) is focused towards the core. We are interested in collecting molecules A (spheres) at the core region ($-R_1<x<R_1$, $y=0$). Inset shows the flux lines for the two compounds, which are bent as a consequence of the anisotropicity of the shell. Simultaneous control of the flux trajectory for the two compounds is the basic principle of operation of the anisotropic membrane. (c) The anisotropic shell can be constructed using multilayer structures made of two isotropic materials M_1 and M_2 with mass resistances adding in series in the radial direction and in parallel in the azimuthal direction.

7.2 Theoretical approach

Diffusive transport processes in isotropic membranes are commonly described by Fick's theory, which establishes that the flux $J_{(i)}$ of species *i* across a planar membrane is given by

$$J_{(i)} = \frac{D_{(i)} S_{(i)} \Delta p_{(i)}}{H}; \quad \alpha_{A/B} = \frac{J_{(A)}/\Delta p_{(A)}}{J_{(B)}/\Delta p_{(B)}} = \left(\frac{D_{(A)}}{D_{(B)}}\right)\left(\frac{S_{(A)}}{S_{(B)}}\right) \tag{7.1}$$

where $D_{(i)}$ is the diffusivity, $S_{(i)}$ the solubility, $\Delta p_{(i)}$ the driving force, and H the membrane thickness[9–13]. In contrast, in our proposed device, anisotropic material properties are engineered to obtain a specific functionality. This can be achieved by engineering the mass diffusivity tensor[2,14–18]

$$J_{(i)} = -\begin{bmatrix} D_{xx(i)} & D_{xy(i)} \\ D_{yx(i)} & D_{yy(i)} \end{bmatrix} \nabla C_{(i)} \tag{7.2}$$

In order to design separation processes using engineered anisotropic membranes, the first task is to define a suitable structural geometry. In the case of isotropic membranes, this selection is performed by considering that the system should fit standard module designs and be easy to manufacture and maintain[9,19,20]. In anisotropic membranes, however, it is also necessary to find a structural geometry that allows the easy collection of the permeate fraction of interest. Towards this end, we introduce a membrane separation device consisting of two concentric half-cylinders as shown in Figure 7.1(b). The cylindrical core of radius R_1 is made of an isotropic material with solubility $S_{c(i)}$ and diffusivity $D_{c(i)}$ for compound *i*. On the other hand, the cylindrical shell with internal radius R_1 and external radius R_2 is made of an anisotropic material with solubility $S_{sh(i)}$ and tensorial diffusivity $\overline{\overline{D}}_{sh(i)}$. The role of the anisotropic shell is to

manipulate the trajectory of the molecules of interest. For example, an ideal anisotropic shell for separation of a binary mixture should detour one compound around the core and focus the other compound towards the core[14,21]. The effectiveness of the anisotropic shell for separation will thus depend on the ability of the shell to differently promote the diffusion of the compounds along the radial and azimuthal directions. Note that in our proposed design, the permeate fraction enriched with the compound of interest is collected at the planar lower surface of the cylindrical core, i.e. at the line $-R_1<x<R_1$, $y=0$.

Our initial objective is to show how the anisotropic shell affects separation of a binary mixture of arbitrary compounds *A* and *B*. The diffusion of species *i* (*A* or *B*) in the core and shell regions can be described using continuity and Fick's law Eqs (7.1) and (7.2), which yields the following differential equations for diffusion

$$\frac{1}{r}\frac{\partial}{\partial r}\left(r\,\frac{\partial C_{c(i)}}{\partial r}\right)+\frac{1}{r^2}\frac{\partial^2 C_{c(i)}}{\partial \theta^2}=0 \qquad \text{for the core} \tag{7.3}$$

$$\frac{1}{r}\frac{\partial}{\partial r}\left(r\,\frac{\partial C_{sh(i)}}{\partial r}\right)+\frac{l_{(i)}^2}{r^2}\frac{\partial^2 C_{sh(i)}}{\partial \theta^2}=0 \qquad \text{for the shell} \tag{7.4}$$

where $l_{(i)}^2 = D_{\theta(i)}/D_{r(i)}$, $D_{\theta(i)}$ and $D_{r(i)}$ are the azimuthal and radial diffusion coefficients of the shell, respectively. Eqs (7.3) and (7.4) have solutions $C_{(i)}(r,\theta) = Y_{(i)}(r)G_{(i)}(\theta)$ in the form of Fourier's series expansion[22]. By considering the mirror symmetry with respect to $x=0$ and a non-divergent concentration at $r=0$, the spatial concentrations $C_{(i)}(r,\theta)$ can be written as

$$C_{c(i)}(r,\theta) = C_{c(i)}^0 + \sum_{n=1}^{\infty} a_{n(i)}\, r^n \sin(n\theta) \tag{7.5}$$

$$C_{sh(i)}(r,\theta) = C_{sh(i)}^0 + \sum_{n=1}^{\infty} \left[b_{n(i)}\, r^{nl_{(i)}} + c_{n(i)}\, r^{-nl_{(i)}}\right] \sin(n\theta) \tag{7.6}$$

where the constants $C^0_{c(i)}$, $C^0_{sh(i)}$ and the coefficients $a_{n(i)}, b_{n(i)}$ and $c_{n(i)}$ are obtained by applying the following boundary conditions. We consider a partial pressure p_i on the upper side ($r = R_2$) and zero at the bottom of the device ($\theta = 0$). At the interface between shell and core ($r = R_1$) we enforce the continuity of the radial flux and the discontinuity in concentration by considering the partition coefficient $K_{(i)} = S_{c(i)}/S_{(i)}$.

$$\begin{aligned} D_{c(i)}\frac{\partial C_{c(i)}}{\partial r} = D_{r(i)}\frac{\partial C_{sh(i)}}{\partial r};\quad C_{c(i)} = K_{(i)}C_{sh(i)} \quad \text{at} \quad r = R_1 \\ C_{sh(i)} = p_{(i)}S_{sh(i)} \quad \text{at} \quad r = R_2 \\ C_{c(i)} = 0;\quad C_{sh(i)} = 0 \quad \text{at} \quad \theta = 0 \end{aligned} \tag{7.7}$$

The above boundary conditions yield the following expressions for the concentration of each compound *i*

$$C_c(r,\theta) = \sum_{n=1}^{\infty} \alpha_n (2\ K\ l\ D'_r)\left(\frac{r}{R_1}\right)^n \sin(n\theta)$$

$$C_{sh}(r,\theta) = \sum_{n=1}^{\infty} \alpha_n \left[(lD'_r + K)\left(\frac{r}{R_1}\right)^{nl} + (lD'_r - K)\left(\frac{r}{R_1}\right)^{-nl}\right] \sin(n\theta) \tag{7.8}$$

$$\alpha_n = PS_{II}\ \frac{2}{\pi}\left[\frac{1-(-1)^n}{n}\right]\left[(lD'_r + K)\left(\frac{R_2}{R_1}\right)^{nl} + (lD'_r - K)\left(\frac{R_2}{R_1}\right)^{-nl}\right]^{-1}$$

and $C^0_{c(i)} = C^0_{sh(i)} = 0$, where $D'_{r(i)} = D_{r(i)}/D_{c(i)}$. We validated the concentrations $C_{(i)}(r,\theta)$ given by Eq. (7.8) against numerical predictions via COMSOL Multiphysics® and obtained excellent agreement.

For operation of the anisotropic membrane, we are interested in the average flux *J* leaving the core along the line $-R_1 < x < R_1$, $y = 0$ (Figure 7.1(b)), which is given by

$$\langle J_{l_y} \rangle = -D_c \left\langle \frac{\partial C_c}{\partial y} \right\rangle = -D_c \sum_{n=1}^{\infty} a_n R_1^{n-1} \tag{7.9}$$

Calculation of the fluxes for compounds *A* and *B* allow us to predict the selectivity $\alpha_{A/B}$

$$\alpha_{A/B} = \frac{\langle J_{cy(A)}\rangle/\Delta p_{(A)}}{\langle J_{cy(B)}\rangle/\Delta p_{(B)}} = \left(\frac{D_{c(A)}}{D_{c(B)}}\right)\left(\frac{S_{c(A)}}{S_{c(B)}}\right)\frac{\sum_{n=1}^{\infty}\left[\frac{1-(-1)^n}{n}\right]\frac{l_{(A)}D'_{r(A)}}{(l_{(A)}D'_{r(A)}+K_{(A)})(R_2/R_1)^{nl_{(A)}}+(l_{(A)}D'_{r(A)}-K_{(A)})(R_2/R_1)^{-nl_{(A)}}}}{\sum_{n=1}^{\infty}\left[\frac{1-(-1)^n}{n}\right]\frac{l_{(B)}D'_{r(B)}}{(l_{(B)}D'_{r(B)}+K_{(B)})(R_2/R_1)^{nl_{(B)}}+(l_{(B)}D'_{r(B)}-K_{(B)})(R_2/R_1)^{-nl_{(B)}}}} \tag{7.10}$$

and permeance $P_{(A)}$ of the membrane

$$P_{(A)} = \frac{\langle J_{cy(A)}\rangle}{\Delta p_{(A)}} = \frac{4D_{c(A)}S_{c(A)}}{\pi R_1}\sum_{n=1}^{\infty}\left[\frac{1-(-1)^n}{n}\right]\frac{l_{(A)}D'_{r(A)}}{(l_{(A)}D'_{r(A)}+K_{(A)})(R_2/R_1)^{nl_{(A)}}+(l_{(A)}D'_{r(A)}-K_{(A)})(R_2/R_1)^{-nl_{(A)}}} \tag{7.11}$$

An analysis of Eq. (7.10) reveals that the anisotropic separation device introduces a new physical mechanism that can be used to enhance separation. Note that the selectivity can be written as the product of three factors

$$\alpha_{A/B} = \left(\frac{D_{c(A)}}{D_{c(B)}}\right)\left(\frac{S_{c(A)}}{S_{c(B)}}\right)\left(\frac{Q_{(A)}}{Q_{(B)}}\right) \tag{7.12}$$

where the third factor $Q_{(A)}/Q_{(B)}$ depends on structural and material properties of the anisotropic shell. The ratio $Q_{(A)}/Q_{(B)}$ is equal to one for an isotropic membrane and its existence in our design opens up a number of possibilities in the sense that combinations of structural and material parameters $R_1, R_2, l, D_r^{'}, K$ can make its value greater than one, thus generating an improvement in the selectivity.

7.3 Results and discussion

We show in Figures 7.2(a) and 7.2(b) the selectivity and permeance of the proposed anisotropic membrane in the case of a binary mixture consisting of oxygen and nitrogen. The isotropic core is considered to be polydimethylsiloxane (PDMS) and the homogeneous shell has anisotropic diffusion coefficients D_r and D_θ that correspond to a layered structure made of *isotropic* polymeric materials PDMS and PSF. This will be discussed in detail in the next section. The solubilities and diffusion coefficient for the

core and shell materials are summarized in Table 7.1. The anisotropic shell is purposely designed to detour N_2 around the PDMS core, thus collecting O_2 at the core. This is done by carefully selecting the materials such that the diffusivity ratio $D_{r(O2)}/D_{r(N2)}$ is much larger than the ratio $D_{\theta(O2)}/D_{\theta(N2)}$. Figure 7.2 clearly shows how the structural properties play a fundamental role on the selectivity and permeance. We observe that for a constant value of R_1 the larger the anisotropic shell (i.e. increasing values of R_2/R_1), the higher the selectivity and the lower the permeance. These results can be understood by considering that by increasing the thickness of the shell, the anisotropic path for the diffusing compounds becomes longer and the effects of the shell on detouring N_2 around the core increase, which increases the selectivity. The increased R_2/R_1 ratio also causes a decrease in the number of molecules that reach the core, thus lowering the permeance. For comparison, we also show the selectivity and permeance in the case that the shell is made of a single isotropic material (either PDMS or PSF). We can see that the separation properties of the proposed device using an anisotropic shell are significantly different from those corresponding to isotropic shells, indicating the possibility of using anisotropic diffusion mechanisms to enhance the separation of O_2 and N_2.

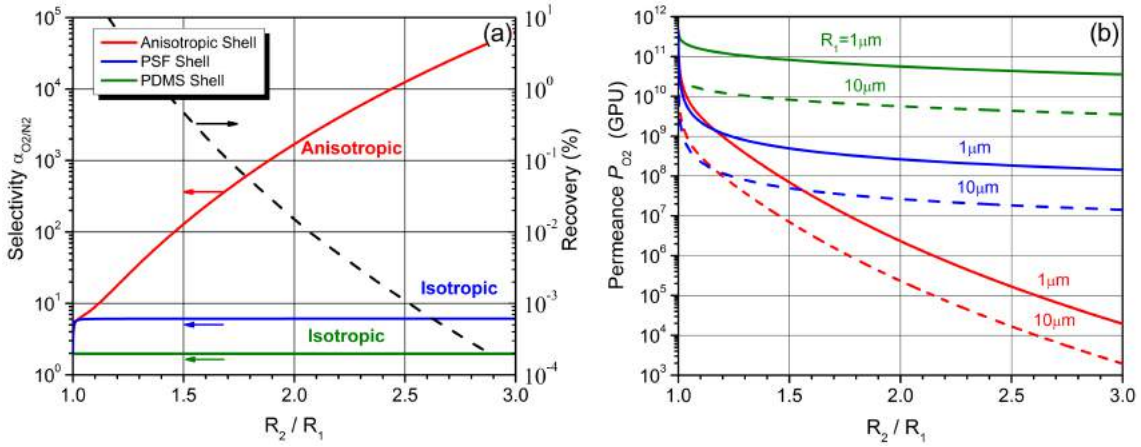

Figure 7.2. (a) Selectivity and (b) permeance for our anisotropic membrane device as a function of R_2/R_1 in the case of separation of a binary mixture of oxygen and nitrogen. The cylindrical core is made of PDMS. Red, blue, and green lines correspond to anisotropic, PSF, and PDMS shells respectively. The anisotropic shell is made of layered PSF and PDMS materials. For the permeance, two R_1 values are considered 1μm and 10μm.

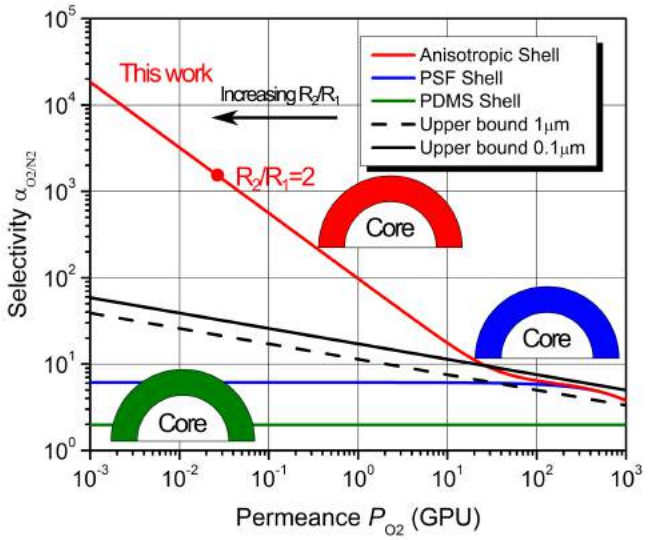

Figure 7.3. Modified Robeson plot for selectivity vs. permeance for anisotropic (red), PSF (blue), and PDMS (green) shells respectively where R_1=1μm. Black solid line shows selectivity vs. permeance upper bounds for a planar isotropic membrane of thickness 1μm. We note that if R_1 is increased (reduced) the plot will shift to the left (right).

A remarkable result from our numerical predictions is that the performance of the proposed anisotropic membranes is above the upper bound limit for most of the permeability spectrum. We show in Figure 7.3 the selectivity vs. permeance plot of the device, which is analogous to the well-known Robeson plot[23,24]. A representative value of R_1=1μm is chosen for the calculations. The most significant result in Figure 7.3 is that the use of an anisotropic shell (red solid line) can make the device to have selectivities significantly higher than the upper bounds (black solid line). For example, for R_2/R_1=2, the selectivity is two orders of magnitude larger than that from conventional membranes. We have also evaluated the collected fraction for increasing R_2/R_1 ratios in the range $1.0<R_2/R_1<3.0$ (Figure 7.2(a)) and found a recovery between ~10% and 0.001%. This indicates that the increase in selectivity is accompanied by a reduction in the oxygen recovery. In terms of process operation, if higher recoveries are needed, larger membrane areas and operational cost will be required. The results presented demonstrate that control of the direction of the mass flux via anisotropy, as proposed here, can be an important factor in the design of separation processes by providing membranes with increased efficiencies. For comparison, we also show in Figure 7.3 the cases where the shell is made of isotropic materials PDMS (green) and PSF (blue). It should be noted that, in contrast to the anisotropic shell, the selectivity of isotropic shells is bounded by the intrinsic properties of the constituent materials.

As mentioned previously, we propose to manufacture the anisotropic shell using a layered structure made of commonly available isotropic materials. Achieving anisotropic properties by means of bilayer structures has been extensively discussed in chapter 4. According to effective medium theory, it is possible to construct a multilayer structure

made of thin layers of alternating materials *1* and *2* with different solubilities and diffusivities, which behaves as an anisotropic medium when the number of layers is large enough. In our proposed membrane, we have a set of concentric cylinders of alternating materials *1* and *2*, in which resistances add in series (parallel) in the radial (azimuthal) direction (Figure 7.1(c)). Effective medium theory establishes the effective radial $D_{r(i)}$ and azimuthal diffusivities $D_{\theta(i)}$ of the layered shell as well as its effective solubility $S_{sh(i)}$ in terms of the properties of the isotropic materials and their volume fractions[15,16,25–28], which are given by

$$D_{\theta(i)} = \frac{1}{(f_1+f_2k_i')}\left[\, f_1 D_{1(i)} + f_2 k_i' D_{2(i)} \,\right];\ \ [D_{r(i)}]^{-1} = (f_1 + f_2 k_i')\left[\frac{f_1}{D_{1(i)}} + \frac{f_2}{k_i' D_{2(i)}}\right] \tag{4.1}$$

$$S_{sh(i)} = f_1 S_{1(i)} + f_2 S_{2(i)} \tag{4.2}$$

where $D_{1(i)}, D_{2(i)}$ are the isotropic diffusion coefficients of compound *i* in materials *1* and *2* respectively, f_1, f_2 are the volume fractions, and $k'_{(i)} = S_{2(i)}/S_{1(i)}$. Using the diffusivities and solubilities given in Table 7.1 for N_2 and O_2 in PDMS and PSF, Eq. (4.1) establishes that a multilayer structure made of PDMS (Material *1*) and PSF (Material *2*) with f_1=0.5 yields the anisotropic properties of the shell previously studied (Table 7.1). In Figure 7.4 we explore the selectivity and permeance as a function of the volume fraction for R_1=1μm and R_2/R_1=2. The results show that the volume fraction of the layered shell is another important factor on the performance of the device. The selectivity increases continuously from f_1=0 until it reaches a maximum at f_1=0.5 and decreases with further increase of the volume fraction. In contrast, the permeance decreases monotonously until f_1=0.5 and increases for larger volume fractions. These results show the richness of behaviors that can be obtained by means of an anisotropic separation device.

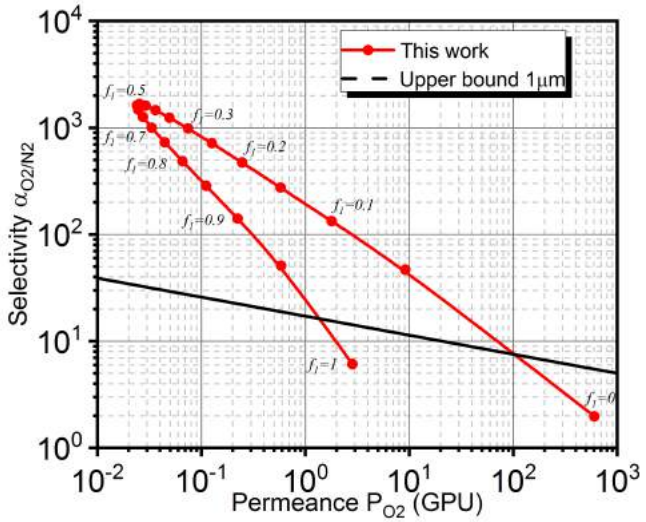

Figure 7.4. Selectivity vs. permeance for a membrane separation device with R_1=1μm and R_2/R_1=2 for different volume fractions of PDMS in the shell.

Table 7.1. Solubilities and diffusivities for polydimethylsiloxane (PDMS), polysulfone (PSF) (Refs.[29,30]) and for an anisotropic shell made of layered PDMS (Material *1*) and PSF (Material *2*) with f_{PDMS}=0.5.

	$S_{(O2)}$ [mol/m^{3}Pa]	$D_{(O2)}$ [m^2/s]	$S_{(N2)}$ [mol/m^{3}Pa]	$D_{(N2)}$ [m^2/s]	$D'_{r\,(O2)}$	$D'_{\theta\,(O2)}$	$D'_{r\,(N2)}$	$D'_{\theta\,(N2)}$
PDMS	7.9×10^{-5}	3.4×10^{-9}	4.0×10^{-5}	3.4×10^{-9}				
PSF	1.1×10^{-4}	4.4×10^{-12}	6.6×10^{-5}	1.2×10^{-12}				
Shell	9.45×10^{-5}		5.30×10^{-5}		3.01×10^{-3}	4.18×10^{-1}	8.78×10^{-4}	3.77×10^{-1}

We note that another design aspect is the number N of bilayers of materials *1* and *2* that are required to obtain an effective anisotropic medium behavior for the shell (Figure 7.1(c)). We thus analyze the role of N in detail in Figure 7.5 for an anisotropic shell made of a PDMS-PSF multilayer structure. As it can be seen in the insets, the selectivity increases while the permeance decreases with increasing numbers of bilayers, both showing an asymptotic behavior for a large number of layers. Note that the difference between layered and continuous anisotropic shell is minimal for a sufficiently large

number of bilayers (N~20)[31]. Figure 7.5 shows that one important consequence of the resultant selectivity/permeance values obtained for different number of bilayers is that the performance of the device in terms of the modified Robeson plot[23] is also a function of N. As a result, N should be selected ensuring that the performance is above the upper bound. Furthermore it is also possible to tailor the number of layers N to tune the permeance of the device. That is, the number of layers N can also be a variable to control to a certain extent the relation between selectivity and permeance.

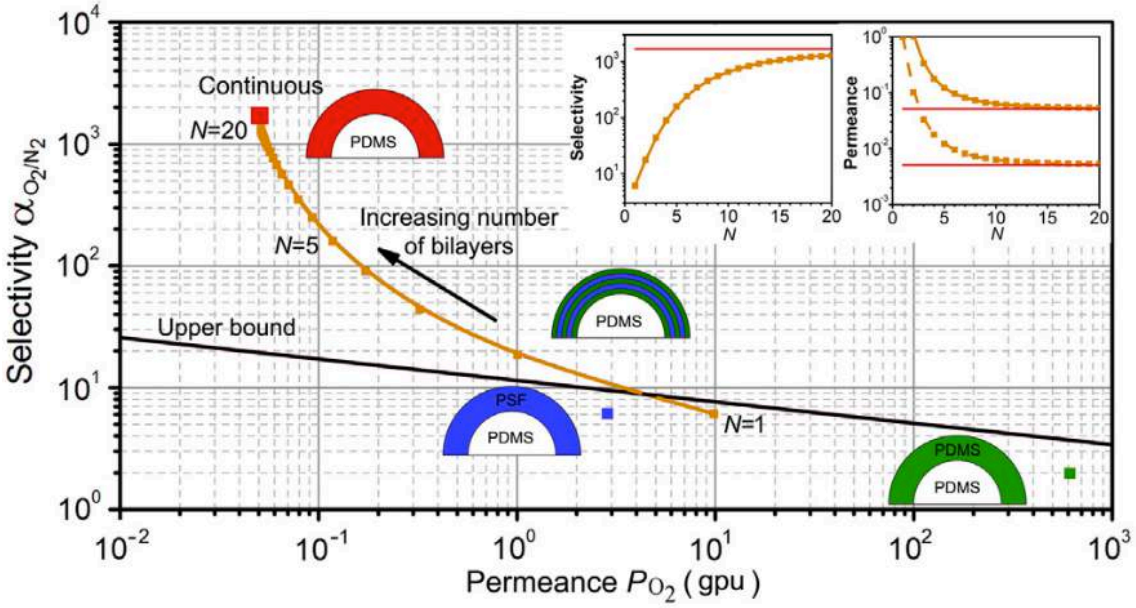

Figure 7.5. Insets: Selectivity (left) and permeability (right) of our membrane design for separation of a binary mixture of oxygen (50%) and nitrogen (50%) as a function of the number N of bilayers. The layered anisotropic shell is made of isotropic PDMS and PSF materials. R_1=1μm (top line), R_1=10μm (bottom line) and R_2/R_1=2. Main panel: Robeson plot of selectivity vs. permeance for a layered anisotropic shell with R_1=1μm and R_2/R_1=2 and increasing number of layers (orange line). For large numbers of bilayers (~20), the performance corresponds to the continuous case (red dot). For reference, PSF and PDMS shells are also shown in the figure.

7.4 Conclusions

We showed that engineered anisotropic structures can give rise to a new class of membranes that can be used for separation of O_2 and N_2. By controlling the flux direction by means of anisotropy, we introduced a new device for separation that allows increasing the selectivity of membranes for O_2 above the limits typically observed in isotropic membranes. The anisotropic membranes proposed here can be fabricated as multilayer structures made of two isotropic materials with contrasting diffusivities. The effective diffusivities and solubilities of the anisotropic structure can be obtained using effective medium theory. Importantly, the present work is a demonstration of a new physical system that breaks separation limits for O_2 and N_2 in membrane technologies.

7.5 References

(1) Zeng, L.; Song, R. Controlling Chloride Ions Diffusion in Concrete. *Sci. Rep.* **2013**, *3*, 3359.

(2) Guenneau, S.; Puvirajesinghe, T. M. Fick's Second Law Transformed: One Path to Cloaking in Mass Diffusion. *J. R. Soc. Interface* **2013**, *10* (83), 20130106.

(3) Guenneau, S.; Petiteau, D.; Zerrad, M.; Amra, C.; Puvirajesinghe, T. Transformed Fourier and Fick Equations for the Control of Heat and Mass Diffusion. *AIP Adv.* **2015**, *5* (5), 053404.

(4) Narayana, S.; Sato, Y. Heat Flux Manipulation with Engineered Thermal Materials. *Phys. Rev. Lett.* **2012**, *108* (21), 214303.

(5) Dede, E. M.; Nomura, T.; Schmalenberg, P.; Seung Lee, J. Heat Flux Cloaking, Focusing, and Reversal in Ultra-Thin Composites Considering Conduction-Convection Effects. *Appl. Phys. Lett.* **2013**, *103* (6), 063501.

(6) Schittny, R.; Kadic, M.; Guenneau, S.; Wegener, M. Experiments on Transformation Thermodynamics: Molding the Flow of Heat. *Phys. Rev. Lett.* **2013**, *110* (19), 195901.

(7) Baker, R. W.; Low, B. T. Gas Separation Membrane Materials: A Perspective. *Macromolecules* **2014**, *47* (20), 6999–7013.

(8) Wijmans, J. G.; Baker, R. W. The Solution-Diffusion Model: A Review. *J. Memb.*

Sci. **1995**, *107* (1–2), 1–21.

(9) Sanders, D. F.; Smith, Z. P.; Guo, R.; Robeson, L. M.; McGrath, J. E.; Paul, D. R.; Freeman, B. D. Energy-Efficient Polymeric Gas Separation Membranes for a Sustainable Future: A Review. *Polymer.* **2013**, *54* (18), 4729–4761.

(10) Koros, W. J.; Fleming, G. K. Membrane-Based Gas Separation. *J. Memb. Sci.* **1993**, *83*, 1–80.

(11) Koros, W. J.; Fleming, G. K.; Jordan, S. M.; Kim, T. H.; Hoehn, H. H. Polymeric Membrane Materials for Solution-Diffusion Based Permeation Separations. *Prog. Polym. Sci.* **1988**, *13* (4), 339–401.

(12) Koros, W. J.; Coleman, M. R.; Walker, D. R. B. Controlled Permeability Polymer Membranes. *Annu. Rev. Mater. Sci.* **1992**, *22*, 47–89.

(13) Klopffer, M. H.; Flaconneche, B. Transport Properties of Gases in Polymers: Bibliographic Review. *Oil Gas Sci. Technol.* **2001**, *56* (3), 223–244.

(14) Restrepo-Flórez, J. M.; Maldovan, M. Mass Separation by Metamaterials. *Sci. Rep.* **2016**, *6* (2), 21971.

(15) Sax, J.; Ottino, J. M. Modeling of Transport of Small Molecules in Polymer Blends: Application of Effective Medium Theory. *Polym. Eng. Sci.* **1983**, *23* (1 l), 165–176.

(16) Shah, N.; Sax, J. E.; Ottino, J. M. Influence of Morphology on the Transport Properties of Polystyrene/Polybutadiene Blends: 2. Modelling Results. *Polymer.* **1985**, *26* (8), 1239–1246.

(17) Csernica, J.; Baddour, R. F.; Cohen, R. E. Gas Permeability of a Polystyrene/Polybutadiene Block Copolymer Possessing a Misorientated Lamellar Morphology. *Macromolecules* **1989**, *22*, 1493–1496.

(18) Kinning, D. J.; Thomas, E. L.; Ottino, J. M. Effect of Morphology on the Transport of Gases in Block Copolymers. *Macromolecules* **1987**, *20* (36), 1129–1133.

(19) Koros, W. J.; Zhang, C. Materials for Next-Generation Molecularly Selective Synthetic Membranes. *Nat. Mater.* **2017**, *16* (3), 289–297.

(20) Baker, R. W. Future Directions of Membrane Gas Separation Technology. *Ind. Eng. Chem. Res.* **2002**, *41* (6), 1393–1411.

(21) Restrepo-Flórez, J.-M.; Maldovan, M. Metamaterial Membranes. *J. Phys. D. Appl. Phys.* **2017**, *50*, 25104.

(22) Incropera, F. P.; DeWitt, D. P.; Bergman, T. L.; Lavine, A. S. *Fundamentals of*

Heat and Mass Transfer, 6th Ed.; John Wiley & Sons, Inc.: New York, 2007.

(23) Robeson, L. M. The Upper Bound Revisited. *J. Memb. Sci.* **2008**, *320* (1–2), 390–400.

(24) Freeman, B. D. Basis of Permeability/Selectivity Tradeoff Relations in Polymeric Gas Separation Membranes. *Macromolecules* **1999**, *32* (2), 375–380.

(25) Belova, I. V; Murch, G. E. Analysis of the Effective Diffusivity in Nanocrystalline Materials. *J. Metastable Nanocrystalline Mater.* **2004**, *19*, 25–34.

(26) Belova, I. V.; Murch, G. E. Diffusion in Nanocrystalline Materials. *J. Phys. Chem. Solids* **2003**, *64*, 873–878.

(27) Van Siclen, C. D. Effective Diffusivity of Solute in Multiphase Materials with Segregation. *J. Phys. Chem. Solids* **2004**, *65* (6), 1199–1200.

(28) Zhang, Y.; Liu, L. On Diffusion in Heterogeneous Media. *Am. J. Sci.* **2012**, *312* (9), 1028–1047.

(29) Merkel, T. C.; Bondar, V. I.; Nagai, K.; Freeman, B. D.; Pinnau, I. Gas Sorption, Diffusion, and Permeation in Poly(Dimethylsiloxane). *J. Polym. Sci. Part B Polym. Phys.* **2000**, *38* (3), 415–434.

(30) McHattie, J. S.; Koros, W. J.; Paul, D. R. Gas Transport Properties of Polysulfones: 1. Role of Symmetry of Methyl Group Placement on Bisphenol. *Polymer.* **1991**, *32* (5), 840–850.

(31) Restrepo-Flórez, J. M.; Maldovan, M. Rational Design of Mass Diffusion Metamaterial Concentrators Based on Coordinate Transformations. *J. Appl. Phys.* **2016**, *120* (8), 084902.

CHAPTER 8: GENERAL CONSIDERATIONS FOR THE DESIGN OF CYLINDICAL ANISOTROPIC MEMBRANES FOR GAS SEPARATIONS[1]

8.1 Introduction

In chapters 3-6 we have demonstrated the possibility of designing materials to achieve control of mass flux *direction*[1–4]. Using these principles we developed the concept of anisotropic membranes in chapter 7[5]. We demonstrated that a membrane that manipulates mass flux direction can control the trajectory of the compounds of interest and create spatial areas where the flux of the desired molecule is focused, or alternatively spatial areas where undesirable molecules are prevented from penetrating[2,5]. Furthermore we have shown that in practice, the fabrication of these anisotropic membrane materials involves the use of layered arrangements of isotropic materials. We note however that despite their unique potential, the design, operation, capabilities, and limitations of anisotropic membrane materials to achieve gas separations are still largely unexplored.

In this chapter, we build on the findings presented in chapter 7[5] and completely characterize the performance of anisotropic membranes. Our findings allow to address some fundamental design questions. For example, which structure geometries can be used and how are they operated to take advantage of flux directional control? What are the governing variables determining the performance of these membranes? How these variables affect the performance and structure requirements for gas separation? As an

[1] Portions of this chapter have been published in: "Restrepo-Flórez, J.M.; Maldovan, M.; Anisotropic membranes for gas separations. *AIChE journal.* ***2019***"

example, at the end of the chapter we apply the findings to design anisotropic membranes for the separation of H_2/CH_4.

8.2 Theoretical analysis

We first present a theoretical and analytical approach that allows designing, characterizing, and enhancing the performance of separation processes using anisotropic membranes. Since separation principles in anisotropic systems are different from those in typical isotropic systems, rationally designed geometries (different from isotropic membranes) need to be considered in the anisotropic case. Specifically, in separation processes using isotropic membranes, separation occurs due to the different flux magnitudes for compounds crossing the membrane and a single permeate develops across the membrane. Flat sheets and hollow fibers are examples of membrane geometries generally used in separation processes involving isotropic materials[6]. In contrast, in the separation processes considered here using anisotropic membranes, both magnitude and direction of mass flux are manipulated and separation occurs due to the different spatial rerouting of molecules *A* and *B* (Figure 8.1). In this case, two permeates develop with compositions that are functions of the position on the permeate side. As a result, when designing anisotropic membranes one has to define the region where the permeate is collected (e.g. permeate 1 or permeate 2) in order to take advantage of the rerouting of molecules trajectories. The basic role of the anisotropic shell is to manipulate the flux directions such that separation efficiency is maximized either for permeate 1 or permeate 2. Thus, in the anisotropic case, it is necessary to design new membrane geometries and operational strategies in order to collect the permeate fraction of interest. In our membrane designs, we consider the collection of the permeate from the core region (i.e.

permeate 1 in Figure 8.1). The membrane composite consists of a half-cylindrical core region surrounded by a cylindrical shell. The core (c) region ($r<R_1$) is made of an isotropic material with diffusivity $D_{c(i)}$ and solubility $S_{c(i)}$ for compound i, whereas the cylindrical shell (sh) ($R_1<r<R_2$) consists of an anisotropic material with diffusivity $D_{\theta(sh)(i)}$ in the azimuthal direction, diffusivity $D_{r(sh)(i)}$ in the radial direction, and solubility $S_{sh(i)}$. Permeation across the membrane develops due to a chemical potential driving force, where a constant partial pressure p_i is applied at $r=R_2$ and complete sweeping $p_i=0$ is imposed at $-R_2<x<R_2$, $y=0$ for all compounds leaving the system. At the interface between the core and the shell ($r=R_1$), flux continuity in the radial direction is enforced and the partition coefficient $K_{(i)} = S_{c(i)}/S_{sh(i)}$ is used to account for concentration discontinuities due to changes in solubilities. By considering Fick's law $J_{(i)} = -\bar{\bar{D}}_{(i)}\nabla C_{(i)}$ and continuity equations, the concentration distribution for species i in the anisotropic membrane is given by the Fourier series expansions[5]:

$$C_{c(i)}(r,\theta) = \sum_{n=1}^{\infty} a_{n(i)} r^n \sin(n\theta) \tag{7.5}$$

$$C_{sh(i)}(r,\theta) = \sum_{n=1}^{\infty} [b_{n(i)} r^{nl_{(i)}} + c_{n(i)} r^{-nl_{(i)}}] \sin(n\theta) \tag{7.6}$$

where $l_{(i)}^2 = D_{\theta(sh)(i)}/D_{r(sh)(i)}$. By applying the boundary conditions, we find that the series coefficients can be written as

$$a_{n(i)} = p_{(i)} S_{sh(i)} \frac{4}{\pi}\left[\frac{1-(-1)^n}{n}\right] K_{(i)} \theta_{n(i)} R_1^{-n} \tag{8.1}$$

$$b_{n(i)} = p_{(i)} S_{sh(i)} \frac{2}{\pi}\left[\frac{1-(-1)^n}{n}\right] \left(1+\delta_{(i)}\right) \theta_{n(i)} R_1^{-nl_{(i)}} \tag{8.2}$$

$$c_{n(i)} = p_{(i)} S_{sh(i)} \frac{2}{\pi}\left[\frac{1-(-1)^n}{n}\right] \left(1-\delta_{(i)}\right) \theta_{n(i)} R_1^{nl_{(i)}} \tag{8.3}$$

$$\theta_{n(i)} = \left[\left(1+\delta_{(i)}\right)\left(\frac{R_2}{R_1}\right)^{nl_{(i)}} + \left(1-\delta_{(i)}\right)\left(\frac{R_2}{R_1}\right)^{-nl_{(i)}}\right]^{-1} \tag{8.4}$$

where $\delta_{(i)} = D_{c(i)}S_{c(i)}/\sqrt{D_{\theta(sh)(i)}D_{r(sh)(i)}}\,S_{sh(i)}$. Using this analytical solution, we calculate the average fluxes $\langle J_{y(i)}\rangle$ for compound *i* leaving the core along the *y*-direction (permeate 1) and obtain analytical expressions for normalized permeance (Eq. (8.5)) and ideal selectivity (Eq. (8.6)) of the anisotropic membrane

$$\frac{P_{(i)}}{P^*_{(i)}} = \left(\frac{1}{P^*_{(i)}}\right)\frac{<J_{y(i)}>}{\Delta p_{(i)}} = \frac{4}{\pi}\sum_{n=1}^{\infty}\left[\frac{1-(-1)^n}{n}\right]\theta_{n(i)} \tag{8.5}$$

$$\frac{\alpha_{A/B}}{\alpha^*_{A/B}} = \frac{\sum_{n=1}^{\infty}\left[\frac{1-(-1)^n}{n}\right]\theta_{n(A)}}{\sum_{n=1}^{\infty}\left[\frac{1-(-1)^n}{n}\right]\theta_{n(B)}} \tag{8.6}$$

where $P^*_{(i)} = D_{c(i)}S_{c(i)}/R_1$ is the isotropic core permeance and $\alpha^*_{A/B} = \frac{D_{c(A)}S_{c(A)}}{D_{c(B)}S_{c(B)}}$ is the isotropic core selectivity. Note that $P_{(i)}/P^*_{(i)}$ and $\alpha_{A/B}/\alpha^*_{A/B}$ measure the changes in permeance and selectivity due to the anisotropic shell with respect to the permeance and selectivity of the core.

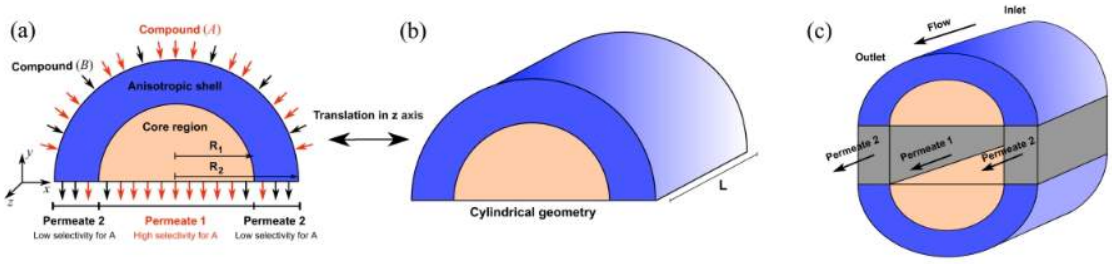

Figure 8.1. Schematic of the proposed anisotropic membranes. The core region is isotropic while the surrounding shell is anisotropic. The role of the shell is to reroute compounds *A* and *B* through the membrane. The driving force is the chemical potential difference at the top and bottom of the membrane. Separation of *A* from *B* is obtained for permeate 1 leaving the core. A schematic of a module design is shown on the right where two permeate streams are generated requiring two independent collection channels (Permeate 1 and Permeate 2).

It is interesting to note that a small number of non-dimensional variables is required to characterize the membrane in terms of normalized selectivities and permeances (Eqs (8.5)-(8.6)). In particular, for the separation of two gases A and B, the variables are: R_2/R_1 , $l_{(A)}$, $l_{(B)}$, $\delta_{(A)}$, and $\delta_{(B)}$. That is $\alpha_{A/B}/\alpha^*_{A/B} = f(R_2/R_1, l_{(A)}, l_{(B),}\delta_{(A),}\delta_{(B)})$ and $P_{(i)}/P^*_{(i)} = g(R_2/R_1, l_{(i)}, \delta_{(i)})$. The first non-dimensional variable R_2/R_1 is geometrical and represents the relative thickness of the shell. The variable $\delta_{(i)}$ is the ratio between the core material intrinsic permeability (i.e. $D_{c(i)}S_{c(i)}$) and the intrinsic permeability of the anisotropic material (i.e. $\sqrt{D_{\theta(sh)(i)}D_{r(sh)(i)}}\, S_{sh(i)}$). In addition, $l_{(A)}$and $l_{(B)}$ are non-dimensional variables that characterize the anisotropicity of the shell. The variables $l_{(A)}$and $l_{(B)}$ are of special interest because they determine the specific anisotropic mass diffusion of A and B induced by the shell. We show in Figure 8.2 (left panels) the preferred trajectories of A and B for different values of $l_{(A)}$and $l_{(B)}$ when a binary mixture is diffusing through the anisotropic membranes. Note that when $l_{(i)} > 1$ $(i = A, B)$, we have $D_{\theta(sh)(i)} > D_{r(sh)(i)}$ and the anisotropic shell causes compound i to mainly detour around the core, whereas for $l_{(i)} < 1$, we have $D_{\theta(sh)(i)} < D_{r(sh)(i)}$ and the shell causes compound i to mainly focus towards the core. Therefore, depending on the values of $l_{(A)}$and $l_{(B)}$there exist four different scenarios. The membrane can (1) focus molecules of A towards the core and shield molecules of B from the core $(l_{(A)} < 1,\ l_{(B)} > 1)$ (Figure 8.2(a)), (2) detour both A and B around the core $(l_{(A)} > 1,\ l_{(B)} > 1)$ (Figure 8.2(b)), (3) focus both A and B $(l_{(A)} < 1,\ l_{(B)} < 1)$ (Figure 8.2(c)), and (4) shield A and focus B $(l_{(A)} > 1,\ l_{(B)} < 1)$ (Figure 8.2(d)). Note that most materials used in membrane science and technology are isotropic and lie at the origin of the plot (i.e. $l_{(i)} = 1$, and $D_{\theta(sh)(i)} = D_{r(sh)(i)}$).

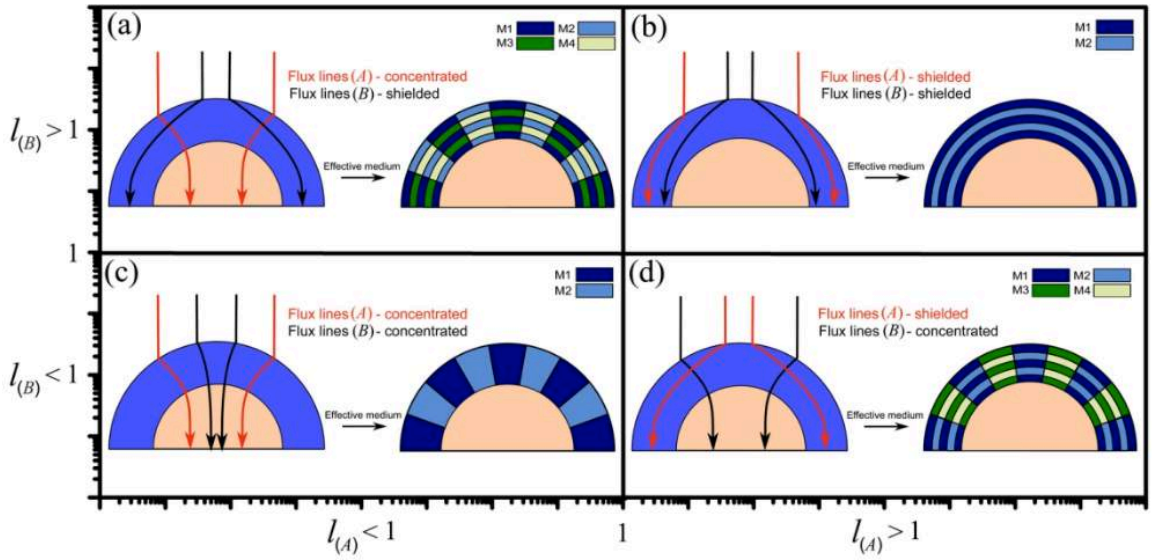

Figure 8.2. Schematic for the effect of the anisotropic shell on the trajectory of compounds *A* and *B* (a) $l_{(A)}<1$, $l_{(B)}>1$ (b) $l_{(A)}>1$, $l_{(B)}>1$ (c) $l_{(A)}<1$, $l_{(B)}<1$ (d) $l_{(A)}>1$, $l_{(B)}<1$. The shell structures made of isotropic materials that can create such mass diffusion trajectories are shown on the right.

We also show in Figure 8.2 (right panels) the corresponding shell structures that provide the anisotropic properties required to obtain the mass diffusion trajectories for *A* and *B*. We note that the shell structures are made of homogeneous and isotropic materials. The anisotropic structures made of isotropic materials are designed by using effective medium theory[4,7,8]. For example, to obtain $l_{(i)} > 1$ (i.e. $D_{\theta(sh)(i)} > D_{r(sh)(i)}$), a multilayer shell made of alternating materials M_1 and M_2 aligned along the azimuthal direction provides the required anisotropic shell structure where compound *i* prefers the azimuthal direction for diffusion (Figure 8.2(b))[4]. In this case, the azimuthal diffusivity $D_{\theta(sh)(i)}$ of the shell is given by a parallel diffusion model (Eq. (4.1)) while the radial diffusivity $D_{r(sh)(i)}$ is given by a series model (Eq. (4.1)). The diffusivities $D_{1(i)}$and $D_{2(i)}$ and solubilities $S_{1(i)}$ and $S_{2(i)}$ of the constitutive materials M_1 and M_2 that yield the

anisotropic structure with properties $D_{r(sh)(i)}$, $D_{\theta(sh)(i)}$, and $S_{sh(i)}$, can be found by solving the effective medium equations

$$D_{sh(i)}^{Parallel} = \frac{1}{(f_1+f_2k_i^*)}\left(f_1D_{1(i)} + f_2k_i^*D_{2(i)}\right); \quad \frac{1}{D_{sh(i)}^{Series}} = (f_1 + f_2k_i^*)\left(\frac{f_1}{D_{1(i)}} + \frac{f_2}{k_i^*D_{2(i)}}\right) \quad (4.1)$$

$$S_{sh(i)} = f_1S_{1(i)} + f_2S_{2(i)} \quad (4.2)$$

where f_1 and f_2 are the volume fractions of materials M_1 and M_2 and $k_i^* = \frac{S_{2(i)}}{S_{1(i)}}$ is the partition coefficient for compound *i* between materials M_1 and M_2. Analogously, to obtain $l_{(i)} < 1$ (i.e. $D_{\theta(sh)(i)} < D_{r(sh)(i)}$) a multilayer shell made of materials M_1 and M_2 aligned along the radial direction (i.e. in series in the azimuthal direction and in parallel in the radial direction) provides the anisotropic shell structure where the radial direction is preferred for diffusion (Figure 8.2(c)). To obtain $l_{(A)} < 1, l_{(B)} > 1$ (Figure 8.2(a)) or $l_{(A)} > 1, l_{(B)} < 1$ (Figure 8.2(d)) different structural arrangements are required. In the first case, compound *A* should effectively see shell layers aligned along the radial direction ($D_{\theta(sh)(A)} < D_{r(sh)(A)}$) while compound *B* should see shell layers along the azimuthal direction ($D_{\theta(sh)(B)} > D_{r(sh)(B)}$), (and vice versa for the second case). The required shell material properties for compounds *A* and *B* can be obtained simultaneously by arranging four materials M_1, M_2, M_3 and M_4 as shown in Figures 8.2(a) and 8.2(d). The properties of these materials must be selected such that for $l_{(A)} < 1, l_{(B)} > 1$

$$\begin{array}{llll} D_{1(A)}=D_{(A)*}, & S_{1(A)}=S_{(A)*}, & D_{1(B)}=D_{(B)*}, & S_{1(B)}=S_{(B)*} \quad M_1 \\ D_{2(A)}=D_{(A)*}, & S_{2(A)}=S_{(A)*}, & D_{2(B)}=D_{(B)\dagger}, & S_{2(B)}=S_{(B)\dagger} \quad M_2 \\ D_{3(A)}=D_{(A)\dagger}, & S_{3(A)}=S_{(A)\dagger}, & D_{3(B)}=D_{(B)*}, & S_{3(B)}=S_{(B)*} \quad M_3 \\ D_{4(A)}=D_{(A)\dagger}, & S_{4(A)}=S_{(A)\dagger}, & D_{4(B)}=D_{(B)\dagger}, & S_{4(B)}=S_{(B)\dagger} \quad M_4 \end{array} \quad (8.7)$$

while for $l_{(A)} > 1, l_{(B)} < 1$ * should be exchanged by † (and vice versa) in the properties of materials M_2 and M_3. The symbols * and † indicate the diffusion coefficients that are required to be similar.

An alternative approach to design the anisotropic shells consists in finding the effective properties of a set of given isotropic materials arranged as in Figures 8.2(a)-8.2(d). For anisotropic shells made of two isotropic materials aligned along the azimuthal or radial directions (Figures 8.2(b) and 8.2(c)), the effective properties can be calculated by the effective medium formulas Eqs (4.1)-(4.2). For the anisotropic shells made of four isotropic materials (Figures 8.2(a) and 8.2(d)) the effective properties can be found using effective medium theory equations deduced by using a resistor network analogy and are given by

$$D_{\theta(sh)(i)} = \frac{1}{(f_1+f_2)+(f_3+f_4)k_{r_1r_2(i)}}\left[\frac{(f_1+f_2)^3 k_{12(i)} D_{1(i)} D_{2(i)}}{(f_1+f_2 k_{12(i)})(f_1 k_{12(i)} D_{2(i)}+f_2 D_{1(i)})} + \frac{(f_3+f_4)^3 k_{r_1r_2(i)} k_{34(i)} D_{3(i)} D_{4(i)}}{(f_3+f_4 k_{34(i)})(f_3 k_{34(i)} D_{4(i)}+f_4 D_{3(i)})}\right] \quad (8.8)$$

$$D_{r(sh)(i)} = \frac{1}{(f_1+f_3)+(f_2+f_4)k_{c_1c_2(i)}}\left[\frac{(f_1+f_3)^3 k_{13(i)} D_{1(i)} D_{3(i)}}{(f_1+f_3 k_{13(i)})(f_1 k_{13(i)} D_{3(i)}+f_3 D_{1(i)})} + \frac{(f_2+f_4)^3 k_{c_1c_2(i)} k_{24(i)} D_{2(i)} D_{4(i)}}{(f_2+f_4 k_{24(i)})(f_2 k_{24(i)} D_{4(i)}+f_4 D_{2(i)})}\right] \quad (8.9)$$

$$S_{sh(i)} = f_1 S_{1(i)} + f_2 S_{2(i)} + f_3 S_{3(i)} + f_4 S_{4(i)} \quad (8.10)$$

$$k_{r1r2(i)} = \left(\frac{f_3 S_{3(i)}+f_4 S_{4(i)}}{f_1 S_{1(i)}+f_2 S_{2(i)}}\right)\left(\frac{f_1+f_2}{f_3+f_4}\right);\ k_{c1c2(i)} = \left(\frac{f_2 S_{2(i)}+f_4 S_{4(i)}}{f_1 S_{1(i)}+f_3 S_{3(i)}}\right)\left(\frac{f_1+f_3}{f_2+f_4}\right);\ k_{jk\,(i)} = \frac{S_{k(i)}}{S_{j(i)}} \quad (8.11)$$

where $D_{\theta(sh)(i)}$ and $D_{r(sh)(i)}$ are the azimuthal and radial diffusivities of the shell, $S_{sh(i)}$ is the solubility of the shell. $f_1, f_2 f_3$ and f_4 , $D_{1(i)}$, $D_{2(i)}$ $D_{3(i)}$ and $D_{4(i)}$, $S_{1(i)}$, $S_{2(i)}$ $S_{3(i)}$ and $S_{4(i)}$, are the volume fractions, diffusivities and solubilities of materials M_1, M_2, M_3, M_4. $k_{jk(i)}$ are the partition coefficients between materials j and k.

From an experimental perspective, the realization of the proposed structures should take advantage of the recent advances in the manufacture of multilayer systems at

the nanoscale, which offer an avenue for the experimental realization of the systems[9–13]. We also note that multilayer composites are one alternative to achieve anisotropic systems but other routes, which are also consistent with the proposed theoretical development, include the use of oriented non-spherical inclusions in a matrix material[14]. The use of intrinsically anisotropic materials, if available, constitutes an additional experimental route. We also note that the particular design shown in Figure 8.2(b) should not be confused with a multistage process. Our devices use a single pressure difference ($P_{\mathrm{HIGH}}-P_{\mathrm{LOW}}$), in contrast to multistage systems, where a set of pressure differences (one at each stage) is employed. We also stress that the proposed theoretical development applies to all the structures in Figure 8.2 and more generally to any anisotropic shell (i.e. beyond layered materials as in Figure 8.2(b)). In addition, the spatial dependence of the flux magnitude on the permeate side allows us to collect the permeate fraction of interest in a region that maximizes the selectivity or permeance of the device, which is in contrast to isotropic systems, where all the permeate that leaves the membrane is typically collected. Clearly, by collecting a fraction of the permeate in our devices there is an implicit trade-off between purity and recovery.

8.3 Results and Discussion

We calculate in Figures 8.3 and 8.4 the performance of the proposed anisotropic membranes in terms of the normalized selectivity and permeance as a function of the design variables $l_{(A)}$, $l_{(B)}$, $\delta_{(A)}$and $\delta_{(B)}$ for an aspect ratio R_2/R_1=2. Figures 8.3(a)-8.3(b) present the relative selectivity $\alpha_{A/B}/\alpha^*_{A/B}$ measuring the increase (or decrease) of the membrane selectivity with respect to the selectivity of the isotropic core without the shell. From the plots it can be seen how, for a fixed value of $\delta_{(A)}$ and $\delta_{(B)}$ the selectivity for *A*

increases when $l_{(A)}$ decreases and $l_{(B)}$ increases. This increase in selectivity can be explained by considering that a higher $\alpha_{A/B}$ is obtained when molecules of *A* are focused towards the core and molecules of *B* are detoured around it. In other words, to improve the performance it is necessary to favor the transport of *A* in the radial direction with respect to the azimuthal direction (i.e. small $l_{(A)}$) and simultaneously hinder the radial transport of *B* (i.e. large $l_{(B)}$). In terms of the structure of the shell, this means that the membranes shown in Figure 8.2(a) offer the best performance. Note that in the opposite case when $l_{(A)} > 1, l_{(B)} < 1$, the anisotropic shell favors the transport of *B* towards the core instead of *A*, this results in an inversion of the selectivity, such that *B* instead of *A* is collected at the core of the device (Figures 8.2(d) and 8.3(c)). Note that the performance is characterized under ideal conditions where boundary conditions are constant in space and time, assuming perfect mixing in the fluid, and neglecting concentration polarization. The shielding effect created when the magnitude of l_i is increased can also be observed in Figure 8.4, where we plot the normalized permeance $P_{(i)}/P^*_{(i)}$ as a function $l_{(i)}$ and $\delta_{(i)}$. It can be seen from the plot that for a fixed value of $\delta_{(i)}$ the normalized permeance of *i* from the core decreases as $l_{(i)}$ increases, which corresponds to a stronger shielding shell. Note that the selectivity increases when permeance of *A* is high ($l_{(A)}$ small) and the permeance of *B* is low ($l_{(B)}$ large).

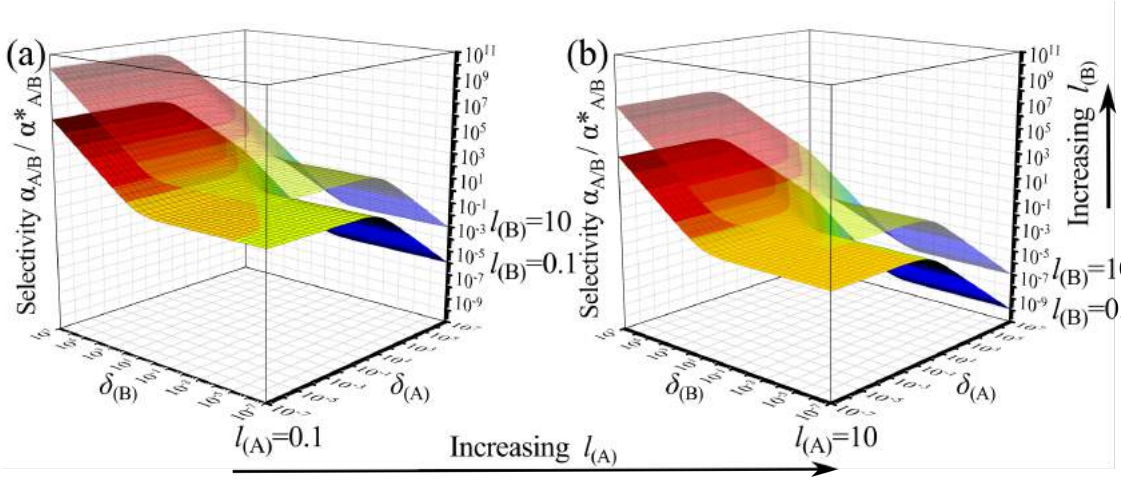

Figure 8.3. Normalized selectivity as a function of the non-dimensional variables $l_{(i)}$ and $\delta_{(i)}$ for a shell/core ratio R_2/R_1=2. (a) $l_{(A)}$=0.1, (b) $l_{(A)}$=10.

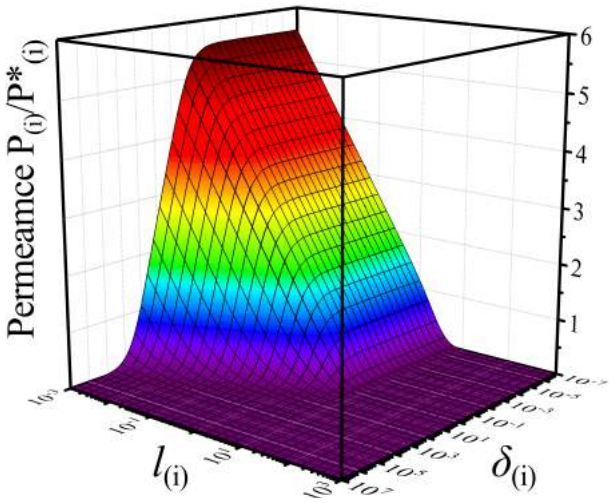

Figure 8.4. Normalized permeance as a function of $l_{(i)}$ and $\delta_{(i)}$ for a ratio R_2/R_1=2.

The performance of the system is also determined by the values of the non-dimensional variables $\delta_{(A)}$, and $\delta_{(B)}$. We can see from Figure 8.4 that for a constant value of $l_{(i)}$ the normalized permeance of i increases when the value of $\delta_{(i)}$ decreases. Therefore $\alpha_{A/B}/\alpha^*_{A/B}$ should increase for small $\delta_{(A)}$ (large permeance of A) and large $\delta_{(B)}$ (small permeance of B), which agrees with the selectivity plots shown in Figure 8.3. This

behavior can also be analyzed by considering a fixed core material ($D_{c(i)}$ and $S_{c(i)}$ are constant) and noting that in order to make $\delta_{(A)}$ small (such that normalized permeance of A increases) it is required to increase the intrinsic permeance $\sqrt{D_{\theta(sh)(A)}D_{r(sh)(A)}}\,S_{sh(A)}$ of the anisotropic shell, thus causing an increase in the amount of compound A that enters the shell and therefore the permeance at the core $P_{(A)}/P^*_{(A)}$. Analogously, to obtain a large $\delta_{(B)}$, we need to reduce the shell permeance for B. This reduction causes a smaller amount of compound B to enter the shell and in the limiting case the normalized permeance tends to zero at the core, in agreement with the trend observed in Figure 8.4.

In Figure 8.5, we plot the normalized selectivity versus permeance of our proposed membranes. For reference, we show with a black star the selectivity and permeance of the core material, which corresponds to $\alpha_{A/B}/\alpha^*_{A/B} = 1$ and $P_{(A)}/P^*_{(A)} = 1$. We can see how different values of selectivities and permeances can be obtained for different values of the non-dimensional variables $l_{(A)}, l_{(B),}\delta_{(A),}\delta_{(B)}$. Figure 8.5 shows that the selectivity and permeance of this system can be broadly manipulated through the structural design of the shell. Note that in many cases, higher selectivity values are achieved in the case of the anisotropic membrane. We note that the feasible region in Figure 8.5 depends on the mix to be separated and needs to be established for each gas pair based on the properties of the available materials for that mix. It is also interesting to note that under certain conditions similar performances can be achieved with different structures. For example, black and blue squares in Figure 8.5 represent membranes with $l_{(B)}$=10 and $\delta_{(B)}$=10^7. The black squares have $l_{(A)}$=10 while for the blue squares $l_{(A)}$=0.1 and the performance is modulated by $\delta_{(A)}$. Note that there are overlapping regions where similar performances can be achieved by using different structures.

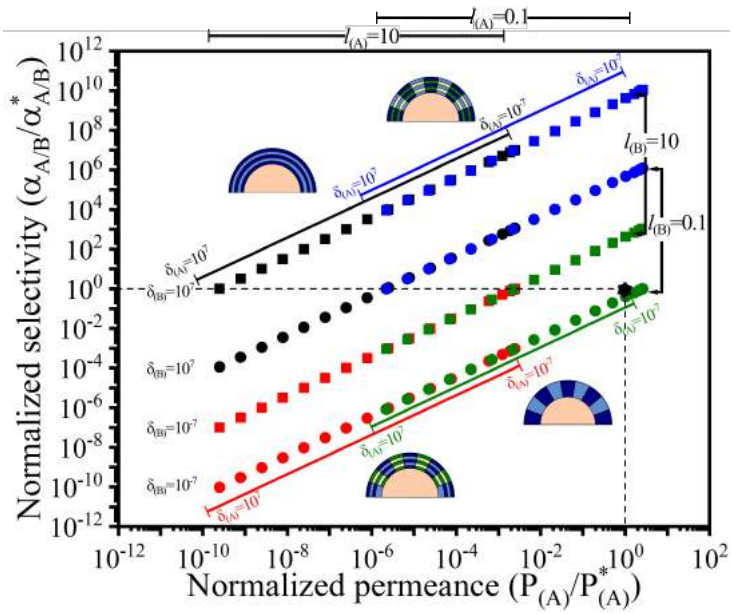

Figure 8.5. Selectivity vs. permeance for different values of the non-dimensional variables $\delta_{(A)}$, $\delta_{(B)}$, $l_{(A)}$ and $l_{(B)}$.

To provide insight on the dynamics of anisotropic mass separation membranes, we show in Figure 8.6 the concentrations profiles (color maps where red corresponds to high concentration and blue to low concentration) and flux lines (white arrows) for compounds *A* and *B* within the membrane for the systems shown in Figures 8.2(a)-(d). On the upper panels, we consider membranes made of homogeneous anisotropic materials, while in the lower panels, we consider the corresponding layered membranes made of isotropic materials, which are obtained via effective medium theory (Eqs (4.1)-(4.2)). The imposed boundary conditions are $p_{(i)} = 1$atm at the upper boundary and $p_{(i)} = 0$atm at the bottom of the structures. The plots clearly show the functionalities of the structures, since it can be seen in Figure 8.6 how compounds *A* and *B* are focused towards the core or shielded from the core depending on the values of $l_{(A)}$ and $l_{(B)}$. For simplicity, we assume constant solubility across the constituent materials. Importantly we

can see that the flux trajectories followed by compounds *A* and *B* in the homogeneous anisotropic material and the effective multilayer composite are similar showing that the layered structures can reproduce the required anisotropy to redirect the flux of *A* and *B*. Clearly, this similarity asymptotically increase with increasing number of layers per unit volume[3,5].

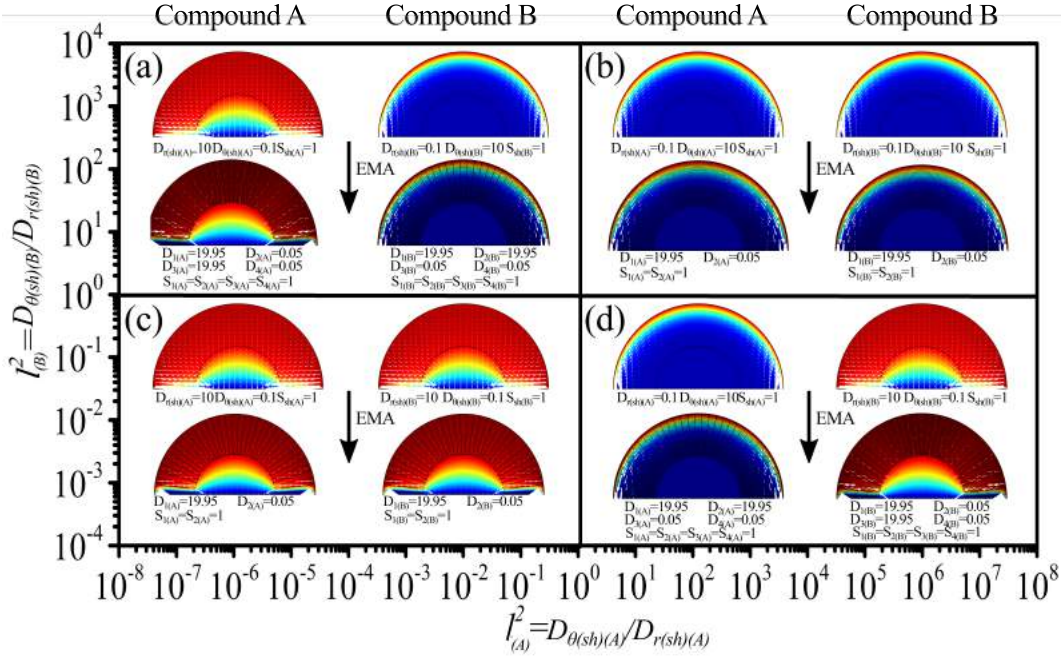

Figure 8.6. Color maps for concentration distribution of compounds *A* (left) and *B* (right) inside the anisotropic membranes. We show both homogeneous anisotropic shells (top) and the corresponding multilayer shells (bottom) obtained by effective medium theory (a) $l_{(A)}<1$, $l_{(B)}>1$ (b) $l_{(A)}>1$, $l_{(B)}>1$ (c) $l_{(A)}<1$, $l_{(B)}<1$ (d) $l_{(A)}>1$, $l_{(B)}<1$. For simplicity, the materials are assumed to have similar solubilities.

We next apply our proposed approach to a realistic system and introduce anisotropic membranes for separation of the binary system H_2/CH_4. This binary mixture was selected due to its relevance in the recovery of hydrogen[15]. We found four isotropic materials PTMSP[16], PDMS[17], PIM-7[18] and PMDA-BATPHF[19] which allow to obtain the shell structures with the different anisotropies for H_2 and CH_4 as shown in Figure 8.7.

These materials have been selected such that the effective properties of the resulting composites satisfy the constraints in terms of the magnitude of $l_{(A)}$ and $l_{(B)}$ in each of the shells (e.g. in Figure 8.7(b) $l_{(A)}>1$ and $l_{(B)}>1$). The physical properties of the materials are listed in Table 8.1 (additional results for PSF[20] and PDMS are presented in the SI). We show in Figure 8.7 our numerical predictions for selectivity α_{H_2/CH_4} vs. permeance $P_{(H_2)}$ for the different types of membranes as a function of the number of building-blocks. In Figure 8.7(b) we plot α vs. P (blue lines) for membranes with increasing number of bilayers N arranged in the azimuthal direction while in Figure 8.7(c) the membranes have increasing number of bilayers m arranged in the radial direction. On the other hand, the membranes in Figures 8.7(a) and 8.7(d) are described in terms of the total number of bilayers N and m in the azimuthal and radial directions respectively. For reference, we also show the selectivity and permeance values when the shells are made of a homogeneous anisotropic material (black stars), which corresponds to the limiting case of a large number of bilayers N and m. We note that the performance of the multilayer membranes approaches that of a homogeneous anisotropic system when the number of bilayers N and m increases. In terms of performance for hydrogen separation, the membranes shown in Figure 8.7(a) offer both large selectivities and permeances. On the other hand, the membranes in Figures 8.7(b) and 8.7(c) show very high selectivities and low permeances (Figure 8.7(b)) and high permeances and low selectivities (Figure 8.7(c)). Interestingly, in Figure 8.7(d) we obtain a selectivity inversion where the membranes become CH_4 selective. Importantly, this selectivity inversion is achieved by only changing the arrangement of isotropic materials, thus changing the effective medium properties, and not by chemical modifications of the constituent materials. The above

results show the rich behavior in terms of selectivities and permeances that can be obtained by considering anisotropic mass diffusion membranes for separation.

Table 8.1. Diffusion properties of the shell materials in Figure 8.7. The effective properties for the shells are calculated using effective medium theory.

	$S_{(H2)}$ [mol/m^{3}Pa]	$D_{(H2)}$ [m^2/s]	$S_{(CH4)}$ [mol/m^{3}Pa]	$D_{(CH4)}$ [m^2/s]	$D_{r(sh)(H2)}$ [m^2/s]	$D_{\theta(sh)(H2)}$ [m^2/s]	$D_{r(sh)(CH4)}$ [m^2/s]	$D_{\theta(sh)(CH4)}$ [m^2/s]
PTMSP	1.74×10^{-4}	2.60×10^{-8}	1.25×10^{-3}	3.60×10^{-9}				
PDMS	2.41×10^{-4}	1.10×10^{-9}	3.62×10^{-3}	5.10×10^{-12}				
PIM-7	1.98×10^{-5}	1.29×10^{-8}	1.67×10^{-4}	2.17×10^{-9}				
PMDA-BATPHF	6.94×10^{-5}	2.20×10^{-10}	4.22×10^{-4}	6.90×10^{-13}				
Figures 8.2(a)-8.7(a)	1.26×10^{-4}		1.40×10^{-3}		2.10×10^{-9}	2.03×10^{-9}	1.37×10^{-11}	2.45×10^{-10}
Figures 8.2(b)-8.7(b)	1.22×10^{-4}		8.36×10^{-4}		2.50×10^{-10}	1.86×10^{-8}	6.95×10^{-13}	2.69×10^{-9}
Figures 8.2(c)-8.7(c)	1.22×10^{-4}		8.36×10^{-4}		1.86×10^{-8}	2.50×10^{-10}	2.69×10^{-9}	6.95×10^{-13}
Figures 8.2(d)-8.7(d)	1.26×10^{-4}		1.40×10^{-3}		2.03×10^{-9}	2.10×10^{-9}	2.45×10^{-10}	1.37×10^{-11}

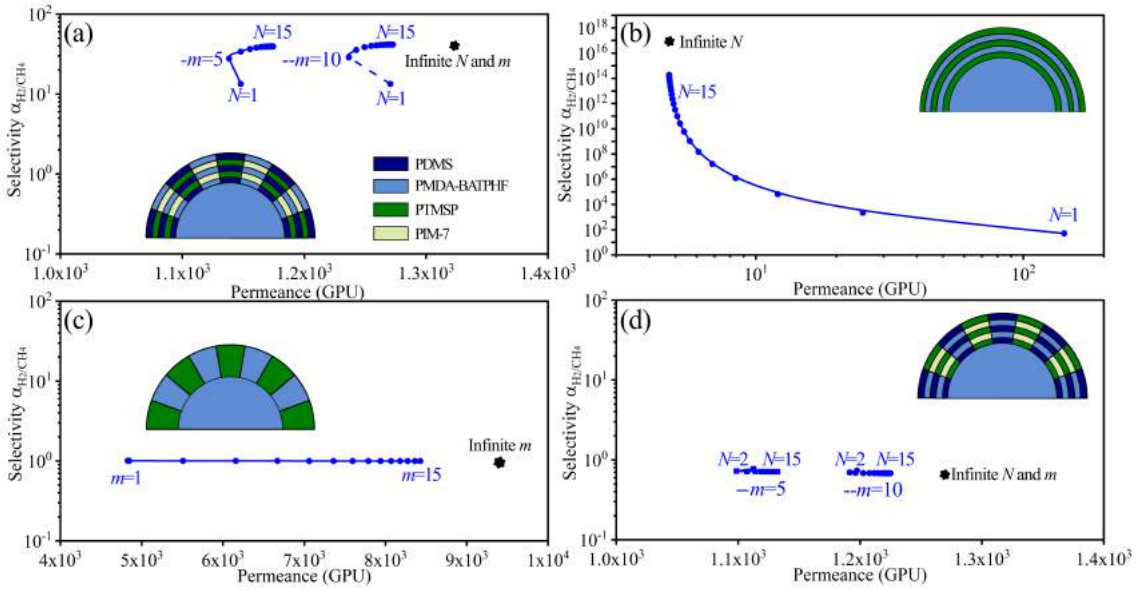

Figure 8.7. Selectivity vs. permeance for different anisotropic membranes for separation of H_2/CH_4 with different number of azimuthal N and radial m layers (blue circles) (a) CH_4 shielded from the core and H_2 focused towards the core (b) Both CH_4 and H_2 are shielded from the core. (c) Both CH_4 and H_2 are focused towards the core (d) CH_4 is focused towards the core and H_2 is shielded from the core. The black stars correspond to homogeneous anisotropic shells. Results are presented for R_1=1μm.

8.4 Conclusions

In this chapter we studied the complete design space for the anisotropic membrane materials developed in chapter 7. We have demonstrated that the performance of these materials can be characterized in terms of three dimensionless parameters: $l_{(i)}$, $\delta_{(i)}$ and R_2/R_1. The required anisotropicity for mass diffusion is obtained in practice by considering composite materials and using effective medium to design their effective anisotropic properties. We have shown the effective medium structures required to realize different flux trajectories based on the nature of the anisotropic shell. We note that the properties of the membrane materials studied are achieved by tailoring anisotropic properties for mass diffusion in order to manipulate the trajectory of the diffusing molecules. This is in contrast to conventional chemical modifications of membrane materials for separations, which only modify the flux magnitude.

8.5 References

(1) Restrepo-Flórez, J.-M.; Maldovan, M. Metamaterial Membranes. *J. Phys. D. Appl. Phys.* **2017**, *50*, 25104.

(2) Restrepo-Flórez, J. M.; Maldovan, M. Mass Separation by Metamaterials. *Sci. Rep.* **2016**, *6* (2), 21971.

(3) Restrepo-Flórez, J. M.; Maldovan, M. Rational Design of Mass Diffusion Metamaterial Concentrators Based on Coordinate Transformations. *J. Appl. Phys.* **2016**, *120* (8), 084902.

(4) Restrepo-Flórez, J. M.; Maldovan, M. Mass Diffusion Cloaking and Focusing with Metamaterials. *Appl. Phys. Lett.* **2017**, *111* (7), 071903.

(5) Restrepo-Flórez, J.-M.; Maldovan, M. Breaking Separation Limits in Membrane Tehnology. *J. Memb. Sci.* **2018**.

(6) Baker, R. W. Future Directions of Membrane Gas Separation Technology. *Ind. Eng. Chem. Res.* **2002**, *41* (6), 1393–1411.

(7) Davis, H. T. The Effective Medium Theory of Diffusion in Composite Media. *J. Am. Ceram. Soc.* **1977**, *60* (11–12), 499–501.

(8) Sax, J.; Ottino, J. M. Modeling of Transport of Small Molecules in Polymer Blends: Application of Effective Medium Theory. *Polym. Eng. Sci.* **1983**, *23* (1 l), 165–176.

(9) Borges, J.; Mano, J. F. Molecular Interactions Driving the Layer-by-Layer Assembly of Multilayers. *Chem. Rev.* **2014**, *114* (18), 8883–8942.

(10) Richardson, J. J.; Björnmalm, M.; Caruso, F. Technology-Driven Layer-by-Layer Assembly of Nanofilms. *Science.* **2015**, *348* (6233).

(11) Ajitha, A. R.; Aswathi, M. K.; H.J., M.; Izdebska, J.; Thomas, S. *Multicomponent Polymeric Materials*; Kim, J., Thomas, S., Saha, P., 1st Ed.; Springer: Dordrecht, 2016; Vol. 223.

(12) Ponting, M.; Hiltner, A.; Baer, E. Polymer Nanostructures by Forced Assembly: Process, Structure, and Properties. *Macromol. Symp.* **2010**, *294* (1), 19–32.

(13) Gupta, M.; Lin, Y.; Deans, T.; Baer, E.; Hiltner, A.; Schiraldi, D. A. Structure and Gas Barrier Properties of Poly (Propylene-Graft-Maleic Anhydride)/ Phosphate Glass Composites Prepared by Microlayer Coextrusion. *Macromolecules* **2010**, *43*, 4230–4239.

(14) Moccia, M.; Castaldi, G.; Savo, S.; Sato, Y.; Galdi, V. Independent Manipulation of Heat and Electrical Current via Bifunctional Metamaterials. *Phys. Rev. X* **2014**, *4* (2), 021025.

(15) Bernardo, P.; Drioli, E.; Golemme, G. Membrane Gas Separation: A Review/State of the Art. *Ind. Eng. Chem. Res.* **2009**, *48* (10), 4638–4663.

(16) Merkel, T. C.; Bondar, V.; Nagai, K.; Freeman, B. D. Perfluorocarbon Gases in Poly (1-Trimethylsilyl-1-Propyne). *J. Polym. Sci. Part B Polym. Phys.* **2000**, *38*, 273–296.

(17) Merkel, T. C.; Bondar, V. I.; Nagai, K.; Freeman, B. D.; Pinnau, I. Gas Sorption, Diffusion, and Permeation in Poly(Dimethylsiloxane). *J. Polym. Sci. Part B Polym. Phys.* **2000**, *38* (3), 415–434.

(18) Budd, P. M.; Msayib, K. J.; Tattershall, C. E.; Ghanem, B. S.; Reynolds, K. J.; McKeown, N. B.; Fritsch, D. Gas Separation Membranes from Polymers of Intrinsic Microporosity. *J. Memb. Sci.* **2005**, *251* (1–2), 263–269.

(19) Tanaka, K.; Kita, H.; Okano, M.; Okamoto, K. Permeability and Permselectivity of Gases in Fluorinated and Non-Fluorinated Polyimides. *Polymer.* **1992**, *33* (3), 585–592.

(20) McHattie, J. S.; Koros, W. J.; Paul, D. R. Gas Transport Properties of Polysulfones: 1. Role of Symmetry of Methyl Group Placement on Bisphenol. *Polymer.* **1991**, *32* (5), 840–850.

CHAPTER 9: ANALYSIS AND CHARACTERIZATION OF ANISOTROPIC HOLLOW FIBERS FOR GAS SEPARATIONS

9.1 Introduction

In previous chapters we have proved that flux directional control is possible by using anisotropic materials[1–4]. Furthermore, we have shown how structured composites (metamaterials) made of multilayers display effective anisotropic behavior, thus enabling the rational design of membrane materials that can control the diffusion trajectory of the species in a binary mixture as they cross the membrane[1,2,5]. We have also described different membrane devices designed to take advantage of flux directional control in anisotropic materials[1]. One of the main challenges associated with our previous devices is the complexity of the structures in terms of experimental fabrication. Towards this end, in this chapter, we study and characterize one of the simplest anisotropic membranes: a multilayer slab. We describe the proposed membrane and illustrate how this membrane can be arranged in a hollow-fiber-like geometry, constituting a significantly simpler configuration. We subsequently study mass diffusion through the anisotropic membrane and the separation performance; which allows us to identify relevant design parameters. Finally, we explore and characterize in detail the design space for these membranes in terms of selectivity and permeability.

9.2 Theoretical analysis

Before discussing the details of the diffusion process across the proposed anisotropic membrane, lets first focus on their operation. Anisotropic materials can guide the diffusion of molecules toward different places[1]. Note that as a consequence of the

physical rerouting of flux lines toward specific locations, a position dependent flux on the permeate site is generated. In order to take advantage of this feature it is necessary to conceive membrane designs in which two permeate fractions are collected. The fact that flux is dependent on position enables to select the region where the species of interest is to be collected. Importantly, anisotropic membranes need to be conceived such that the two permeate fractions generated can be collected independently without mixing.

In this chapter, we are interested in studying a simple case scenario in terms of both geometry and material properties. We consider a slab of length L and thickness H (Figure 9.1(a)). The anisotropic slab is operated such that permeation of species i occurs as a result of applying a partial pressure $p_{(i)}$ at the upper boundary and complete sweeping (i.e. $p_{(i)} = 0$) at the bottom, left, and right sides (i.e. a 2D driving force). This mode of operation generates two different and independent permeates: a permeate leaving the system through the bottom, and a permeate leaving the system through the sides (Figure 9.1(a)). At the material level, we consider that the slab is made of a material with anisotropic diffusivity $\overline{\overline{D}}_{(i)}$ (Eq. (9.1)) and solubility $S_{(i)}$. Importantly, in this case, the off-diagonal elements of the diffusivity tensor are considered equal to zero (i.e. $D_{xy(i)} = D_{yx(i)} = 0$). An ideal anisotropic material for the separation of a binary mixture should be able to direct the species of interest A towards the bottom of the device, while simultaneously rerouting the other species B to the sides. In this manner, by collecting the permeate fraction at the bottom, one is recovering the purified species of interest. An important advantage of this anisotropic slab design arises from the possibility of adapting it to an "anisotropic hollow fiber". As it is shown in Figure 9.1(a), the slab can be transformed into a cylindrical shell via bending. We next study the performance of the

anisotropic slab in terms of separation, which can be adapted to form an anisotropic hollow fiber.

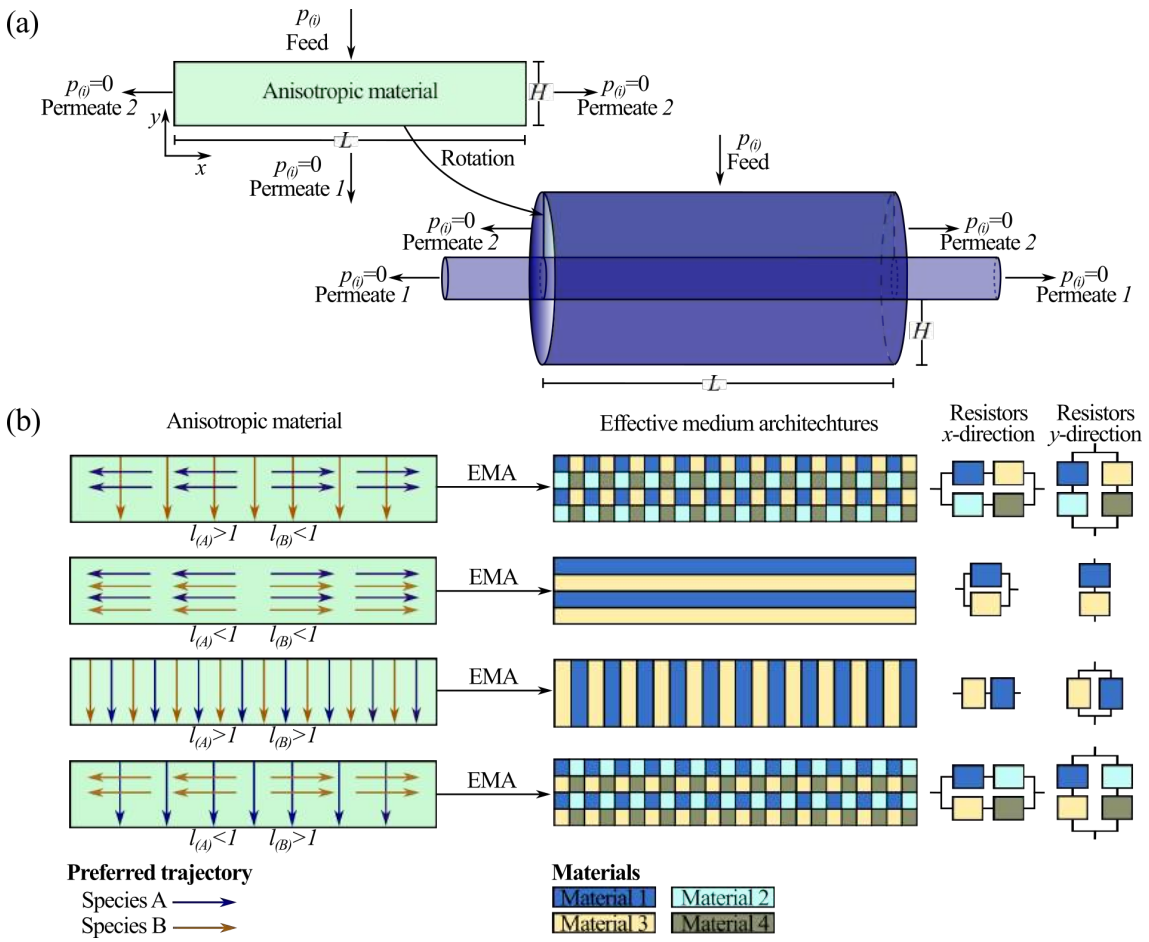

Figure 9.1. (a) Anisotropic membrane slab (light green) and operating conditions. The slab can be transformed into a cylindrical shell via bending/rotation. (b) A schematic of the anisotropic membrane slab with different preferred directions of transport for *A* and *B* as a function of $l_{(A)}$ and $l_{(B)}$ (left). Effective medium architectures for the required anisotropicity (center. A resistors network analogy representing the resistance to diffusion in different effective media (right). The resistor network analogy is used to calculate the effective properties of the composites.

$$\bar{\bar{D}}_{(i)} = \begin{bmatrix} D_{xx(i)} & 0 \\ 0 & D_{yy(i)} \end{bmatrix} \tag{9.1}$$

Mathematically, we model mass diffusion through the membrane using the anisotropic version of Fick's law (Eq. (9.2)), which along with the continuity equation yield the partial differential equation governing the diffusion of species *i* at steady state (Eq. (9.3)),

$$J_{(i)} = \overline{\overline{D}}_{(i)} \nabla C_{(i)} \tag{9.2}$$

$$\frac{\partial^2 C_{(i)}}{\partial x^2} + l_{(i)}^2 \frac{\partial^2 C_{(i)}}{\partial y^2} = 0 \tag{9.3}$$

where $l_{(i)}^2 = D_{yy(i)}/D_{xx(i)}$ defines the *contrast* of the anisotropic material.

Eq. (9.3) can be solved using separation of variables by postulating a solution of the form $C_{(i)}(x,y) = G_{(i)}(x)H_{(i)}(y)$. With a general concentration profile given by Eq. (9.4).

$$C_{(i)}(x,y) = \sum_{n=1}^{\infty} \left(A_{n(i)} e^{-\frac{\lambda}{l_{(i)}} y} + B_{n(i)} e^{\frac{\lambda}{l_{(i)}} y} \right) \sin\left(\frac{n\pi}{L} x\right) \tag{9.4}$$

Using the boundary conditions of the problem, we find the value of the unknown constants $A_{n(i)}$, $B_{n(i)}$ and λ, such that the concentration profile is finally given by Eq. (9.5). Results obtained using this equation were validated against numerical solutions using the finite elements software Comsol Multiphysics® version 5.3[6] and we found excellent agreement.

$$C_{(i)}(x,y) = \frac{2p_{(i)}S_{(i)}}{\pi} \sum_{n=1}^{\infty} \frac{((-1)^n - 1)}{n} \left(\frac{\sinh\left(\frac{n\pi(y-H)}{Ll_{(i)}}\right)}{\sinh\left(\frac{n\pi H}{Ll_{(i)}}\right)} \right) \sin\left(\frac{n\pi x}{L}\right) \tag{9.5}$$

We consider permeate 1 (Figure 9.1) as the fraction of the permeate to be collected and use the formulas for permeability (Eq. (9.6)) and selectivity (Eq. (9.7)) to characterize the performance of the anisotropic membrane[7–9]

$$P'_{(i)} = \frac{\langle J_{y(i)} \rangle H}{\Delta p_{(i)}} = \frac{4S_{(i)}D_{yy(i)}}{\pi l_{(i)}}\left(\frac{H}{L}\right)\sum_{n=1}^{\infty}\frac{(1-(-1)^n)}{n}\frac{1}{\sinh\left(\frac{n\pi}{l_{(i)}}\left(\frac{H}{L}\right)\right)} \tag{9.6}$$

$$\alpha_{A/B} = \frac{P_{(A)}}{P_{(B)}} = \frac{S_{(A)}D_{yy(A)}l_{(B)}}{S_{(B)}D_{yy(B)}l_{(A)}}\left(\frac{H}{L}\right)\frac{\sum_{n=1}^{\infty}\frac{(1-(-1)^n)}{n}\frac{1}{\sinh\left(\frac{n\pi}{l_{(A)}}\left(\frac{H}{L}\right)\right)}}{\sum_{n=1}^{\infty}\frac{(1-(-1)^n)}{n}\frac{1}{\sinh\left(\frac{n\pi}{l_{(B)}}\left(\frac{H}{L}\right)\right)}} \tag{9.7}$$

where $\langle J_{y(i)} \rangle$ is the average flux in the in the *y* direction.

As it can be seen from Eqs (9.6)-(9.7) the performance of the membrane can be characterized using a small number of variables. Both permeabilities and selectivities depend on the dimensionless numbers $l_{(i)}$ describing the anisotropy and the aspect ratio H/L. Note that the magnitudes of $P'_{(i)}$ and $\alpha_{A/B}$ are modulated by the products $P^{*\prime}_{(i)} = S_{(i)}D_{yy(i)}$, and $\alpha^*_{A/B} = S_{(A)}D_{yy(A)}/S_{(B)}D_{yy(B)}$, respectively. We note that $P^{*\prime}_{(i)}$ can be interpreted as the permeability of an isotropic material with solubility $S_{(i)}$and diffusivity $D_{yy(i)}$, operated under a one-dimensional driving force; likewise $\alpha^*_{A/B}$ can be understood as the selectivity of this isotropic membrane under a one-dimensional driving force [7–10]. If $l_{(i)} > 1$ the preferred direction of transport is toward the bottom of the membrane, while if $l_{(i)} < 1$ the preferred direction is toward the sides. This gives rise to four different cases as illustrated in Figure 9.1(b): $l_{(A)} > 1$ and $l_{(B)} < 1$, $l_{(A)} > 1$ and $l_{(B)} > 1$, $l_{(A)} < 1$ and $l_{(B)} < 1$, $l_{(A)} < 1$ and $l_{(B)} > 1$. Note that each of the cases can be realized in practice by using a specific structured metamaterial composite (Figure 9.1(center)). If $l_{(A)} > 1$ and $l_{(B)} > 1$, the composite consist of a stack of layered polymers oriented vertically; in this case resistances add in parallel in the *y*-direction and in series in the *x*-direction, ensuring that *y* is the preferred direction of transport. Similarly, if $l_{(A)} < 1$ and $l_{(B)} < 1$,

the composite consists of a stack of layered polymers oriented horizontally. In this case, mass resistances add in series in the *y*-direction and in parallel in the *x*-direction; thus the preferential direction of transport is inverted. For the cases $l_{(A)} > 1, l_{(B)} < 1$, and $l_{(A)} < 1, l_{(B)} > 1$, where there is a decoupling between the diffusion trajectories of the two species *A* and *B* it is necessary to use four materials. From the figure, note that two resistor networks arise in this case: one network in the *x*-direction and one network in the *y*-direction. To ensure that the preferred direction of transport is different for the two species of interest it is required to rationally choose a spatial material distribution. The equations to calculate the effective medium properties for these more complex cases can be found in chapters (Eqs. (4.1)-(4.2) and (8.8)-(8.10)). Although the experimental realization of these configurations is challenging, recent advances in polymer multilayer manufacturing opening a path that enable the realization of complex multilayer systems[11–14].

9.3 Results and discussion

In Figure 9.2 we calculate the normalized permeability for species *i* ($P'_{(i)}/P^{*\prime}_{(i)}$) as a function of the dimensionless variables $l_{(i)}$ and H/L. From Figure 9.2(a) we see that the magnitude of $l_{(i)}$ controls the magnitude of the normalized permeability ($P'_{(i)}/P^{*\prime}_{(i)}$), where an increase in $l_{(i)}$ translates into an increase in the relative permeability (Figure 9.2(a)). Likewise, if $l_{(i)}$ decreases, the normalized permeability is reduced, such that if $l_{(i)} \to 0$ we have $P'_{(i)}/P^{*\prime}_{(i)} \to 0$. This behavior is explained by realizing that $l_{(i)}$ measures the preference of the membrane for transporting species *i* into the *y*-direction. Larger values of $l_{(i)}$ mean a stronger ability to reroute molecules of species *i* toward the bottom. The

physical effect of increasing $l_{(i)}$ is clearly observed by comparing the results obtained for different anisotropic membranes with those obtained for isotropic membranes where $l_{(i)} = 1$ (i.e. $D_{yy(i)} = D_{xx(i)}$) (dashed line in Figure 9.2(a)). For constant *H/L* ratio, it is observed from Figure 9.2(a), that if $l_{(i)} < 1$ (i.e. $D_{yy(i)} < D_{xx(i)}$) the predicted relative permeability is smaller than that of an isotropic material ($l_{(i)} = 1$), a consequence of the fact that in this case the *x*-direction is the preferred direction for transport and species *i* is rerouted to the sides of the membrane. Similarly, if $l_{(i)} > 1$ (i.e. $D_{yy(i)} > D_{xx(i)}$) the predicted relative permeability is larger than that obtained with an isotropic material ($l_{(i)} = 1$) operated under the same conditions. The value of $P'_{(i)}/P^{*\prime}_{(i)}$ is smaller than one meaning that the relative permeability is reduced in comparison with the reference permeability $P^{*\prime}_{(i)}$. This reference value corresponds to the permeability of an isotropic membrane with diffusivity $D_{yy(i)}$ and solubility $S_{(i)}$ operated under a one-dimensional driving force. This result is a consequence of the fact that in the proposed design we use a two-dimensional driving force (pressure equal to zero at the bottom and the sides of the membrane), generating two independent permeates. We only collect the fraction of species *i* that leaves through the bottom and there is a fraction of species *i* that leaves the membrane through the sides. Thus, it is consistent to observe a permeability reduction in comparison with an isotropic material with permeability $P^{*\prime}_{(i)}$ under a one-dimensional field in which flux moves in the *y*-direction and it is all collected at the bottom. We note that in the limiting case when $l_{(i)} \to \infty$ the membrane behaves as an isotropic material ($P'_{(i)}/P^{*\prime}_{(i)} \to 1$) operated under a one-dimensional driving force. This trend can be explained by considering that as the value of $l_{(i)}$ increases, the preference for diffusing in

the x-direction is reduced. As a result, if $l_{(i)} \to \infty$, mass diffusion in x is negligible in comparison with mass diffusion in y and the system is essentially one-dimensional. The asymptotic convergence to the isotropic one-dimensional case as the value of $l_{(i)}$ increases can be observed in Figure 9.2(c), where the flux lines become vertical for larger values of $l_{(i)}$. This behavior is also corroborated in Figure 9.2(b) where the local permeability at the bottom of the system flattens (i.e. its dependence on the position is reduced $P'_{(i)}(x) \to P'_{(i)}$) as $l_{(i)}$ increases. This profile is similar to an isotropic material in a one-dimensional gradient in which the flux leaving the membrane is independent of the position. In addition, we note the different trends for $P'_{(i)}/P^{*\prime}_{(i)}$ bounds when $l_{(i)} \to 0$ or $l_{(i)} \to \infty$. Specifically, we note that increasing the magnitude of $l_{(i)}$ above a certain value has a small effect on $P'_{(i)}/P^{*\prime}_{(i)}$ (e.g. for $H/L = 0.5$ the critical $l_{(i)}$value is ~3). In contrast, by decreasing the value of $l_{(i)}$, the predicted $P'_{(i)}/P^{*\prime}_{(i)}$ is reduced monotonically. Another physical variable that influences the resultant relative permeability is the aspect ratio of the membrane H/L. There are two trends that can be observed in Figure 9.2(a). First, note that when the aspect ratio decreases, the critical $l_{(i)}$ value also decreases. For example, if $H/L = 0.5$, the critical $l_{(i)}$ above which there is no significant change in $P'_{(i)}/P^{*\prime}_{(i)}$ is ~3 while if $H/L = 5$ the critical $l_{(i)}$ is ~10. Secondly, for a constant value of $l_{(i)}$, when the aspect ratio increases, the relative permeability $P'_{(i)}/P^{*\prime}_{(i)}$ decreases. Both of these trends can be explained by analyzing the trajectory that a gas molecule follows as it reaches the bottom of the membrane. We note that a molecule can move both in the x and y directions under the described operating conditions. For simplicity, let us consider a membrane with constant L. When the aspect ratio increases (i.e. increasing H), the minimum distance that

a molecule travels in the y-direction before leaving the membrane increases, while the distance in the x-direction remains constant. Increasing the aspect ratio causes a reduction in $P'_{(i)}/P^{*\prime}_{(i)}$. Similarly, $P'_{(i)}/P^{*\prime}_{(i)}$ increases when the aspect ratio decreases.

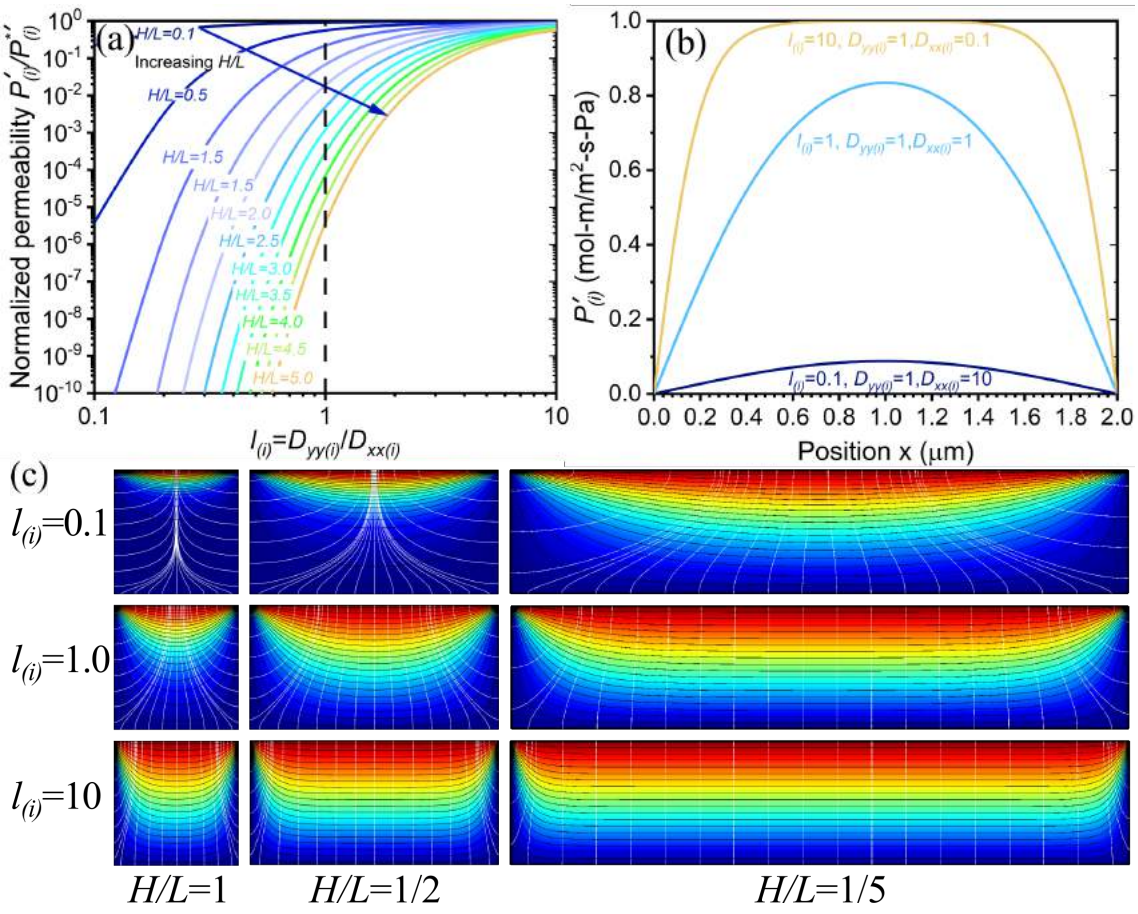

Figure 9.2. (a) Normalized permeability $P'_{(i)}/P^{*\prime}_{(i)}$ as a function of $l_{(i)}$ for different aspect ratios H/L. Dashed line represents the permeability for an isotropic material with $l_{(i)} = 1$. (b) Local permeability $P'_{(i)}(x)$ of the system at the bottom of the membrane as a function of the x-coordinate for representative values of $l_{(i)}$ and $H/L = 2$. (c) Color maps of the concentration profiles for representative values of $l_{(i)}$ and H/L. Isoconcentration lines are presented in black, and flux lines are displayed in white.

In Figure 9.3 we study the effects of $l_{(A)}$, $l_{(B)}$ and H/L on the relative selectivity $\alpha_{A/B}/\alpha^*_{A/B}$ of the membrane. As we have discussed, $\alpha^*_{A/B}$ represents the selectivity of an isotropic material with permeabilities $P^{*\prime}_{(A)}$ and $P^{*\prime}_{(B)}$ for species A and B, respectively. Note that in this material, separation occurs exclusively due to the difference in the flux magnitude of species A and B. Therefore, the ratio $\alpha_{A/B}/\alpha^*_{A/B}$ can be interpreted as an enhancement factor obtained when flux directional control is enabled in the membrane. We found that an increment in the relative selectivity is observed when $l_{(A)}$ increases or $l_{(B)}$ decreases (Figure 9.3). This behavior is consistent with the fact that, by increasing $l_{(A)}$, the ability of the membrane to direct molecules A towards the bottom is increased thus raising the selectivity for A. Likewise, when of $l_{(B)}$ decreases, the ability of the membrane to reroute B to the sides is enhanced, creating a permeate fraction at the bottom with a reduced amount of species B, thus enhancing the selectivity. We note that the maximum and minimum selectivities occur at different locations. The selectivity is maximum in the quadrant where $l_{(A)} > 1$ (A is send to the bottom) and $l_{(B)} < 1$ (B is send to the sides), and it is minimum in the quadrant where these conditions are inverted. Note that when $l_{(A)} = l_{(B)}$ (Figure 9.3) we have $\alpha_{A/B}/\alpha^*_{A/B} = 1$. In this case, the membrane is unable to control independently the flux trajectory of species A and B, and there is no net gain in selectivity. In terms of the aspect ratio of the membrane H/L, we can see that if $H/L \to 0$ then $\alpha_{A/B}/\alpha^*_{A/B} \to 1$. This means that the ability to enhance selectivity via flux directional control in thinner (i.e. $H/L \ll 1$) membranes is reduced; or equivalently that a membrane material with stronger anisotropic properties is required to obtain a selectivity enhancement. These trends are in agreement with the results presented in Figure 9.2(c), where we can see that when the aspect ratio increases the

concentration profile approaches that of an isotropic material in a one-dimensional driving force.

The results in Figures 9.2 and 9.3 can be summarized using a modified Robeson representation[15,16] of relative selectivity $\alpha_{A/B}/\alpha^*_{A/B}$ vs. relative permeability ($P'_{(i)}/P^{*\prime}_{(i)}$) as shown in Figure 9.4. In this figure, we see that the performance of the membrane can be divided in two regions. The upper part of the plot where $l_{(A)} > l_{(B)}$ presents an enhancement in selectivity (i.e. $\alpha_{A/B}/\alpha^*_{A/B} > 1$). In contrast, in the lower part we observe that $\alpha_{A/B}/\alpha^*_{A/B} < 1$ when $l_{(A)} < l_{(B)}$. These two regions are separated by a horizontal line for which $\alpha_{A/B}/\alpha^*_{A/B} = 1$ and $l_{(A)} = l_{(B)}$. The figure clearly shows how increasing the value of $l_{(A)}$ for a constant value of $l_{(B)}$ causes an increase in selectivity (upper region). Similarly, increasing the value of $l_{(B)}$ for a constant value of $l_{(A)}$ causes a reduction in the observed selectivity (bottom region). The effect of the aspect ratio on the performance of the membranes is also clearly described, where the smaller the aspect ratio the lower the ability of the membrane to enhance the selectivity.

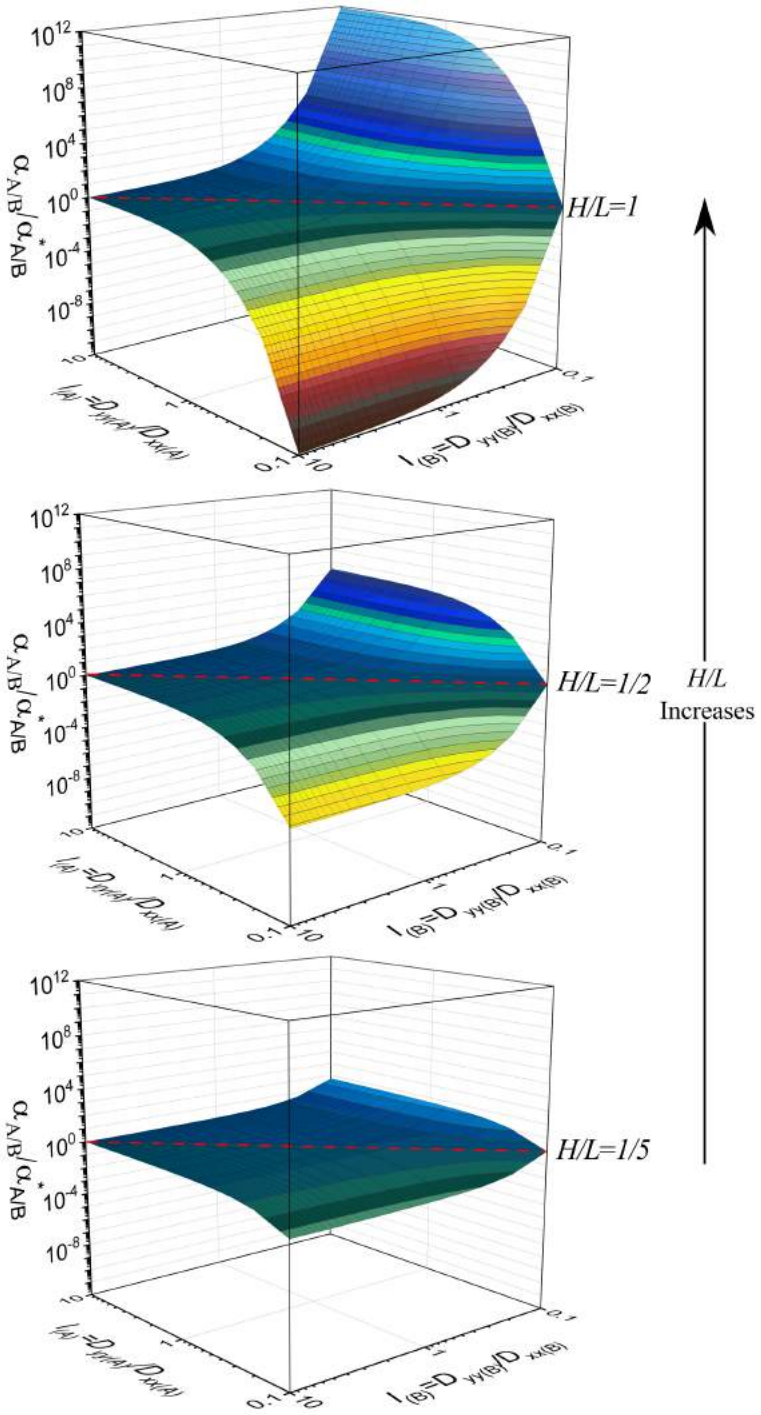

Figure 9.3. Selectivity as a function of $l_{(A)}$ and $l_{(B)}$ for three representative aspect ratios $H/L = 1/5$, $H/L = 1/2$, $H/L = 1$**.** The dashed red line represents the set of materials for which $l_{(A)} = l_{(B)}$ and $\alpha_{A/B(i)}/\alpha^*_{A/B(i)} = 1$.

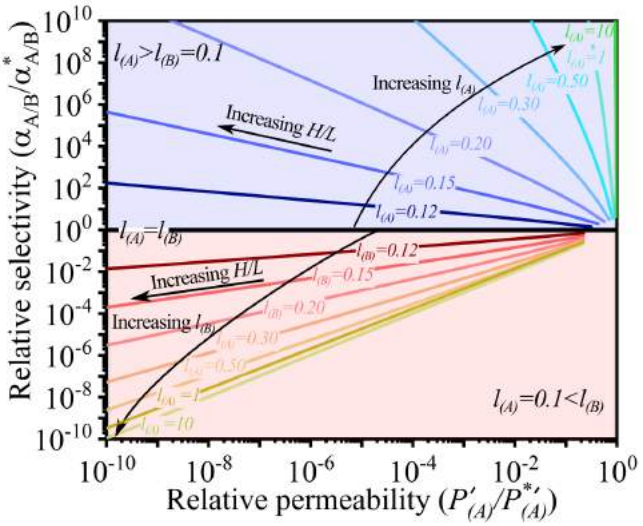

Figure 9.4. Modified Robeson representation of relative selectivity $\alpha_{A/B}/\alpha^*_{A/B}$ vs. relative permeability $P'_{(i)}/P^{*\prime}_{(i)}$ for representative membranes. The upper panel present membranes with $l_{(A)} > l_{(B)} = 0.1$. Different lines correspond to different values of $l_{(A)}$ increasing from bottom to top from $l_{(A)} = 0.12$ to $l_{(A)} = 10$. The lower panel presents membranes with $l_{(A)} = 0.1 < l_{(B)}$. Different lines correspond to different $l_{(B)}$ increasing increases from top to bottom from $l_{(B)} = 0.12$ to $l_{(B)} = 10$.

9.4 Conclusions

In this chapter, we have studied the separation performance of anisotropic multilayer membranes under a two-dimensional driving force. The membrane consist of a planar slab constituting a simple geometry that can potentially be transformed into an anisotropic hollow fiber membrane. We showed that these planar membranes under two-dimensional driving forces can significantly enhance selectivities. We have also introduced an analytical approach to describe mass diffusion in these membranes, which allows studying the performance of the membranes for different structural and material conditions.

9.5 References

(1) Restrepo-Flórez, J.-M.; Maldovan, M. Breaking Separation Limits in Membrane Tehnology. *J. Memb. Sci.* **2018**.

(2) Restrepo-Flórez, J. M.; Maldovan, M. Mass Separation by Metamaterials. *Sci. Rep.* **2016**, *6* (2), 21971.

(3) Restrepo-Flórez, J. M.; Maldovan, M. Rational Design of Mass Diffusion Metamaterial Concentrators Based on Coordinate Transformations. *J. Appl. Phys.* **2016**, *120* (8), 084902.

(4) Restrepo-Flórez, J. M.; Maldovan, M. Mass Diffusion Cloaking and Focusing with Metamaterials. *Appl. Phys. Lett.* **2017**, *111* (7), 071903.

(5) Restrepo-Flórez, J.-M.; Maldovan, M. Metamaterial Membranes. *J. Phys. D. Appl. Phys.* **2017**, *50*, 25104.

(6) Multiphysics, C. Comsol Multiphysics. 2018.

(7) Koros, W. J.; Zhang, C. Materials for Next-Generation Molecularly Selective Synthetic Membranes. *Nat. Mater.* **2017**, *16* (3), 289–297.

(8) Park, H. B.; Kamcev, J.; Robeson, L. M.; Elimelech, M.; Freeman, B. D. Maximizing the Right Stuff: The Trade-off between Membrane Permeability and Selectivity. *SciencE.* **2017**, *356*, eab0530.

(9) Jue, M. L.; Lively, R. P. Targeted Gas Separations through Polymer Membrane Functionalization. *React. Funct. Polym.* **2015**, *86*, 40–43.

(10) Koros, W. J.; Coleman, M. R.; Walker, D. R. B. Controlled Permeability. *Annu. Rev. Mater. Sci.* **1992**, *22*, 47–89.

(11) Ponting, M.; Hiltner, A.; Baer, E. Polymer Nanostructures by Forced Assembly: Process, Structure, and Properties. *Macromol. Symp.* **2010**, *294* (1), 19–32.

(12) Gupta, M.; Lin, Y.; Deans, T.; Baer, E.; Hiltner, A.; Schiraldi, D. A. Structure and Gas Barrier Properties of Poly (Propylene-Graft-Maleic Anhydride)/ Phosphate Glass Composites Prepared by Microlayer Coextrusion. *Macromolecules* **2010**, *43*, 4230–4239.

(13) Richardson, J. J.; Björnmalm, M.; Caruso, F. Technology-Driven Layer-by-Layer Assembly of Nanofilms. *Science (80-.).* **2015**, *348* (6233).

(14) Ajitha, A. R.; Aswathi, M. K.; H.J., M.; Izdebska, J.; Thomas, S. *Multicomponent Polymeric Materials*; Kim, J., Thomas, S., Saha, P., Eds.; Springer: Dordrecht, 2016; Vol. 223.

(15) Robeson, L. M. Correlation of Separation Factor versus Permeability for Polymeric Membranes. *J. Memb. Sci.* **1991**, *62* (2), 165–185.

(16) Robeson, L. M. The Upper Bound Revisited. *J. Memb. Sci.* **2008**, *320* (1–2), 390–400.

CHAPTER 10: PERMEABILITIES AND SELECTIVITIES IN ANISOTROPIC PLANAR MEMBRANES FOR GAS SEPARATIONS

10.1 Introduction

As we have shown in previous chapters, a starting point for the rational design of anisotropic membrane materials for separations is metamaterials engineering[1,2,11–13,3–10]. Inspired by metamaterials theory, we have postulated the possibility of designing anisotropic membrane materials that reroute the trajectory of diffusing chemical compounds in a prescribed way[14,15] (See chapters 7-9). In this chapter, we explore the use of metamaterial-inspired anisotropic *planar* membranes for the separation of gas mixtures (e.g. O_2 and N_2, as well as H_2 and CH_4 separation). Our work is based on the generalization of Fick's law for anisotropic materials $J_{(i)} = \overline{\overline{D}}_{(i)} \nabla C_{(i)}$, where different components of the diffusivity tensor are rationally designed such that diffusing molecules follow specific trajectories within the membrane. We demonstrate large selectivities for benchmark separations such as O_2/N_2 and H_2/CH_4 by incorporating anisotropy in separation processes and discuss existing trade-off relations between the variables characterizing the performance of anisotropic membranes: selectivity, permeability, and collected permeate proportion (CPP). Furthermore from a theoretical perspective we study the separation of binary mixtures made of two species *A* and *B* using two types of anisotropic planar membranes. In the first case, the planar membrane is designed to reroute one of the species in the mixture (e.g. species *B*) (Figure 10.1(b)) while in the second case the membrane simultaneously guides both species *A* and *B* (Figure 10.1(c)). The goal in both cases is to have species *A* and *B* at different locations after they cross the

membrane. Importantly, the fluxes of species *B* in Figure 10.1(b) and species *A* and *B* in Figure 10.1(c) are spatially dependent on the permeate side, i.e. $J_{(i)}(x)$. This is in contrast to isotropic membranes where the fluxes of species *A* and *B* are spatially constant under the same conditions (i.e. spatially constant high pressure on the top and low pressure on the bottom) (Figure 10.1(a)). The spatial dependence of the permeate flux $J_{(i)}(x)$ is the fundamental property that will be leveraged to achieve separations.

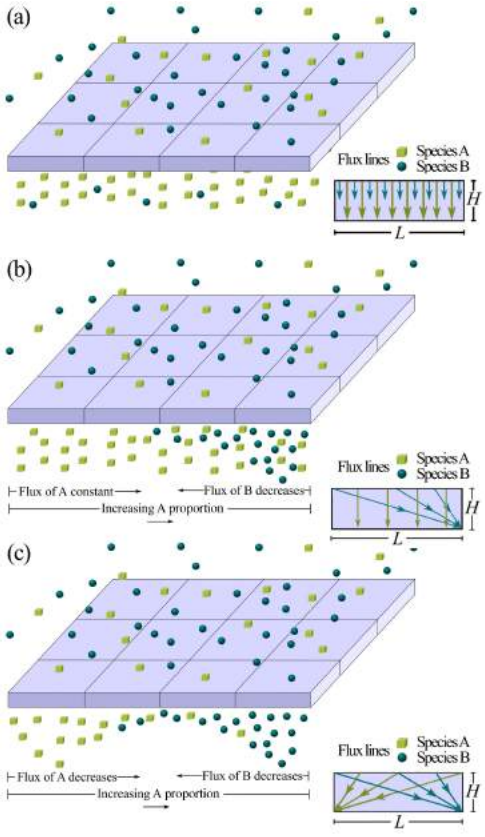

Figure 10.1. Schematic representation of a planar membrane of thickness *H* and length *L* (a) Isotropic membrane: Difference in flux magnitude creates a permeate enriched in one of the species diffusing through the membrane (species *A* in this case). (b) Anisotropic membrane: flux directional control of species *B*, creates a permeate depleted on this species at the left side, thus if the collection area is located at the left the side the permeate will be enriched in species *A* (c) Anisotropic membrane: flux directional control of species *A* and *B* creates a permeate where flux of these species is a function of the position. If the collection area is located at the left, the permeate is enriched in species *A*, whereas if the collection area is located at the right the permeate is enriched in species *B*.

10.2 Results and discussion

10.2.1 Rerouting one species (Ideal case)

We first study the separation of *A* and *B* by modifying the trajectory of *B* (Figure 10.1(b)), and engineer the membrane anisotropy such that the flux of *B* is bent to the right as *B* crosses the membrane. We employ a multilayer structure made of two homogeneous isotropic materials M_1 and M_2 where the plane of the layers is rotated by an angle θ with respect to the direction of the driving force (Figure 10.2). Such multilayer structure enables anisotropic mass diffusion due to the different mass diffusion properties along the parallel $\parallel$ and perpendicular $\perp$ directions to the layers (i.e. parallel and series, respectively). The effective mass diffusion tensor $\overline{\overline{D}}_{(i)}$ for these structures is given by Eqs (10.1) and (4.1) where $D_{\parallel(i)}$ and $D_{\perp(i)}$ are the effective diffusion coefficients along the parallel and perpendicular directions to the layers, respectively, f_1 and f_2 are the volume fractions of constitutive layered materials M_1 and M_2, and k_i is the partition coefficient between the materials, *i.e.* $k_{(i)} = S_{1(i)}/S_{2(i)}$, where *S* is the solubility. The effective solubility of the multilayer structure is calculated as $S_{(i)} = f_1 S_{1(i)} + f_2 S_{2(i)}$.

$$\begin{bmatrix} D_{\parallel(i)}\, cos^2\theta_{(i)} + D_{\perp(i)}\, sin^2\theta_{(i)} & \left(D_{\perp(i)} - D_{\parallel(i)}\right) sin\theta_{(i)}\, cos\theta_{(i)} \\ \left(D_{\perp(i)} - D_{\parallel(i)}\right) sin\theta_{(i)}\, cos\theta_{(i)} & D_{\perp(i)}\, cos^2\theta_{(i)} + D_{\parallel(i)}\, sin^2\theta_{(i)} \end{bmatrix} \tag{6.1}$$

$$D_{\parallel(i)} = \frac{1}{(f_1 + f_2 k_{(i)})}\left(f_1 D_{1(i)} + f_2 k_{(i)} D_2\right); \frac{1}{D_{\perp(i)}} = \left(f_1 + f_2 k_{(i)}\right)\left(\frac{f_1}{D_{1(i)}} + \frac{f_2}{k_i D_{2(i)}}\right) \tag{4.1}$$

We first consider that the layered structure is made of two ideal homogeneous isotropic materials M_1 and M_2 whose diffusivities and solubilities are selected such that the membrane modifies only the trajectory of species *B* to the right. We consider two cases $D_{\parallel(B)}/D_{\perp(B)} = 100$ and $D_{\parallel(B)}/D_{\perp(B)} = 4$, with $D_{\parallel(A)}/D_{\perp(A)} = 1$ (Table 10.1). We

show in Figures 10.2(a) and 10.2(b) the predicted permeability $P'_{(B)}(x)$ for species *B* as a function of the position *x* on the permeate side. The permeability $P'_{(i)} = J_{(i)}H/\Delta p_{(i)}$ of species *i* is defined as the flux $J_{(i)}$ times the membrane thickness *H* normalized by the driving force $\Delta p_{(i)}$ across the membrane[16,17]. Note that for isotropic membranes $P'_{(i)}$ is also equivalent to $D_{(i)}S_{(i)}$. For calculations, we assume a partial pressure of 1 atm on the upper side and complete sweeping on the lower (permeate) side. The thickness of the membrane is *H*=1μm and the lengths are *L*=1μm, 2μm, and 5μm. Figure 10.2(a) shows the development of a position dependent permeability profile $P'_{(B)}(x)$ for the controlled species *B* due to the engineered bending of the trajectory of species *B*. Specifically, we observe species *B* depletion on the membrane left side (low local permeability $P'_{(B)}$), and enrichment of species *B* on the right side (high local permeability $P'_{(B)}$). Clearly, the magnitude of the depletion of species *B* on the left side is dependent on the ratio $D_{\parallel(B)}/D_{\perp(B)}$. On the other hand, the permeability $P'_{(A)}$ of species *A* remains constant for all positions *x* on the permeate side since the trajectory of species *A* is not modified. Importantly, we note that due to the rerouting of species *B* there exist a spatial area on the permeate side of the membrane (left side) where the permeability of *B* is dramatically reduced. This lack of species *B* will be leveraged next to perform separations. To quantify the strong reduction in the permeability of *B* on the left side, we compare in Figure 10.2(a) the position-dependent metamaterial permeability $P'_{(B)}(x)$ against the constant permeabilities corresponding to membranes made of the constituent homogeneous isotropic materials M_1 or M_2 as well as the permeabilities of membranes consisting of series and parallel composite structures made of materials M_1 and M_2. Note that all the membranes are operated under the same conditions such that adequate comparisons

between the physical effects arising from the use of anisotropic and isotropic membranes can be drawn. Figure 10.2(a) shows that, due to the rerouting of species *B* via anisotropy, the permeability of *B* on the left side can be orders of magnitude smaller than that corresponding to the constituent materials as well as the series and parallel arrangements.

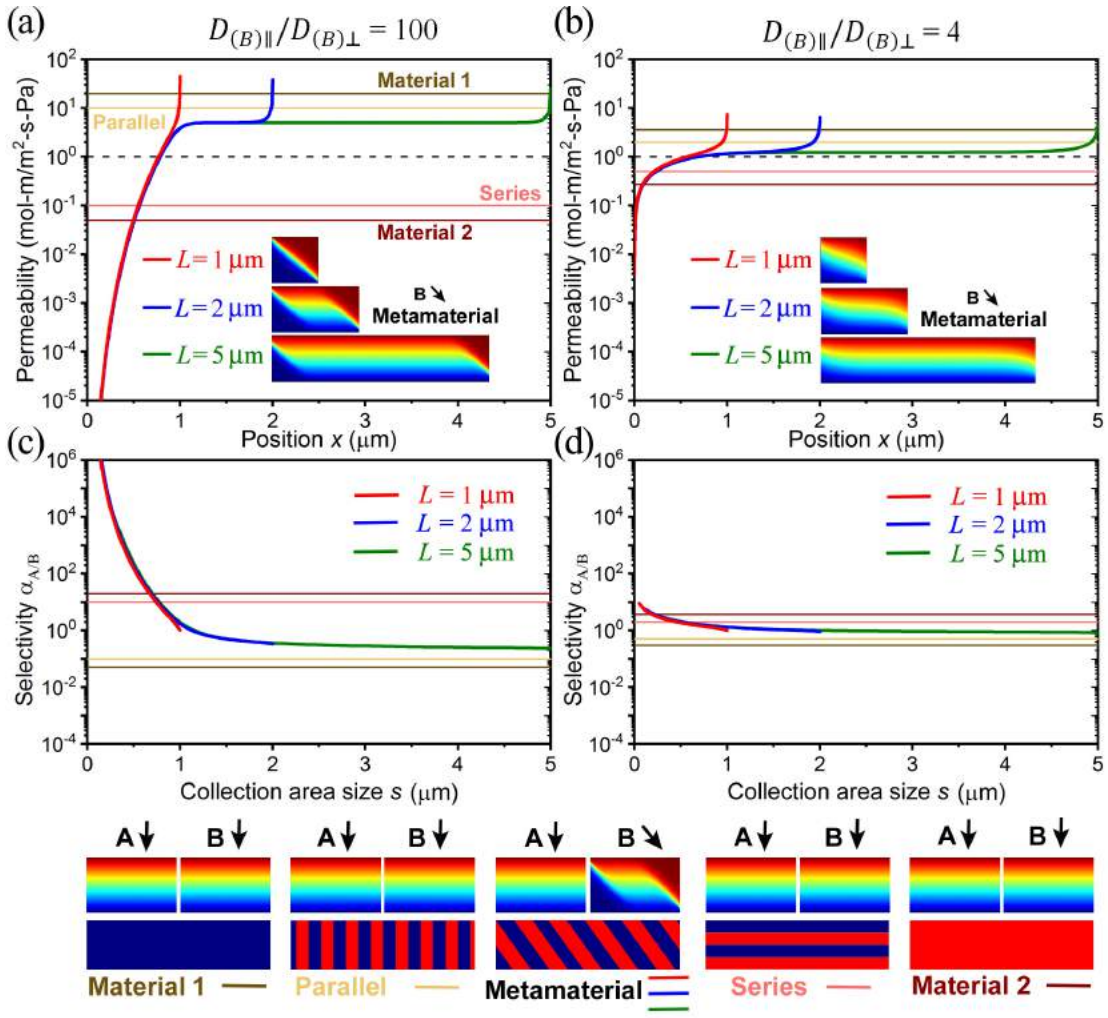

Figure 10.2. Separation of a binary mixture of species *A* and *B* using an anisotropic planar membrane that reroutes species *B* toward the right side while not affecting the diffusion of *A*. The figure also presents the performance of related isotropic systems and their series and parallel arrangements (a)-(b) Permeability of species *B* as a function of the position x on the permeate side for $D_{\parallel(B)}/D_{\perp(B)} = 100$ and $D_{\parallel(B)}/D_{\perp(B)} = 4$, with $D_{\parallel(A)}/D_{\perp(A)} = 1$. (c)-(d) Corresponding selectivities $\alpha_{A/B}$ as a function of the length s of a collection area placed at the left side of the membrane. Color maps show the concentration profiles for *A* and *B*.

Table 10.1. Material properties for separation of species A and B (left), and O_2 and N_2 (right). For O_2/N_2 separation M_1 is PDMS and M_2 is PSF. Units $[D]=m^2/s$, $[S]=mol/m^3Pa$

	A/B separation				O_2/N_2 separation	
Property	A	B	A	B	O_2	N_2
D_1	1	19.95	1	3.73	3.4×10^{-9}	3.4×10^{-9}
S_1	1	1	1	1	7.9×10^{-5}	4.0×10^{-5}
D_2	1	0.05	1	0.27	4.4×10^{-12}	1.2×10^{-12}
S_2	1	1	1	1	1.1×10^{-4}	6.6×10^{-5}
$D_\parallel$	1	10	1	2	1.42×10^{-9}	1.28×10^{-9}
$D_\perp$	1	0.1	1	0.5	1.02×10^{-11}	2.98×10^{-12}
S_{eff}	1	1	1	1	9.45×10^{-5}	5.30×10^{-5}
θ	45	45	45	45	45	45
$D_\parallel/D_\perp$	1	100	1	4	139.2	429.5

We next exploit this unconventional permeation behavior to perform the separation of *A* and *B*. To obtain a mixture enriched in species *A*, the area where the products are collected should be on the left side of the membrane (where *B* is depleted). Note that in contrast to isotropic membranes, in our anisotropic membranes the selectivity $\alpha_{A/B} = \langle P'_{(A)}\rangle/\langle P'_{(B)}\rangle$ depends on the size and location of the collection area due to the spatial dependence of the permeability $P'_{(B)}(x)$. We show in Figures 10.2(c) and 10.2(d) the selectivities $\alpha_{A/B}$ for the membranes in Figures 10.2(a) and 10.2(b) for different collection areas on the permeate side. We consider that the collection area starts from the left side of the membrane (*i.e.* we are interested in a permeate enriched in species *A*) and we collect the permeate leaving the membrane through the area defined by $0 \leq x \leq s$, where s is the length of collection area. We find that the ability of the membrane to produce a permeate enriched in the species *A* significantly increases when the collection area is decreased (Figures 10.2(c)-10.2(d)). Importantly, depending on the size of the area where the permeate is collected, it is possible to achieve selectivities $\alpha_{A/B}$ that are orders of magnitude larger than those of the constituent homogeneous isotropic materials as well

as the series and parallel composite structures. These large selectivities $\alpha_{A/B}$ are a consequence of the low permeability of *B* on the left side of the membrane.

We note that as the collection area is reduced on the permeate side in order to obtain high selectivities one is reducing the collected permeate proportion (CPP) which is given by CPP=$\int_0^s J_{(i)}(x)dx \,/\, \int_0^L J_{(i)}(x)dx$. Note that in conventional isotropic membranes, the entire permeate fraction (with spatially constant composition on the permeate side of the membrane) is collected, thus CPP=1. On the contrary, in anisotropic membrane materials, selecting the size of the collection area is critical to incorporate the advantages of flux directional control, therefore CPP < 1. In other words, anisotropic membranes enable a novel property since one can increase the selectivity while reducing the CPP under single stage operation, which is contrast to isotropic membranes. Note that if the collection area comprises the entire anisotropic membrane on the permeate side, there is no advantage in rerouting the flux lines and the permeate composition obtained lies between the limits imposed by the constituent materials (Figures 10.2(c)-10.2(d), for x=L).

One important variable controlling the performance of anisotropic membranes is the rotation angle θ associated with the multilayer structure. In Figure 10.3 we present the local permeability results for systems with different rotation angles for a membrane in which L=5μm. The effects of θ on the performance of the system are explained by considering that the rotation angle of the multilayer structure determines the bending angle of the flux line. Importantly, $\theta = 0$ and $\theta = \pi/2$ correspond to the limiting cases in which materials are connected in series and parallel, respectively, and there is not flux directional control as it is in fact observed in the plot.

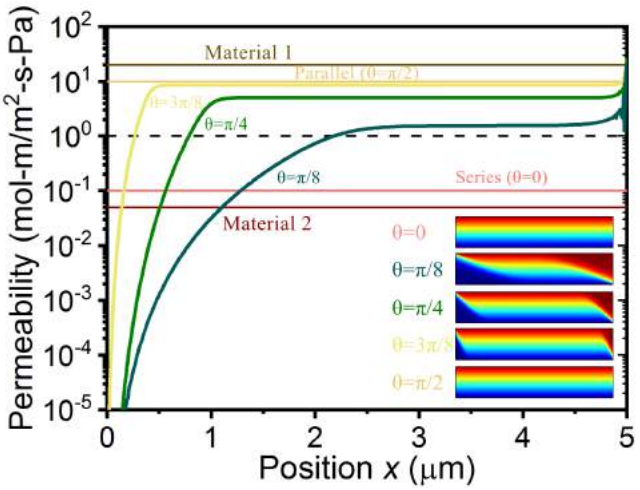

Figure 10.3. Effect of the rotation angle of the multilayer material on the local permeability for systems L=5μm.

10.2.2 Rerouting one species (Real case)

After studying separation of mixtures by ideal anisotropic planar membranes, we next focus on a real separation process and study the permeability and selectivity of oxygen and nitrogen through anisotropic membranes made of realistic materials. To achieve different anisotropic properties for the diffusion of oxygen and nitrogen[15], we consider layered membranes made of PDMS[18] and PSF[19] (Table 10.1). In Figures 10.4(a)-10.4(c) we show the predicted permeability for nitrogen $P'_{(N_2)}(x)$ and oxygen $P'_{(O_2)}(x)$ as a function of the position x along the membrane on the permeate side, as well as the selectivities α_{O_2/N_2} as a function of the size of the collection area. In contrast with the idealized systems discussed in the first part of this chapter, in this case, the diffusion paths of the two species are influenced by the anisotropic membrane. That is, for the realistic material case under study, the trajectories of both oxygen and nitrogen are modified by the anisotropic membrane and the species are rerouted toward the right edge. Note however that the rerouting is more pronounced for nitrogen since $P'_{(N_2)}(x) <$

$P'_{(O_2)}(x)$ on the left side. We show in Figure 10.4(c) that the preferential rerouting of nitrogen toward the right side causes a significant increase in the oxygen selectivity α_{O_2/N_2} when the collection area is located at the left side of the membrane. Importantly, the selectivity of the anisotropic membrane can be made larger than the selectivities of the isotropic materials comprising the membrane. As mentioned previously, the obtained selectivities are correlated to the CPP, which is shown in Figure 10.4(c)-inset. The relation between permeability, selectivity, and CPP for the separation of oxygen and nitrogen using an anisotropic membrane material made of layered PDMS and PSF materials is shown in Figure 10.5. This representation is a 3D expansion of the Robeson plot allowing for a complete characterization of the anisotropic membrane[20,21]. Note that in this plot it is possible to compare the performance of anisotropic materials, isotropic materials, and the upper bound. Isotropic materials have fixed selectivity vs. permeability values. On the other hand, the upper bound for isotropic materials appears as a plane[20,21]. Figure 10.5 shows the trade-off between selectivity α and CPP, which is a property exclusive of anisotropic membranes. Note that in isotropic membranes made of PDMS, PSF or their series and parallel combinations, a reduction in the CPP does not cause an increase in the selectivity. These results demonstrate the novel properties of anisotropic membranes in terms of selectivity values that depend on the area where the products are recovered, achieving enhanced selectivities beyond the values to the constituent materials.

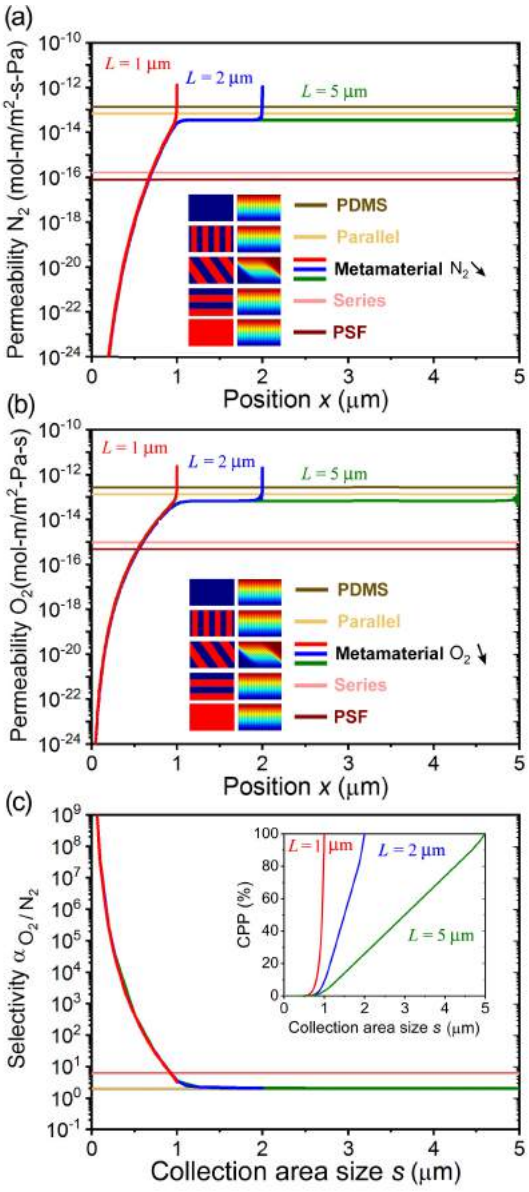

Figure 10.4. Separation of a binary mixture of O_2 and N_2 using an anisotropic planar membrane that preferentially reroutes N_2 to the right. O_2 is also rerouted to the right but to a lesser extent (a)-(b) Permeabilities of N_2 and O_2 as a function of the position x on the permeate side. (c) Selectivity α_{O_2/N_2} as a function of the length s of a collection area placed at the left side of the membrane. Inset shows collected permeate proportion (CPP).

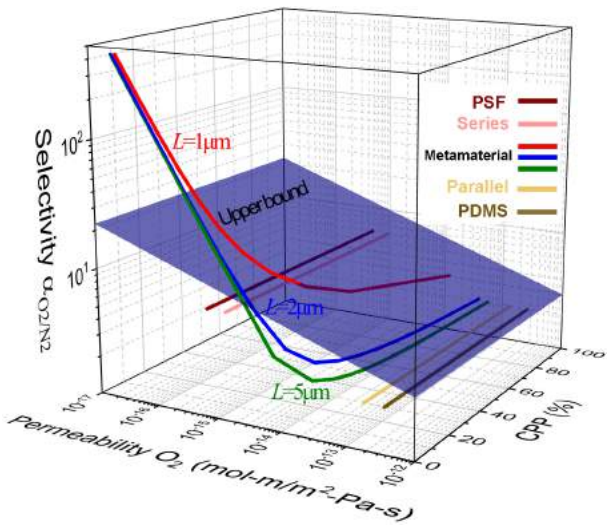

Figure 10.5. Modified Robeson plot for the separation of O_2 and N_2 using an anisotropic planar membrane. The plot shows the relation between the selectivity, permeability, and CPP. For comparison we show the results for the isotropic constituent materials PDMS and PSF, and their series and parallel arrangements. The blue plane is the upper bound.

10.2.3 Rerouting two species (Ideal case)

We also study the permeability and selectivity of anisotropic planar membranes that manipulate the diffusion paths of both species A and B[14]. Specifically, we consider planar membranes made of materials M_1, M_2, M_3 and M_4 spatially arranged as shown in Figure 10.6(a), which allows to reroute species A and B toward opposite directions after they cross the membrane. The diffusivities along each principal axis $D_{\parallel(i)}$ and $D_{\perp(i)}$ are obtained by using a resistors network analogy (See Eqs 8.8-8.10). The material properties are presented in Table 10.2. Importantly, in this case we have $D_{\parallel(A)}/D_{\perp(A)} < 1$ and $D_{\parallel(B)}/D_{\perp(B)} > 1$, allowing us to reroute species A and B toward different places. Figures 10.6(a) and 10.6(c) show the permeabilities $P'_{(A)}(x)$ and $P'_{(B)}(x)$ as a function of the position on the permeate side, where it can be seen how the species A is depleted near the right edge (low $P'_{(A)}(x)$) and the species B is depleted near the left (low $P'_{(B)}(x)$). That is,

species A is directed to the left while species B is directed to the right. These opposite trends cause an interesting result in terms of selectivities. If one collects the permeate near the left side, the membrane is selective in species A (Figure 10.6(b)). On the other hand, if one collects near the right side the membrane is selective in species B (Figure 10.6(d)). In contrast to the case where only B was rerouted, here the membrane is able to achieve selectivities that are higher than any of the constituent materials for both species A (Figure 10.6(b)) and species B (Figure 10.6(d)). This is a consequence of the development of simultaneous spatially-dependent permeability profiles for A and B, where $P'_{(A)}(x)$ is low on the right and $P'_{(B)}(x)$ is low on the left. Another advantage of this anisotropic membrane is the increase in the CPP factor, note that if species A is not controlled a linear trend of CPP vs collection area is established, in contrast as we see in 10.5(c), controlling the two species yields a concave profile.

Table 10.2. Material properties for separation of species A and B (left), and H_2 and CH_4 (right), which are designed to independently control the diffusion trajectory of the two species. For H_2/CH_4 separation M_1 is PTMSP, M_2 PDMS, M_3 PIM-7, and M_4 PMDA-BATPHF. Units $[D]=m^2/s$, $[S]=mol/m^3Pa$

	A/B separation		H_2/CH_4 separation	
Property	A	B	H_2	CH_4
D_1	19.95	19.95	2.60×10^{-8}	3.60×10^{-9}
S_1	1	1	1.74×10^{-4}	1.25×10^{-3}
D_2	0.05	19.95	1.10×10^{-9}	5.10×10^{-12}
S_2	1	1	2.41×10^{-4}	3.62×10^{-3}
D_3	19.95	0.05	1.29×10^{-8}	2.17×10^{-9}
S_3	1	1	1.98×10^{-5}	1.67×10^{-4}
D_4	0.05	0.05	2.20×10^{-10}	6.90×10^{-13}
S_4	1	1	6.94×10^{-5}	4.22×10^{-4}
D_P	10	10	1.00×10^{-8}	8.94×10^{-10}
D_S	0.1	0.1	4.32×10^{-10}	8.39×10^{-13}
$D_\parallel$	0.1	10	2.03×10^{-9}	2.45×10^{-10}
$D_\perp$	10	0.1	2.10×10^{-9}	1.37×10^{-11}
S_{eff}	1	1	1.26×10^{-4}	1.40×10^{-3}
θ	45	45	45	45
$D_\parallel/D_\perp$	0.01	100	0.95	17.86

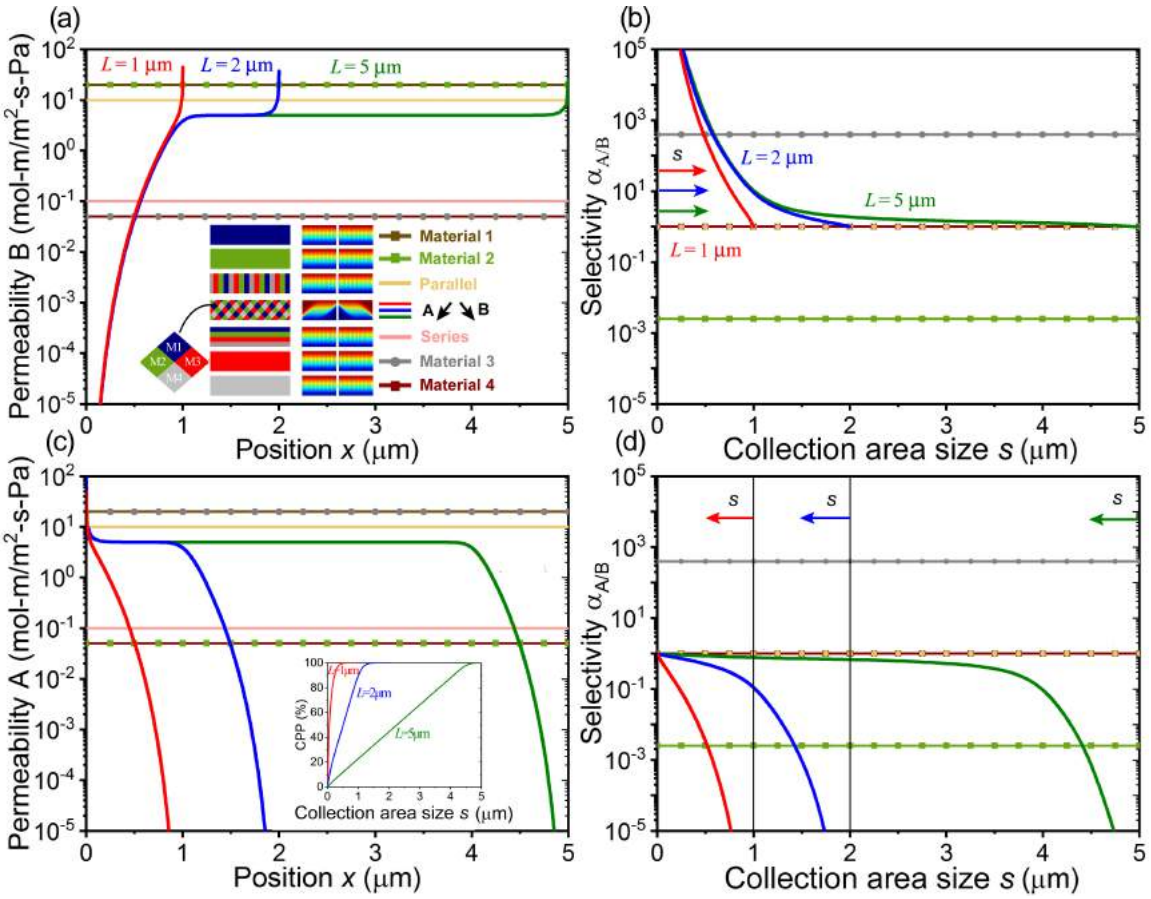

Figure 10.6. Separation of a binary mixture of species A and B using an anisotropic membrane that reroutes species B to the right side and species A toward the left side. (a)-(c) Permeabilities of species A and B as a function of the position on the permeate side. (b)-(d) Selectivities ($\alpha_{A/B}$) as a function of the length s of a collection area placed at the left side (c) and right side (d) of the membrane. Inset: CPP of species A as a function of the length s of a collection area placed at the left side of the membrane.

10.2.4 Rerouting two species (Real case)

In Figure 10.7 we study the performance of the proposed structure for the separation of a binary mixture of H_2 and CH_4. In this case, the anisotropic membrane is made of PTMSP[22], PDMS[18], PIM-7[23] and PMDA-BATPHF[24] (Table 10.2). These materials have been selected such that the effective medium has $D_{\parallel(H_2)}/D_{\perp(H_2)} < 1$ and $D_{\parallel(CH_4)}/D_{\perp(CH_4)} > 1$, and CH_4 is rerouted to the right and H_2 to the left side of the membrane. The

permeability profiles shown in Figures 10.7(a)-10.7(c) show that in the membrane made of realistic materials CH_4 is detoured toward the right side and H_2 essentially moves in the vertical direction. This effect is significant since it proves that independent control of the trajectory of diffusing molecules can be obtained (e.g. we reroute CH_4 to the right without affecting H_2). In terms of CPP of H_2, the dependence with respect to the collection area size (Figure 10.7(c), inset) follows a nearly linear dependence. This result is in sharp contrast with the case of O_2 separation (Figure 10.4(c), inset) where the CPP is non-linear with respect to the collection area size. This is because in the present case, H_2 is not being rerouted to the right side. A summary of the relation between selectivity, permeability, and CPP is shown in Figure 10.8 where we can observe the described trade-off between selectivity and CPP. Additionally, it is also possible to observe that in contrast to Fig. 10.4 there is not a significant change in the permeability of the membrane when the CPP is reduced, *i.e.* when the collection area decreased. This is also a consequence of the fact that H_2 is not being rerouted to the right side.

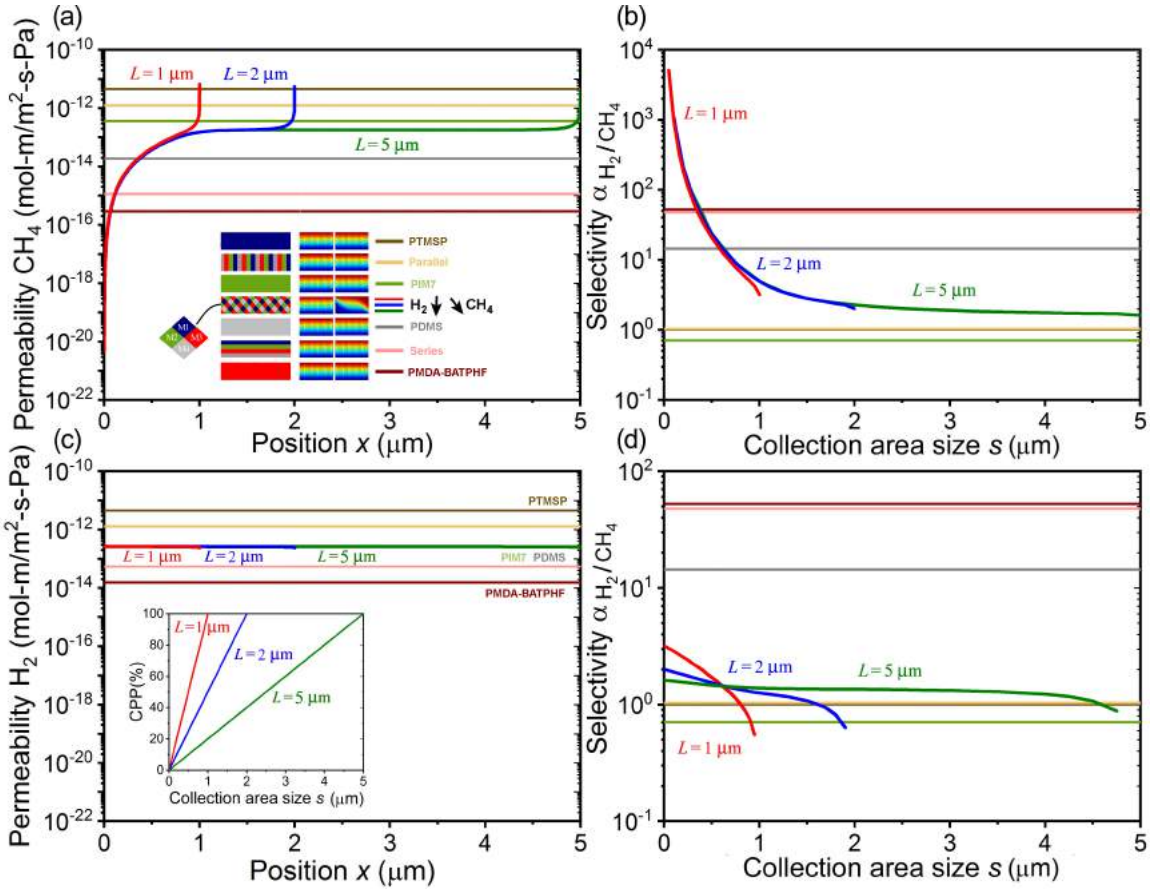

Figure 10.7. Separation of H_2 and CH_4 in a planar membrane that reroutes CH_4 to the right side and H_2 to the left side. (Note: The effect on H_2 is very small). (a)-(b) Permeability of CH_4 and H_2 as a function of the position x on the permeate side. (c)-(d) Ideal selectivity α_{H_2/CH_4} as a function of the length s of a collection area placed at the left (c) and right (d) side of the membrane. Inset: CPP of H_2 as a function of the length s of a collection area placed at the left side of the membrane.

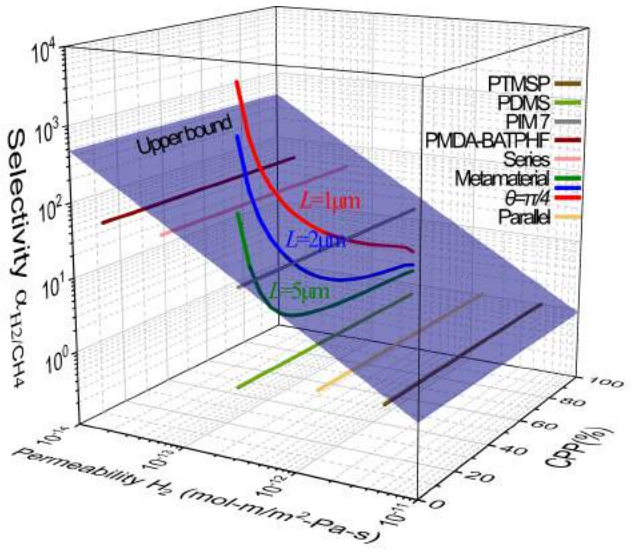

Figure 10.8. Modified Robeson plot for the separation of N_2 and CH_4 using an anisotropic planar membrane. The plot shows the relation between the selectivity, permeability, and CPP. For comparison we also show the selectivity and permeability for the isotropic constituent materials PTMSP, PDMS, PIM-7, and PMDA-BATPHF), as well as their series and parallel arrangements. The blue plane represents the upper bound for this separation.

10.3 Conclusions

In summary, we presented a complete framework for the characterization of anisotropic planar materials for gas separations. We used metamaterials theory to design and study anisotropic planar membrane materials in which the flux direction of the species is controlled as the species diffuse within the membrane. We showed that the incorporation of this new physical mechanism leads to significant changes in the performance of the membrane. Due to the development of spatially-dependent permeability profiles, we found selectivities that are larger than the selectivities of the constituent materials and corresponding series and parallel models under single stage operation. Our results also show the existence of a trade-off relation between the

selectivity and the collected permeate proportion for anisotropic planar membranes, a relation that is absent for isotropic membranes in single stage operation.

10.4 References

(1) Pendry, J. B.; Schurig, D.; Smith, D. R. Controlling Electromagnetic Fields. *Science.* **2006**, *312* (5781), 1780–1782.

(2) Guenneau, S.; Puvirajesinghe, T. M. Fick's Second Law Transformed: One Path to Cloaking in Mass Diffusion. *J. R. Soc. Interface* **2013**, *10* (83), 20130106.

(3) Guenneau, S.; Amra, C.; Veynante, D. Transformation Thermodynamics: Cloaking and Concentrating Heat Flux. *Opt. Express* **2012**, *20* (7), 8207–8218.

(4) Narayana, S.; Sato, Y. Heat Flux Manipulation with Engineered Thermal Materials. *Phys. Rev. Lett.* **2012**, *108* (21), 214303.

(5) Maldovan, M. Sound and Heat Revolutions in Phononics. *Nature* **2013**, *503* (7475), 209–217.

(6) Guenneau, S.; Petiteau, D.; Zerrad, M.; Amra, C.; Puvirajesinghe, T. Transformed Fourier and Fick Equations for the Control of Heat and Mass Diffusion. *AIP Adv.* **2015**, *5* (5), 053404.

(7) Kadic, M.; Bückmann, T.; Schittny, R.; Wegener, M. Metamaterials beyond Electromagnetism. *Reports Prog. Phys.* **2013**, *76* (12), 126501.

(8) Schittny, R.; Kadic, M.; Guenneau, S.; Wegener, M. Experiments on Transformation Thermodynamics: Molding the Flow of Heat. *Phys. Rev. Lett.* **2013**, *110* (19), 195901.

(9) Dede, E. M.; Nomura, T.; Lee, J. Thermal-Composite Design Optimization for Heat Flux Shielding, Focusing, and Reversal. *Struct. Multidiscip. Optim.* **2014**, *49* (1), 59–68.

(10) Zeng, L.; Song, R. Controlling Chloride Ions Diffusion in Concrete. *Sci. Rep.* **2013**, *3*, 3359.

(11) Restrepo-Flórez, J. M.; Maldovan, M. Mass Separation by Metamaterials. *Sci. Rep.* **2016**, *6* (2), 21971.

(12) Restrepo-Flórez, J. M.; Maldovan, M. Rational Design of Mass Diffusion Metamaterial Concentrators Based on Coordinate Transformations. *J. Appl. Phys.* **2016**, *120* (8), 084902.

(13) Restrepo-Flórez, J. M.; Maldovan, M. Mass Diffusion Cloaking and Focusing with

Metamaterials. *Appl. Phys. Lett.* **2017**, *111* (7), 071903.

(14) Restrepo-Flórez, J.-M.; Maldovan, M. Metamaterial Membranes. *J. Phys. D. Appl. Phys.* **2017**, *50*, 25104.

(15) Restrepo-Flórez, J.-M.; Maldovan, M. Breaking Separation Limits in Membrane Technology. *J. Memb. Sci.* **2018**, *566* (April), 301–306.

(16) Koros, W. J.; Zhang, C. Materials for Next-Generation Molecularly Selective Synthetic Membranes. *Nat. Mater.* **2017**, *16* (3), 289–297.

(17) Park, H. B.; Kamcev, J.; Robeson, L. M.; Elimelech, M.; Freeman, B. D. Maximizing the Right Stuff: The Trade-off between Membrane Permeability and Selectivity. *Science.* **2017**, *356*, eab0530.

(18) Merkel, T. C.; Bondar, V. I.; Nagai, K.; Freeman, B. D.; Pinnau, I. Gas Sorption, Diffusion, and Permeation in Poly(Dimethylsiloxane). *J. Polym. Sci. Part B Polym. Phys.* **2000**, *38* (3), 415–434.

(19) McHattie, J. S.; Koros, W. J.; Paul, D. R. Gas Transport Properties of Polysulfones: 1. Role of Symmetry of Methyl Group Placement on Bisphenol. *Polymer.* **1991**, *32* (5), 840–850.

(20) Robeson, L. M. The Upper Bound Revisited. *J. Memb. Sci.* **2008**, *320* (1–2), 390–400.

(21) Robeson, L. M. Correlation of Separation Factor versus Permeability for Polymeric Membranes. *J. Memb. Sci.* **1991**, *62* (2), 165–185.

(22) Merkel, T. C.; Bondar, V.; Nagai, K.; Freeman, B. D. Perfluorocarbon Gases in Poly (1-Trimethylsilyl-1-Propyne). *J. Polym. Sci. Part B Polym. Phys.* **2000**, *38*, 273–296.

(23) Budd, P. M.; Msayib, K. J.; Tattershall, C. E.; Ghanem, B. S.; Reynolds, K. J.; McKeown, N. B.; Fritsch, D. Gas Separation Membranes from Polymers of Intrinsic Microporosity. *J. Memb. Sci.* **2005**, *251* (1–2), 263–269.

(24) Tanaka, K.; Kita, H.; Okano, M.; Okamoto, K. Permeability and Permselectivity of Gases in Fluorinated and Non-Fluorinated Polyimides. *Polymer.* **1992**, *33* (3), 585–592.

CHAPTER 11: CONCLUSIONS AND FUTURE DIRECTIONS

11.1 Conclusions

In this thesis we have explored the design of metamaterials for mass diffusion control. Specifically we have applied metamaterial ideas and concepts to expand the universe of available membrane materials for gas separations. The main findings of this dissertation are presented below:

1. We have shown that the use of coordinate transformations enables the design of metamaterial devices that can control the direction and magnitude of mass flux. Interestingly, as we showed in chapter 3 for the case of concentrators, the ability of these devices to achieve precise control of the flux trajectory is highly tunable. Specifically, we have proved that by modifying the different design variables associated with metamaterial systems it is possible to adjust the concentration gradient developed in a region of interest, the mass flow rate, and the disturbance of the external field. We have also demonstrated that composite materials consisting of multilayers can be used to approximate the anisotropic diffusivity characteristic of metamaterials. Clearly, the accuracy of the multilayer approach increases as the number of layers increases.

2. In chapter 4 we have demonstrated that the design of mass diffusion metamaterials requires the use of effective medium theory that takes into consideration the correct driving force for mass diffusion: the chemical potential. We note that typical approaches based on effective medium theory for heat diffusion consider the use of constituent materials with identical solubility, an assumption that is not satisfied in

metamaterial systems. Our results prove that the partitioning coefficient between constituent materials with different solubilities has a significant effect on the physical behavior of the metamaterial structure. The developed theoretical framework provides an avenue to incorporate solubility differences into the design process of mass diffusion metamaterials.

3. After establishing the fundamental theoretical ground enabling the design of metamaterials for the control of a single chemical species, we showed in chapters 5 and 6 that it is possible to design metamaterial structures that can simultaneously control the diffusion of two chemical species. Specifically, we have demonstrated how a rationally designed metamaterial can control the trajectory of different molecules in a binary mixture by directing them toward different places. In this thesis, we have established the relation between the desired flux trajectory for the species of interest and the required anisotropic diffusivity for the metamaterial that can realize such trajectory. Moreover, we have introduced an effective medium based metamaterial architecture that would allow the experimental realization of metamaterial devices using only isotropic materials.

4. Inspired by the results obtained in chapters 3-6. We showed in chapters 7 and 8 how anisotropic materials can be used in gas separations.

    a. We developed analytical models for mass diffusion in cylindrical geometries in order to fully describe mass diffusion processes in anisotropic cylindrical core-shell membranes. Interestingly the permeance and selectivity obtained using anisotropic cylindrical membranes depends on a few number of dimensionless variables: $l_{(i)}$ which characterizes the anisotropy of the shell,

$\delta_{(i)}$ which represents the core/shell material permeability ratio, and R_2/R_1 which represents the characteristic dimensions of the problem. A complete characterization of the design space is presented by considering the above variables.

b. Our results show that anisotropic membranes can be tuned to obtain very high selectivities significantly higher than those of the constituent materials.

c. Finally, we show how the operation of anisotropic membrane systems is significantly different than that in typical isotropic membranes. In the isotropic case, one retentate and one permeate fraction are generated; in contrast when using anisotropic membranes at least two permeate fractions are created. The development of two permeates arises from the rerouting of mass flux lines toward specific locations on the permeate side.

5. In chapter 9, we present a discussion of the simplest anisotropic system to perform separation: a slab with diagonal anisotropic coefficient operated under a two-dimensional driving force. We characterize the selectivity and permeability of this system in terms of the dimensionless variables $l_{(i)}$ and H/L. We also draw a direct connection between the performance of our system and that of an anisotropic hollow fiber.

6. In chapter 10, we focus our attention to the study of anisotropic diffusion in planar anisotropic membranes. In this chapter, we show how the use of metamaterials leads to permeabilities and selectivities that cannot be attained by the metamaterial constituent materials or their series or parallel composites. Furthermore, we show how in anisotropic planar membranes there exists a trade-off relation that allows to

increase the selectivity of the process by reducing the size of the collection area. This relation is unique of anisotropic membranes and provides a broader picture for mass diffusion through membranes applied to gas separations. We have also shown that this trade-off relation can be incorporated in a modified Robeson representation containing all variables relevant to characterize the performance of anisotropic membranes for gas separation: selectivity, permeability and collected fraction.

11.2 Future work

Throughout this thesis we have demonstrated the use of metamaterials theory for the control of mass diffusion and we have applied metamaterial ideas and concepts to the design of anisotropic membranes for gas separations. Based on the understanding developed in this thesis, we find some interesting future research paths both at the fundamental level as well as in applications.

1. The most useful strategy to achieve effective mass diffusion metamaterials that behave anisotropically is the use of multilayer structures. In the case of heat conduction, there is extensive experimental works that prove the principles behind metamaterial engineering to control thermal diffusive processes. In contrast, in the case of mass diffusion there is no experimental work on the design of metamaterials to control the diffusion paths of molecules. Towards this end, there is interesting recent experimental work that can provide opportunities for experimental fabrication of mass diffusion metamaterials via the manufacturing of polymeric multilayer structures[1–4]. These polymer multilayers of different compositions can be used as a platform for the experimental realization of mass diffusion metamaterials. More

specifically, we believe these novel technologies can provide a path to enable metamaterial membranes for gas separations.

2. In this thesis we have demonstrated the use anisotropic metamaterial membranes for gas separations. The use of metamaterials to control of mass diffusion has not been attempted in the past. We have demonstrated that high selectivities can be obtained in rationally designed metamaterial membranes. The increase in selectivity is accompanied by a reduction in the amount of the species that is collected. An important question that remains open is how these metamaterial membranes would benefit a given separation process in terms of a trade-off between efficiency, easy of fabrication, and costs. Additional research needs to be performed to answer this question, which requires a complete design of a metamaterial membrane in addition to the module and characterization of the entire system as a function of different process conditions.

3. The results presented in this dissertation have been obtained under the assumption that Fick's law can be applied to describe the diffusion process. This assumption is reasonable in multiple cases but there are instances in which classical Fick's law is not valid. One particular case for example is when multicomponent effects on mass diffusion are significant. In this case, the Stefan-Maxwell formulation or a generalized Fick's law can be used to describe the diffusion process[5,6]. Future research can be focused on understanding mass diffusion in anisotropic membranes in which multicomponent effects are important.

4. In this thesis, we have explored the possibility of tailoring the diffusivity tensor $\overline{\overline{D}}_{(i)}$ to achieve control of the mass flux direction. We should note that in all cases the

resulting equation and the transformation techniques used translated into diffusion coefficients that are independent on concentration. As a result, the differential equations are linear in nature. An interesting research avenue that have recently emerged in the case of heat conduction involves the design of non-linear metamaterials. In the case of mass diffusion, this means to be able to design metamaterials having a concentration-dependent diffusivity tensor (i.e. $\overline{\overline{D}}_{(i)}(C_{(i)})$). The design of these non-linear metamaterials can enable the realization of responsive metamaterials that provide different properties depending on the concentration of the species of interest in the environment. These metamaterial functionalities may find applications in the design of mass diffusion sensors.

5. Finally, we point out that most of the results presented in this dissertation have been obtained under steady state conditions. The transient control of mass diffusion processes is also a critically important aspect. An interesting research avenue both at the theoretical level and also from an applied perspective consists of the use of metamaterials for the control of transient mass diffusion[7,8]. This research area is largely unexplored and it may have significant impact in a number of problems of practical interest.

11.3 References

(1) Gupta, M.; Lin, Y.; Deans, T.; Baer, E.; Hiltner, A.; Schiraldi, D. A. Structure and Gas Barrier Properties of Poly (Propylene-Graft-Maleic Anhydride)/ Phosphate Glass Composites Prepared by Microlayer Coextrusion. *Macromolecules* **2010**, *43*, 4230–4239.

(2) Ponting, M.; Hiltner, A.; Baer, E. Polymer Nanostructures by Forced Assembly: Process, Structure, and Properties. *Macromol. Symp.* **2010**, *294* (1), 19–32.

(3) Borges, J.; Mano, J. F. Molecular Interactions Driving the Layer-by-Layer Assembly of Multilayers. *Chem. Rev.* **2014**, *114* (18), 8883–8942.

(4) Richardson, J. J.; Björnmalm, M.; Caruso, F. Technology-Driven Layer-by-Layer Assembly of Nanofilms. *Science.* **2015**, *348* (6233).

(5) Krishna, R.; Wesselingh, J. A. The Maxwell-Stefan Approach to Mass Transfer. *Chem. Eng. Sci.* **1997**, *52* (6), 861–911.

(6) Taylor, R.; Krishna, R. *Multicomponent Mass Transfer*, 1st Ed.; John Wiley & Sons, Inc: New York, 1995.

(7) Zeng, L.; Song, R. Controlling Chloride Ions Diffusion in Concrete. *Sci. Rep.* **2013**, *3*, 3359.

(8) Li, Y.; Liu, C.; Bai, Y.; Qiao, L.; Zhou, J. Ultrathin Hydrogen Diffusion Cloak. *Adv. Theory Simulations* **2017**, *1* (1), 1700004.

AIP PUBLISHING LICENSE
TERMS AND CONDITIONS

Mar 04, 2019

This Agreement between Georgia Institute of Technology -- Juan Manuel Restrepo Flórez ("You") and AIP Publishing ("AIP Publishing") consists of your license details and the terms and conditions provided by AIP Publishing and Copyright Clearance Center.

License Number	4542071245772
License date	Mar 04, 2019
Licensed Content Publisher	AIP Publishing
Licensed Content Publication	Journal of Applied Physics
Licensed Content Title	Rational design of mass diffusion metamaterial concentrators based on coordinate transformations
Licensed Content Author	Juan Manuel Restrepo-Flórez, Martin Maldovan
Licensed Content Date	Aug 28, 2016
Licensed Content Volume	120
Licensed Content Issue	8
Type of Use	Thesis/Dissertation
Requestor type	Author (original article)
Format	Electronic
Portion	Excerpt (> 800 words)
Will you be translating?	No
Title of your thesis / dissertation	Exploring metamaterials for mass diffusion control
Expected completion date	May 2019
Estimated size (number of pages)	182
Requestor Location	Georgia Institute of Technology 311 Ferst Drive NW ATLANTA, GA 30332 United States Attn: Juan Manuel Restrepo
Billing Type	Invoice
Billing Address	Georgia Institute of Technology 311 Ferst Drive NW ATLANTA, GA 30332 United States Attn: Juan Manuel Restrepo

Total 0.00 USD

Terms and Conditions

AIP Publishing -- Terms and Conditions: Permissions Uses

AIP Publishing hereby grants to you the non-exclusive right and license to use and/or distribute the Material according to the use specified in your order, on a one-time basis, for the specified term, with a maximum distribution equal to the number that you have ordered. Any links or other content accompanying the Material are not the subject of this license.

1. You agree to include the following copyright and permission notice with the reproduction of the Material:"Reprinted from [FULL CITATION], with the permission of AIP Publishing." For an article, the credit line and permission notice must be printed on the first page of the article or book chapter. For photographs, covers, or tables, the notice may appear with the Material, in a footnote, or in the reference list.
2. If you have licensed reuse of a figure, photograph, cover, or table, it is your responsibility to ensure that the material is original to AIP Publishing and does not contain the copyright of another entity, and that the copyright notice of the figure, photograph, cover, or table does not indicate that it was reprinted by AIP Publishing, with permission, from another source. Under no circumstances does AIP Publishing purport or intend to grant permission to reuse material to which it does not hold appropriate rights.
   You may not alter or modify the Material in any manner. You may translate the Material into another language only if you have licensed translation rights. You may not use the Material for promotional purposes.
3. The foregoing license shall not take effect unless and until AIP Publishing or its agent, Copyright Clearance Center, receives the Payment in accordance with Copyright Clearance Center Billing and Payment Terms and Conditions, which are incorporated herein by reference.
4. AIP Publishing or Copyright Clearance Center may, within two business days of granting this license, revoke the license for any reason whatsoever, with a full refund payable to you. Should you violate the terms of this license at any time, AIP Publishing, or Copyright Clearance Center may revoke the license with no refund to you. Notice of such revocation will be made using the contact information provided by you. Failure to receive such notice will not nullify the revocation.
5. AIP Publishing makes no representations or warranties with respect to the Material. You agree to indemnify and hold harmless AIP Publishing, and their officers, directors, employees or agents from and against any and all claims arising out of your use of the Material other than as specifically authorized herein.
6. The permission granted herein is personal to you and is not transferable or assignable without the prior written permission of AIP Publishing. This license may not be amended except in a writing signed by the party to be charged.
7. If purchase orders, acknowledgments or check endorsements are issued on any forms containing terms and conditions which are inconsistent with these provisions, such inconsistent terms and conditions shall be of no force and effect. This document, including the CCC Billing and Payment Terms and Conditions, shall be the entire agreement between the parties relating to the subject matter hereof.

This Agreement shall be governed by and construed in accordance with the laws of the State of New York. Both parties hereby submit to the jurisdiction of the courts of New York County for purposes of resolving any disputes that may arise hereunder.

V1.2

Questions? customercare@copyright.com or +1-855-239-3415 (toll free in the US) or +1-978-646-2777.

AIP PUBLISHING LICENSE TERMS AND CONDITIONS

Mar 04, 2019

This Agreement between Georgia Institute of Technology -- Juan Manuel Restrepo Flórez ("You") and AIP Publishing ("AIP Publishing") consists of your license details and the terms and conditions provided by AIP Publishing and Copyright Clearance Center.

License Number	4542081311478
License date	Mar 04, 2019
Licensed Content Publisher	AIP Publishing
Licensed Content Publication	Applied Physics Letters
Licensed Content Title	Mass diffusion cloaking and focusing with metamaterials
Licensed Content Author	Juan Manuel Restrepo-Flórez, Martin Maldovan
Licensed Content Date	Aug 14, 2017
Licensed Content Volume	111
Licensed Content Issue	7
Type of Use	Thesis/Dissertation
Requestor type	Author (original article)
Format	Electronic
Portion	Excerpt (> 800 words)
Will you be translating?	No
Title of your thesis / dissertation	Exploring metamaterials for mass diffusion control
Expected completion date	May 2019
Estimated size (number of pages)	182
Requestor Location	Georgia Institute of Technology 311 Ferst Drive NW ATLANTA, GA 30332 United States Attn: Juan Manuel Restrepo
Billing Type	Invoice
Billing Address	Georgia Institute of Technology 311 Ferst Drive NW ATLANTA, GA 30332 United States Attn: Juan Manuel Restrepo

Total 0.00 USD

Terms and Conditions

AIP Publishing -- Terms and Conditions: Permissions Uses

AIP Publishing hereby grants to you the non-exclusive right and license to use and/or distribute the Material according to the use specified in your order, on a one-time basis, for the specified term, with a maximum distribution equal to the number that you have ordered. Any links or other content accompanying the Material are not the subject of this license.

1. You agree to include the following copyright and permission notice with the reproduction of the Material:"Reprinted from [FULL CITATION], with the permission of AIP Publishing." For an article, the credit line and permission notice must be printed on the first page of the article or book chapter. For photographs, covers, or tables, the notice may appear with the Material, in a footnote, or in the reference list.
2. If you have licensed reuse of a figure, photograph, cover, or table, it is your responsibility to ensure that the material is original to AIP Publishing and does not contain the copyright of another entity, and that the copyright notice of the figure, photograph, cover, or table does not indicate that it was reprinted by AIP Publishing, with permission, from another source. Under no circumstances does AIP Publishing purport or intend to grant permission to reuse material to which it does not hold appropriate rights.
   You may not alter or modify the Material in any manner. You may translate the Material into another language only if you have licensed translation rights. You may not use the Material for promotional purposes.
3. The foregoing license shall not take effect unless and until AIP Publishing or its agent, Copyright Clearance Center, receives the Payment in accordance with Copyright Clearance Center Billing and Payment Terms and Conditions, which are incorporated herein by reference.
4. AIP Publishing or Copyright Clearance Center may, within two business days of granting this license, revoke the license for any reason whatsoever, with a full refund payable to you. Should you violate the terms of this license at any time, AIP Publishing, or Copyright Clearance Center may revoke the license with no refund to you. Notice of such revocation will be made using the contact information provided by you. Failure to receive such notice will not nullify the revocation.
5. AIP Publishing makes no representations or warranties with respect to the Material. You agree to indemnify and hold harmless AIP Publishing, and their officers, directors, employees or agents from and against any and all claims arising out of your use of the Material other than as specifically authorized herein.
6. The permission granted herein is personal to you and is not transferable or assignable without the prior written permission of AIP Publishing. This license may not be amended except in a writing signed by the party to be charged.
7. If purchase orders, acknowledgments or check endorsements are issued on any forms containing terms and conditions which are inconsistent with these provisions, such inconsistent terms and conditions shall be of no force and effect. This document, including the CCC Billing and Payment Terms and Conditions, shall be the entire agreement between the parties relating to the subject matter hereof.

This Agreement shall be governed by and construed in accordance with the laws of the State of New York. Both parties hereby submit to the jurisdiction of the courts of New York County for purposes of resolving any disputes that may arise hereunder.

V1.2

Questions? customercare@copyright.com or +1-855-239-3415 (toll free in the US) or +1-978-646-2777.

IOP Publishing LICENSE TERMS AND CONDITIONS

Mar 06, 2019

This is a License Agreement between Georgia Institute of Technology -- Juan Manuel Restrepo Flórez ("You") and IOP Publishing ("IOP Publishing") provided by Copyright Clearance Center ("CCC"). The license consists of your order details, the terms and conditions provided by IOP Publishing, and the payment terms and conditions.

All payments must be made in full to CCC. For payment instructions, please see information listed at the bottom of this form.

License Number	4543190432444
License date	Mar 04, 2019
Licensed content publisher	IOP Publishing
Licensed content title	Journal of Physics D : Applied Physics
Licensed content date	Jan 1, 1970
Type of Use	Thesis/Dissertation
Requestor type	Author of requested content
Format	Electronic
Portion	chapter/article
The requesting person/organization is:	Juan Manuel Restrepo Florez
Title or numeric reference of the portion(s)	Introduction, methods, results and discussion, conclusions, references
Title of the article or chapter the portion is from	Metamaterial membranes
Editor of portion(s)	N/A
Author of portion(s)	N/A
Volume of serial or monograph.	N/A
Issue, if republishing an article from a serial	50
Page range of the portion	
Publication date of portion	1 December 2016
Rights for	Main product
Duration of use	Life of current and all future editions
Creation of copies for the disabled	no
With minor editing privileges	yes
For distribution to	Worldwide

In the following language(s)	Original language of publication
With incidental promotional use	no
The lifetime unit quantity of new product	Up to 499
Title	Exploring metamaterials for mass diffusion control
Institution name	n/a
Expected presentation date	May 2019
Billing Type	Invoice
Billing Address	Georgia Institute of Technology 311 Ferst Drive NW ATLANTA, GA 30332 United States Attn: Juan Manuel Restrepo
Total (may include CCC user fee)	0.00 USD
Terms and Conditions	

TERMS AND CONDITIONS

The following terms are individual to this publisher:

These special terms and conditions are in addition to the standard terms and conditions for CCC's Republication Service and, together with those standard terms and conditions, govern the use of the Works.

As the "User" you will make all reasonable efforts to contact the author(s) of the article which the Work is to be reused from, to seek consent for your intended use. Contacting one author who is acting expressly as authorised agent for their co-author(s) is acceptable.

User will reproduce the following wording prominently alongside the Work:

- the source of the Work, including author, article title, title of journal, volume number, issue number (if relevant), page range (or first page if this is the only information available) and date of first publication. This information can be contained in a footnote or reference note; and
- a link back to the article (via DOI); and
- if practicable, and IN ALL CASES for new works published under any of the Creative Commons licences, the words "© IOP Publishing. Reproduced with permission. All rights reserved"

Without the express permission of the author(s) and the Rightsholder of the article from which the Work is to be reused, User shall not use it in any way which, in the opinion of the Rightsholder, could: (i) distort or alter the author(s)' original intention(s) and meaning; (ii) be prejudicial to the honour or reputation of the author(s); and/or (iii) imply endorsement by the author(s) and/or the Rightsholder.

This licence does not apply to any article which is credited to another source and which does not have the copyright line '© IOP Publishing Ltd'. User must check the copyright line of the article from which the Work is to be reused to check that IOP Publishing Ltd has all the necessary rights to be able to grant permission. User is solely responsible for identifying and

obtaining separate licences and permissions from the copyright owner for reuse of any such third party material/figures which the Rightsholder is not the copyright owner of. The Rightsholder shall not reimburse any fees which User pays for a republication license for such third party content.

This licence does not apply to any material/figure which is credited to another source in the Rightsholder's publication or has been obtained from a third party. User must check the Version of Record of the article from which the Work is to be reused, to check whether any of the material in the Work is third party material. Third party citations and/or copyright notices and/or permissions statements may not be included in any other version of the article from which the Work is to be reused and so cannot be relied upon by the User. User is solely responsible for identifying and obtaining separate licences and permissions from the copyright owner for reuse of any such third party material/figures where the Rightsholder is not the copyright owner. The Rightsholder shall not reimburse any fees which User pays for a republication license for such third party content.

User and CCC acknowledge that the Rightsholder may, from time to time, make changes or additions to these special terms and conditions without express notification, provided that these shall not apply to permissions already secured and paid for by User prior to such change or addition.

User acknowledges that the Rightsholder (which includes companies within its group and third parties for whom it publishes its titles) may make use of personal data collected through the service in the course of their business.

If User is the author of the Work, User may automatically have the right to reuse it under the rights granted back when User transferred the copyright in the article to the Rightsholder. User should check the copyright form and the relevant author rights policy to check whether permission is required. If User is the author of the Work and does require permission for proposed reuse of the Work, User should select 'Author of requested content' as the Requestor Type. The Rightsholder shall not reimburse any fees which User pays for a republication license.

If User is the author of the article which User wishes to reuse in User's thesis or dissertation, the republication licence covers the right to include the Accepted Manuscript version (not the Version of Record) of the article. User must include citation details and, for online use, a link to the Version of Record of the article on the Rightsholder's website. User may need to obtain separate permission for any third party content included within the article. User must check this with the copyright owner of such third party content. User may not include the article in a thesis or dissertation which is published by ProQuest. Any other commercial use of User's thesis or dissertation containing the article would also need to be expressly notified in writing to the Rightsholder at the time of request and would require separate written permission from the Rightsholder.

User does not need to request permission for Work which has been published under a CC BY licence. User must check the Version of Record of the CC BY article from which the Work is to be reused, to check whether any of the material in the Work is third party material and so not published under the CC BY licence. User is solely responsible for identifying and obtaining separate licences and permissions from the copyright owner for reuse of any such third party material/figures. The Rightsholder shall not reimburse any fees which User pays for such licences and permissions.

As well as CCC, the Rightsholder shall have the right to bring any legal action that it deems necessary to enforce its rights should it consider that the Work infringes those rights in any way.

For STM Signatories ONLY (as agreed as part of the STM Guidelines)
Any licence granted for a particular edition of a Work will apply also to subsequent editions of it and for editions in other languages, provided such editions are for the Work as a whole in situ and do not involve the separate exploitation of the permitted illustrations or excerpts.

Other Terms and Conditions:

STANDARD TERMS AND CONDITIONS

1. Description of Service; Defined Terms. This Republication License enables the User to obtain licenses for republication of one or more copyrighted works as described in detail on the relevant Order Confirmation (the "Work(s)"). Copyright Clearance Center, Inc. ("CCC") grants licenses through the Service on behalf of the rightsholder identified on the Order Confirmation (the "Rightsholder"). "Republication", as used herein, generally means the inclusion of a Work, in whole or in part, in a new work or works, also as described on the Order Confirmation. "User", as used herein, means the person or entity making such republication.
2. The terms set forth in the relevant Order Confirmation, and any terms set by the Rightsholder with respect to a particular Work, govern the terms of use of Works in connection with the Service. By using the Service, the person transacting for a republication license on behalf of the User represents and warrants that he/she/it (a) has been duly authorized by the User to accept, and hereby does accept, all such terms and conditions on behalf of User, and (b) shall inform User of all such terms and conditions. In the event such person is a "freelancer" or other third party independent of User and CCC, such party shall be deemed jointly a "User" for purposes of these terms and conditions. In any event, User shall be deemed to have accepted and agreed to all such terms and conditions if User republishes the Work in any fashion.

3. Scope of License; Limitations and Obligations.

3.1 All Works and all rights therein, including copyright rights, remain the sole and exclusive property of the Rightsholder. The license created by the exchange of an Order Confirmation (and/or any invoice) and payment by User of the full amount set forth on that document includes only those rights expressly set forth in the Order Confirmation and in these terms and conditions, and conveys no other rights in the Work(s) to User. All rights not expressly granted are hereby reserved.
3.2 General Payment Terms: You may pay by credit card or through an account with us payable at the end of the month. If you and we agree that you may establish a standing account with CCC, then the following terms apply: Remit Payment to: Copyright Clearance Center, 29118 Network Place, Chicago, IL 60673-1291. Payments Due: Invoices are payable upon their delivery to you (or upon our notice to you that they are available to you for downloading). After 30 days, outstanding amounts will be subject to a service charge of 1-1/2% per month or, if less, the maximum rate allowed by applicable law. Unless otherwise specifically set forth in the Order Confirmation or in a separate written agreement signed by CCC, invoices are due and payable on "net 30" terms. While User may exercise the rights licensed immediately upon issuance of the Order Confirmation, the license is automatically revoked and is null and void, as if it had never been issued, if complete payment for the license is not received on a timely basis either from User directly or through a payment agent, such as a credit card company.
3.3 Unless otherwise provided in the Order Confirmation, any grant of rights to User (i) is "one-time" (including the editions and product family specified in the license), (ii) is non-exclusive and non-transferable and (iii) is subject to any and all limitations and restrictions (such as, but not limited to, limitations on duration of use or circulation) included in the

Order Confirmation or invoice and/or in these terms and conditions. Upon completion of the licensed use, User shall either secure a new permission for further use of the Work(s) or immediately cease any new use of the Work(s) and shall render inaccessible (such as by deleting or by removing or severing links or other locators) any further copies of the Work (except for copies printed on paper in accordance with this license and still in User's stock at the end of such period).

3.4 In the event that the material for which a republication license is sought includes third party materials (such as photographs, illustrations, graphs, inserts and similar materials) which are identified in such material as having been used by permission, User is responsible for identifying, and seeking separate licenses (under this Service or otherwise) for, any of such third party materials; without a separate license, such third party materials may not be used.

3.5 Use of proper copyright notice for a Work is required as a condition of any license granted under the Service. Unless otherwise provided in the Order Confirmation, a proper copyright notice will read substantially as follows: “Republished with permission of [Rightsholder’s name], from [Work's title, author, volume, edition number and year of copyright]; permission conveyed through Copyright Clearance Center, Inc. ” Such notice must be provided in a reasonably legible font size and must be placed either immediately adjacent to the Work as used (for example, as part of a by-line or footnote but not as a separate electronic link) or in the place where substantially all other credits or notices for the new work containing the republished Work are located. Failure to include the required notice results in loss to the Rightsholder and CCC, and the User shall be liable to pay liquidated damages for each such failure equal to twice the use fee specified in the Order Confirmation, in addition to the use fee itself and any other fees and charges specified.

3.6 User may only make alterations to the Work if and as expressly set forth in the Order Confirmation. No Work may be used in any way that is defamatory, violates the rights of third parties (including such third parties' rights of copyright, privacy, publicity, or other tangible or intangible property), or is otherwise illegal, sexually explicit or obscene. In addition, User may not conjoin a Work with any other material that may result in damage to the reputation of the Rightsholder. User agrees to inform CCC if it becomes aware of any infringement of any rights in a Work and to cooperate with any reasonable request of CCC or the Rightsholder in connection therewith.

4. Indemnity. User hereby indemnifies and agrees to defend the Rightsholder and CCC, and their respective employees and directors, against all claims, liability, damages, costs and expenses, including legal fees and expenses, arising out of any use of a Work beyond the scope of the rights granted herein, or any use of a Work which has been altered in any unauthorized way by User, including claims of defamation or infringement of rights of copyright, publicity, privacy or other tangible or intangible property.

5. Limitation of Liability. UNDER NO CIRCUMSTANCES WILL CCC OR THE RIGHTSHOLDER BE LIABLE FOR ANY DIRECT, INDIRECT, CONSEQUENTIAL OR INCIDENTAL DAMAGES (INCLUDING WITHOUT LIMITATION DAMAGES FOR LOSS OF BUSINESS PROFITS OR INFORMATION, OR FOR BUSINESS INTERRUPTION) ARISING OUT OF THE USE OR INABILITY TO USE A WORK, EVEN IF ONE OF THEM HAS BEEN ADVISED OF THE POSSIBILITY OF SUCH DAMAGES. In any event, the total liability of the Rightsholder and CCC (including their respective employees and directors) shall not exceed the total amount actually paid by User for this license. User assumes full liability for the actions and omissions of its principals, employees, agents, affiliates, successors and assigns.

6. Limited Warranties. THE WORK(S) AND RIGHT(S) ARE PROVIDED "AS IS". CCC HAS THE RIGHT TO GRANT TO USER THE RIGHTS GRANTED IN THE ORDER CONFIRMATION DOCUMENT. CCC AND THE RIGHTSHOLDER DISCLAIM ALL OTHER WARRANTIES RELATING TO THE WORK(S) AND RIGHT(S), EITHER EXPRESS OR IMPLIED, INCLUDING WITHOUT LIMITATION IMPLIED WARRANTIES OF MERCHANTABILITY OR FITNESS FOR A PARTICULAR PURPOSE. ADDITIONAL RIGHTS MAY BE REQUIRED TO USE ILLUSTRATIONS, GRAPHS, PHOTOGRAPHS, ABSTRACTS, INSERTS OR OTHER PORTIONS OF THE WORK (AS OPPOSED TO THE ENTIRE WORK) IN A MANNER CONTEMPLATED BY USER; USER UNDERSTANDS AND AGREES THAT NEITHER CCC NOR THE RIGHTSHOLDER MAY HAVE SUCH ADDITIONAL RIGHTS TO GRANT.
7. Effect of Breach. Any failure by User to pay any amount when due, or any use by User of a Work beyond the scope of the license set forth in the Order Confirmation and/or these terms and conditions, shall be a material breach of the license created by the Order Confirmation and these terms and conditions. Any breach not cured within 30 days of written notice thereof shall result in immediate termination of such license without further notice. Any unauthorized (but licensable) use of a Work that is terminated immediately upon notice thereof may be liquidated by payment of the Rightsholder's ordinary license price therefor; any unauthorized (and unlicensable) use that is not terminated immediately for any reason (including, for example, because materials containing the Work cannot reasonably be recalled) will be subject to all remedies available at law or in equity, but in no event to a payment of less than three times the Rightsholder's ordinary license price for the most closely analogous licensable use plus Rightsholder's and/or CCC's costs and expenses incurred in collecting such payment.
8. **Miscellaneous.**
8.1 User acknowledges that CCC may, from time to time, make changes or additions to the Service or to these terms and conditions, and CCC reserves the right to send notice to the User by electronic mail or otherwise for the purposes of notifying User of such changes or additions; provided that any such changes or additions shall not apply to permissions already secured and paid for.
8.2 Use of User-related information collected through the Service is governed by CCC's privacy policy, available online here: http://www.copyright.com/content/cc3/en/tools/footer/privacypolicy.html.
8.3 The licensing transaction described in the Order Confirmation is personal to User. Therefore, User may not assign or transfer to any other person (whether a natural person or an organization of any kind) the license created by the Order Confirmation and these terms and conditions or any rights granted hereunder; provided, however, that User may assign such license in its entirety on written notice to CCC in the event of a transfer of all or substantially all of User's rights in the new material which includes the Work(s) licensed under this Service.
8.4 No amendment or waiver of any terms is binding unless set forth in writing and signed by the parties. The Rightsholder and CCC hereby object to any terms contained in any writing prepared by the User or its principals, employees, agents or affiliates and purporting to govern or otherwise relate to the licensing transaction described in the Order Confirmation, which terms are in any way inconsistent with any terms set forth in the Order Confirmation and/or in these terms and conditions or CCC's standard operating procedures, whether such writing is prepared prior to, simultaneously with or subsequent to the Order Confirmation, and whether such writing appears on a copy of the Order Confirmation or in a

separate instrument.
8.5 The licensing transaction described in the Order Confirmation document shall be governed by and construed under the law of the State of New York, USA, without regard to the principles thereof of conflicts of law. Any case, controversy, suit, action, or proceeding arising out of, in connection with, or related to such licensing transaction shall be brought, at CCC's sole discretion, in any federal or state court located in the County of New York, State of New York, USA, or in any federal or state court whose geographical jurisdiction covers the location of the Rightsholder set forth in the Order Confirmation. The parties expressly submit to the personal jurisdiction and venue of each such federal or state court.If you have any comments or questions about the Service or Copyright Clearance Center, please contact us at 978-750-8400 or send an e-mail to info@copyright.com.
v 1.1

Questions? customercare@copyright.com or +1-855-239-3415 (toll free in the US) or +1-978-646-2777.